The Role of Microglia in Activity-Dependent Neuronal Network Maturation and Maintenance



Auguste Vadisiute

Christ Church College, University of Oxford

Department of Anatomy, Physiology and Genetics

Trinity Term 2022

Thesis submitted for the degree of Doctor of Philosophy

Abstract

Neurons comprise only less than half of the nervous system, yet some of all those other cells have been largely ignored. Microglia are the tissue resident macrophages of the brain. These cells play a key role in shaping neuronal network formation during development and subsequently help to maintain a stable and healthy brain. After birth our brain contains overabundant neuronal connections and some of these must be refined and eliminated. Microglia scavenge the unnecessary connections via synaptic pruning and shape the neuronal network. Any abnormality in this interaction during neuronal network formation and maintenance can lead to a variety of neurodevelopmental disorders such as autism or schizophrenia. Yet, neither the risk factors underlying these disorders nor the mechanisms that regulate synaptic pruning in the developing brain are well understood.

My DPhil project tested the hypothesis that excitation or inhibition of specific neurons in a neuronal network changes microglial behaviour and dynamics leading to altered communication between microglia and neurons. Using a mouse model, I selectively removed parts of the Snap25 gene and it produced a non-functioning protein in a subset of cortical layer 5 projection neurons and some hippocampal dentate gyrus neurons and thus also eradicated their ability to release synaptic vesicles in a regulated manner from around the time of birth in a chronic fashion. I observed that abolition of Snap25 expression reduced microglial activity and altered synaptic maturation. Also, it affected microglia-neuron communication by disrupting normal chemokine and phagocytic signalling. Lastly, I observed sex-specific changes in microglia-neuron communications and this indicated that male mice were more sensitive to abolished Snap25-mediated release of synaptic vesicles during brain development. To test whether the same changes would apply for more acute silencing, I used

chemogenetic manipulation to increase or reduce network activity of the same subpopulation of layer 5 and hippocampal neurons for hours rather than weeks. I observed that chronic synaptic and acute chemogenetic 'silencing' affects microglia in the same manner. Moreover, acute chemogenetic activation alters microglial morphology leading to retraction of processes and shift to a highly phagocytic active amoeboid form. Findings from my doctoral project suggest that interaction between microglia and neurons is bidirectional in an activity-dependent and sex-specific manner. Given the differential effects of synaptic 'silencing' on microglial cell morphology and activity in males and females, it would be interesting to speculate that microglia may contribute to the sex-specific effects of synaptic 'silencing' on microglia-neuron communications and synaptic maturation during development.

Abbreviations

ADP	Adenosine diphosphate
ATP	Adenosine triphosphate
BCA	Bicinchoninic acid assay
C3	Complement component 3
CA1	Cornu ammonis 1
CA3	Cornu ammonis 3
CD11b	Cluster of differentiation 11 b
CD11c	Cluster of differentiation 11 c
CD68	Cluster of differentiation 68 or phagosomal marker
cDNA	Complementary DNA
cKO	Conditional knock-out
CNS	Central Nervous System
CNO	Clozapine-N-oxide
CR3	Complement receptor 3
CX3CL1	CX3C Mofit chemokine ligand 1 or fractalkine ligand
CX3CR1	CX3C Mofit chemokine receptor 1 or fractalkine receptor
DAPI	4’,6-diamidino-2-phenylindole
DNA	Deoxyribonucleic acid
DREADDs	Designer receptors exclusively activated by designer drugs
EM	Electron microscopy
GAPDH	Glyceraldehydre-3-phosphate dehydrogenase
hM3Dq	Modified form of the human M3 muscarine (hM3) receptor

hM4Di	Modified form of the human M4 muscarine (hM4) receptor
HRP	Horseradish peroxidase
GIRK	G protein inwardly rectifying potassium channels
GO	Gene ontology
GPCR	G protein-coupled receptor
GW	Gestational week
Iba1	Ionized calcium-binding adaptor molecule
IgG	Immunoglobulin G
L5	Cortical layer 5
MHC	Major histocompatibility complex
mRNA	Messenger ribonucleic acid
PCR	Polymerase chain reaction
PSD95	Postsynaptic density protein 95
qPCR	Quantitative PCR
Rbp4	Retinol binding protein 4
RIPA	Radioimmunoprecipitation assay buffer
RNA	Ribonucleic acid
SC	Superior colliculus
Snap25	Synaptosomal-associated protein 25 kDa
SNARE	Soluble N-ethylmaleimide attachment protein receptor
TBS	Tris-buffer saline
VAMP	Vesicle-associated membrane protein
vGlut1	Vesicular glutamate transporter 1
WT	Wild type mice

Statement and credits

I declare that no part of my thesis has been submitted for any qualification other than the degree of Doctor of Philosophy at the University of Oxford.

When it is not stated otherwise, the work is my own. However, some of the experimental work and writing a general review was the result of collaborations with other group members. Part of my introduction of chapter 4 was based on the review that we recently submitted to *Developmental Neurobiology* (I as a first co-author). I adopted the SNARE complex figure and several text elements from this review that were my own work and overlap between this publication and the thesis presented here.

Several parts of the thesis were performed in collaboration with fellow students and supervisors. Firstly, control and Snap25 cKO mouse perfusions and genotyping was performed together with co-supervisor Dr. Anna Hoerder-Suabedissen, and tissue collection for WB and qPCR was performed by supervisors Prof. Zoltán Molnár and Dr. Anna Hoerder-Suabedissen. Secondly, the WB protocol for fractalkine ligand (CX3CL1) and receptor (CX3CL1) was obtained together with biochemistry part 2 student Penny Sherlock who worked under my direct supervision. A series of WB experiments for CX3CL1-CX3CR1 and corresponding data analysis was performed by Penny Sherlock and was used for her MSc thesis that I supervised. For my DPhil project I repeated all of these experiments and did not include her data. Moreover, Penny assisted with the brain tissue sectioning, and staining and confocal imaging of the hippocampal CA3 region. Data analysis of the hippocampal CA3 region performed by Penny Sherlock was only used for her thesis, but I re-analysed some of the images acquired by her. For my DPhil project I repeated image analysis, collected missing data points and reimaged some of the CA3 region due to the issues with the confocal microscope at the time of Penny's stay at our laboratory. All experiments and data analysis were either repeated or

reanalysed because Penny was not able to finish the full developmental profile of the CA3 region due to COVID-19 pandemic (03-2020). Third, semi-automatic and automatic analysis tools described in chapter 2 were created in collaboration with a previous colleague Alfonsas Jursenas from Vilnius University, who currently works at Baltic Institute of Advanced Technology, Lithuania. Moreover, tissue homogenization for WB and qPCR was performed together with a fellow student, Javier Gilbert Jaramillo from the Molnár and James research groups. Finally, DREADDs experiments, tissue collection and brain sectioning were performed together with Elise Meijer from the Molnár and Vyazovskiy research groups. CNO for IP injections was prepared by Dr. Lukas Krone from the Molnár and Vyazovskiy groups. Some of the brain imaging of cFos staining was performed by Elise Meijer but this data was not presented in my thesis. Visual cortex layer 5, superior colliculus, and the hippocampal CA1 and CA3 regions imaging and data analysis presented in thesis chapter 5 was performed only by me.

Acknowledgements

First and foremost, I would like to express my special gratitude to my supervisors Professor Zoltán Molnár and Dr. Anna Hoerder-Suabedissen. Thank you for being amazing supervisors and mentors, for your relentless support, encouragement and advice. Thank you for teaching me how to see a bigger perspective in science and life, your help has been invaluable and I could never be grateful enough.

The work presented in this thesis would not be possible without funding. I would like to thank the State Studies Foundation of Lithuania and the University of Oxford for financial support during my DPhil.

To all my dear colleagues and friends in the lab and in particular Javier, Sara, Florina, Elise, Luana and etc, I wish I could name you all. My beloved friends, I would like to thank you for accepting nothing less than excellence from me, it is hard to express in words how grateful I am to all of you who inspired and supported me: Daria, Dainius, Evaldas, Inga, Burcu, Paul, and Dovile. Especially, I would like to thank to Andrew, Rishi, Mina, Jodie, Claire, and Mandy for sharing this journey together since day one, for reminding me to live outside the lab, for challenging and supporting me no matter what, and for being the best partners in crime.

Finally, I would love to thank my family who provided me with moral and emotional support. I am grateful for your understanding and all the opportunities you have given me.

Table of Contents

Abstract *2*

Abbreviations *4*

Statement and credits *6*

Acknowledgements *8*

Chapter 1: Introduction *15*

1.1 The origin of microglia *15*

1.2 Microglial entry routes and colonization 17

1.3 Microglial classification 20
1.3.1 Classification based on morphological features 21
1.3.1.1 Amoeboid microglia 21
1.3.1.2 Ramified microglia 22
1.3.1.3 Other morphologies of microglia 22
1.3.2 Classification based on microglial function and gene expression 25

1.4 Microglial regional heterogeneity in the developing and mature brain 26
1.4.1 Microglial distribution across CNS 26
1.4.2 Sexually-dimorphic microglia 27

1.5 Multitasking microglia: from protectors to scavengers 30

1.6 Microglia-neuron interactions via signalling pathways during critical periods of the postnatal development 33
1.6.1 Chemokine signalling through fractalkine axis 33
1.6.1.1 Fractalkine ligand 33
1.6.1.2 Fractalkine receptor 35
1.6.1.3 Biological functions of fractalkine 36
1.6.1.4 The role of fractalkine signaling 37
1.6.2 Phagocytic signalling through classic complement system pathway 38
1.6.2.1 Microglia-neuron interactions via the classical complement system pathway 38
1.6.2.2 The role of complement system in synapse elimination 40
1.6.3 Signalling molecules in microglia-neuron interactions 41

1.7 The role of microglia in the context of disease 43

1.8 Hypothesis and project aims 46

Chapter 2: Methods *48*

2.1 Animals 48
2.1.1 Breeding and maintenance 48
2.1.2 Snap25 conditional KO mice 48
2.1.3 DREADD animals 49

2.2 Tissue collection 49
2.2.1 Perfusion 49

2.3 Molecular techniques 50

2.3.1 Genotyping 50
2.3.1.1 DNA extraction 50
2.3.1.2 Polymerase Chain Reaction (PCR) 50
2.3.1 Western Blots 52
2.3.1.1 Sample preparation 52
2.3.1.2 Loading, running and transferring the protein 53
2.3.1.3 Antibody staining 53
2.3.1.4 Western Blot analysis 54
2.3.2 Quantitative polymerase chain reaction (qPCR) 54
2.3.1.1 Tissue homogenisation and RNA extraction for qPCR 54
2.3.1.2 cDNA synthesis 55
2.3.1.3 qPCR and analysis 55
2.4 Immunohistochemistry and microscopy 57
2.4.1 Fixed-tissue sectioning 57
2.4.1 Immunohistochemical labelling 57
2.4.2 Confocal microscopy 58
2.5 Image analysis 59
2.5.1 Automatic and semi-automatic tools for the analysis of microglia morphology 59
2.5.1.1 Cell counter 59
2.5.1.2 Automatic 3D microglia volume counter 60
2.5.1.3 3D Sholl analysis 61
2.5.2 Manual analysis of microglial morphology 63
2.5.2.1 Microglial soma size and roundness 63
2.5.2.2 Primary branches 65
2.5.2.3 Microglial complexity 65
2.5.3 Analysis of phagocytic pouches 66
5.2.4 Analysis of microglia active areas and presynaptic engulfment 67
2.5.5 Analysis of synaptic density 67
2.6 Statistics 68
2.7 Additional information 69
Chapter 3: Changes in microglial cells dynamic during normal brain development 70
3.1 Introduction 70
3.1.1 Variety of microglial features 71
3.1.2 Synaptic pruning by microglia 73
3.2 Results 77
3.2.1 Brain region-specific distribution of microglia during development 77
3.2.2 CD68 in microglia changes during development 80
3.2.3 Morphological differences of microglia in the developing brain 83
3.3 Discussion 89
3.3.1 Region- and sex-specific heterogeneity in microglia during development 89
3.3.2 Microglial phagocytic activity follows different trajectories in male and female brains during development 90
3.3.3 Morphological changes of microglia in the developing male and female brains 91

Chapter 4: Microglia are involved in activity-dependent neuronal network formation and maturation 95

4.1 Introduction 95
4.1.1 SNARE complex and microglia 95
4.1.2 Synaptosomal-associated protein 25 (Snap25) 98

4.2 Results 100
4.2.1 Conditional Snap25 knockout mouse model 100
4.2.1 Synaptic 'silencing' affects microglial cell distribution and morphological features across brains during development 102
4.2.2 Abolished regulated release of neurotransmitter vesicles affects microglial activity and microglia-neuron interactions in the developing brain 119
4.2.3 Synaptic 'silencing' affects chemokine and phagocytic signalling pathways in the developing brain 128
4.2.3.1 Lack of Snap25 downregulates CX3CL1 but upregulates CX3CR1 expression 128
4.2.3.2 Lack of Snap25 affects C3 and CD11b expressions across the brain during development 136

4.3 Discussion 143
4.3.1 Synaptic 'silencing' affects microglia distribution and morphological features across developing brain in a sex-specific manner 145
4.3.2 Abolished release of synaptic vesicles affects microglial function and excitatory synapse density in a sex-specific manner 147
4.3.3 Synaptic 'silencing' affects microglia-neuron interactions via chemokine and phagocytic signalling pathways 150

Chapter 5: Acute chemogenetic inhibition and activation of cortical layer 5 neurons and dentate gyrus affects microglial behaviour and dynamics 153

5.1 Introduction 153

5.2 Results 155
5.2.1 Inhibitory and excitatory DREADDs mouse models 155
5.2.2 Experimental design and procedures 156
5.2.2.1 Inhibitory DREADD: $Rbp4^{Cre}$;hM4Di 157
5.2.2.2 Excitatory DREADD: $Rbp4^{Cre}$;hM3Dq 157
5.2.2.3 $Rbp4^{Cre}$, hM4Di and hM3Dq control experiments 159
5.2.3 DREADDs validation 160
5.2.3.1 Methods 160
5.2.3.2 Inhibitory DREADD validation 161
5.2.3.3 Excitatory DREADD validation 163
5.2.3.4 $Rbp4^{Cre}$, hM4Di and hM3Dq control validation 165
5.2.3 Chronic and acute 'silencing' and acute activation of cortical layer 5 subtypes and dentate gyrus neurons affects microglial behaviour and synaptic density in the visual cortex layer 5, superior colliculus, hippocampal CA1 and CA3 regions of the mature brain 167

5.3 Discussion 178

5.3.1 Inhibitory and excitatory DREADDs model to study microglial behaviour and dynamics 178
5.3.2 Chronic synaptic and acute chemogenetic 'silencing', and acute chemogenetic activation affects microglial distribution and morphology 180
5.3.3 Chronic synaptic and acute chemogenetic 'silencing', and acute chemogenetic activation affects CD68 in microglia and excitatory synaptic density 183

Chapter 6: Discussion 187

6.1: Inhibition or excitation of neuronal activity affects microglial distribution in the developing brain in a sex-specific manner 188

6.2: Microglia adapt their morphology in activity-dependent manner 190

6.3: Changes in microglial activity during postnatal development in activity-dependent manner 192

6.4: Changes in neuronal activity alters microglia-neuron interactions during development 194
6.4.1: Changes in excitatory synaptic density and microglial trogocytic activity 194
6.4.2: Molecular mechanisms of microglia-neuron interactions 195

6.5: Limitations and future directions 198

Bibliography 200

Appendix 1 239

Table of Figures

Figure 1: Microglial migration to the brain 16
Figure 2: Timeline of microglial development 19
Figure 3: Variable morphology of microglia 24
Figure 4: Sexual-dimorphism of microglia 29
Figure 5: The role of microglia in the developing CNS 32
Figure 6: The schematic structure of fractalkine ligand 35
Figure 7: CX3CL1/CX3CR1 signalling role in the healthy brain 38
Figure 8: The schematic overview of the complement system 39
Figure 9: Synaptic pruning via complement system 41
Figure 10: 'Eat-me' signals 42
Figure 11: 'Don't eat-me' signals 43
Figure 12: The role of microglia in neuropathological conditions 45
Figure 13: Microglial cells counter 60
Figure 14: Automatic 3D Iba1+ signal reconstruction voxel-based method 61
Figure 15: 3D Sholl analysis tool 62
Figure 16: 3D Sholl analysis results 63
Figure 17: Analysis of soma area and roundness 64
Figure 18: Fractal box counting 66
Figure 19: Analysis of phagocytic pouches 67
Figure 20:Synapse formation and synaptic pruning during human brain development 71
Figure 21: Different subtypes of microglia classified based on their morphology 72
Figure 22: Basic cytoarchitectonic subdivisions and their connectivity of hippocampus 74
Figure 23: Large-scale axonal pruning 76
Figure 24: Brain region-specific changes in microglial density during early postnatal development 80
Figure 25:Differences in microglial phagocytic activity across developing brain 82
Figure 26: Morphological changes of microglia during early brain development 85
Figure 27: Ramification pattern dynamics of microglia in the developing brain 87
Figure 28: Sex-specific differences in microglial morphology during brain development 93
Figure 29: Overview of the functions of SNAREs, Snap25, and some of their accomplices at the synaptic terminal 97
Figure 30: Cre-LoxP system to develop Snap25 cKO ($Rbp4^{Cre}$/+;Ai14;$Snap25^{fl/fl}$) mice strain 101
Figure 31: Cre expression in Snap25 cKO ($Rbp4^{Cre}$/+;Ai14;$Snap25^{fl/fl}$) mouse brains 101
Figure 32: Sex-specific changes of microglial cells density across the brain in developing control and Snap25 cKO ($Rbp4^{Cre}$/+;Ai14;$Snap25^{fl/fl}$) mice 104
Figure 33:Lack of Snap25 affects microglial volume and primary branches in the developing brain 108
Figure 34: Increased microglial soma size in Snap25 cKO ($Rbp4^{Cre}$/+;Ai14;$Snap25^{fl/fl}$) mice 110
Figure 35: 3D Sholl analysis of microglia in the developing control and Snap25 cKO mice cortex 112
Figure 36: 3D Sholl analysis of microglia in the developing control and Snap25 cKO mice hippocampus 114

Figure 37: Changes of microglial ramification and complexity during development in Snap25 cKO mice brain 118
Figure 38: Reduced phagocytic activity of microglia in 'silenced' brains 121
Figure 39: Microglial phagocytic capacity and presynaptic compartment engulfment differ between control and Snap25 cKO (Rbp4^{Cre}/+;Ai14;Snap25$^{fl/fl}$) brains 124
Figure 40: Synaptic density increases in sex-specific manner in 'silenced' brain during development 127
Figure 41: Abolition of Snap25 from a selected population of layer 5 projection neurons in Rbp4^{Cre}/+;Ai14;Snap25$^{fl/fl}$ affects chemokine signalling in the developing cortex 132
Figure 42: Abolition of Snap25 from dentate gyrus neurons in the Rbp4^{Cre}/+;Ai14;Snap25$^{fl/fl}$ affects chemokine signalling in the developing hippocampus 135
Figure 43: Synaptic 'silencing' of a subpopulation of layer 5 pyramidal neurons affects the expression of C3 and CD11b in the developing cortex 138
Figure 44: Synaptic 'silencing' of neurons in the dentate gyrus affects the expression of C3 and CD11b in the developing hippocampus 141
Figure 45: Abolition of Snap25 affected bidirectional communication between microglia and neurons in a sex-specific manner 145
Figure 46: Excitatory and inhibitory DREADDs activation pathways 154
Figure 47: cFos+ cells density decreases in Rbp4^{Cre};hM4Di mice 90 minutes after CNO application 162
Figure 48: cFos+ cells increases in Rbp4^{Cre};hM3Dq mice 90 minutes after CNO application 164
Figure 49: Changes in cFos+ density in mice injected with saline 166
Figure 50: Changes in microglial distribution and phagocytic activity in the chronic 'silencing' model of Snap25 cKO (Rbp4^{Cre};Snap25$^{fl/fl}$), and after 90 minutes of chemogenetic manipulation in the inhibitory (Rbp4^{Cre};hM4Di) and excitatory (Rbp4Cre;hM3Dq) DREADDs mice 170
Figure 51: Changes in microglial morphology in in the chronic 'silencing' model of Snap25 cKO, and after 90 minutes of chemogenetic manipulation in the inhibitory (Rbp4^{Cre};hM4Di) and excitatory (Rbp4^{Cre};hM3Dq) DREADDs mice 173
Figure 52: Changes in microglia ramification patterns in the chronic 'silencing' model of Snap25 cKO, and after 90 minutes of chemogenetic manipulation in the inhibitory (Rbp4^{Cre};hM4Di) and excitatory (Rbp4^{Cre};hM3Dq) DREADDs mice 175
Figure 53: Changes in synaptic density in in the chronic 'silencing' model of Snap25 cKO, and after 90 minutes of chemogenetic manipulation in the inhibitory (Rbp4^{Cre};hM4Di) and excitatory (Rbp4^{Cre};hM3Dq) DREADDs mice 177
Figure 54: Microglial cells morphological and functional adaptation to the changes of synaptic activity 185

Chapter 1: Introduction

1.1 The origin of microglia

In 1919, Pío Del Río-Hortega identified phagocytic cells in the CNS and introduced the term '*microglia*' (del Rio-Hortega, 1932; Rio-Hortega, 1939). Microglia are the tissue resident macrophages of the central nervous system (CNS) (London et al., 2013). Depending on the brain region, microglia make up 0.5 – 16.6% of the total cellular population in the normal adult human brain (Mittelbronn et al., 2001) and 5 – 12 % in the adult mouse brain (Lawson et al., 1990, 1992). In the human brain, the origin of microglia has been a subject of debate and two theories have been presented. The first theory, known as the neuroectodermal, suggests that microglia originate from the pluripotent glioblasts (Fujita & Kitamura, 1975; Menassa & Gomez-Nicola, 2018; Rezaie & Male, 2002). The second theory, the mesodermal, argues that microglia originate in the yolk sac from hematopoietic stem cell progenitors similar to primitive macrophages and migrate to the brain from the fourth week of gestation (Menassa & Gomez-Nicola, 2018). Human and mouse brain studies support the mesoderm theory that microglia are derived from primitive yolk sac macrophages (Ginhoux et al., 2010, 2013; Hertz & Fedoroff, 1980; Hutchins et al., 1990; Konigsmark & Sidman, 1963; Menassa & Gomez-Nicola, 2018). In the mouse, microglia formation starts early at embryonic day 7.5 – 8.0 in the yolk sac (Figure 1) (Ginhoux et al., 2010; Kierdorf et al., 2013). These early microglia populate the brain mesenchyme from embryonic day 9.5 (Askew & Gomez-Nicola, 2018; Ginhoux et al., 2010; Prinz & Priller, 2014) and their migration is blood circulation-dependent (Prinz & Priller, 2014).

Microglia are not the only population of macrophages in the brain. In brain tissue, extraparenchymal or border-associated macrophages (BAMs), like microglia, are generated

by yolk sac-derived progenitors and are divided in three categories (Brioschi et al., 2020; Goldmann et al., 2016; Prinz et al., 2017). First, perivascular macrophages (pvMPs) are found in the perivascular Virchow-Robin spaces of the cortical blood vessels. Second, meningeal macrophages (mMPs) are found within the meningeal membrane and on the pia mater or within the dura. Third, choroid plexus macrophages (cpMPs) are located beneath the epithelial cell layer of the choroid plexus. BAMs interference between the brain and the periphery suggest that they might be involved in immune surveillance, vascular permeability regulation and the homeostasis of cerebrospinal fluid and CNS (Brioschi et al., 2020; Mildenberger et al., 2022). However, it remains largely unknown how BAMs contribute to brain homeostasis and different pathological conditions.

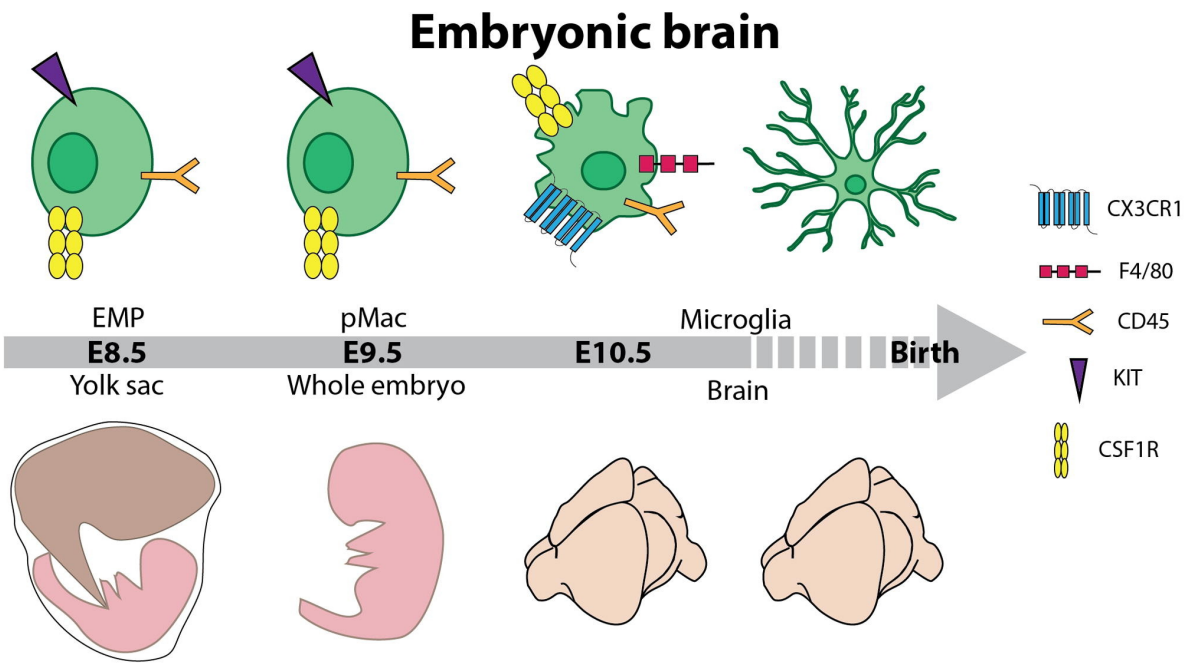


Figure 1: Microglial migration to the brain

At E8.5 microglia derive from erythromyeloid progenitors (EMP): colony-stimulating factor-1 receptor (CSF1R), KIT and pan-leukocyte marker CD45. EMPs mature into premacrophages (pMacs) and colonise the embryo in fractalkine receptor (CX3CR1)-dependent manner from E9.5. pMacs in the developing brain express CX3CR1, CSF1R, CD45 as well as glycoproteins F4/80 from E10.5. Adapted from (Askew & Gomez-Nicola, 2018).

1.2 Microglial entry routes and colonization

Microglia colonise the human brain between the 4th and 24th week of gestation (GW) and the first wave of microglial entry into the developing brain precedes the peak of neurogenesis and neuronal migration (Menassa & Gomez-Nicola, 2018) (Figure 2). Migrating microglial cells, which invade the brain through the entry routes, are amoeboid (Fujimoto et al., 1989; Kershman, 1939; Lawson et al., 1990). When nearing their resting areas, microglia extend their processes, and become elongated and branched. By the time they reach their stable location, microglia are characterized as ramified (Fujimoto et al., 1989; Kershman, 1939; Lawson et al., 1990). Microglial entry areas used to be called 'fountains' (Kershman, 1939; Penfield, 1928) and three entry routes have been described. First, the leptomeningeal route occurs around 4.5th GW. Microglia are presumed to enter from the pial surface and amoeboid microglial cells accumulate in the superficial marginal zone (Monier et al., 2006, 2007). Second, the ventricular lumen route occurs around 4.5 – 5.5th GW and amoeboid microglia are detected in the ventricular lumen and ventricular zone (B. H. Choi, 1981; Monier et al., 2006, 2007). Third, the choroid plexus route occurs around 5.5th GW and amoeboid microglial cells enter the brain from the choroid plexus into the parenchyma of the thalamic eminence (B. H. Choi, 1981; Fujimoto et al., 1989; Monier et al., 2006, 2007).

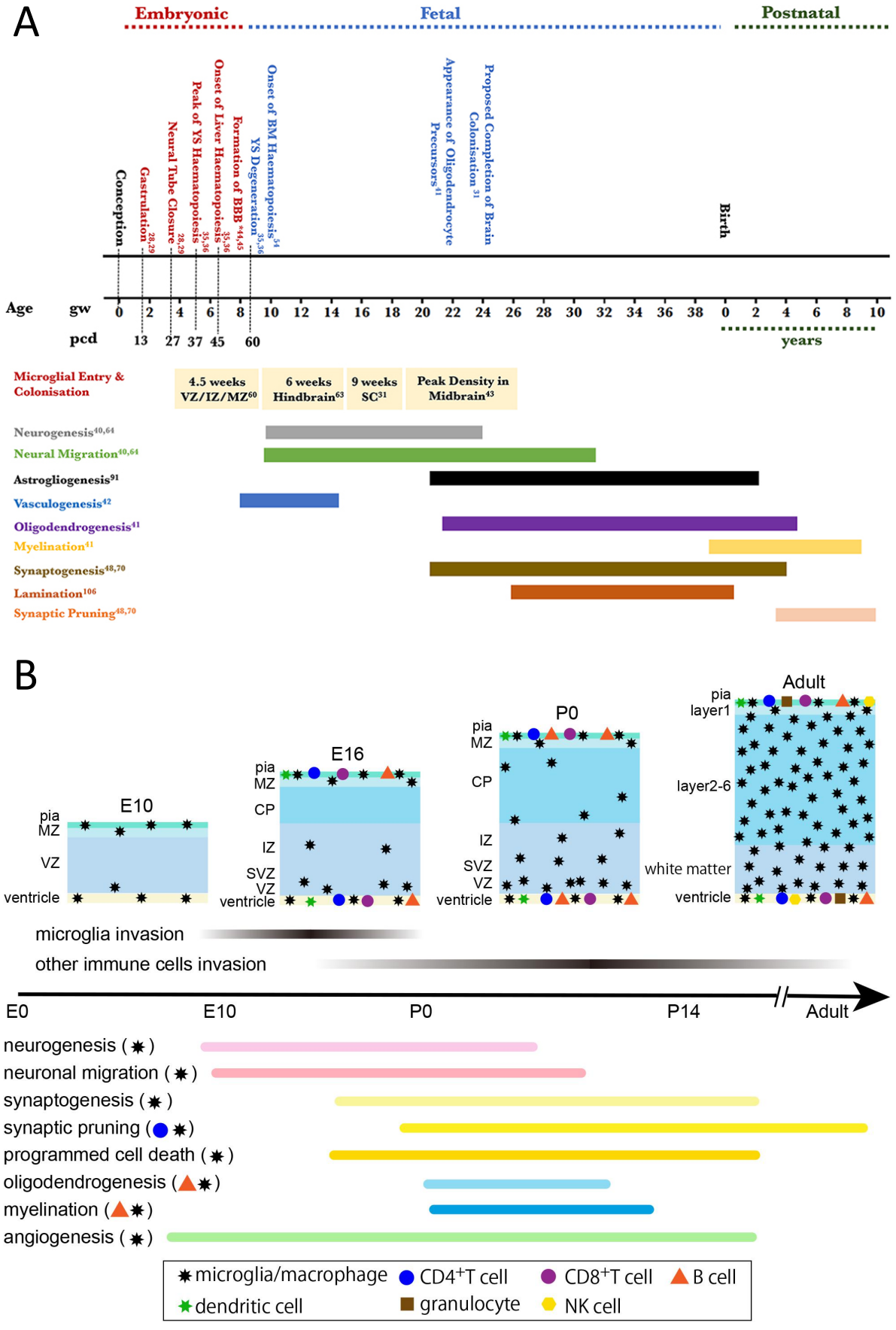

A
Embryonic
Fetal
Postnatal
Conception
Gastrulation [28,29]
Neural Tube Closure [28,29]
Peak of YS Haematopoiesis [35,36]
Onset of Liver Haematopoiesis [35,36]
Formation of BBB [44,45]
YS Degeneration [35,36]
Onset of BM Haematopoiesis [54]
Appearance of Oligodendrocyte Precursors [41]
Proposed Completion of Brain Colonisation [31]
Birth
Age
gw 0 2 4 6 8 10 12 14 16 18 20 22 24 26 28 30 32 34 36 38 0 2 4 6 8 10
pcd 13 27 37 45 60
years
Microglial Entry & Colonisation
4.5 weeks VZ/IZ/MZ [60]
6 weeks Hindbrain [63]
9 weeks SC [31]
Peak Density in Midbrain [43]
Neurogenesis [40,64]
Neural Migration [40,64]
Astrogliogenesis [91]
Vasculogenesis [42]
Oligodendrogenesis [41]
Myelination [41]
Synaptogenesis [48,70]
Lamination [106]
Synaptic Pruning [48,70]
B
E10
pia
MZ
VZ
ventricle
E16
pia
MZ
CP
IZ
SVZ
VZ
ventricle
P0
pia
MZ
CP
IZ
SVZ
VZ
ventricle
Adult
pia
layer1
layer2-6
white matter
ventricle
microglia invasion
other immune cells invasion
E0
E10
P0
P14
Adult
neurogenesis (✸)
neuronal migration (✸)
synaptogenesis (✸)
synaptic pruning (●✸)
programmed cell death (✸)
oligodendrogenesis (▲✸)
myelination (▲✸)
angiogenesis (✸)
microglia/macrophage
CD4+T cell
CD8+T cell
B cell
dendritic cell
granulocyte
NK cell

Figure 2: Timeline of microglial development

Microglial entry and colonisation in the developing human brain (A). Timeline of cortex development and microglial distribution in mice (B). Abbreviations: BBB – blood-brain barrier, BM – bone marrow, CP – cortical plate, CSF – cerebrospinal fluid, E – embryonic days, IZ – intermediate zone, MZ – marginal zone, PCD – post conceptional days, GW – gestational week, SVZ – subventricular zone, VZ – ventricular zone. Adapted from (Menassa & Gomez-Nicola, 2018; Morimoto & Nakajima, 2019).

As soon as microglia enter, they colonise the developing brain in a time-dependent manner (Table 1.1) and are very likely to play a pivotal role in neurogenesis, neuronal migration and many other cellular processes. In mice, microglia enter the brain at E9.5 yet other immune cells infiltrate the brain later in the development by E16 (Figure 1.2) (Morimoto & Nakajima, 2019). In the developing cortex, microglia are located in the pia, marginal zone and ventricles at E10 suggesting that in mice microglial entry routes may be similar to humans. Within days, microglia migrate through cortical plate, intermediate zone, subventricular and ventricular zones (De et al., 2018; Morimoto & Nakajima, 2019) and before birth distribute through the entire cortex and dramatically increase in number (Reemst et al., 2016; Silva et al., 2019).

GW	Microglia	Brain regions
4-24th	Microglia colonise brains	
4.5th	Amoeboid	Leptomeningeal route
4.5-5.5th	Amoeboid	Ventricular lumen
5.5th	Amoeboid	Choroid plexus
8th	Amoeboid	Cortical plate (CP) thickens, microglia appear in marginal zone (MZ). Density increases in ventricular zone (VZ), subventricular zone (SVZ), intermediate zone (IZ) and subplate (SP)
8-12th	Cells suggested to be proliferating	
10th	Amoeboid	Fetal blood vessels appear in the telencephalic wall
11th	Amoeboid/ resting	Found in the forebrain, internal capsule, vena terminalis, choroid plexus, corpus callosum, ventricles, and thalamus
9-13th	Amoeboid/ resting	Proliferating amoeboid microglia aligned along the subplate-cortical plate. ***NOTE: these cells suggested to support thalamocortical synaptic development.***
14th	Amoeboid/ resting	Amoeboid microglia appear around the cerebral peduncles and optic tracts. Smaller groups occur just under the meninges lining the lower border which penetrate the brain.
14-17th	Amoeboid/ resting	Microglia cluster near the white matter at the junction between the thalamus and the internal capsule, the optic tract, and the junction between the internal capsule and the cerebral peduncle. Microglia are observed in the corpus callosum and the periventricular hypothalamus.
16th	Amoeboid/ resting	Much larger group of amoeboid microglia in outer and inner ventricular areas and corpus callosum
18th	Amoeboid/ resting	Microglia migrate radially within the cortical plate to transform into ramified gray matter microglia. Tangential migration occurs within the IZ. Microglia populate the cortex and are distribute across the various layers.
19-30th	Amoeboid/ resting	Tangentially oriented microglia are founded in white matter tracts such as the corpus callosum and the external capsule.
By 29th	Ramified microglia gradually accumulate in all the zones of the developing brain.	
By 35th	Microglia density decreases.	
End of GW	Amoeboid/ resting	By the end of the gestation – ramified microglia can be seen across the cortical layers, and the white matter shows a higher density of cells compared to the gray matter.

Table 1: Timeline of microglial development in the developing embryonic human brain Summary adapted from (B. H. Choi, 1981; Fujimoto et al., 1989; Monier et al., 2006, 2007; Penfield, 1928).

1.3 Microglial classification

Microglia undergo highly adaptive changes in morphology and function during embryonic and postnatal development. Microglial morphological transformation during embryonic mouse development is regulated by runt-related transcription factor 1 (Runx1) (Zusso et al., 2012).

In the mouse brain, lineage-tracing experiments showed that primitive macrophages progenitor cells express Runx1 during late embryogenesis and the first two weeks of postnatal development (Zusso et al., 2012). Runx1 expression loss during postnatal development correlates with morphological transformation from ameboid to ramified at postnatal day 10 (P10) (Prinz & Priller, 2014; Zusso et al., 2012).

1.3.1 Classification based on morphological features

1.3.1.1 Amoeboid microglia

Amoeboid microglia are (also known as active, macrophage-like, unramified, reactive, activated, phagocytic) the most common type of microglia in embryonic brains and in different neuropathological conditions (A. Karperien et al., 2013; Lawson et al., 1990; Soltys et al., 2005; Torres-Platas et al., 2014). Amoeboid microglia have a few short thick processes, or thin filopodia, or no processes and an irregular, amoeboid-shape body (Torres-Platas et al., 2014). Embryonic amoeboid microglia shift to a ramified microglial morphology during postnatal development by extending processes and the irregular shaped body reduces to a small and round static soma. In the context of different neuropathological conditions and neuroinflammation, ramified microglia retract their processes followed by cellular locomotion and shift-back to amoeboid, highly active, microglia (Brockhaus et al., 1996; Dailey & Waite, 1999; Stence et al., 2001). Amoeboid microglia migrate to the sites where they are needed and make clusters around damaged areas (e.g. injury, neuronal degeneration induced injury, tumours, beta-amyloid plaques etc.) (Arcuri et al., 2017; Brockhaus et al., 1996; Gutmann & Kettenmann, 2019; Heppner et al., 1998; Wierzba-Bobrowicz et al., 2002). It has been hypothesized that amoeboid microglia in embryonic mice play a role in myelogenesis (Hagemeyer et al., 2017). Microglia are a highly dynamic cell population that

respond to environmental changes. Surprisingly, microglia can transform from ramified to amoeboid morphology within 30 – 60 minutes (Davalos et al., 2005; Nimmerjahn et al., 2005).

1.3.1.2 Ramified microglia

Ramified microglia, also known as resting, quiescent, surveillant, or unactivated, are the most common type of microglia in the mature brain (A. Karperien et al., 2013; Lawson et al., 1990; Soltys et al., 2005; Torres-Platas et al., 2014). Ramified microglia have a round and small soma, and regularly branched processes (Soltys et al., 2005). They extend and retract thin, highly ramified processes as they survey their environment (Nimmerjahn et al., 2005). Microglial soma remains static, does not change its morphology, and processes constantly make transient contacts with neurons and blood vessels (Nimmerjahn et al., 2005). Using a multiphoton imaging, Wake et al. demonstrated that ramified microglial processes make direct contact with neuronal synapses at approximately one contact per hour (Wake et al., 2009). Furthermore, ramified microglia contact astrocytes and oligodendrocytes, and this cross-talk between different glial cells plays an important role in angiogenesis (Biswas et al., 2020; Nimmerjahn et al., 2005) and myelination (Domingues et al., 2016) respectively. These dynamic ramified microglial cells play a role in neuroprotection (Vinet et al., 2012), pinocytotic activity (Glenn et al., 1991), synaptic pruning (Chugh & Ekdahl, 2016), and maintain a stable brain environment (Glenn et al., 1991; Wierzba-Bobrowicz et al., 2002).

1.3.1.3 Other morphologies of microglia

Microglia have been categorized in many different subtypes based on their morphology. These subtypes describe microglia in transition form from ramified to amoeboid or from amoeboid to ramified (Figure 3). Thus, these morphologies are related to their functional

state (Davis et al., 1994). In 1990, Lawson et al. categorized microglia into three distinct subtypes: compact, longitudinal and radial (Figure 3) (Lawson et al., 1990). Growing interest in microglia and advances in histology and microscopy helped differentiate these cells into ramified, hypertrophic, bushy and amoeboid (Soltys et al., 2005). In 2013, microglia were described as: ramified, ramifying or re-ramifying/de-ramifying and amoeboid (A. Karperien et al., 2013). Ramifying microglia were subdivided into intermediate, hypertrophied and bushy (A. Karperien et al., 2013). The most commonly used classification of microglia across the literature: ramified, primed, hypertrophic/hypertrophied, reactive/bushy and amoeboid (Figure 1.3) (Constanzo et al., 2020; Torres-Platas et al., 2014). In pathological conditions even more distinct subtypes of microglia have been described (Figure 3) (F. R. Walker et al., 2014). For example, dystrophic microglia were identified in normal-aged human samples (Streit et al., 2014) and are present near beta amyloid plaques in Alzheimer's disease (Streit et al., 2014). Rod microglia have very small nuclei, are elongated with few processes and have been described in epilepsy, encephalitis and Alzheimer's disease (Bachstetter et al., 2017; Y.-M. Ho et al., 2014; Wirenfeldt et al., 2009).

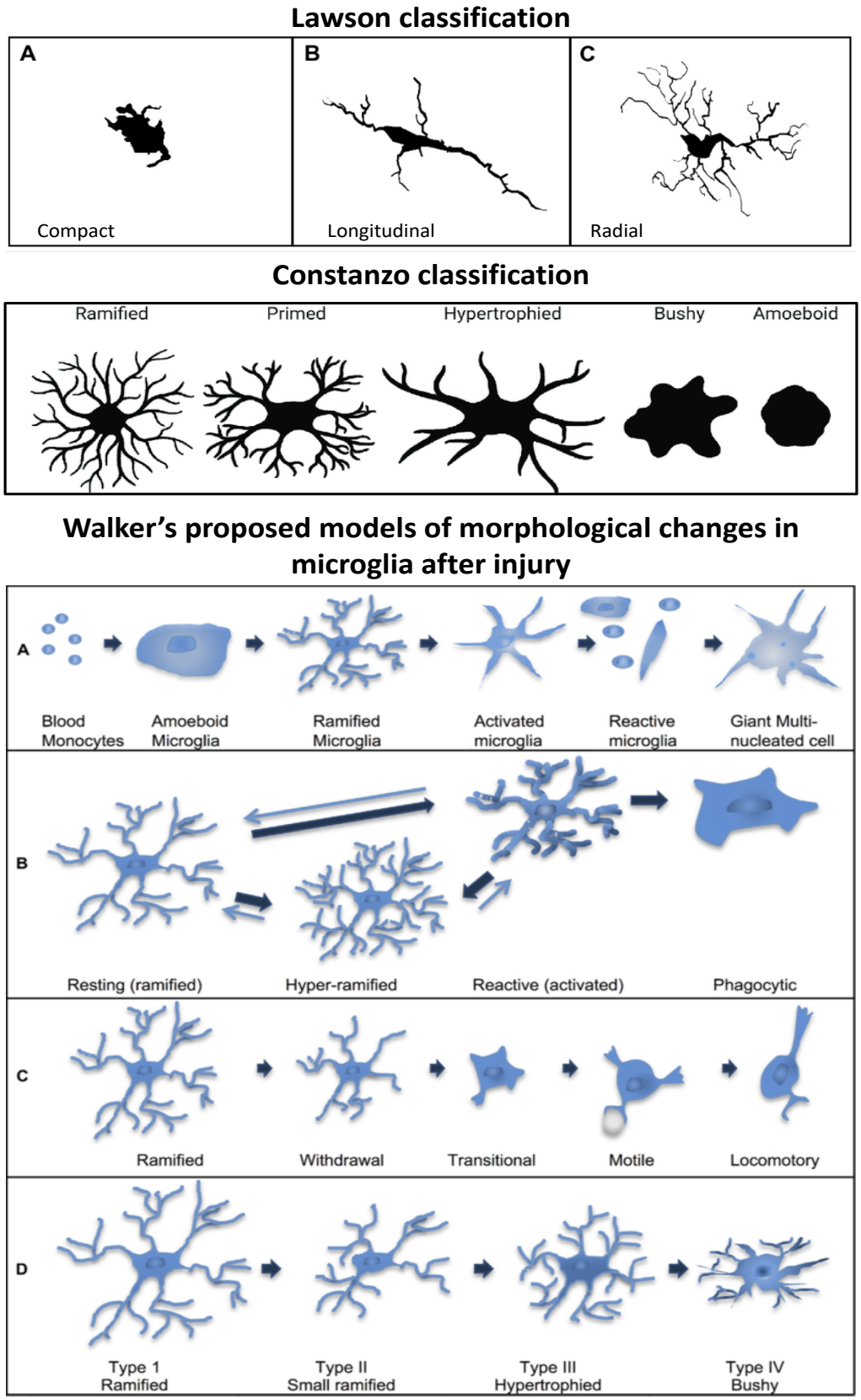


Figure 3: Variable morphology of microglia

Adapted from (Constanzo et al., 2020; A. Karperien et al., 2013; Lawson et al., 1990; F. R. Walker et al., 2014).

1.3.2 Classification based on microglial function and gene expression

Another approach to define different types of microglia is based on gene expression and microglial functions in physiological and pathological conditions. Differential expression of markers among microglia helps to better understand microglia interaction with environmental factors, neurons and other glial cells, and microglial roles in pathological conditions.

Satellite microglia were first described by Pío Del Río-Hortega (del Rio-Hortega, 1932; Rio-Hortega, 1939). This type of microglia is very unique since its soma is associated with neuronal cell bodies (Baalman et al., 2015). It has been shown that less than 3% of cortical neurons have linked satellite microglia that extend a single process and interact with the axon initial segment (Baalman et al., 2015). This type of microglia is usually found in adult animals and is more common in the cortex (Baalman et al., 2015). Satellite microglia can be defined by the following markers: ionized calcium-binding adaptor molecule 1 (Iba1), cluster of differentiation 11b (CD11b), and chemokine (CX3C motif) receptor 1 (CX3CR1) (Baalman et al., 2015; De Haas et al., 2008).

Dark microglia were recently identified using electron microscopy (EM) in the adult and aged mouse hippocampus. This type of microglia is called *dark* due to their electron-dense cytoplasm and nucleoplasm (Bisht et al., 2016). Dark microglia display markers of oxidative and metabolic stress and appear to be extremely active. Another interesting feature of dark microglia is that their processes contact capillaries suggesting a possible implication in vascular remodelling or maintenance (Bisht et al., 2016). Dark microglia express CD11b, but levels of Iba1 and CX3CR1 are downregulated (Bisht et al., 2016; De Haas et al., 2008).

CD11c-microglia express the integrin CD11c. It has been demonstrated that 20% of the total microglial population in P3-P5 developing brains are CD11c-microglia (Wlodarczyk et al.,

2017). CD11c-microglia express genes associated with myelination and neurogenesis in the neonatal brain and play a role in these processes (Wlodarczyk et al., 2017). Moreover, CD11c-microglia also express insulin-like growth factor 1 (IGF1), Iba1, CD11b and CX3CR1 (De Haas et al., 2008; Wlodarczyk et al., 2017).

Less common types of microglia have been demonstrated in pathological conditions. *Gitter cell-like microglia* have been found in the context of age-related sensory function loss and they are Iba1 positive (Das, 1976; Tremblay et al., 2012).

1.4 Microglial regional heterogeneity in the developing and mature brain

Rapid progression in microglial research demonstrated heterogenous distribution of microglia. Microglial regional heterogeneity includes temporospatial (Silvin & Ginhoux, 2018; Tay et al., 2017), sex-specific (Lenz et al., 2013; Villa et al., 2019), morphology and gene expression (Eggen et al., 2019; Tay et al., 2017)

1.4.1 Microglial distribution across CNS

In human brains, microglial density differs across different regions: only 0.3% of cells are microglia in the gray matter of the cerebellum, 11% in the medulla oblongata, and 5% in the cortical gray matter (Mittelbronn et al., 2001; Pelvig et al., 2008).

In rodents, microglial regional heterogeneity has been demonstrated in the developing and mature brain. In the developing CNS, microglial distribution changes very rapidly during the first month of postnatal development in the hippocampus (Paolicelli et al., 2011) and somatosensory cortex (Mondo et al., 2020). In the adult rat prefrontal cortex, higher microglial density has been found in cortical layer 5 compared to layer 1 (Kongsui et al., 2014). Interestingly, it has been demonstrated that differences in microglial density do not alter their

morphological features (Kongsui et al., 2014). Moreover, areas of particularly high density of microglia include hippocampus, basal ganglia, substantia nigra and olfactory telencephalon, and areas of lower density are the cerebellum and brainstem (Lawson et al., 1990; Stowell et al., 2018). Some early studies reported higher density of microglia in the forebrain, lower in the midbrain, and the lowest in the brainstem as well as cerebellum (Ehninger & Kempermann, 2003; Savchenko et al., 2000). In the adult mouse brain, only 5 % of cells are microglia in the cerebral cortex and corpus collosum, and approximately 12% in the substantia nigra (Lawson et al., 1990). It has been estimated that microglial cells fell in the range of 3000 – 9000 cells/mm^3 even in regions were neuronal density is high such as the cerebellum, and particularly high density of microglia in the striatum, at approximately 12000 cells/mm^3 (Kongsui et al., 2014).

1.4.2 Sexually-dimorphic microglia

In recent years, our understanding of microglial importance and involvement in brain development has increased rapidly. A lot of studies revealed that microglia are sexually dimorphic, and their behaviour and morphology can differ between male and female brains (Guillot-Sestier et al., 2021; Hui et al., 2020; Kerr et al., 2019; Weinhard, Neniskyte, et al., 2018). It has been speculated that microglial sexual-dimorphism may arise as early as hematopoiesis in the yolk sac or as soon as microglia enter the brain during early days of embryonic development (Lenz et al., 2013; VanRyzin et al., 2018; Villa et al., 2019). Microglial density, morphology and activity vary between males and females in several brain areas. Sex-specific significant differences in the number of microglia have been reported in the preoptic area (Lenz et al., 2013), hippocampus (Guneykaya et al., 2018; Schwarz et al., 2012; Weinhard, Neniskyte, et al., 2018), parietal cortex and amygdala (Guneykaya et al., 2018; Schwarz et al.,

2012). In the developing hippocampus of female mice, higher density and phagocytic activity of microglia has been observed at P8 yet decreased at P28 compared to males (Weinhard, Neniskyte, et al., 2018). Similar results were found for 3 weeks old males where microglia density was lower in the hippocampus (Guneykaya et al., 2018). In the mature brain, higher density of microglia and larger microglial soma has been observed in cortex, hippocampus and amygdala in 13 week old males (Guneykaya et al., 2018).

The peak of microglial activity during the third postnatal week (Schafer et al., 2012) corresponds to the critical period for hormonally mediated sexual differentiation of the developing brain. During this period, androgen from the male testis supplies testosterone to the brain, which is aromatized into estradiol to induce brain masculinization and defeminisation (McCarthy et al., 2009). Lenz et al. demonstrated that perinatal treatments with microglial activity blocker minocycline inhibited masculinization of the brain (Lenz et al., 2013). In fact, microglia are able to maintain the same sex-specific properties *in vitro* (Villa et al., 2018). This interesting feature of microglia has been observed in microglia isolated from adult brain and placed in culture of the opposite sex (Villa et al., 2018). In microglial cell lines, mRNA of estrogen receptors α and β were expressed (Crain & Watters, 2010). In addition, it has been shown that estrogen blocked pro-inflammatory cytokine expression in microglia (Ishihara et al., 2015).

Physiological sex differences of microglia have been demonstrated (Figure 4). In males, microglia have higher migration capacity, enlarged soma and higher expression of two primary classes of major histocompatibility complex (MHC) molecules 1 and 2 (MHC1 and MHC2), and P2Y12 purinergic receptor for adenosine diphosphate (ADP) (Guneykaya et al., 2018). In females, microglia have higher phagocytic capacity and expression of phagocytic receptors as well as inflammatory genes (Nelson et al., 2017; Yanguas-Casás et al., 2018).

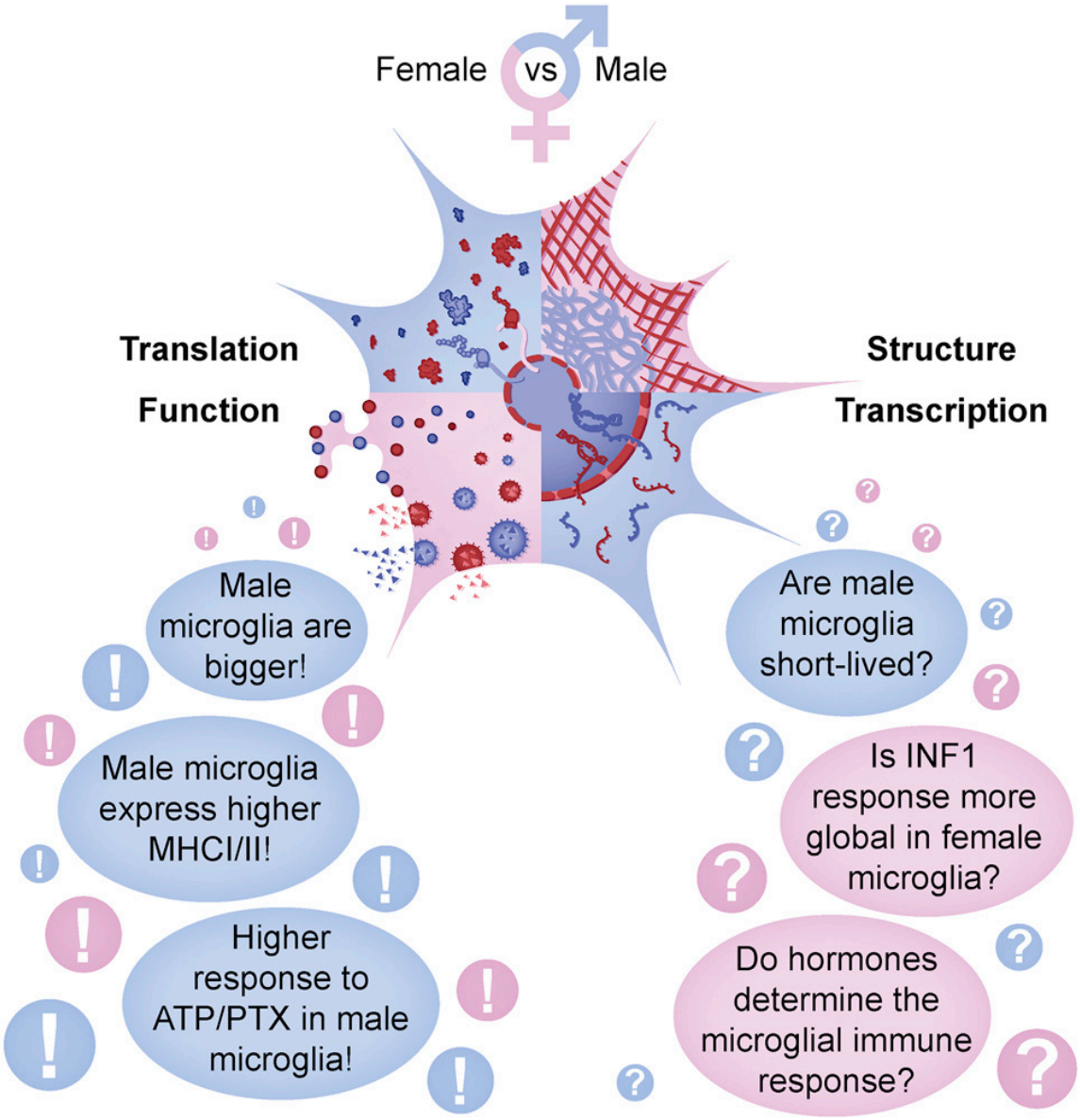


Figure 4: Sexual-dimorphism of microglia

Summary illustration from (Guneykaya et al., 2018).

In terms of gene expression, different molecular signatures of microglia have been observed in male and female brains. Guneykaya et al. found 1109 genes differentially expressed by microglia between males and females in the hippocampus, and 55 genes in the cortex (Guneykaya et al., 2018). In the cortex, 72 highly expressed and 27 lower expressed genes were identified in males compared to females. In the hippocampus, 324 genes were expressed at a higher level and 867 genes at lower level in males compared to females

(Guneykaya et al., 2018). Gene Ontology (GO) analysis showed that higher expression of genes in male hippocampus were linked to genes related to defence response to bacteria, differentiation and insulin receptor pathway (Guneykaya et al., 2018). The same study showed sex-specific protein expression in microglia. Highly expressed proteins in the male brains are myosin related, purinoreceptors, and Toll-like receptors (Guneykaya et al., 2018). GO analysis revealed that in a P20 brain, genes related to inflammatory and immune response, and response to lipopolysaccharide (LPS) were upregulated in females suggesting that microglia are in the primed state (Thion et al., 2018).

There are many unanswered questions about the sexual-dimorphism of microglia. Recent studies indicate that male and female microglia may play different roles in a time- and region-dependent manner. The sexual dimorphisms of microglia should be considered when explaining and understanding microglia-related processes in the brain.

1.5 Multitasking microglia: from protectors to scavengers

Until 20 years ago, it was believed that microglia just guard the brain as a part of the immune system. In recent years, our understanding of microglia involvement in brain functions increased rapidly (Figure 5). Microglia are able to check every volume unit of the brain in under a couple of hours and help to maintain a stable and healthy brain environment by controlling homeostasis of the CNS (Prinz & Priller, 2014). Furthermore, microglia contribute to pathological neuroinflammation by release of cytokines and active, amoeboid microglia respond to brain injury by removing cell debris and promoting wound repair (Casano & Peri, 2015; Prinz & Priller, 2014). Microglia also play a role in neurogenesis, blood-brain barrier integrity and angiogenesis by releasing pro- and anti-inflammatory cytokines, neurotrophic

and growth factors (Biswas et al., 2020; Kierdorf & Prinz, 2013; Lyu et al., 2021; Nimmerjahn et al., 2005; Prinz & Priller, 2014)

In the developing brain, microglia play a key role in shaping the neuronal network by remodelling of neuronal circuits (Casano & Peri, 2015; Neniskyte & Gross, 2017; Wake et al., 2013) and shape the developing CNS by scavenging synapses. This process, when excessive synapses are eliminated, and necessary synapses are sustained is known as synaptic pruning.

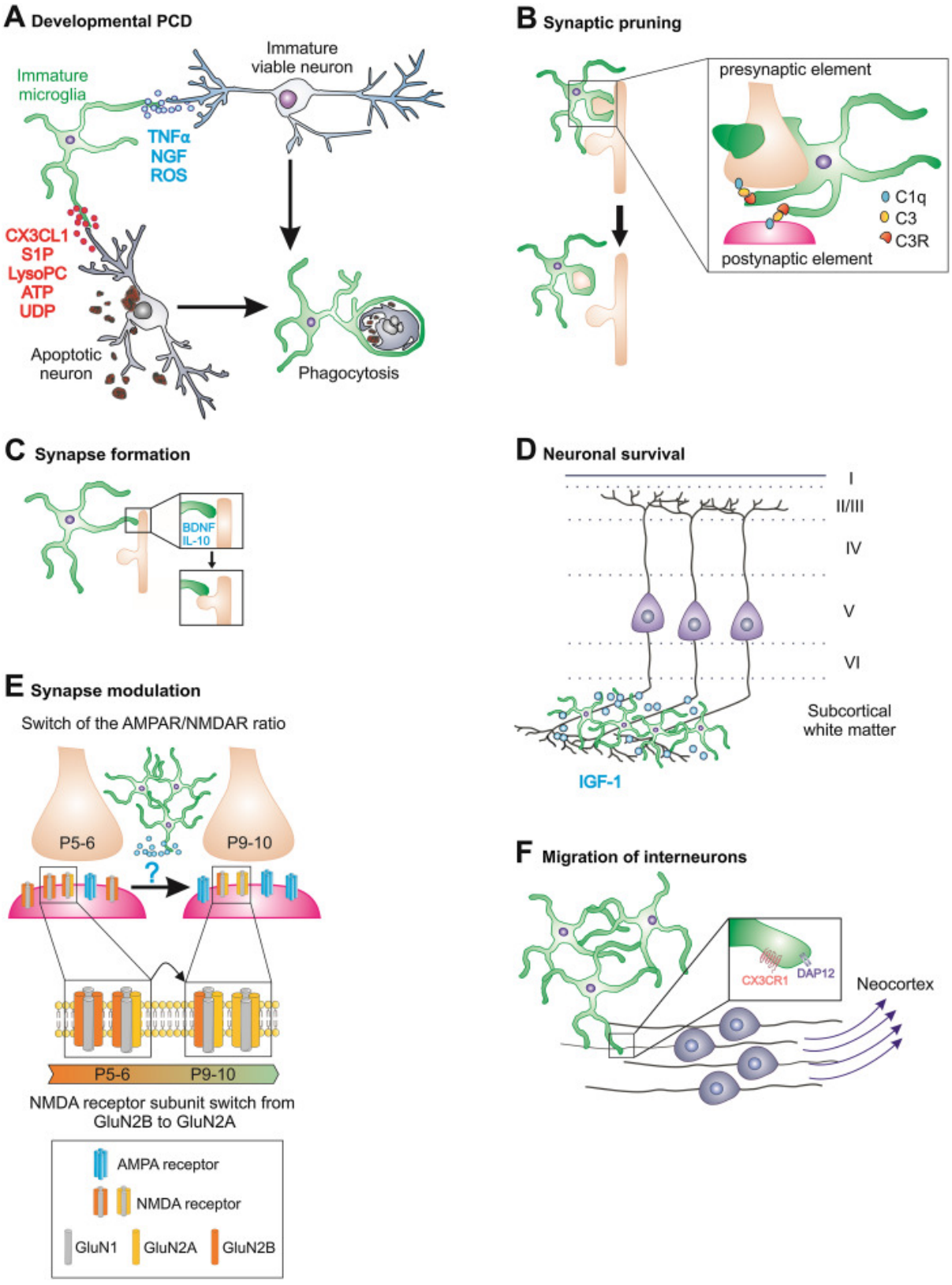


Figure 5: The role of microglia in the developing CNS

Main functions of microglia during early postnatal development of the brain. (A) microglial phagocytic activity, 'eat-me' signals (red), neuronal apoptosis signalling pathways (blue). (B) Synaptic pruning via complement system. (C) Synapse formation. (D) Survival of layer 5 neurons through IGF-1. (E) Receptor

regulation at thalamocortical synapses of the barrel cortex. (F) Interneuron migration in CX3CR1 and DAP12-dependent manner. PCD -programmed cell death. Figure from (Mosser et al., 2017).

1.6 Microglia-neuron interactions via signalling pathways during critical periods of the postnatal development

During the development of the nervous system, tightly controlled and region-specific synaptic pruning eliminates the overabundantly generated synapses in order to induce the effectiveness of neuronal transmissions. To understand how microglia-mediated synapse elimination implicates the regulation of neuronal connectivity, two molecular pathways have been identified that modulate microglia function in the developing brain.

1.6.1 Chemokine signalling through fractalkine axis

1.6.1.1 Fractalkine ligand

In 1997 Bazan et al. first identified and described the CX3C(delta) subfamily of chemokines and for the first time used the term *'fractalkine'* (Bazan et al., 1997). Fractalkine ligand (CX3CL1) is the only representative of the CX3C subfamily which is classified as a dual-function chemokine: 1) homeostatic (category D) and 2) inflammatory cytokine (category I) (Jones et al., 2010; G. Y. Liu et al., 2005; Maciejewski-Lenoir et al., 1999; Poniatowski et al., 2017). In the human genome, CX3CL1 is located within the long arm of chromosome 16 (16q13) (Nomiyama et al., 1998) and is highly conserved between humans, mice and rats. In mice, CX3CL1 is located within the long arm of chromosome 8 (8qC5) (Rossi et al., 1998), and in rats it is located within the small arm of chromosome 19 (19p12) (Nishiyori et al., 1998; Tarozzo et al., 2003; Xiao et al., 2009).

Fractalkine ligand has two different isoforms (Chapman et al., 2000). First, membrane-bound (mCX3CL1) provides direct interaction with its sole receptor CX3CR1, cell-cell adhesion, and keeps microglia in a surveying state. Second, soluble (sCX3CL1) is produced by proteolytic cleavage of the N-terminal chemokine domain of the membrane bound form working as an extracellular mediator and chemotaxis (Kim et al., 2011). Proteolytic cleavage or 'shedding' can be enhanced by stimulation of phorbol-12-myristate-13-acetate (PMA) or disintegrin-like metalloproteinase 10/17 (ADAM10/ADAM17) (Figure 6) (Nishiyori et al., 1998; Poniatowski et al., 2017; Wojdasiewicz et al., 2014). CX3CL1 is produced in high levels by neurons within the telencephalon and diencephalon and particularly in the cerebral cortex, hippocampus, amygdala, basal ganglia, thalamus, and olfactory bulb (Kim et al., 2011; Tarozzo et al., 2003). In addition, high levels of expression of CX3CL1 mRNA is present in the hippocampal formation demonstrating the highest concentration in cornu ammonis 1 (CA1), CA2 and CA3 regions and in the cortex in layers 2, 3, 5 and 6 (Nishiyori et al., 1998; Tarozzo et al., 2003).

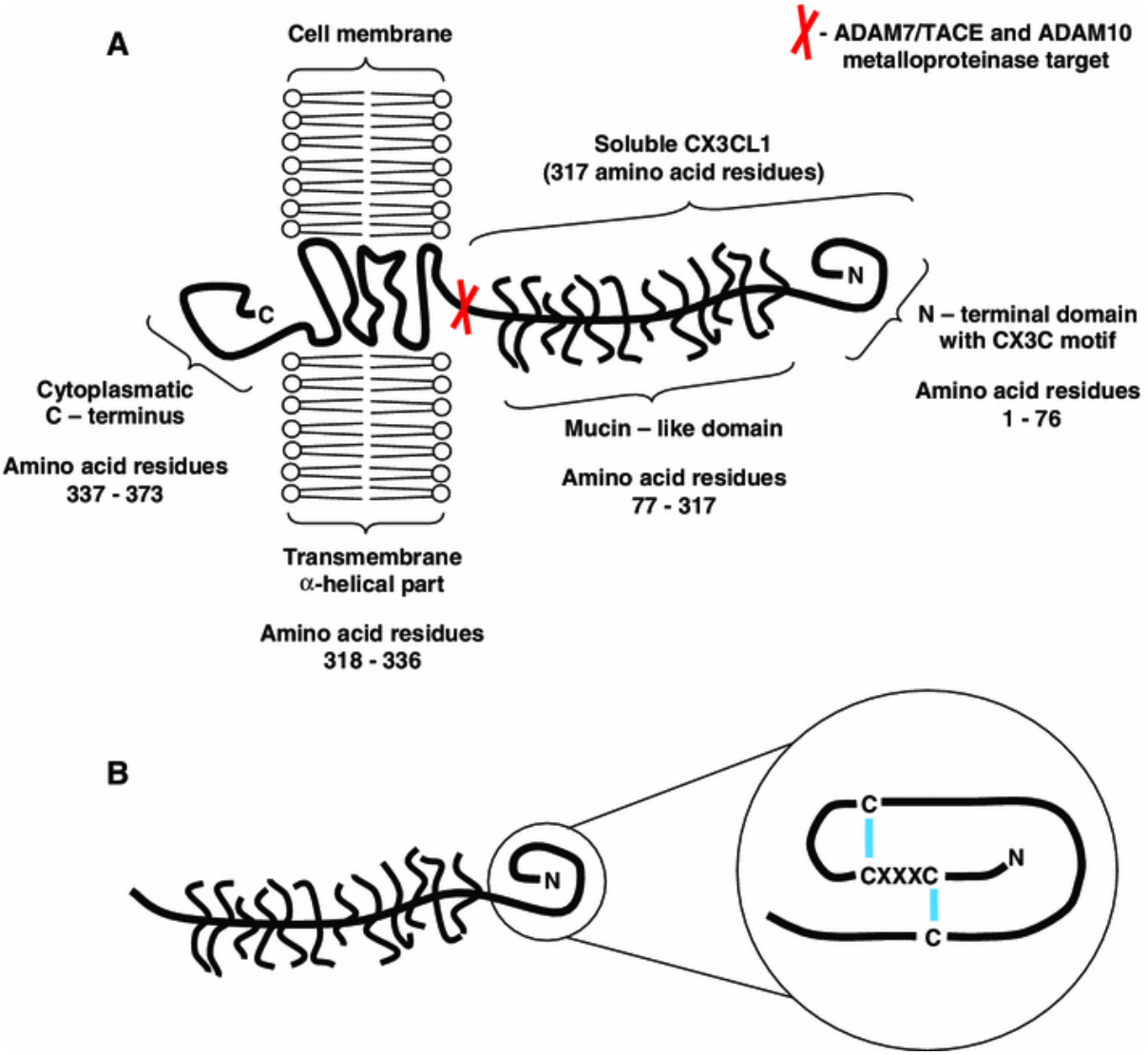


Figure 6: The schematic structure of fractalkine ligand

(A) mCX3CL1 showing regions of the molecule and the site of the cleaving action of ADAM10 and ADAM17. (B) sCX3CL1 produced by proteolytic cleavage. Figure from (Wojdasiewicz et al., 2014).

1.6.1.2 Fractalkine receptor

In the CNS, CX3CL1 is mostly expressed in neurons and its unique receptor is exclusively expressed by microglia. Fractalkine receptor (CX3CR1) belongs to the A class (rhodopsin-like receptors) of G protein-coupled receptor (GPCR) proteins (Imai et al., 1997; Raport et al., 1995). In the human genome, the CX3CR1 coding gene is composed of four exons and is located within the short arm of chromosome 3 (3p21.3) (Maho et al., 1999; Nomiyama et al.,

1998). Moreover, it is highly conserved between human, mouse and rat. In mouse, CX3CR1 is located on chromosome 9 (9qF4) and in rat within chromosome 8 (Combadiere et al., 1998; DeVries et al., 2003).

1.6.1.3 Biological functions of fractalkine

sCX3CL1 chemoattracts T cells as well as monocytes while mCX3CL1 promotes adhesion of leukocytes (Bazan et al., 1997). sCX3CL1 plays a role in recruitment of immune cells, vascular remodulation, wound healing, proliferation and survival. So far, only one more CXC family chemokine, known as CXCL16, also functions as cell adhesion molecule (Shimaoka et al., 2004). It has been shown that sCX3CL1 induces survival pathways in other cell types of myeloid origin such as monocytes (White et al., 2014) and drives the migration of neoplastic cell (P. Liu et al., 2018). The relationship between CX3CL1 and CX3CR1 signalling was first described by Imai et al. in 1997 (Imai et al., 1997). In 1998 Harrison et al. first showed evidence of a modulatory role of fractalkine in mediating microglia-neuron interactions (Harrison et al., 1998). To understand microglia-neuron interactions through fractalkine signalling, Liang et al., 2009 evaluated the effects of fractalkine receptor on microglia dynamics *ex vivo* by using time-lapse imaging and showed reduction of microglia motility in the CX3CR1-deficient model (Liang et al., 2009). However, it remains unclear how CX3CL1-CX3CR1 signalling contributes to directly regulating pruning itself. Paolicelli et al, 2011 first published evidence *in vivo* that synaptic pruning by microglia is necessary for normal brain development (Paolicelli et al., 2011). In this study, they used CX3CR1 knock-out mice and observed higher dendritic spine density on hippocampal CA1 region pyramidal neurons and showed that deficiency in the fractalkine receptor caused impaired synaptic pruning (Paolicelli et al., 2011, 2014). Importantly, their results showed that the second and third postnatal week might be a critical

time period for microglia-mediated synaptic pruning. Overall, the authors suggested that fractalkine signalling promotes microglial migration into the developing brain or the release of the fractalkine might be necessary in synapse recognition by microglia. CX3CL1-CX3CR1 axis also is involved in cell survival and recruitment of immune cell subpopulations. In pathological conditions, fractalkine signalling induces cell proliferation, migration, invasion and apoptosis (Rivas-Fuentes et al., 2021).

1.6.1.4 The role of fractalkine signaling

The communication between CX3CL1 and CX3CR1 allows microglia-neuron interactions and determines proper neuronal network, synapse maturation and plasticity (Figure 7) (Lauro et al., 2015; Paolicelli et al., 2014; Yamagata et al., 2003). In the developing brain, CX3CL1/CX3CR1 signalling plays a role in synaptic refinement in the CNS during the postnatal critical periods for synaptic pruning (Hoshiko et al., 2012; Paolicelli et al., 2011, 2014). However, CX3CL1/CX3CR1 signalling inactivation has neurotoxic effects (Cardona et al., 2006). High level of CX3CL1 expressed in neurons limits CX3CR1 activation on microglia and keeps microglia in a silenced state (Biber et al., 2007a; Ransohoff & Perry, 2009) yet soluble CX3CL1 overexpression improves cognitive function (Finneran et al., 2019). CX3CL1 decrease has been shown in the aged mouse brain and might be linked with neuronal loss and altered effector state of microglia (Lyons et al., 2009; Wynne et al., 2010). However, it remains unknown whether CX3CL1/CX3CR1 signalling acts as regulator of microglial infiltration and migration or as a synapse-specific chemotactic signal for synapse recognition by microglia during brain maturation and maintenance.

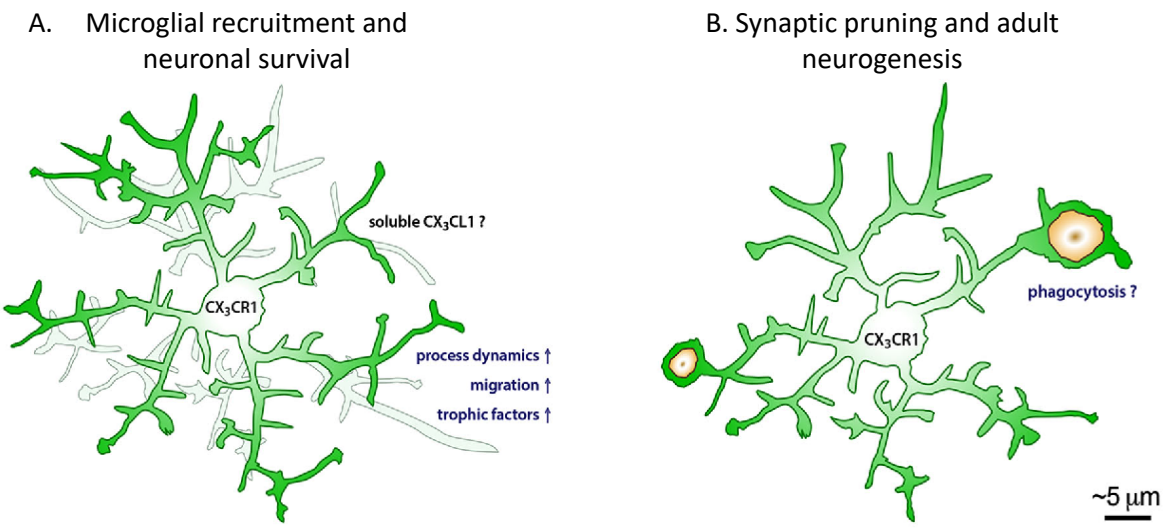


Figure 7: CX3CL1/CX3CR1 signalling role in the healthy brain

(A) Fractalkine axis promotes microglial recruitment to neuronal network by increasing microglial process dynamics, migration and modulates neuronal survival by releasing trophic factors. (B) Fractalkine signalling plays a role in the developmental synaptic pruning and neurogenesis. Adapted from (Paolicelli et al., 2014).

1.6.2 Phagocytic signalling through classic complement system pathway

1.6.2.1 Microglia-neuron interactions via the classical complement system pathway

One of the mechanisms by which microglia interact with developing synapses is the complement system. The complement system or complement cascade was discovered by Jules Bordet who was awarded the 1919 Nobel Prize. Complement represents a major part of the innate immunity and contributes to the rapid clearance of pathogens, dead or dying cells and plays a critical role in the inflammatory immune response (Sarma & Ward, 2011). The complement cascade components have been indicated to play a role in synapse elimination during development. The complement system has three distinct pathways: the classical pathway, the lectin pathway, and the alternative pathway (Figure 8) (Sarma & Ward, 2011).

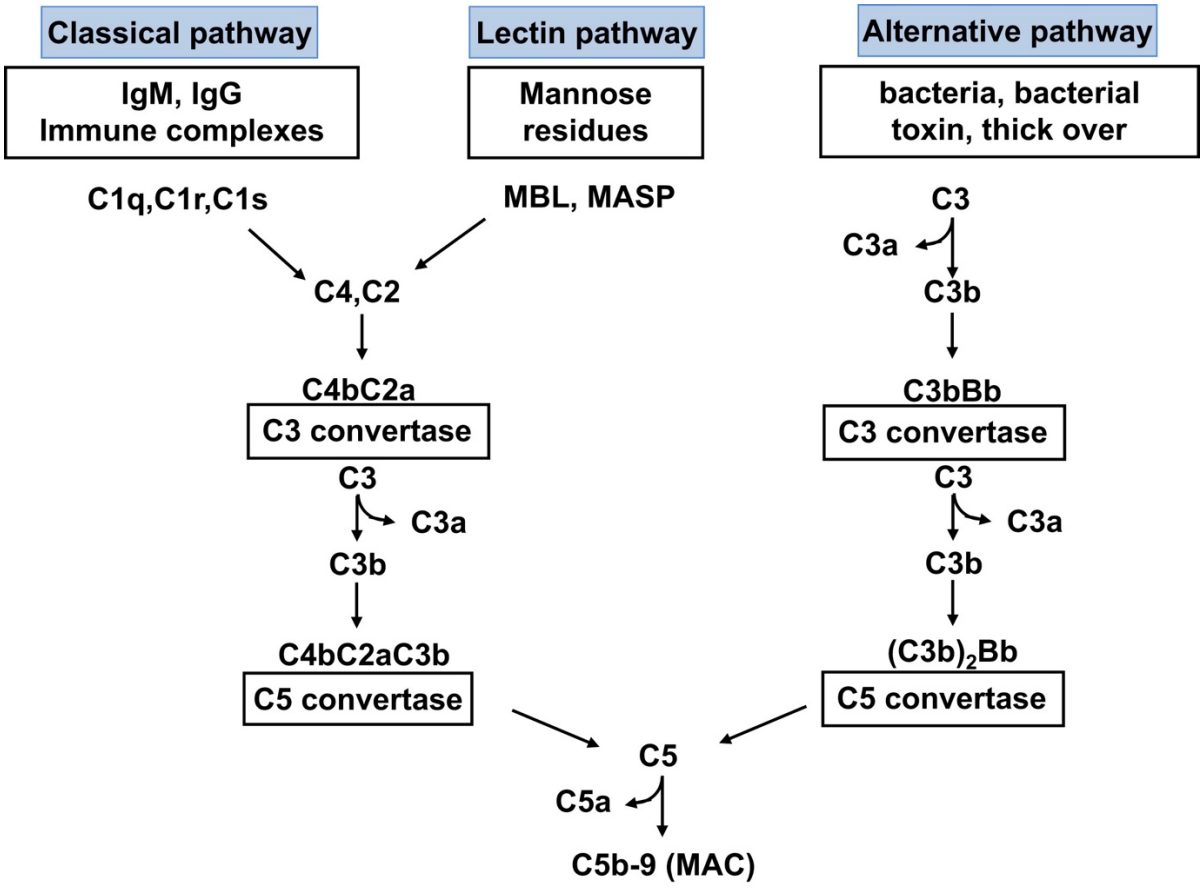


Figure 8: The schematic overview of the complement system

Three activation pathways: classical, lectin and alternative. Figure from (Noris & Remuzzi, 2013).

It has been indicated that the classical complement system pathway is involved in synaptic elimination and pruning (Schafer et al., 2012; Stevens et al., 2007). The classical pathways contain C1q which binds to its target and leads to conformational changes of C1q that activates C1r and C1s proenzymes. C1s proenzyme activation leads to C2 and C4 cleavage, resulting in C3 activation (Wouters et al., 2005). It has been shown that neurons and microglia express complement molecules: neurons express complement components - C1q, C2, C3, C4, C5-9 (Shen et al., 1997); microglia express classical pathway components – C1q, C1r, C1s, C2, C3, C4 and complement receptors C1qR, CR2, C3aR, C4R (Gasque et al., 1998; D. G. Walker et al., 1995).

The complement cascade proteins C3 and C1q allocate to synapses in the thalamus of the developing mouse (Schafer et al., 2012; Stephan et al., 2012), and act as “eat-me” signals for microglia. Microglia then engulf synapses via complement receptor 3 (CR3). CR3 (also known as CD11b/CD18 and Mac-1) is a phagocytic receptor expressed on microglia (Ehlers, 2000). Complement receptor 3 is a dimeric receptor which consists of the two integrin chains: CD11b and CD18 (Linnartz & Neumann, 2013; van den Elsen & Isenman, 2011). CD11b or complement receptor 3 alfa is involved in adhesion processes and uptake of complement-coated molecules (Jurga et al., 2020).

1.6.2.2 The role of complement system in synapse elimination

The phagocytic signalling pathway through the complement system plays a role in synaptic pruning. Synaptic pruning via complement system is activity-dependent; complement proteins label synapses according to their activity (Katz & Shatz, 1996; Presumey et al., 2017). It has been demonstrated in the cortex (Huttenlocher, 1979), cerebellum (Hashimoto & Kano, 2013), retinogeniculate system (Hooks & Chen, 2006; Katz & Shatz, 1996; Schafer et al., 2012), and neuromuscular junction (Darabid et al., 2014). The expression of high affinity CR3 is important for synapse elimination (Presumey et al., 2017; Stephan et al., 2012) and results in permanent defects of synaptic pruning (Presumey et al., 2017; Schafer et al., 2012; Stephan et al., 2012) in mouse models where complement cascade proteins and/or CR3 expression is genetically deleted. In the visual thalamus of CR3 knock-out mice, microglial phagocytosis decreased between postnatal day 5 and 20, and microglia engulfed inputs from the eye with less active neurons suggesting that microglia can be a mediator of synaptic remodelling in the developing retinothalamic system (Figure 9) (Schafer et al., 2012). Moreover, it has been demonstrated that the complement system contributes to synaptic pruning of the

somatosensory cortex layer 5 neurons (Chu et al., 2010) and hippocampus (Zhan et al., 2014). CR3, its subunit CD11b together with CX3CR1 and P2Y12 are associated with synaptic pruning through microglial phagocytosis (Tuan & Lee, 2019). Moreover, it has been shown that changes in CD11b and DAP12 expression trigger the death of neurons in the developing hippocampus (Wakselman et al., 2008).

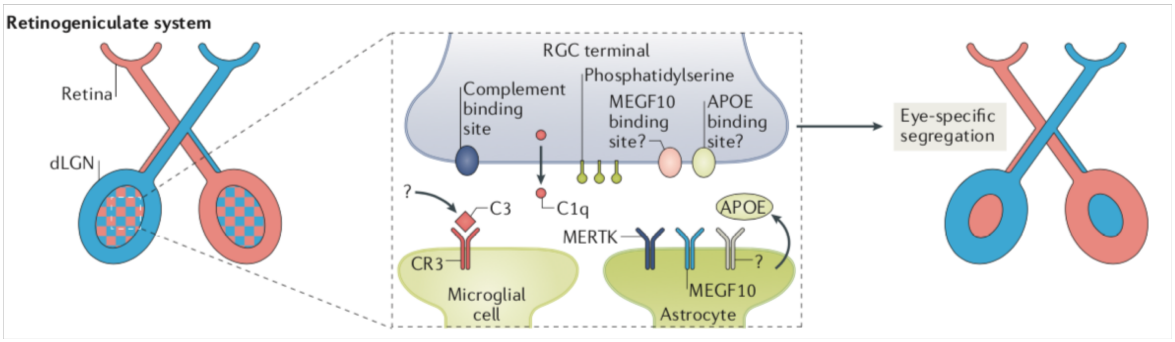


Figure 9: Synaptic pruning via complement system

In developing visual system to achieve the segregation of eye-specific inputs in dorsal lateral geniculate nucleus (dLGN), immature inputs from the contralateral eye that terminate in the region receiving ipsilateral projections are eliminated by microglia in a complement-dependent manner. RGCs – retina ganglion cells, MERTK – MER receptor tyrosine kinase, MEGF10 – multiple epidermal growth factor-like domains protein 10, APOE – apolipoprotein E. Figure from: (Neniskyte & Gross, 2017).

1.6.3 Signalling molecules in microglia-neuron interactions

Molecular signals that mediate microglia-neuron communications can be divided into 'find-me', 'eat-me', 'don't eat-me', and 'spare-me'. Microglia first need to recognize 'find-me' signals and then migrate to their sources, and detect 'eat-me' signals. 'Eat-me' signals help microglia to recognise synapses that need to be eliminated and induce phagocytosis (Brown & Neher, 2014; Elward & Gasque, 2003). Opposite, 'don't eat-me' signals, protect synapses from damage during pruning (Elward & Gasque, 2003) and 'spare-me' signals inhibit synaptic phagocytosis (Lehrman et al., 2018)

‘Eat-me’ signals are complement system components C1q and C3 (Elward & Gasque, 2003; Ogden et al., 2001; Wouters et al., 2005), calreticulin (Gardai et al., 2005), carbohydrates such as mannose (Ogden et al., 2001), lipid molecule phosphatidylserine (Nagata et al., 2016) and opsonins such as growth arrest-specific 6 (Gas6), milk fat globule epidermal growth factor 8 (MFG-E8) and MER tyrosine kinase (MerTK) (Figure 10) (Vilalta & Brown, 2018).

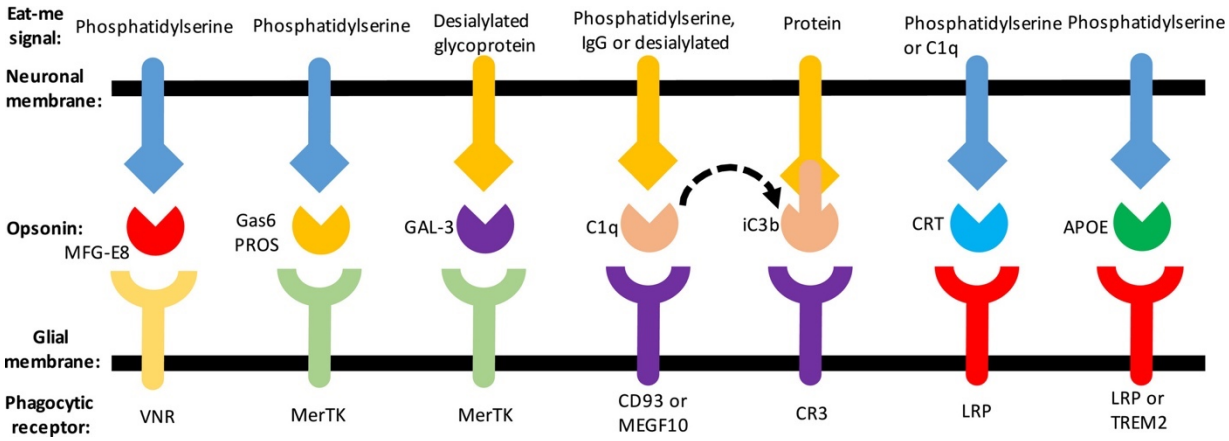


Figure 10: ‘Eat-me’ signals

Intracellular phagocytic signalling for microglia or astrocytes. Figure from (Vilalta & Brown, 2018).

The most common ‘don’t eat-me signals are CD200 (Gordon et al., 2017; Hayakawa et al., 2016), CD24 (Barkal et al., 2019), adenosine (Nakamura et al., 2020), sialic acid (Jia et al., 2022; Nomura et al., 2017) and CD47 which might also act as ‘find me’ signal (Figure 11) (Elward & Gasque, 2003; Lehrman et al., 2018). Fractalkine has been determined as ‘find me/eat-me’ signal (Paolicelli et al., 2011).

Other potential ‘eat-me’ and ‘don’t eat-me’ signals have been recently described by Cockram et al. and authors discussed possible implications of phagocytic code leading to novel therapies for multiple diseases (Cockram et al., 2021).

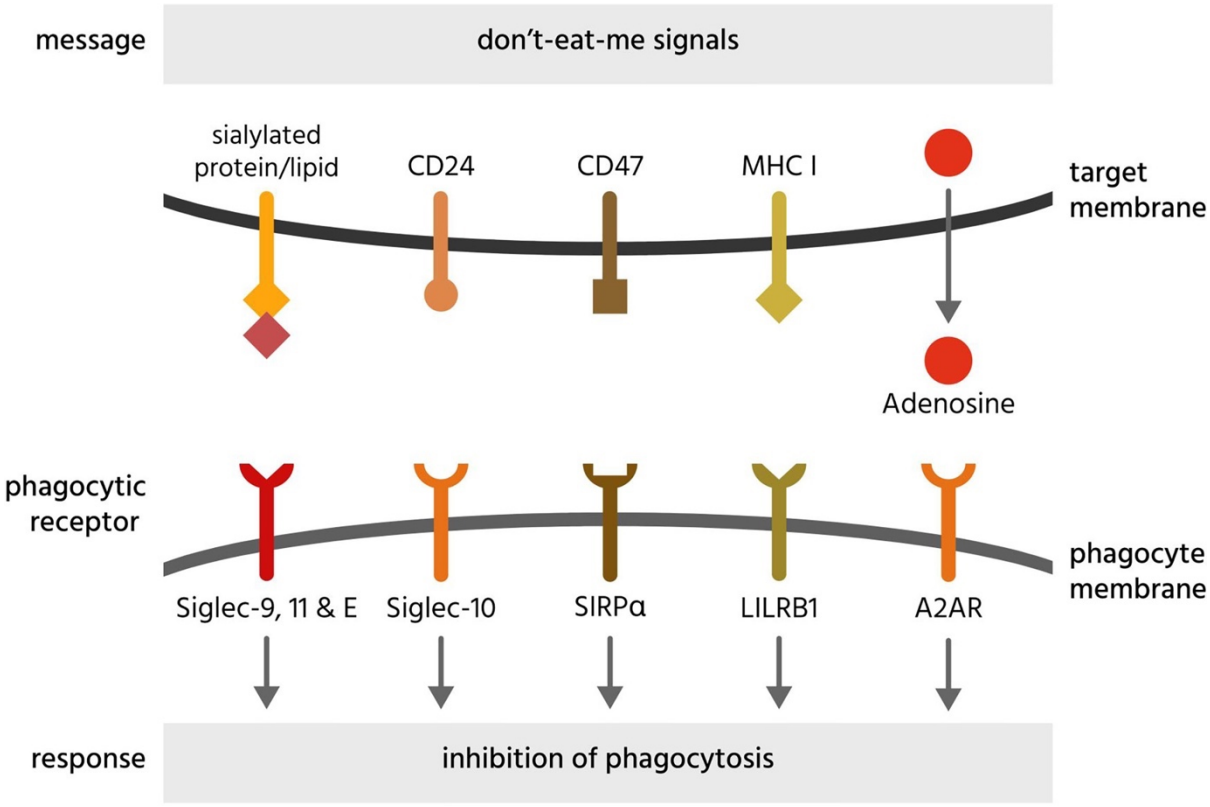


Figure 11: 'Don't eat-me' signals

Molecular 'don't eat-me' signalling for microglia and macrophages. Figure (Cockram et al., 2021).

1.7 The role of microglia in the context of disease

Microglial involvement in various neurological disorders has been demonstrated in stroke (Qin et al., 2019; S. Zhang, 2019), multiple sclerosis (Guerrero & Sicotte, 2020; Monroe & Di Paolo, 2021), sleep disorders (Chianella et al., 1999; Green et al., 2020; H. Liu et al., 2021), Huntington's disease (Palpagama et al., 2019; Savage et al., 2020; Yang et al., 2017), epilepsy (Andoh et al., 2019; Hiragi et al., 2018), neuropathic pain (Fiore et al., 2021; H. Zhao et al., 2017; Zhuo et al., 2011), traumatic brain injury (Hernadez-Ontiveros et al., 2013; Karve et al., 2016), Rett syndrome (Maezawa & Jin, 2010; D. Zhao et al., 2017), Parkinson's (M. S. Ho, 2019; Pabon et al., 2011) and Alzheimer's disease (Cheng et al., 2021; Crehan et al., 2012; Hansen et al., 2018).

Furthermore, microglia might be involved in various neurodevelopmental disorders and neuropsychiatric disorders such as psychosis (Dalman et al., 2008). Synaptic pruning by microglia needs to be strictly controlled since defective neuronal connectivity may lead to autism spectrum disorders (Sellgren et al., 2019) and schizophrenia (Glantz & Lewis, 2000; Sellgren et al., 2019) When synaptic pruning activity is suppressed, or microglial cells are less active, a too dense network may cause autism spectrum disorders (Velmeshev et al., 2019) and this process is known as under-pruning. It has been demonstrated in a human single cell genomics study where the strongest cell type-specific molecular changes in autism occurred in microglia (Sellgren et al., 2019). The opposite, over-pruning, when the neuronal network becomes too sparse after very active pruning occurs in schizophrenia (Glantz & Lewis, 2000; Sellgren et al., 2019). Moreover, it has been shown that microglial activation through the stimulation of β2-adrenoreceptor was associated with behaviour abnormalities similar to autism (Zerrate et al., 2007). In post-mortem tissue, microglial density was decreased in the cerebral cortex of autistic patients (Tetreault et al., 2012) and decreased fractalkine expression was observed in the prefrontal cortex in schizophrenia (Hill et al., 2021).

In fact, environmental changes can have an impact on microglia that may lead to different neuropathological conditions (Figure 12). Environmental factors can be stress (Bolton et al., 2013; Shankardass et al., 2009), pollution (Hartz et al., 2008; Levesque et al., 2011), diet (Lin et al., 2017), bacterial and viral infections (Antonson et al., 2017; de Cossío et al., 2017; Enayati et al., 2012; Pang et al., 2005; Roumier et al., 2008; Schaafsma et al., 2017), sensory deprivation (Denizet et al., 2017; Gunner et al., 2019), and toxins (Bolton et al., 2017; Klocke et al., 2017).

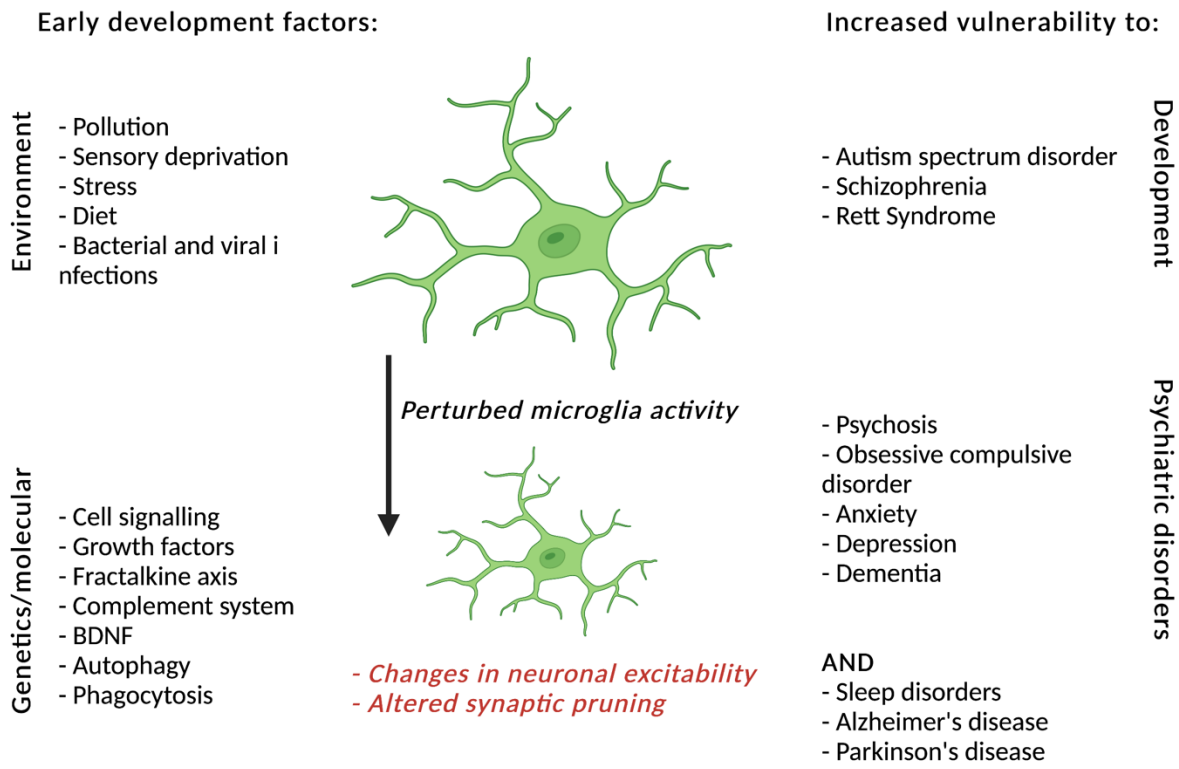


Figure 12: The role of microglia in neuropathological conditions

Created with BioRender.com

1.8 Hypothesis and project aims

One of the paradigms explaining synapse elimination and neuronal circuit remodelling in the developing brain suggest that microglia-neuron interactions may be activity dependent. Neuronal communication underlies brain activity, yet microglia-neuron interactions in systems with silenced or activated specific synapses remain largely unexplored. My DPhil project tested the hypothesis that excitation or inhibition of specific cerebral cortical projection neurons in the neuronal network affects microglial behaviour and dynamics leading to altered microglia-neuron interactions.

Following from this hypothesis, I specified the following aims for my DPhil project:

1. To determine the morphological and functional changes of microglia in the developing mouse visual cortex layer 5, superior colliculus and hippocampal CA1 and CA3 regions;
2. To further examine sex-specific changes of microglia in the developing mouse visual cortex layer 5, superior colliculus, and hippocampal CA1 and CA3 areas;
3. To investigate whether abolished Snap25-mediated regulated release of synaptic vesicles on affected synapses of the cortical layer 5 projection neurons affects microglial behaviour and function in the developing mouse visual cortex layer 5, superior colliculus, and hippocampal CA1 and CA3 areas;
4. To determine sex-specific changes of microglia as the consequence of Snap25-mediated synaptic 'silencing' in specific cortical projection neuron population in the mouse visual cortex layer 5, superior colliculus, and hippocampal CA1 and CA3 regions;
5. To examine microglia-neuron interactions via molecular pathways of fractalkine and complement signalling in activity-dependent formation of neuronal network through synaptic pruning by microglia in mouse;

6. To determine the effect of chronic (conditional Snap25 KO) and acute chemogenetic ‘silencing’, and acute chemogenetic activation of selected cortical projection neurons on microglial behaviour and changes between microglia and neuron communications in the mature visual cortex layer 5, superior colliculus, and hippocampal CA1 and CA3 areas.

Chapter 2: Methods

2.1 Animals

2.1.1 Breeding and maintenance

All animal experiments were approved by a local ethical review committee and conducted in accordance with the UK Animals (Scientific Procedures) Act, 1986 (ASPA), under valid personal and project licenses. All animals were held in individually ventilated cages (IVCs) on a 12 hour light/dark cycle in the Biomedical Sciences Building (BSB), Oxford. Water and food were given *ad libitum*.

2.1.2 Snap25 conditional KO mice

To obtain a conditional ablation of Snap25 expression from a subpopulation of cortex layer 5 neurons (L5 Snap25$^{fl/fl}$ cKO) animals B6-Snap25tm3mcw (Snap25$^{fl/fl}$) were crossed to B6;129S6-Gt(ROSA)26Sortm14(CAG-tdTomato)Hez/J (*Ai14*) and they were crossed to a mouse expressing Cre recombinase Tg(Rbp4-cre)KL100Gsat/Mmucd (*Rbp4-Cre*; Jackson Laboratories)(Hoerder-Suabedissen et al., 2019). Experimental mice were produced by crossing female breeders Cre/+;Snap25$^{fl/+}$;*Ai14* (Rbp4-Cre) with male breeders Snap25$^{fl/fl}$;*Ai14/Ai14*. For experiments comparing control and cKO animals, mice of the following genotypes were used: +/+;*Ai14*;Snap25$^{+/+}$ (control) and Cre/+;Ai14;Snap25$^{fl/fl}$ (Snap25 cKO). The identification of Cre positive mice was performed using fluorescence goggles (Biological Laboratory Equipment Maintenance and Service, BLS) and genotyping (Hoerder-Suabedissen et al., 2019).

2.1.3 DREADD animals

In order to understand the effect of acute activation and silencing on layer 5 neurons, I used a chemogenetic approach and the same layer 5 driver line (described in detail in Chapter 2, 2.1. Animals). I crossed the layer 5 driver mouse expressing Cre recombinase Tg(Rbp4-cre)KL100Gsat/Mmucd (Rbp4-Cre) with the inhibitory DREADD (designer receptors exclusively activated by designer drugs) reporter line B6.129-Gt(ROSA)26Sortm1(CAG-CHRM4*,-mCitrine)Ute/J (R26-LSL-hM4Di-DREADD, The Jackson Laboratory, No:026219) to generate recombinant mice abbreviated as 'Rbp4-Cre::hM4Di' and with the excitatory DREADD reporter line B6N;129-Tg(CAG-CHR3*,-mCitrine)1Ute/J (CAG-LSL-hM3Dq-DREADD, The Jackson Laboratory, No:026220) to generate recombinant mice abbreviated as 'Rbp4-Cre::hM3Dq'. All animal genotyping was performed by Transnetyx (Transnetyx → Genotyping).

2.2 Tissue collection

2.2.1 Perfusion

The mice were perfused at postnatal age P8, P14, P21 and 16 weeks. Animals were anesthetized with 0.6 ml/kg Pentobarbital administered via intraperitoneal (IP) injection and anesthesia was confirmed by pedal reflex test before the perfusion. Animals were transcardially perfused with 0.1 M phosphate buffered saline (PBS, pH 7.4) and 4% formaldehyde (PFA diluted in PBS, F8775; Sigma Aldrich). Afterwards, brains were removed and post-fixed in 4% PFA overnight at 4 °C. The perfused brains were transferred to 1x PBS with 0.05% sodium azide (26628-22-8; Sigma Aldrich) the following day and stored at 4 °C until further usage.

2.2.2 Tissue collection for molecular experiments

Mice were culled by cervical dislocation (Schedule 1). Brains were micro-dissected to collect hippocampus and cortex at P8, P14 and P21 of control and Snap2 cKO mice. All brain tissue samples were fresh-frozen in liquid nitrogen. Left-hemisphere samples were used for WB and right-hemisphere samples were used for qPCR.

2.3 Molecular techniques

2.3.1 Genotyping

2.3.1.1 DNA extraction

Tail tips (obtained from perfused animals) or ear clips (from living animals) were incubated overnight or for 2-3 hours at 55 °C in 200 µl of digest tail-buffer (Table 2.1) containing Proteinase K. After incubation, Proteinase K was inactivated for 30 minutes at 99 °C, the samples were cooled down to room temperature and diluted 1:10 in nano water.

2.3.1.2 Polymerase Chain Reaction (PCR)

The genotype was determined by polymerase chain reaction (PCR). Reaction mix was prepared according to Tables 2.2 and 2.3. Extracted and diluted DNA (1 µl) was added to 19 µl of PCR reaction mix. The thermal cycler conditions are indicated in Tables 2.4 and 2.5. Then 10 µl (Cre) and 12 µl (Snap25 with loading buffer) of PCR products were run on a 1.0 – 1.5 % agarose gel for 30 minutes at 95 V (small boxes) or 125 V (big boxes) in TAE. For DNA counterstaining, GelRed (1:10000, VWR) was used and to identify DNA fragment length DNA ladder (NEB, 100bp) applied. Gel imaging was carried out with Dual Intensity Transilluminator (UVP Bioimaging systems).

Reagent	Initial concentration	Volume (ml)
Tris CC (Trischloride)	1 M	5 ml
EDTA (pH 8.0)	0.5 M	0.5 ml
NaCl	5 M	2 ml
SDS	10 %	1 ml

Table 2: Tail tip buffer solution. Made up to 50 ml in nano water

Stock solution	Volume for 10 samples (µl)
OneTaq Quick-Load® 2xMM w/std Buffer	100 µl
Forward primer (5' TGGAAAATGCTTCTGTCCGT 3')	10 µl
Revere primer (5' CATCGCTCGACCAGTTTAGT 3')	10 µl
nH_2O	72.5 µl

Table 3: Cre primer mix

Stock solution	Concentration	Volume for 20 samples (µl)
nH_2O		346 µl
Taq 10x PCR buffer		50 µl
MgCl	50 mM	30 µl
dNTPs	10 mM	10 µl
Forward primer (5' CCCTGGGGAACCACGGCAGA 3')	0.5 µM	20 µl
Reverse primer (5' TCCCAGGAAACAGCACAGCGT 3')	0.5 µM	20 µl
Platinum Taq		4 µl

Table 4: Snap25 primer mix

Step	Time (min)	Temperature	Action
1	3:00	95 °C	1x
2	0:20	95 °C	40x
3	0:30	62 °C	
4	0:45	72 °C	
5	10:00	72 °C	1x
6	Forever	10 °C	

Table 5: PCR program for Snap25

Step	Time (min)	Temperature	Action
1	3:00	95 °C	1x
2	0:20	95 °C	40x
3	0:30	54 °C	
4	0:45	72 °C	
5	10:00	72 °C	1x
6	Forever	10 °C	

Table 6: PCR program for Cre

2.3.1 Western Blots

2.3.1.1 Sample preparation

Samples were homogenized in RIPA buffer (Abcam, ab156034) and protease inhibitors (Roche cOmplete Mini cocktail inhibitor, 11836153001), left hemisphere of hippocampus in 250 µl and cortex in 500 µl. Tissue homogenization was performed using a tissue homogenizer Ultra-Turrax T25 (Janke&Kunkel, IKA – Labortechnik) for 30 sec and incubated at 4 °C for 30 min, then centrifuged at 12,000 rpm for 15 min at 4 °C and the supernatant was collected. Protein concentration was determined using a Bicinchoninic Acid Assay (BCA) (ThermoFisher Scientific). Tissue lysate samples were diluted 1:100 for hippocampus and 1:200 for cortex.

For loading, samples were made using 1:2 Laemmli loading buffer (078K6153; Sigma Aldrich) and were incubated for 10 min at 95 °C to denature.

2.3.1.2 Loading, running and transferring the protein

All samples were run on pre-cast 4-15% or 4-20% SDS-PAGE gels (Mini-Protean TGX Gels, Bio-Rad) alongside with a protein standard Spectra Multicolor Broad Range Protein Ladder (ThermoFisher Scientific, 26634) for 90 min at 100 volts. The protein was transferred to polyvinylidene difluoride (PVDF) membrane (Bio-Rad) by running in a transfer buffer for 90 min at 250 mA. PonceauS (Abcam) staining was used for total protein visualization and imaged on Bio-Rad ChemiDoc XRS+.

2.3.1.3 Antibody staining

The blots were blocked using a 5% blocking buffer (5% skim milk, Sigma Aldrich) for 1h. After blocking, membranes were probed with the appropriate primary antibody (Table 2.6) overnight at 4 °C: anti-CX3CL1, anti-CX3CR1, anti-C3 and anti-CD11b. The blots were washed three times with TBS containing 0.1% Tween-20 (TBST) (Sigma) and then incubated with horseradish peroxidase-linked (HRP) secondary antibodies (Table 6) for 2-4h at room temperature. Afterwards, the membranes were washed three times with TBST, and the immunoblots were visualized with ECL Western blotting substrate (Clarity, Bio-Rad) using GAPDH and β-actin (Table 2.6) levels for normalization.

Primary Antibodies			
Target	Host-Species	Concentration	Manufacturer
Anti-CX3CL1	Rabbit	1:1000	Abcam, ab25088
Anti-CX3CR1	Mouse	1:2000	Abcam, ab8021
Anti-CD11b	Rabbit	1:2000	Abcam, ab133357
Anti-C3	Mouse	1:1000	Abcam, ab200999
GAPDH	Mouse	1:2000	Abcam, ab9482
β-actin	Rabbit	1:5000	Abcam, ab8227
HRP -conjugated antibodies			
HRP	Species	Concentration	Manufacturer
HRP	Goat Anti-Rabbit IgG	1:2000	Abcam, ab97051
HRP	Goat Anti-Mouse IgG	1:2000	Millipore, AP124P

Table 7: Primary and HRP-conjugated antibodies

2.3.1.4 Western Blot analysis

Image acquisition was conducted by using Bio-Rad ChemiDoc XRS+ and ImageLab 6.0.1. software (Bio-Rad). GAPDH and β-actin were used for loading normalization. The software creates a 3D map of the bands based on the intensity of each pixel and uses rolling disc background removal to quantify each bands intensity. Data was expressed as the ratio between the band intensity of the protein of interest and that of GAPDH or β-actin.

2.3.2 Quantitative polymerase chain reaction (qPCR)

2.3.1.1 Tissue homogenisation and RNA extraction for qPCR

All samples were lysed in QIAzol lysis reagent (RNeasy Lipid Tissue Mini Kit, Qiagen, Cat.No.74804) and homogenized using a tissue homogenizer Ultra-Turrax T25 (Janke & Kunkel, IKA – Labortechnik) for 30 sec for isolation of total RNA. For RNA extraction RNeasy Lipid Tissue Mini Kit (Qiagen, Cat.No. 74804) was used and performed as described by the

manufacturer. The quality and yield of RNA was verified using NanoDrop One (ThermoFisher Scientific).

2.3.1.2 cDNA synthesis

For RT-qPCR, reverse transcription (RT) reaction was performed in a ProFlex PCR System thermocycler (ThermoFisher Scientific) using LunaScript RT SuperMix Kit (New England BioLabs, No. E3010S/L) and performed as described by manufacturer (Table 2.7, 2.8 and 2.9).

Components	20ul Reactions	Final concentration
LunaScript RT SuperMix (x5)	4 µl	X1
RNA Sample	Variable	(up to 1 µg)
Nuclease-free water	To 20 µl	

Table 8: cDNA synthesis protocol

Components	20ul Reactions	Final concentration
No-RT Control Mix (x5)	4 µl	X1
RNA Sample	variable	(up to 1ug)
Nuclease-free water	To 20 µl	

Table 9: no-RT control protocol

Step	Temperature	Time
Primer Annealing	25 °C	2 min
cDNA Synthesis	55 °C	10 min
Heat Inactivation	95 °C	1 min

Table 10: cDNA synthesis program

2.3.1.3 qPCR and analysis

qPCR analysis of CX3CL1, CX3CR1, C3 and CD11b mRNA expression was performed by using QuantStudio™ 5 Real-Time PCR Systems (ThermoFisher Scientific) and each mRNA expression

was normalized to TATA-box binding protein (TBP) expression as internal control for gene level. qPCR was performed using Luna Universal qPCR Master Mix (New England BioLabs, No. M3003X) as described by the manufacturer (Table 2.10 and Table 2.11). The primer sequences for qPCR were summarized in Table 2.12.

Components	20ul reaction	Final concentration
Luna Universal PCR Mix	10 µl	1x
Forward primer (10uM)	0.5 µl	0.25 µM
Reverse primer (10uM)	0.5 µl	0.25 µM
Template cDNA	Variable	< 100 ng
Nuclease-free water	To 20 µl	

Table 11: Master Mix for qPCR. 1 µl of cDNA product was used as input in a 20 µl qPCR reaction

Cycle step	Temperature	Time	Cycles
Initial denaturation	95 °C	60 sec	1
Denaturation	95 °C	15 sec	40-45
Extension	60 °C	30 sec (+ plate read)	
Melt Curve	60-95 °C	Various	1

Table 12: qPCR program

Gene	Species	Forward primer	Reverse primer
CX3CL1	Mouse	GCAACCCCACCCCTTATCAA	CTTGCCAGCCCTCAGAATCA
CX3CR1	Mouse	CACCATGTCCACCTCCTTCC	CACCAGACCGAACGTGAAGA
CD11b	Mouse	GAGGCCCCCAGGACTTTAAC	CTTCTTGGTGAGCGGGTTCT
C3	Mouse	GCCCCTTACCCCTTCATTCC	CGATGGTCTCTTCGCTCTCC

Table 13: Primer sequences

For quantification analysis, the comparative Threshold Cycle (Ct) method was used. The values of Ct from each gene were normalized to the Ct value of TBP for each sample. Relative quantification was performed using the $2^{-\Delta\Delta Ct}$ method (Schmittgen & Livak, 2008) and expressed as fold increase in arbitrary units.

2.4 Immunohistochemistry and microscopy

2.4.1 Fixed-tissue sectioning

PFA-fixed brains were embedded in 5 % agarose (Bioline, DM50-113D) and cut with a vibrating microtome (VT1000S, Leica Systems) with speed 9 and frequency 6-7 at 50 µm thickness coronal sections. All slices were collected and stored in 24-well plates (Costar) in 1x PBS with 0.05 % sodium azide (26628-22-8, Sigma Aldrich).

2.4.1 Immunohistochemical labelling

To investigate microglial cell density, activity, phagocytic capacity and analyze synaptic density at various postnatal ages, and microglial engulfment of vGlut1+ puncta, the brain sections of control and Snap25cKO mice were blocked in 10 – 20 % normal goat serum (Sigma Aldrich) and 0.3 % Triton X-100 in PBS for 2 hours at room temperature. Iba1 (ionized calcium-binding adapter molecule 1 – specific marker for microglia), CD68 (phagosomal marker commonly used to determine microglia phagocytic activity), vGlut1 (vesicular glutamate transporter 1), PSD95 (postsynaptic density 95) were immunodetected by overnight or 48 hours incubation at 4 °C with primary antibodies (Table 2.13) followed by secondary antibodies (Table 2.13) in PBS with 5% normal goat serum and 0.3% Triton X-100 for 2 hours at room temperature. Immunolabelled sections were counterstained with DAPI, mounted with FluorSave™ reagent (MerkMillipore) and imaged as described below. Imaging and analysis were carried out blind to the animal genotype and gender (Table 2.14).

Primary Antibodies			
Target	**Host-Species**	**Concentration**	**Manufacturer**
Anti-Iba1	Rabbit	1:500	FUJIFILM Wako 019-19741

Anti-vGlut1	Guinea Pig	1:500	Merck Millipore AB5905
Anti-PSD95	Mouse	1:500	Thermo Xe3-1B8
Anti-CD68	Mouse	1:500	Abcam, ab955
Secondary Antibodies			
Fluorophore	**Species**	**Concentration**	**Manufacturer**
Alexa Fluor®488	Goat Anti-Rabbit IgG (H+L)	1:500	ThermoFisher, A11034
Alexa Fluor®488	Goat Anti-Mouse IgG (H+L)	1:500	Lifetech, A21041
Alexa Fluor®633	Goat Anti-Guinea Pig IgG (H+L)	1:500	Molecular Probes, A21105

Table 14: Primary and secondary antibodies

Number of Animals				
Genotype	**Control**		**Snap25$^{fl/fl}$ cKO**	
Age/Gender	**Male**	**Female**	**Male**	**Female**
P8	3	3	3	2
P14	3	3	3	3
P21	3	2	2	4
16 weeks	-	4	-	2

Table 15: Number of animals

2.4.2 Confocal microscopy

To evaluate microglial cell density, phagocytic activity and capacity in visual cortex layer 5 (n = 3 images/animal), superior colliculus (n = 6 images/animal) and hippocampus CA1 and CA3 regions (n = 3 images/animal), immunolabeled sections were imaged with a laser-scanning confocal microscope (Zeiss LSM710) using 20x/0.6 air objective and 1x optical zoom at 0.42 µm pixel size, and frame size 1024 x 1024. Image size for cortex was 424.7 x 1275.29 µm, and for superior colliculus and hippocampus CA1 and CA3 area: 424.7 x 424.7 µm.

To examine individual microglial cell morphological features, microglia presynaptic compartment (vGlut1+ puncta) engulfment and vGlut1/PSD95 synaptic density in visual cortex layer 5 (n = 9 images/animal) and hippocampus CA3 region (n = 9 images/animal) the same immunolabeled sections were imaged with laser-scanning confocal (Zeiss LSM710) using 63x/1.4NA oil-immersion objective and 2x optical zoom.

2.5 Image analysis

2.5.1 Automatic and semi-automatic tools for the analysis of microglia morphology

All automatic and semi-automatic tools for microglia analysis were developed in collaboration with Alfonsas Jursenas (Baltic Institute of Advanced Technology, Lithuania).

2.5.1.1 Cell counter

To evaluate microglial cells density, I created an automatic cell counter program with cell overlapping nuclei (overlap between DAPI (nucleus) and Iba1 (microglia)) to count the total number of microglial cells per field of view. The image processing was done using Python language package Scikit-Image in particular the *skimage.morphology* module to find, filter and count connected volumes (Van Der Walt et al., 2014). Image filtering operations (Gaussian filter) were performed using skimage.filters module.

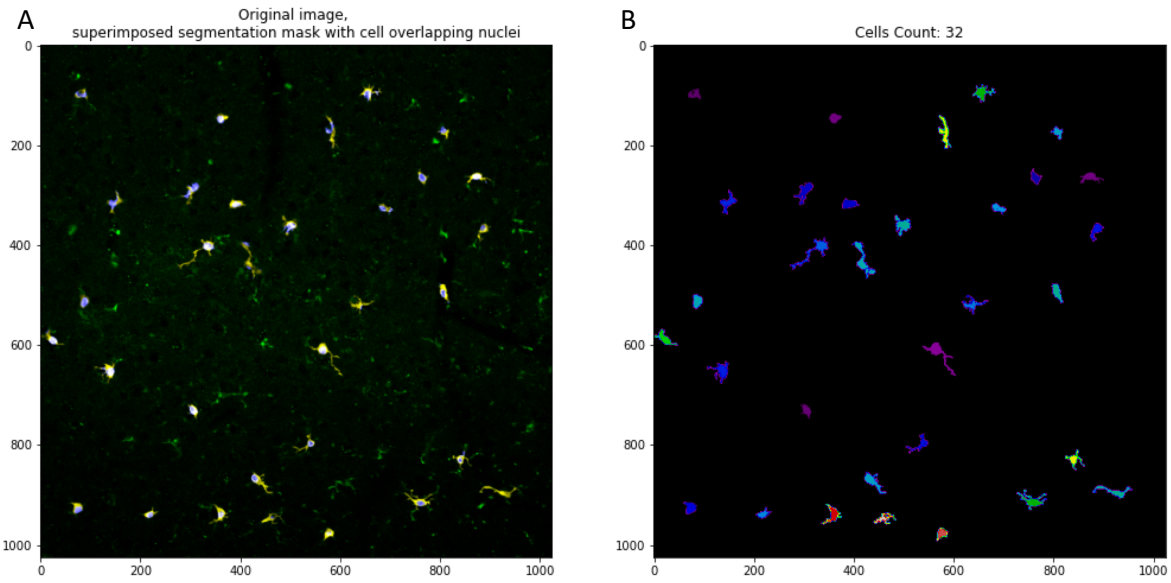


Figure 13: Microglial cells counter

Microglia labelled in green, and nuclei labelled in blue. Original image with superimposed segmentation mask with cell overlapping nuclei (A). Filtered image using skimage.filters module shows total number of microglia per field of view (B).

2.5.1.2 Automatic 3D microglia volume counter

To visualize microglial cells, anti-Iba1 immunohistochemical labeling was used. Iba1+ signal volume was computed by counting all voxels in the connected element (this was done by using the morphology module of the skimage ((Van Der Walt et al., 2014) Python package) corresponding to the cell. Connected element segmentation was done by using 26 neighbour's connectivity (that is the voxels are connected if their edges, corners, or faces touch). Since small ($> 0.7\ \mu m^3, \sim 300$ voxels) connected, volumes cannot correspond to a whole cell, connected regions with smaller voxel count than 300 and considered to be noise are removed. Voxel depth and pixel size was taken from laser-scanning confocal microscope (Zeiss LSM710) image acquisition settings (voxel depth z = 0.55 µm, pixel size x = y = 0.0658941 µm). Iba1 channel was smoothed using Gaussian kernels (with standard deviation of 2 voxels) and binarized using intensity threshold:

$$I_{\text{th}} = 2\sigma = 2\sqrt{\sum_{x,y,z} \frac{\left(I_{x,y,z} - \overline{I}\right)^2}{N}}$$

where x, y, z - intensity channel 3D coordinates, N - voxel count, where σ is standard deviation of the channel 3D matrix, $\overline{I}$ - average intensity.

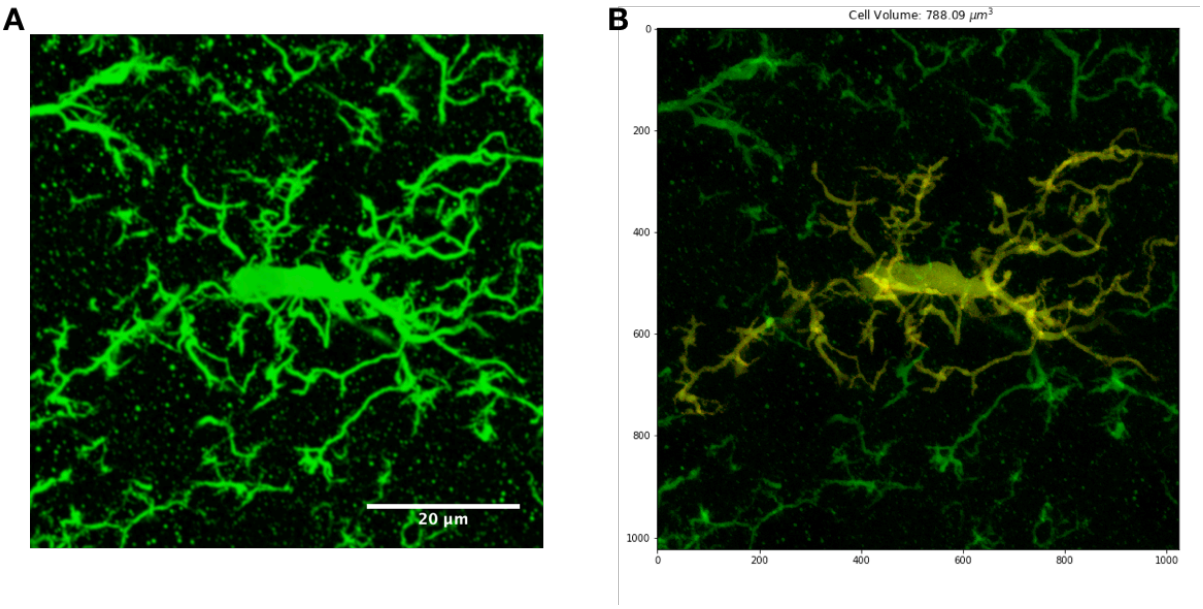


Figure 14: Automatic 3D Iba1+ signal reconstruction voxel-based method

2.5.1.3 3D Sholl analysis

This analysis was performed with the following steps

1. Apply 3D Gaussian blur to reduce high spatial frequency noise.
2. Thresholding the image to obtain a 3D segmentation mask of the cell.
3. Removing small connected components (we obtain the image A in Figure 2.3).
4. Generating binary masks of a fixed radius and thickness of x pixels.
5. Multiplication of spherical shell mask with 3D mask of the cell (for the resulting 3D mask see image B in Figure 15).

a. The sphere is centered in the center of mass of the cell or nucleus of the cell.

6. Counting the connected components in spherical shell mask intersection with the mask of the cell (the intersection is displayed in image B, Figure 15).
7. Repetition of steps 4-6 with increasing radius of the spherical shell mask results in radial distribution of spherical shell intersections.
8. By mapping the intersections distribution to: $y = ln\left(\frac{N_{intersections}}{V_{shpere}}\right); x = r_{sphere}$ and fitting a linear regression model $\hat{y} = m - kr$ we obtain the 3D Sholl regression coefficient k.
9. Results displayed in Figure 16.

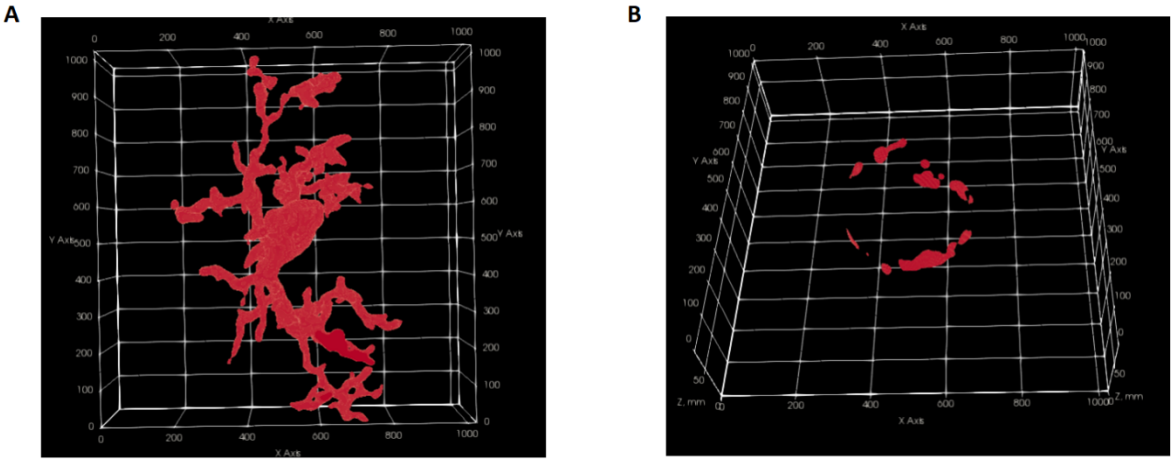
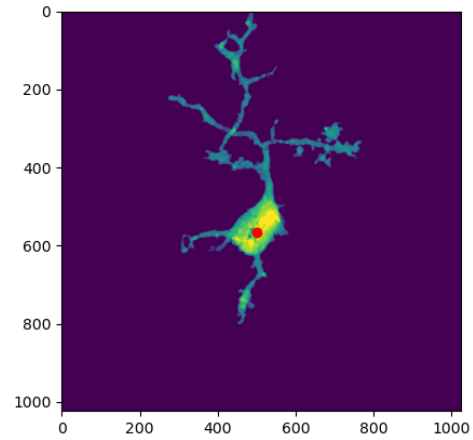


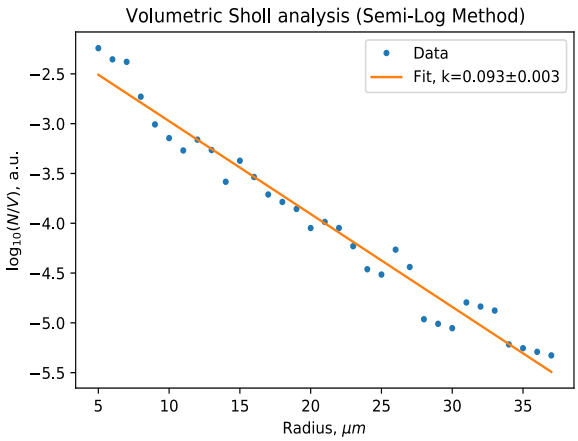
Figure 15: 3D Sholl analysis tool

Segmentation mask of the cell (A). Spherical shell intersection with the cell segmentation mask (B). The connected components in B are interpreted as being analogous to intersections in the 2D Sholl analysis case. The volumetric rendering was performed using Paraview software.

A



B



C

Cell No	k	k_err	R2	Volume
No 1	0.093239167	0.003103574	0.966793517	872.7699398
3D Sholl	**radius, µm**	**Intersections**	**Intersections/Volume**	**log_10(Intersections/Volume)**
0	5	3	0.005729578	-2.241877368
1	6	4	0.004420971	-2.354482369
2	7	6	0.004176077	-2.379231479
3	8	4	0.001865097	-2.729298579
4	9	3	0.000982438	-3.007694883
5	10	3	0.000716197	-3.144967355
6	11	3	0.00053809	-3.26914541
7	12	5	0.000690777	-3.160662343
8	13	5	0.000543315	-3.264948662
9	14	3	0.000261005	-3.583351462
10	15	6	0.000424413	-3.372211136
11	16	5	0.000291421	-3.535478553
12	17	4	0.000194368	-3.711375382
13	18	4	0.00016374	-3.785846133
14	19	4	0.000139223	-3.856289421
15	20	3	8.95247E-05	-4.048057342
16	21	4	0.000103113	-3.986686502
17	22	4	8.96816E-05	-4.04729666
18	23	3	5.88639E-05	-4.230150863
19	24	2	3.45388E-05	-4.461692339
20	25	2	3.05577E-05	-4.51487864
21	26	4	5.43315E-05	-4.264948662
22	27	3	3.63866E-05	-4.439058647
23	28	1	1.08752E-05	-4.963562703
24	29	1	9.78853E-06	-5.009282603
25	30	1	8.84194E-06	-5.053452373
26	31	2	1.60272E-05	-4.795143695
27	32	2	1.45711E-05	-4.836508549
28	33	2	1.32862E-05	-4.876600433
29	34	1	6.074E-06	-5.21652536
30	35	1	5.5681E-06	-5.254292742
31	36	1	5.11686E-06	-5.290996112
32	37	1	4.7131E-06	-5.326693782

D

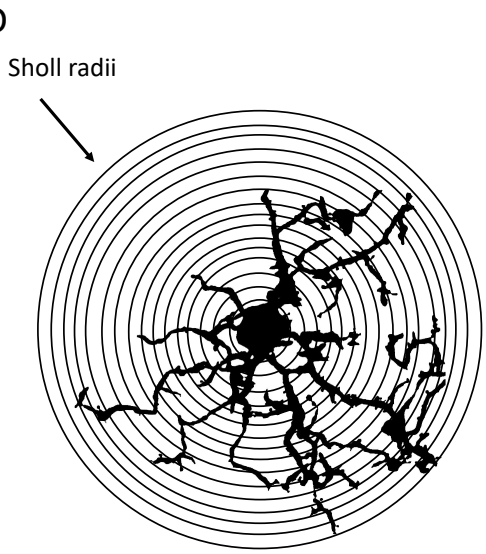


Figure 16: 3D Sholl analysis results

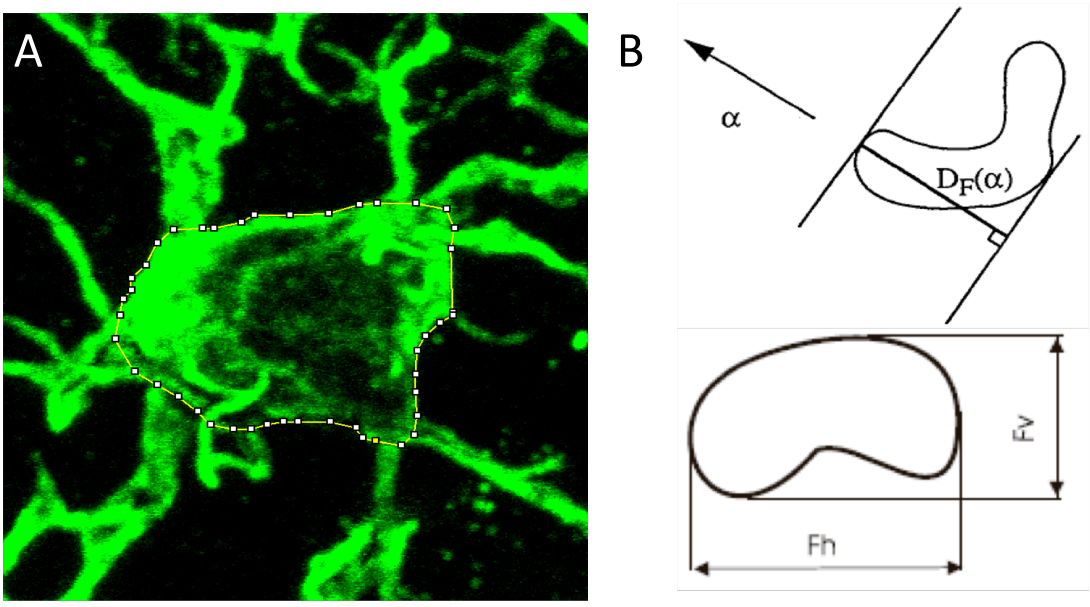
3D reconstructed microglia (A). Volumetric Sholl analysis using semi-log method (B). 3D Sholl analysis results of individual cell presented in the table (C). Example of Sholl radii (D).

2.5.2 Manual analysis of microglial morphology

2.5.2.1 Microglial soma size and roundness

Analysis of microglial soma was performed using ImageJ (NIH). Soma was manually measured using a polygon selection tool (Figure 17A). At the set measurements box of the ImageJ

toolbar, I selected area and Feret's diameter. Feret's diameter is defined as the distance between the two parallel planes restricting the object (soma) perpendicular to that direction (WALTON, 1948). The longest distance between two points along the selection boundary, also known as maximum caliper. *Feret Angle* is described as the angle between the Feret's diameter and a line parallel to the x-axis of the image. *Min Feret* - minimum caliper diameter. The starting coordinates of the Feret's diameter (*Feret X* and *Feret Y*) were displayed. Soma roundness was calculated: Feret Min/Feret (Figure 17C).



Soma size and distance between two parallel tangent lines

$F = P / \pi$

C

Area	Feret	Feret X	Feret Y	Feret Angle	Feret Min	Roundness
70.197671	16.509468	504	510	80.3497	7.560423	0.45794468

Figure 17: Analysis of soma area and roundness

Polygon selection of microglia soma (A). Feret's diameter (B). Microglial soma results displayed in the table (C).

2.5.2.2 Primary branches

Analysis of primary branches was performed using ImageJ (NIH). Primary branches were manually quantified based on visual investigation. Primary branches are described as the main branches that are directly connected to the soma of microglia.

2.5.2.3 Microglial complexity

Analysis of microglial cell complexity was performed using ImageJ (NIH) Fractal box counting method (FracLac plugin; Karperien, 1999-2015). Fractal analysis is used to quantify difficult to describe patterns. Fractal box counting is analogous to the perimeter measuring. Image is covered with a grid and the number of boxes covered by part of the image is counted. then count how many boxes of the grid are covering part of the image. Then the same procedure is done with a finer grid with smaller boxes. By shrinking the size of the grid repeatedly it allows more accurately capture the structure of the pattern (Figure 18). Fractal box count was used on the selected skeleton with box size: 2, 3, 4, 6, 8, 12, 16, 32, and 64. This gave the Fractal dimension of the microglia. Fractal dimension (D_F or D) is a meter of complexity and is the slope of the line when values are plotted by log(N) on the Y-axis against the value of log(r) on the X-axis (Figure 18).

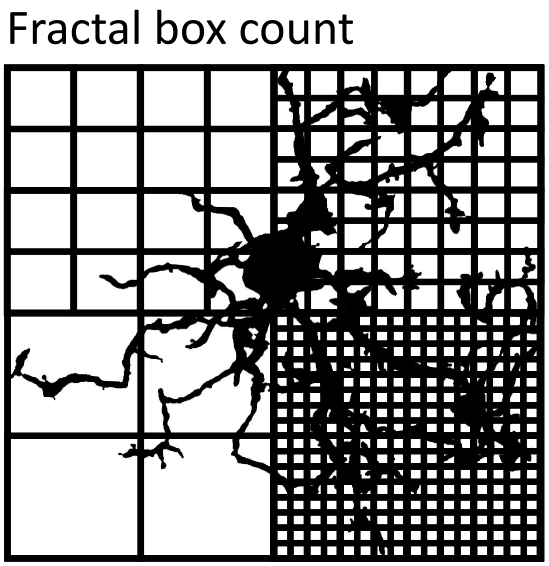


Figure 18: Fractal box counting

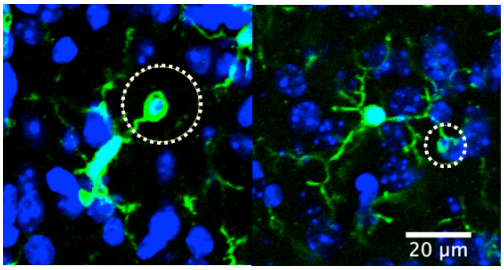
Fractal dimension is used to evaluate microglial complexity (A. L. Karperien & Jelinek, 2015, 2016) and box counting method is exquisitely sensitive to morphological features that are analogous to structural features of microglia. Fractal dimension values range from 1 to 2, where 1 is considered to be a simple circle shape.

All calculations are summarized in the reference guide provided for FracLac plugin https://imagej.nih.gov/ij/plugins/fraclac/FLHelp/BoxCounting.htm and additional associated references (A. Karperien et al., 2013; A. L. Karperien & Jelinek, 2015, 2016).

2.5.3 Analysis of phagocytic pouches

Apoptotic cells were identified based on their nuclear morphology with lost chromatin structure and condensed nuclei revealed with DAPI staining. Phagocytosis was defined as the formation of a three-dimensional (3D) enclosed pouch of microglial branches around an apoptotic cell (Sierra et al., 2010) (Figure 19). 3D phagocytic pouches were counted manually

for each image and the number of phagocytic pouches was divided by the total number of microglial cells per field of view (Sierra et al., 2010).



$$\text{Ph capacity} = \frac{(mgPh1 + 2mgPh2 + \ldots + nmgPhn)}{mg}$$

ph - phagocytic capacity
mg - total no of microglia
mgPh - microglia w/ phagocytic pouches

Figure 19: Analysis of phagocytic pouches

Microglia (green), nuclei (blue). Phagocytic pouches are indicated by circles.

5.2.4 Analysis of microglia active areas and presynaptic engulfment

Analysis was performed using ImageJ (NIH) by manually counting CD68 and vGlut1+ signal co-localization with Iba1+ microglial cells (Gunner et al., 2019). Afterwards, to count the percentage of engulfment, engulfed vGlut1+ was divided by total number of vGlut1+ particles per field of view and multiplied by 100 (Gunner et al., 2019). To calculate the percentage of CD68+/Iba1+ microglia, CD68+ microglial cells were divided by total number of Iba1+ microglia per field of view and multiplied by 100.

2.5.5 Analysis of synaptic density

vGlut1 and PSD95 particle number and volume were analyzed with ImageJ software (NIH) using 3D ROI manager after subtracting background (50 pixels) to remove spatial variations of the background intensities for 3D particle reconstruction, applying Gaussian blur 3D smoothing filter (x sigma = 2, y sigma = 2, z sigma = 2) and manual thresholding. Afterwards, data was normalized based on number of planes in image and image volume (Table 16).

Colocalization between PSD95 and vGlut1 particles was quantified using the ImageJ JACoP plugin. All analysis and calculations are summarized in the reference guide provided for JACoP plugin: https://imagej.net/plugins/jacop and additional associated references (Bolte & Cordelières, 2006).

vGlut1 and PSD95 normalization	
n	Number of animals
vGlut1 and PSD95 Vol (microns)	Volume of vGlut1 and PSD95 signal in microns (μm^3)
No of particles	Number of particles in field of view
z	Number of planes in image
h	0.5500000 x z - image height (voxel depth x z)
V, μm^3	Image volume in microns (h x $(1024 \times 0.0658941)^2$)
p_density	Particle density (No of particles divided by image volume)
p_density x 1000	Particle density x1000
p_vol_sum	Sum of all volume of particles in field of view
p_vol_norm	Normalized volume of volume of all particles in field of view
p_vol_norm x1000	Normalized volume of volume of all particles in field of view x 1000
Image size	67.48 x 67.48 µm

Table 16: vGlut1 and PSD95 data normalization based on imaging features.

2.6 Statistics

Data are reported as means ± standard error of the mean (SEM). Analysis was performed on data from at least 2 brain per group and for each analysis a minimum of 3 sections per brain (visual cortex n = 3 images/animal, superior colliculus n = 6 images/animal and hippocampus CA3 region n = 3 images/animal and 3D data of layer 5 and CA3 area n = 9 images/animal).

Sample size (*n*) refers to individual animals for microglial density, microglial phagocytic activity and capacity, vGlut1 engulfment, synaptic density, protein levels and mRNA expression, cFos+ cell density, while it refers to individual microglia for morphological analysis: microglial volume, microglial soma size and roundness, the number of primary branches, Fractal box count and 3D Sholl analysis. Statistical analyses were conducted using Prism 9 (v.9.3.1, GraphPad Software, San Diego, CA, USA). Normality was verified using Shapiro-Wilk and assessed by QQ plot. For normally distributed data, two-way ANOVA with *post hoc* Šídák was used to determine differences between individual animals and determine genotype effect between control and Snap25 cKO mice, saline and $Rbp4^{Cre}$;hM4Di, and saline $Rbp4^{Cre}$;hM4Dq. For non-normally distributed dataset, non-parametric test followed by two-stage step-up method of Benjamini, Krieger and Yekutieli was used to determine differences between genotype and sex effects at P8, P14 and P21. Threshold for significance levels was set at $P < 0.05$.

2.7 Additional information

- Detailed explanation about Snap25 cKO transgenic mouse model will be discussed in Chapter 4.
- Detailed explanation about inhibitory and excitatory DREADDs mouse models and methods for the DREADD validation and analysis will be discussed in Chapter 5.

Chapter 3: Changes in microglial cells dynamic during normal brain development

3.1 Introduction

Microglia – tissue-resident macrophages – are different from other brain cells in their origin, variety of functions and morphological flexibility (Stratoulias et al., 2019). It was previously believed that microglia simply guard the brain as a part of the immune system, however, our understanding of their importance and involvement in brain functions increased rapidly in recent years. Microglial cells help to maintain a stable and healthy brain environment and also play a key role in shaping neuronal network formation during development (Wake et al., 2013). After birth, our brain contains overabundant neuronal connections (Figure 20) (Seeman et al., 1987) that must be refined and eliminated to secure the most effective and efficient brain activity (LaMantia & Rakic, 1990; A. Miyamoto et al., 2016). Microglia act as gardeners and scavenge unnecessary connections, and this process is known as synaptic pruning. Pruning does not happen in a haphazard fashion, these intelligent cells detect neuronal subtypes, their activity and remodel circuits in a highly regulated manner.

Pruning has a dramatic impact on neuronal network connectivity and helps to shape a neuronal network that is systematically organised to subserve its complex functions (Seeman et al., 1987). Impaired microglial functions can lead to altered neuronal network formation in the developing brain. Abnormal neuronal network development may result in a variety of neurodevelopmental disorders such as autism spectrum disorder (Tang et al., 2014; Velmeshev et al., 2019) and schizophrenia (Glantz & Lewis, 2000; Sellgren et al., 2019). Thus, in order to understand and potentially prevent neurodevelopmental disorders, a better insight into microglia function during early brain development is pivotal.

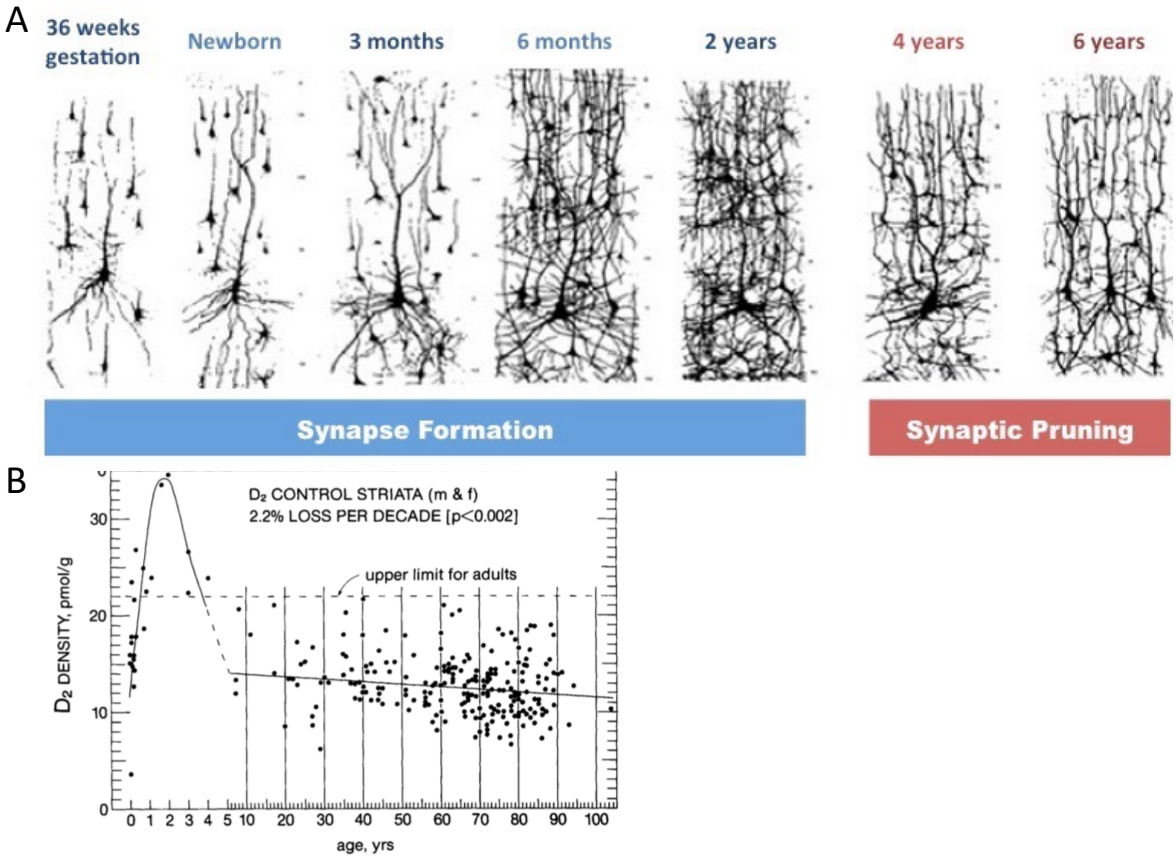


Figure 20:Synapse formation and synaptic pruning during human brain development

(A) During the first two years after birth, neuronal network density increases dramatically. The developmental task of childhood years is to prune and select the most used neurons and synapses. The first peak of synaptic pruning occurs at 2 years old, and the second peak around 6 years old. (B) The density of dopamine D_2 receptor is plotted at various ages. The highest density of D_2 is around 2-3 years of age and decreases thereafter. Adapted from *Cornell et al., 2016* and *Seeman et al., 1987*.

3.1.1 Variety of microglial features

Microglia have a highly variable morphology (A. Karperien et al., 2013) (Figure 21) ; individual cells can cycle reversibly from amoeboid (described as big round cells with a few short or no processes and an irregular, amoeboid body) to a ramified form (described as highly branched cells with small and round soma) and functional activity of microglia correlates with their

morphological changes. However, due to highly variable morphology, it is difficult to classify microglial cells and a few major problems arise (F. R. Walker et al., 2014). First issue: we still have not categorised how many different morphological classes of microglia the brain has. The number of different microglia classes changes from three to more than ten depending on physiological/pathological conditions, brain region, marker expression and even environmental factors (Kosonowska et al., 2015; F. R. Walker et al., 2014). There are no sharp boundaries between morphological subtypes and functional states, thus causing difficulties in classifying microglia based on morphological features. Second issue: we are still using visual investigation to classify microglia; however, this approach is biased and sometimes the same cell can be put into different categories depending on the classification used.

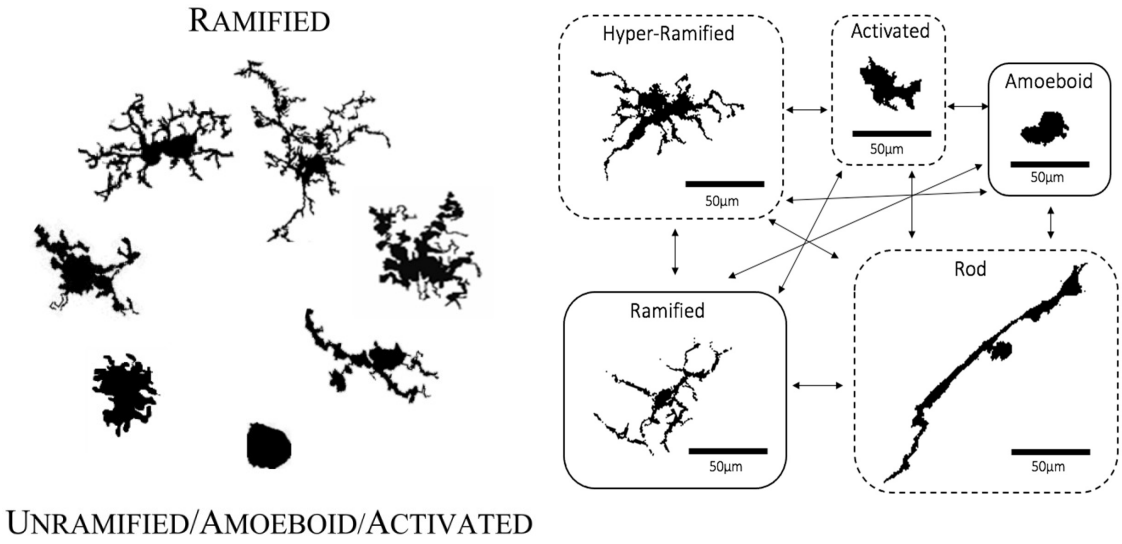


Figure 21: Different subtypes of microglia classified based on their morphology

Microglia are morphologically dynamic cells. Individual cells are able to change from ramified to lacking processes of amoeboid form and back to ramified. Adapted from (A. Karperien et al., 2013) and (S. Choi et al., 2021).

Moreover, microglia transition from ramified to amoeboid morphology can be very rapid in neuroinflammatory processes or can be absent for years in the healthy brain (Casano & Peri, 2015). Yet another important feature of microglia is sexual dimorphism. In recent years it was shown that microglia are sexually dimorphic in both physiological and pathological conditions (Guillot-Sestier et al., 2021; Hui et al., 2020; Kerr et al., 2019; Weinhard, Neniskyte, et al., 2018).

3.1.2 Synaptic pruning by microglia

Synaptic pruning has been well documented in various parts of postnatal mouse brains such as cerebral cortex, hippocampus, and thalamus (Bilimoria & Stevens, 2015; Casano & Peri, 2015; Paolicelli et al., 2011), and showed changes in microglial functions and distribution during postnatal brain development. Microglial density is tightly controlled throughout development (DiBona et al., 2019; Li et al., 2019; Paolicelli et al., 2011). To have an appropriate number of microglia is necessary to maintain brain connectivity and homeostasis throughout life (Prinz & Priller, 2014). Microglia undergo significant changes in their density, morphology and phagocytic abilities during early postnatal brain development (Nimmerjahn et al., 2005; Prinz & Priller, 2014; Zusso et al., 2012). These changes are important for their role in sculpting the developing brain (Casano & Peri, 2015; Wake et al., 2013).

The hippocampus is one region of the brain where microglia have been studied the most. Developmental synaptic pruning has been demonstrated in Schaffer collaterals of the hippocampus (Figure 22) (Zhan et al., 2014). Microglia recognize Schaffer collateral to CA1 pyramidal neurons via fractalkine signalling that is required for synaptic pruning (Paolicelli et al., 2011; Zhan et al., 2014). Furthermore, it has been demonstrated that microglial density

may be involved in region-specific vulnerability of the hippocampus and the heterogeneous distribution of microglia may play a role in the modulation of hippocampal neuronal activity (Jinno et al., 2007).

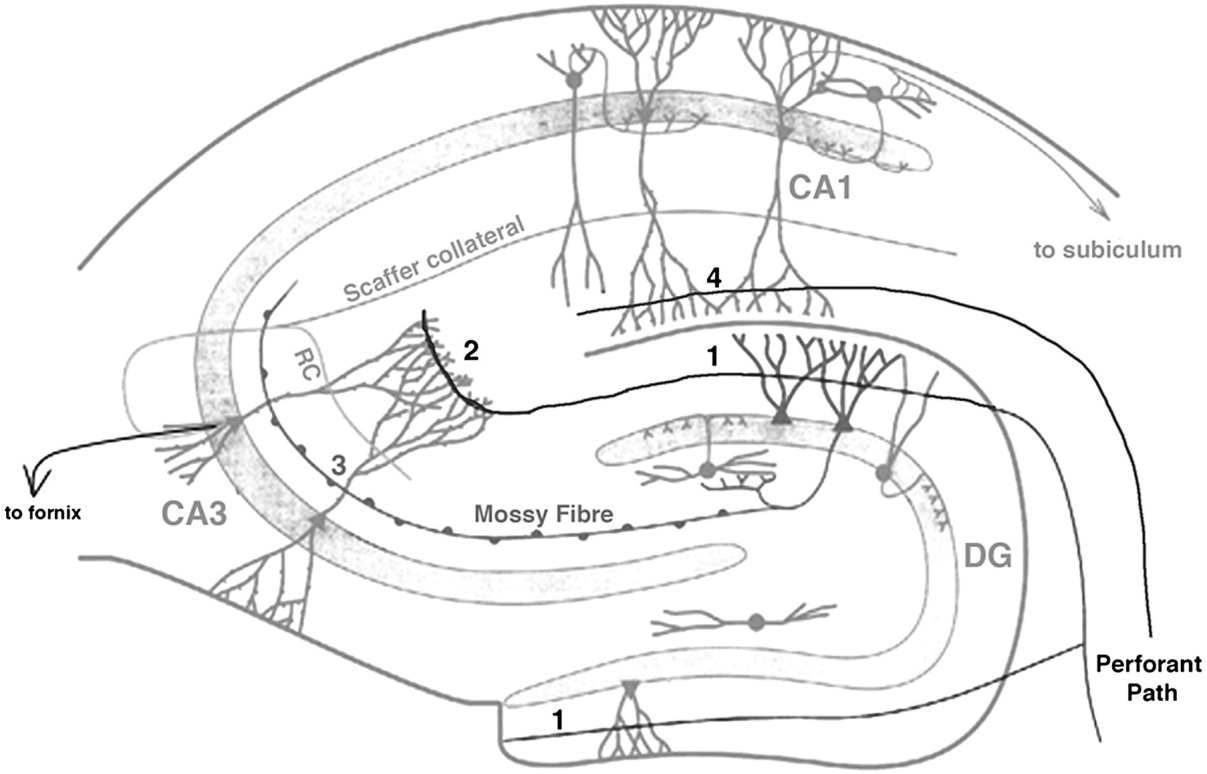


Figure 22: Basic cytoarchitectonic subdivisions and their connectivity of hippocampus

Prefrontal pathway – neurons from EC layer 2 bypass the subiculum and project to the DG, and additional collaterals project to the CA3. Mossy fiber pathway – granule cells in the DG project to the CA3 through the mossy fiber. Third pathway – the CA3 pyramidal neurons project to the CA1 via Shaffer collaterals and from CA1 pyramidal neurons project to the subiculum and to the EC. Cornu ammonis (CA) 1 (CA1), CA2, CA3; entorhinal cortex (EC); dentate gyrus (DG). Original image from (Daumas et al., 2009)

Synapse formation in the developing visual system is also dependent on microglia. It has been demonstrated in the lateral geniculate nucleus of the thalamus that microglia engulfed retinal synaptic inputs from the eye with less active neurons suggesting that microglia can be a mediator of synaptic remodelling in the developing retinogeniculate system (Schafer et al., 2012). In mouse layer 4 of the visual cortex, where most of the geniculocortical projections terminate, microglia responded to monocular deprivation with the increased phagocytic

activity (Schecter et al., 2017). Furthermore, it has been shown that microglial fractalkine receptor (CX3CR1) is not required for activity-dependent plasticity in the binocular segment of the mouse primary visual cortex, and may has more heterogeneous role in different brain regions (Lowery et al., 2017). Moreover, binocular deprivation at P20 and P28 reduced microglial motility in the primary visual cortex. In the primary visual cortex of juvenile mice, sensory deprivation and light exposure affected microglia behaviour. Tremblay and colleagues demonstrated that microglia-synapse interactions are regulated by sensory experience (Tremblay et al., 2010).

Large-scale cortical region-specific axonal pruning has been demonstrated during development (Figure 23). Visual and motor cortices both extend projections to the spinal cord and superior colliculus during early postnatal development, but only the motor cortex maintain the spinal cord projections and only the visual cortex maintain the projections to the superior colliculus (O'Leary et al., 1990; O'Leary & Koester, 1993; Stanfield, 1992; Stanfield et al., 1982; Vanderhaeghen & Cheng, 2010). The rest are eliminated in an area-specific manner during development. It has been shown that in the motor cortex layer 5, microglia support neuronal survival during early postnatal development (Ueno et al., 2013). However, the role of microglia in the developing visual cortex layer 5 neurons and their projections to superior colliculus remains unclear.

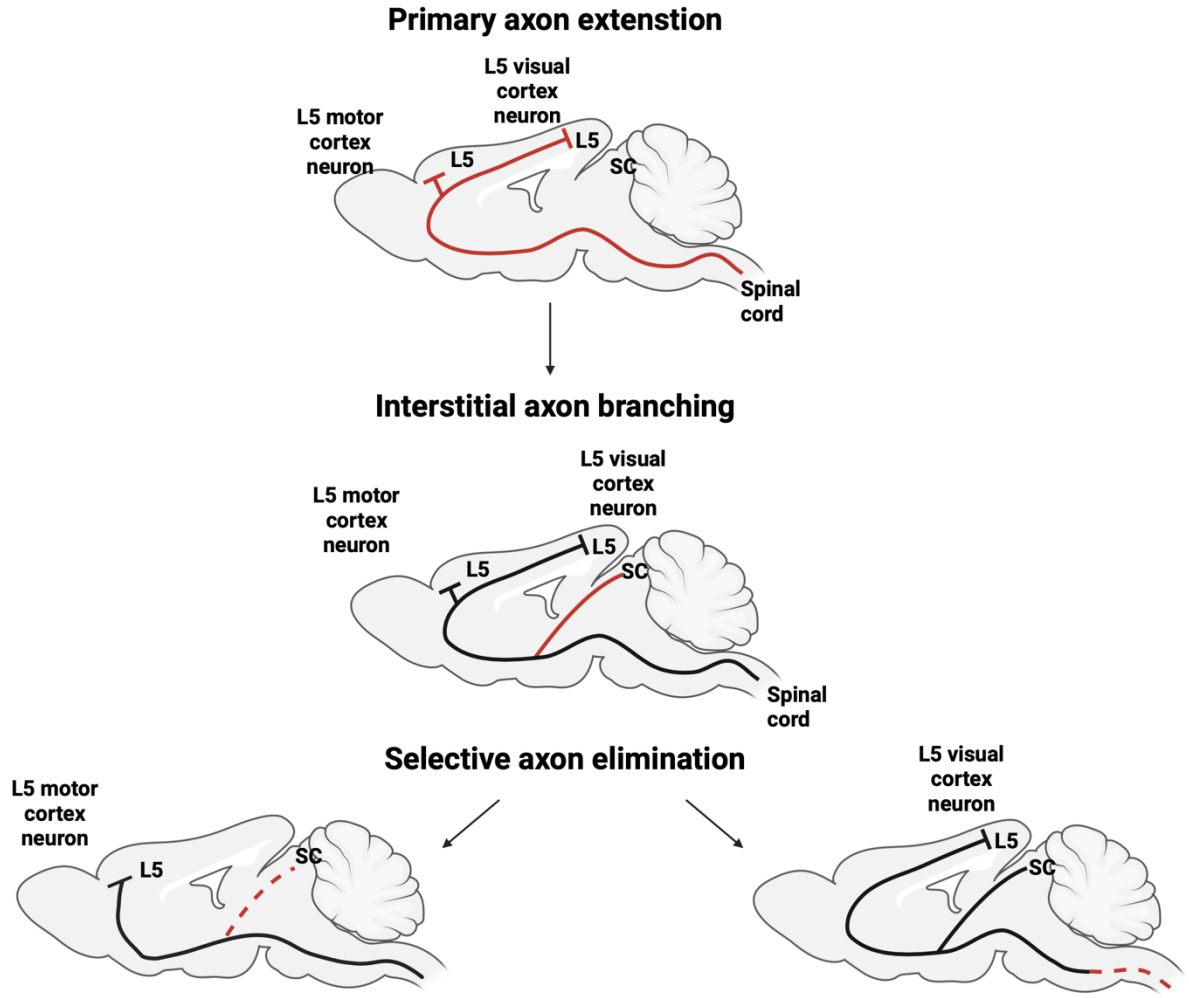


Figure 23: Large-scale axonal pruning

Adapted from (O'Leary et al., 1990; O'Leary & Koester, 1993; Stanfield, 1992; Stanfield et al., 1982; Vanderhaeghen & Cheng, 2010). Created with BioRender.com

My DPhil project focused on microglial morphological and functional changes in the developing visual cortex layer 5, superior colliculus, and hippocampal CA1 and CA3 regions. Moreover, I further investigated microglial behaviour in the developing male and female brains.

3.2 Results

3.2.1 Brain region-specific distribution of microglia during development

To better understand microglial dynamic across different brain regions during normal postnatal development I first evaluated microglial cells density in the developing visual cortex (Figure 24A), superior colliculus (Figure 24B) and hippocampal CA1 (Figure 24C) and CA3 (Figure 24D) areas at postnatal day 8 (P8), P14 and P21. Microglia were immunodetected using anti-Iba1 antibody (Korzhevskii & Kirik, 2016) and visualized by confocal microscopy.

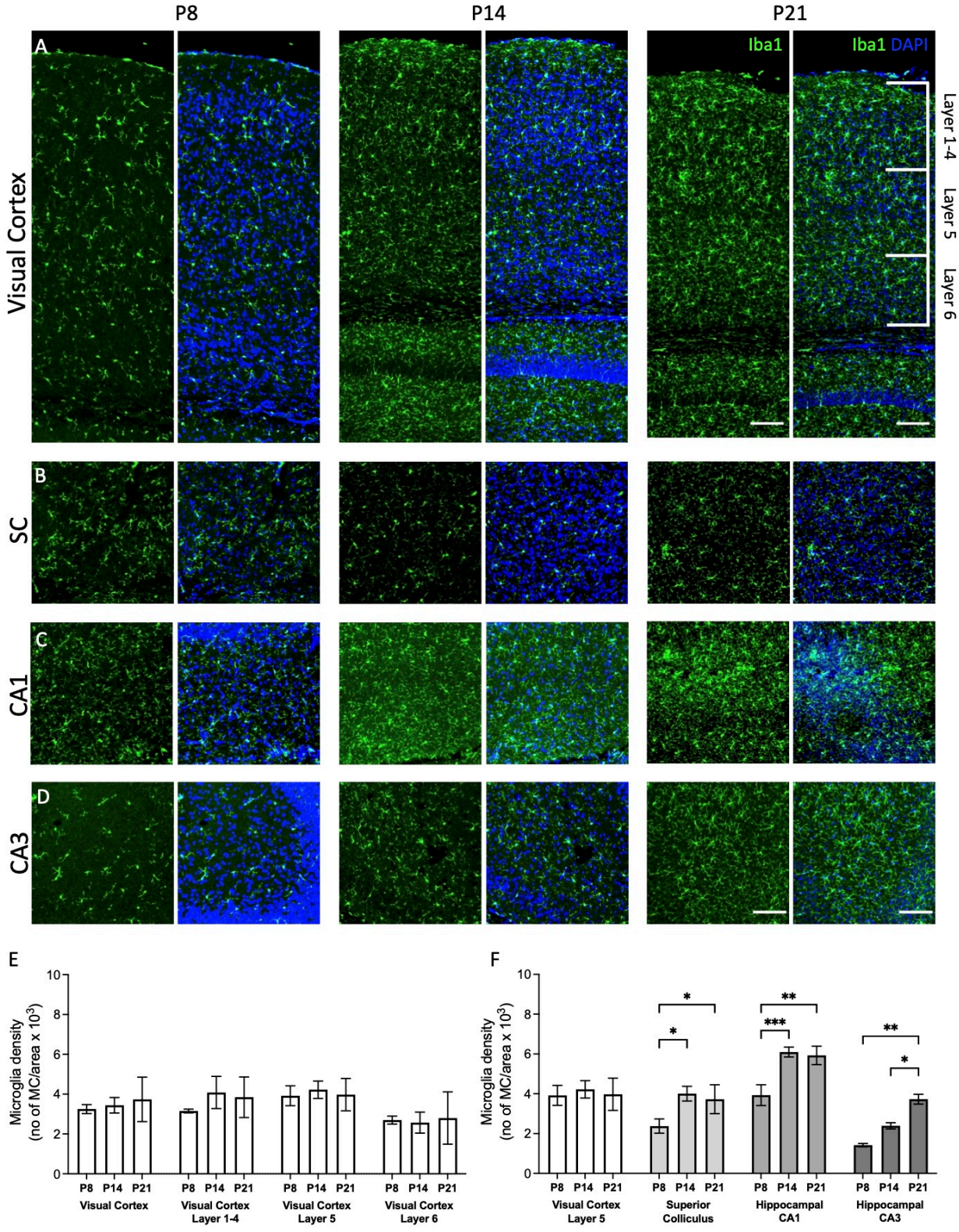
No differences in microglial density in the developing visual cortex and across different cortical layers were observed (Figure 24E), however I observed sex-specific differences (Figure 24E1-4). In the developing visual cortex, microglial density was increased in female mice compared to male at P8 ($p = 0.0141$), P14 ($p < 0.0001$), and P21 ($p < 0.0001$). Across different cortical layers microglial density was higher in females compared to male brains as well. In layers 1-4, microglial density was increased in females compared to males at P14 ($p < 0.0001$) and P21 ($p < 0.0001$). In layer 5, microglial density was increased in females compared to males at P8 ($p = 0.0029$), P14 ($p = 0.0072$), and P21 ($p < 0.0001$). In layer 6, microglial density was increased in females compared to males at P14 ($p < 0.0001$) and P21 ($p < 0.0001$).

In superior colliculus (Figure 24F) microglial density was higher at P14 ($p = 0.0093$) and P21 ($p = 0.0377$) compared to P8. Moreover, sex-specific distribution of microglia was observed in the developing superior colliculus as well. Microglial density was increased in females (Figure 24F-F1) at P8 ($p = 0.0003$), P14 ($p = 0.0006$), and P21 ($p < 0.0001$) compared to males.

Similar results were observed in the hippocampal CA1 area (Figure 24F-F2). Density peaks at P14 and is higher at P14 ($p = 0.0007$) and P21 ($p = 0.0026$) than at P8 (Figure 24F) and was higher in females compared to males at P8 ($p < 0.0001$) and P21 ($p = 0.0012$).

Interestingly, in the hippocampal CA3 area, microglial density peaks later in development, and was higher at P21 compared to P8 (p = 0.0006) and P14 (p = 0.0396), and no differences in microglial density was observed between males and females.

These findings indicate non-uniform and heterogenous distribution of microglia across the developing brain. The sexual dimorphism of microglia appears to emerge slower in visual cortex, especially in layers 1-4 and layer 6, and in the hippocampal CA3 region than in superior colliculus and hippocampal CA1 during first week of postnatal development. Thereafter, sexual dimorphism of microglia become evident across all the brain regions that I investigated in my study and higher density of microglial cells are observed in female brains.


P8
P14
P21
A
Iba1
Iba1 DAPI
Visual Cortex
Layer 1-4
Layer 5
Layer 6
B
SC
C
CA1
D
CA3
E
Microglia density
(no of MC/area x 10³)
P8 P14 P21
Visual Cortex
Visual Cortex Layer 1-4
Visual Cortex Layer 5
Visual Cortex Layer 6
F
Visual Cortex Layer 5
Superior Colliculus
Hippocampal CA1
Hippocampal CA3

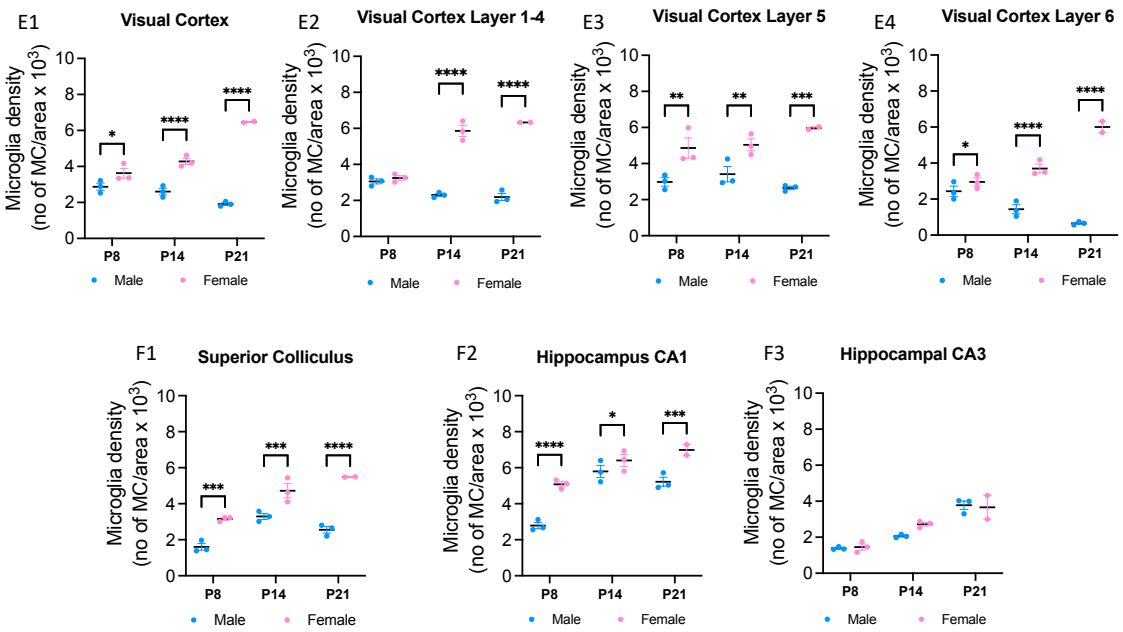


Figure 24: Brain region-specific changes in microglial density during early postnatal development

Representative images of Iba1+ microglia (green) in developing visual cortex at postnatal day 8 (P8), P14 and P21 (A); superior colliculus at P8, P14, P21 (B); hippocampal CA1 region at P8, P14, P21 (C); hippocampal CA3 region at P8, P14, P21 (D). Iba1+ microglia density changes between cortical layers 1 to 6 and differences between male (blue) and female (pink) mice in developing visual cortex (each dot represents an individual mouse, n = 5-6 per age group) (E and E1-4). Microglial cell density increases in SC, CA1, CA3 from P8 to P21 but not in visual cortex layer 5, and shows differences between male and female mice (each dot represents an individual mouse, n = 5-6 per age group) (Fand F1-3). All data presented as mean ± SEM, * $p < 0.05$, ** $p < 0.01$, *** $p < 0.001$, **** $p < 0.0001$. SC – superior colliculus, CA1 – hippocampal cornu ammonis 1, CA3 – hippocampal cornu ammonis 3. Scale bar, 100 µm.

3.2.2 CD68 in microglia changes during development

In order to better understand microglial cells dynamic during postnatal brain development and to further investigate sexual-dimorphism in microglia, I measured CD68 in Iba1 labelled microglia in the visual cortex, superior colliculus, hippocampal CA1 and CA3 regions of male and female mice at P8, P14 and P21. I performed analysis of Iba1-immunolabelled microglia with the phagosomal marker CD68 (Wierzba-Bobrowicz et al., 2002) in fixed brain sections at

P8, P14 and P21. Significant differences in microglial phagocytic activity were observed in the developing superior colliculus, and hippocampal CA1 and CA3 regions (Figure 25E). In superior colliculus and hippocampal CA1, CD68 in Iba1 was decreased at P21 compared to the earlier ages (SC: P8 vs P21 $p < 0.0001$, P14 vs P21 $p < 0.0001$; CA1: P8 vs P21 $p = 0.0005$, P14 vs P21 $p = 0.0004$) (Figure 25E). In the hippocampal CA3 area, percentage of CD68 in Iba1 steadily decreased from P8 to P21 (P8 vs P14 $p = 0.0310$, P8 vs P21 $p < 0.0001$, P14 vs P21 $p = 0.0015$). Sex-specific differences in percentage of CD68 in Iba1 followed the same direction across the developing brain (Table 17). In visual cortex layer 5, superior colliculus, and hippocampal CA1 and CA3 regions percentage of CD68 in Iba1 was higher in females at P8 and P14 (Table 17). However, in males, higher percentage of CD68 in Iba1 was observed when overall CD68 in Iba1 drops at P21.

These results indicate that phagocytic active areas in microglia peaks during the first two weeks of postnatal development and drops thereafter and does not follow the same trajectory in the developing male and female brain. In females, microglia get activated and deactivated earlier than in males.

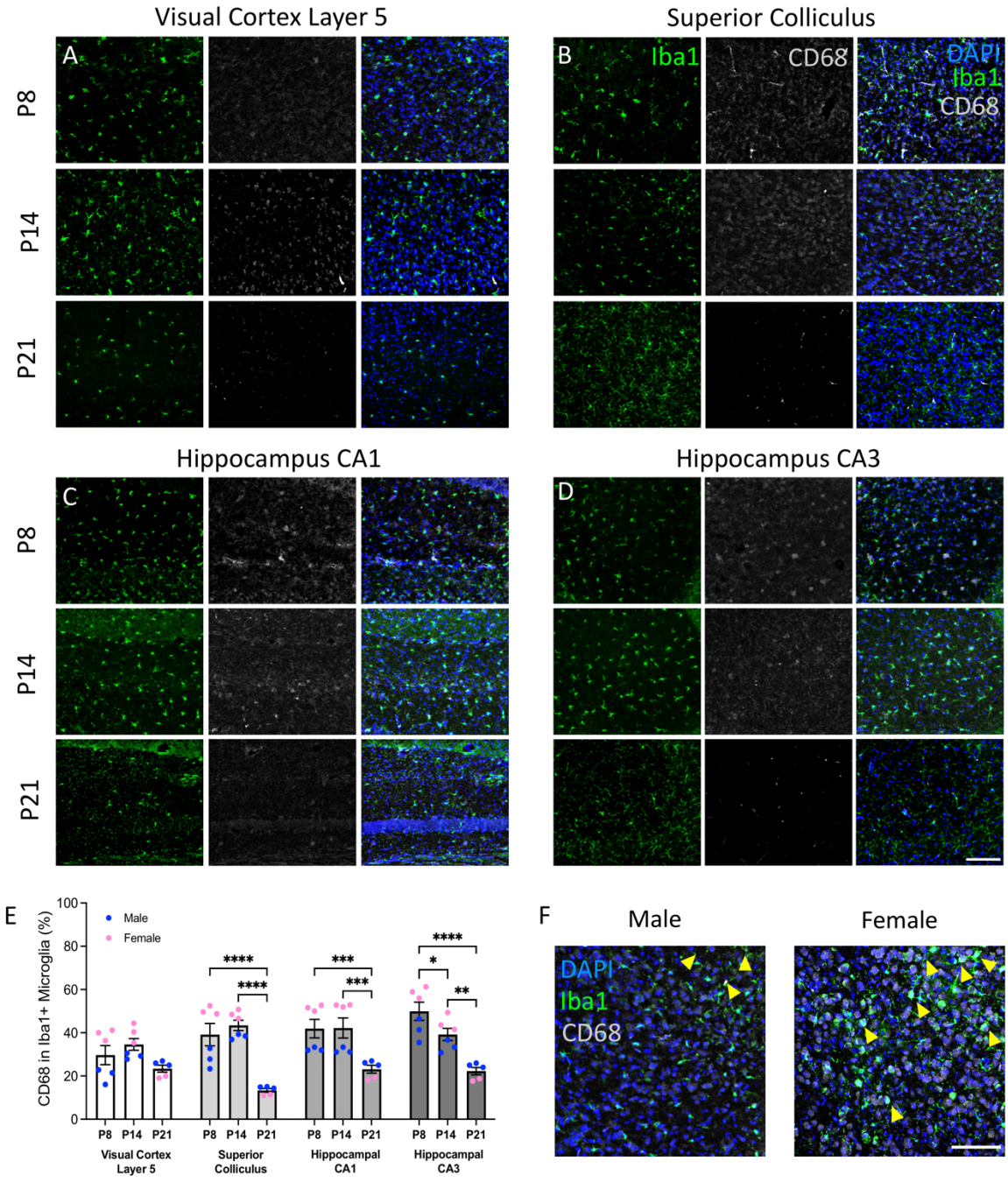


Figure 25:Differences in microglial phagocytic activity across developing brain

Representative images of Iba1 immunolabelled microglia (green) containing phagocytic compartments immunostained for CD68 (grey) at P8, P14, and P21 in visual cortex layer 5 (A), superior colliculus (B), CA1 (C), and CA3 (D). Immunoreactivity for CD68 expressed as a percentage of CD68+ microglial cells with respect to total Iba1+ microglial cells in the visual cortex layer 5, SC, CA1, CA3 at P8, P14, and P21 (two-way ANOVA, each dot represents an individual mouse, n = 5-6 per age group, male mice labelled in blue, female mice labelled in pink) (E). Representative images of Iba1/CD68 immunofluorescence showing microglial cells positive for CD68 (arrowheads) in the male and female. All data presented as mean ± SEM, * $p < 0.05$, ** $p < 0.01$, *** $p < 0.001$, **** $p < 0.0001$. Scale bar, 100 µm.

Microglia Phagocytic Activity (CD68 in Iba1+ microglia, %)						
	Visual Cortex L5			Superior Colliculus		
P8	**Male, n = 3**	**Female, n = 3**	***p***	**Male, n = 3**	**Female, n = 3**	***p***
	20.1092 ± 2.0477	39.1800 ± 1.4486	<0.0001	27.9792 ± 2.7257	50.2831 ± 1.1315	<0.0001
P14	**Male, n = 3**	**Female, n = 3**	***p***	**Male, n = 3**	**Female, n = 3**	***p***
	29.2005 ± 0.8026	39.9822 ± 2.6139	0.0006	38.2330 ± 0.7031	48.6004 ± 1.2135	0.0003
P21	**Male, n = 3**	**Female, n = 2**	***p***	**Male, n = 3**	**Female, n = 2**	***p***
	25.9497 ± 0.5553	19.5238 ± 0.4762	0.0278	14.7400 ± 0.2126	11.2212 ± 0.2004	0.1395
	Hippocampus CA1			Hippocampus CA3		
P8	**Male, n = 3**	**Female, n = 3**	***p***	**Male, n = 3**	**Female, n = 3**	***p***
	32.4023 ± 0.4657	51.4224 ± 0.7799	<0.0001	41.1114 ± 3.1501	58.7315 ± 1.5296	<0.0001
P14	**Male, n = 3**	**Female, n = 3**	***p***	**Male, n = 3**	**Female, n = 3**	***p***
	31.8260 ± 0.7538	52.5648 ± 0.3225	<0.0001	33.5897 ± 1.7073	44.8205 ± 2.3328	0.0019
P21	**Male, n = 3**	**Female, n = 2**	***p***	**Male, n = 3**	**Female, n = 2**	***p***
	26.0033 ± 0.5567	18.8131 ± 0.6313	<0.0001	24.9753 ± 0.5561	18.1985 ± 3.1787	0.05

Table 177: Microglial phagocytic activity changes in sex-specific manner

The percentage of Iba1 immunolabelled microglia containing phagocytic compartments immunostained for CD68 at P8, P14, and P21 in visual cortex layer 5, superior colliculus, and hippocampal CA1 and CA3 areas. All data presented as mean ± SEM, n = 2 – 3 mice per sex group.

3.2.3 Morphological differences of microglia in the developing brain

Since microglia have highly variable morphology which correlates with different functions of these cells I measured microglial volume, soma area, soma roundness, fractal dimension, primary branches and 3D Sholl analysis in the developing visual cortex layer 5 and hippocampal CA3 area of male and female mice. I performed all measurements on Iba1-immunolabelled microglia.

Significant differences in microglial volume were observed only in the developing visual cortex layer 5 (Figure 26A). Microglial volume was increased at P14 and P21 compared to P8 (p = 0.0162 and p = 0.0082, respectively, Figure 26B). Sex-specific differences in microglial volume

were observed (Figure 26B'). Microglial volume was only increased in males at P8 ($p = 0.0088$) and in females at P21 ($p = 0.0004$) in visual cortex but increased in females at P14 in both visual cortex layer 5 ($p < 0.0001$) and hippocampal CA3 ($p < 0.0001$, Figure 26B").

In the developing visual cortex layer 5 and hippocampal CA3 microglial soma size steadily decreased from P8 to P21 (L5: P8 vs P14 $p = 0.0245$, P8 vs P21 $p < 0.0001$, P14 vs P21 $p = 0.0047$; CA3: P8 vs P14 p = 0.0098, P8 vs P21 $p < 0.0001$, P14 vs P21 $p = 0.0100$, Figure 26C). Sex-specific differences in microglial soma size were observed only in visual cortex layer 5. Microglial soma size was slightly increased in females compared to males at P14 ($p = 0.0056$, Figure 26C'). Soma roundness was measured using Feret's method (WALTON, 1948), but no significant brain-region, development and sex-specific changes were observed (L5: P8 vs P14 $p = 0.3325$, P8 vs P21 $p = 0.2131$, P14 vs P21 $p = 0.5494$; CA3: P8 vs P14 $p = 0.4388$, P8 vs P21 $p = 0.4417$, P14 vs P21 $p = 0.9751$, Figure 26D, D', D").

To evaluate microglial cell complexity, I used the Fractal box count method (KARPERIEN et al., 2008). In the developing visual cortex layer 5 and hippocampal CA3, microglial complexity decreased from P8 to P21 (L5: P8 vs P14 $p < 0.0001$, P8 vs P21 $p < 0.0001$, P14 vs P21 $p < 0.0001$; CA3: P8 vs P21 $p < 0.0001$, P14 vs P21 $p < 0.0001$, Figure 26E). Sex-specific differences in microglial complexity were observed only in the developing visual cortex layer 5 (Figure 26E'). Increased microglial complexity was observed in males at P8 ($p = 0.0015$), but in females at P14 ($p < 0.0001$).

In visual cortex layer 5 and hippocampal CA3, the number of primary branches of microglia increased from P8 to P21 (L5: P8 vs P21 $p < 0.0001$, P14 vs P21 $p < 0.0001$; CA3: P8 vs P21 $p < 0.0001$, P14 vs P21 $p < 0.0001$, Figure 26F). Sex-specific differences in the number of primary branches were observed. The number of primary branches was increased in the female visual

cortex layer 5 (p = 0.0440) and hippocampal CA3 (p = 0.0167) at P8, but only in the female visual cortex at P14 (p = 0.0003).

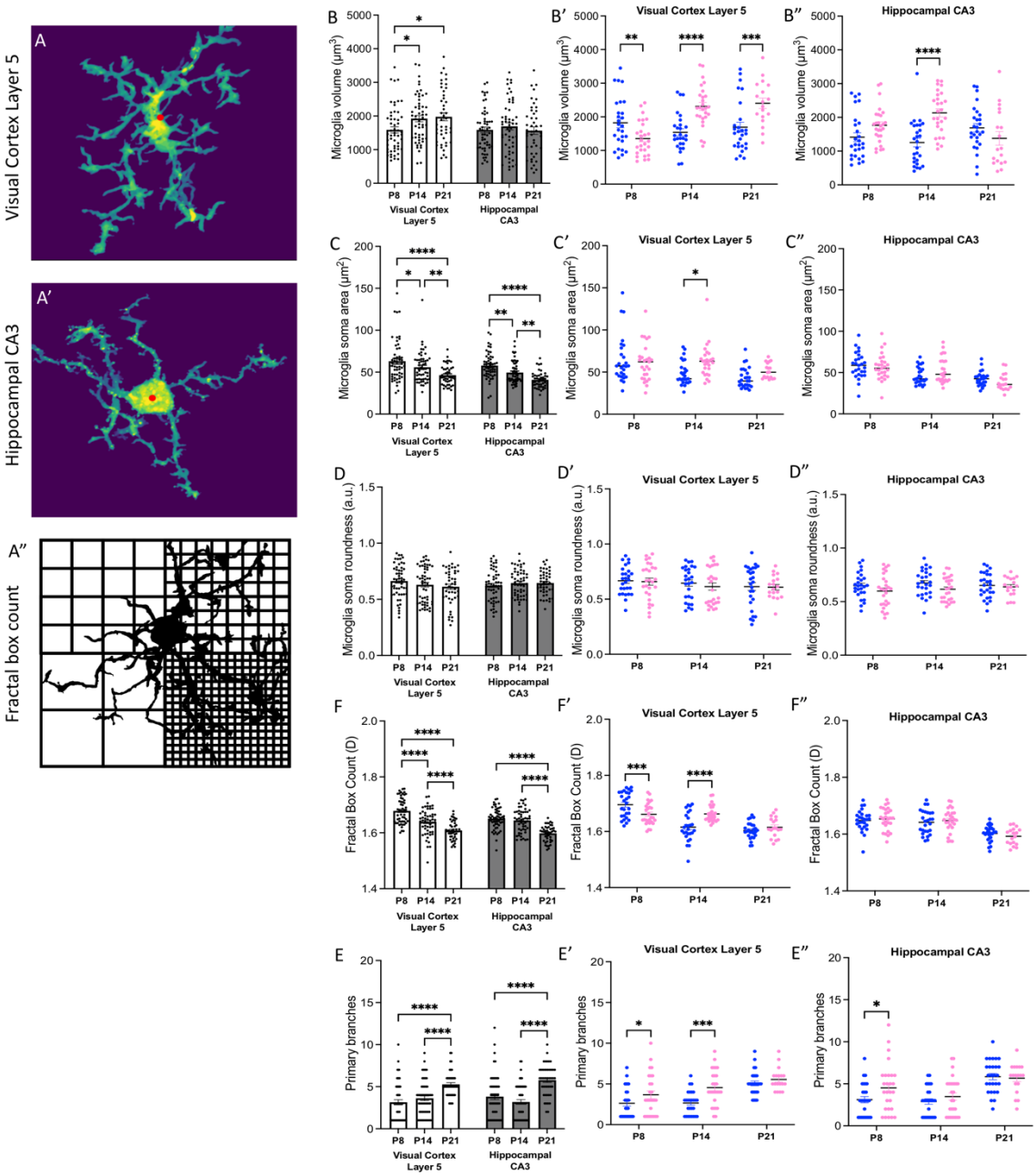


Figure 26: Morphological changes of microglia during early brain development

Representative images of 3D reconstructed Iba1+ microglia in visual cortex layer 5 (A) and hippocampal CA3 region (A'). Microglial size was assessed as Iba1+ volume and microglial volume changes between P8, P14 and and P21 in visual cortex layer 5 and hippocampus CA3 region (B) (each dot represents an individual cell, n = 45-54 per age group). Sex differences in microglial volume were

observed in developing visual cortex layer 5 (B') and hippocampal CA3 (B") at P8, P14 and P21 (each dot represents an individual cell, n = 18-27 per age group, males labelled in blue, females labelled in pink). In both, visual cortex layer 5 and hippocampal CA3 (C) microglial soma size (manually measured using ImageJ software NIH polygon selection tool) differs between P8, P14 and P21 (each dot represents an individual cell, n = 45-54 per age group). Sex-differences were observed in microglial soma size in visual cortex layer 5 (C') but no sex differences in hippocampal CA3 region (C") (each dot represents an individual cell, n = 18-27 per age group, males labelled in blue, females labelled in pink).. Soma roundness was calculated using Feret's method (Feret min divided by Feret max), no developmental, brain-region specific (D) (each dot represents an individual cell, n = 45-54 per age group) and sex differences (D', D") (each dot represents an individual cell, n = 18-27 per age group, males labelled in blue, females labelled in pink) were observed. Fractal analysis was used to determine microglia complexity (Fractal dimension, D) by using Fractal box count method (ImageJ NIH), in both, visual cortex layer 5 and hippocampal CA3 fractal dimension changes during development (E) (each dot represents an individual cell, n = 45-54 per age group). Sex-specific differences in fractal dimensions in visual cortex layer 5 (E') but no changes were observed in hippocampal CA3 (E") (each dot represents an individual cell, n = 18-27 per age group, males labelled in blue, females labelled in pink).. Manually quantified number of microglial primary branches increases during development in visual cortex layer 5 and hippocampal CA3 (F) (each dot represents an individual cell, n = 45-54 per age group). Sex differences in the number of microglial primary branches were observed in visual cortex layer 5 (F') and hippocampal CA3 region (F") (each dot represents an individual cell, n = 18-27 per age group, males labelled in blue, females labelled in pink). All data presented as mean ± SEM, * $p < 0.05$, ** $p < 0.01$, *** $p < 0.001$, **** $p < 0.0001$.

Sholl analysis of intersections were performed on 3D reconstructed Iba1+ cells. No significant changes in the sum of intersections were observed in the developing visual cortex layer 5 and hippocampal CA3 region, only sex-specific differences in the number of intersections were observed. In the developing visual cortex layer 5, the number of intersections was increased in females at P8 ($p = 0.0013$, Figure 27E' and 27G') and P21 ($p = 0.0467$, Figure 27E' and 27G"'). Although, in the hippocampal CA3 area, the number of intersections was increased in males at P14 ($p = 0.0031$, Figure 27E" and 27H"). Similar to the number of intersections, only sex-specific differences in 3D Sholl regression coefficient were observed. In hippocampal CA3, the regression coefficient was increased in females at P8 ($p = 0.0018$) and P21 ($p = 0.0030$), but decreased at P14 ($p < 0.0001$, Figure 27F").

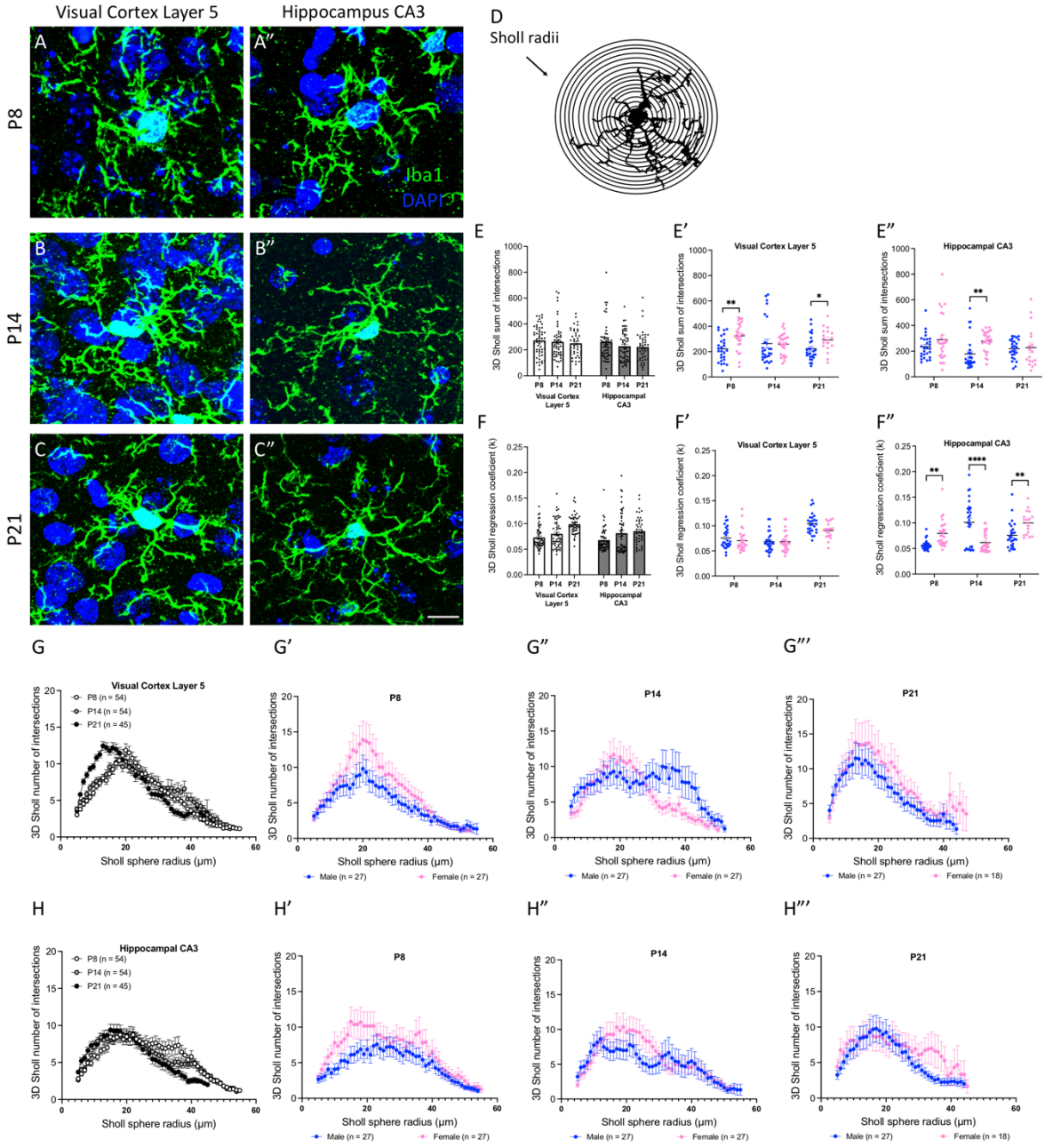


Figure 27: Ramification pattern dynamics of microglia in the developing brain

Representative cells immunolabelled with Iba1 (green) with different ramification patterns in visual cortex layer 5 at P8 (A), P14 (B), and P21 (C) and hippocampal CA3 area at P8 (A'), P14 (B'), and P21 (C'). Sholl analysis from 3D reconstruction (D – H"'). During the first three weeks of postnatal development, no differences in the number of intersections were observed (E) in visual cortex layer 5 (each dot represents an individual cell, n = 45-54 per age group). Sex-specific differences in the number of intersections were observed in visual cortex layer 5 (E') and hippocampal CA3 (E") (each dot represents an individual cell, n = 18-27 per age group, males labelled in blue, females labelled in pink). The regression coefficient describes how quickly branching of microglia decreases when moving away from the soma. No changes in the regression coefficient were observed at P8, P14 and P21 (F) (each

dot represents an individual cell, n = 45-54 per age group) as well as sex differences (each dot represents an individual cell, n = 18-27 per age group, males labelled in blue, females labelled in pink). in visual cortex (F'). Sex-specific differences in the regression coefficient were observed in hippocampal CA3 at P8, P14 and P21 (F") (each dot represents an individual cell, n = 18-27 per age group, males labelled in blue, females labelled in pink). 3D sholl analysis of microglia in developing visual cortex layer 5 (G) and hippocampal CA3 area (H) (each dot represents an individual cell, n = 45-54 per age group), and male and female mice (G' – G"', H'-H"') (each dot represents an individual cell, n = 18-27 per age group, males labelled in blue, females labelled in pink). All data presented as mean ± SEM, * $p < 0.05$, ** $p < 0.01$, *** $p < 0.001$, **** $p < 0.0001$.

These results indicate substantial morphological changes of microglia during early postnatal brain development. Between the first and third week of development, microglial cells become bigger with smaller soma. The number of microglial primary branches increase yet microglial processes remain consistent during development. Moreover, developmental changes of microglial morphology start earlier in females and microglial morphology reaches similar features at P21 in both male and female brains.

3.3 Discussion

3.3.1 Region- and sex-specific heterogeneity in microglia during development

Microglial cells are present in all brain regions, but are not evenly distributed and have different size, number of primary branches and branches/processes ramification patterns across different regions in the mammalian brain (Tan et al., 2020). In the adult mouse brain, areas of particularly high microglia density include hippocampus, basal ganglia, substantia nigra and olfactory telencephalon, and areas of lower density are the cerebellum and brainstem (Lawson et al., 1990; Stowell et al., 2018). Some early studies reported higher density of microglia in the forebrain, lower in the midbrain, and the lowest in the brainstem as well as cerebellum (Ehninger & Kempermann, 2003; Savchenko et al., 2000). In human brains, microglia density is lower in gray matter compared with white matter (Mittelbronn et al., 2001). In the developing CNS, microglia distribution changes very rapidly during the first month of postnatal development. For example in mice hippocampus, microglia density peaks at P15 (Paolicelli et al., 2011), in retina it peaks at P3 (Li et al., 2019), in parietal association cortex at P9 (DiBona et al., 2019), in frontal and somatosensory cortex at P14 (Mondo et al., 2020). To investigate microglial distribution during early postnatal brain development I measured microglial density in visual cortex, superior colliculus and hippocampal CA1 and CA3 regions at P8, P14 and P21. Characterizing microglial density provided a more detailed understanding of microglia's heterogeneous distribution across different brain regions. In the superior colliculus and hippocampal CA1 region, microglial density peaks at P14, but peaks later in hippocampal CA3. Interestingly, microglial density in the visual cortex and across different cortical layers remained unchanged and homogenous across the developmental time period studied. Since sex-specific differences in microglial cells have been demonstrated,

I further tested whether microglial distribution across the developing brain could differ between male and female mice. Although microglial density was homogeneous in the visual cortex, I observed higher microglial density in females than males across different cortical layers. Moreover, higher density of microglia was observed in female superior colliculus and hippocampal CA1, and yet remained homogenous and non-sex-specific in the hippocampal CA3 region. My results support uniform distribution of microglia across different brain regions, but this distribution has sex-specific differences.

3.3.2 Microglial phagocytic activity follows different trajectories in male and female brains during development

In the postnatal brain, microglia utilise a broad number of surface molecules in order to regulate their extracellular environment (Tay et al., 2017) and express markers such as CX3CR1, CD11b, CD45 and CD68. CD68 is a glycoprotein that is expressed at high levels by macrophages and amoeboid (or activated) microglia and at low levels by ramified (or resting) microglia (Tay et al., 2017). Recent studies showed that microglial activity is sexually dimorphic in the mouse hippocampus (Nelson et al., 2017) and higher activity was observed in females at P8 and males at P28 (Weinhard, Neniskyte, et al., 2018). Since microglia play an active role during early postnatal brain development, I further investigated active areas of microglia using CD68 labelling. Similar to microglial distribution, no differences in the percentage of CD68 in microglia were observed in visual cortex layer 5. In superior colliculus and hippocampal CA1, the percentage of CD68 in microglia is higher during the first two weeks of postnatal development and decreases at P21. Moreover, in the hippocampal CA3 region, more active areas of microglia were observed during the first week of postnatal development and steadily decreased until the end of the third week. Furthermore, CD68

signal in Iba1+ microglia was observed significantly earlier and more active areas of microglia were present at P8 and P14 in females than in males. After P14, more active regions of microglia were detected in males than in females. My results suggest that microglia in males get activated and deactivated later. It may be explained that microglial phagocytosis occurs earlier in females during development, and later in males (Weinhard, Neniskyte, et al., 2018).

3.3.3 Morphological changes of microglia in the developing male and female brains

It was believed that microglia as tissue resident macrophages only responded to brain injury, yet these cells are physiologically active, scanning their microenvironment by extending and retracting their branches and changing morphology. These functionally dynamic cells display a broad range of morphologies yet there is little agreement on subtypes or classification used to describe microglia. The terms “activated”, “reactive”, “ramified” “bushy”, “hypertrophic”, “deramified”, “resting” and “dystrophic” have been used to describe microglia (A. Karperien et al., 2013; Lawson et al., 1990; Soltys et al., 2005; Torres-Platas et al., 2014). However, it is still unclear how many subtypes microglia have. Different analysis methods are used for individual microglial morphology: cell and cell soma size, number of primary branches, Sholl analysis to describe ramification of processes (Morrison & Filosa, 2013), motility and mobility, fractal analysis to evaluate complexity of microglial structure (A. L. Karperien & Jelinek, 2015), process thickness, cell roundness and many more. In recent years, machine learning (ML) has been used to classify microglia (Leyh et al., 2021; Sagar et al., 2020) however this approach has many limitations. First, to get any statistically meaningful differences between microglia, thousands of images of microglia must be used with the same resolution and imaging features, and it would be difficult to apply if imaging properties were different. Second, while

mathematically the results are relevant, they are not biologically significant. Principal component (PC) analysis is another new approach to classify microglia. Principal components can provide a compound score based on multiple microglia morphological features and cluster microglia into different subtypes (Mabrouk, 2022). However, different mathematical approaches can be used to cluster microglia cells. Some authors showed that multiple shape properties have higher robustness than any single feature, yet no indication for distinct morphology types (Heindl et al., 2018). ML and PC are powerful and promising tools for microglia classification, however, the majority of those studies focused on pathological conditions (Heindl et al., 2018; Mabrouk, 2022; Soltys et al., 2005). In fact, microglial behaviour is different from physiological conditions or performed *in silico* (Mabrouk, 2022).

To better understand microglial morphological dynamics during development, I used many different analysis methods, and created an automated 3D Sholl analysis tool to evaluate microglial morphology, and I started microglia classification based on principal component analysis. However, due to time limitations, the principal component analysis based on different features of microglial morphology was not finished on time for thesis submission.

Morphology changes of individually analysed cells were similar between both visual cortex layer 5 and hippocampal CA3 microglia during development. In both brain regions, during the first three weeks of postnatal development, microglia increased in volume but reduced in soma size, as well as increased in primary branches but reduced in complexity/fractal dimension. 3D Sholl analysis showed homogeneity in microglial ramification patterns during early postnatal brain development and between two different brain regions.

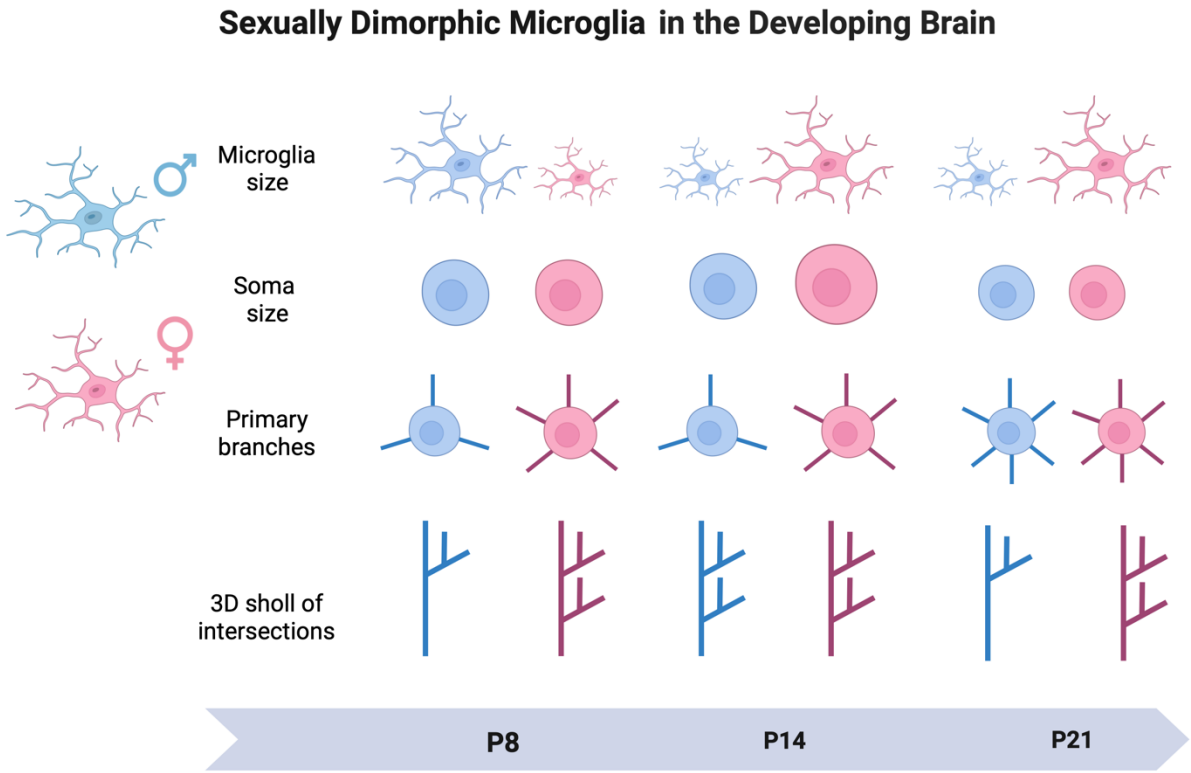


Figure 28: Sex-specific differences in microglial morphology during brain development

Created with BioRender.com

Microglial morphology was different between male and female during brain development (Figure 28). During the first week of postnatal development, microglia are smaller in female brains yet have more primary branches. Microglia increase in cell and cell soma size during the second postnatal week in female brains and have more primary branches compared to males. 3D Sholl analysis indicated that in females, microglial cells have more branches at P8 and at P21 in the visual cortex, but less at P14 in the hippocampus compared to males. At the first week of postnatal development, microglia have similar features in the developing male and female mice, yet cells are bigger in females.

This detailed morphological analysis of microglia indicates that these cells do not follow the same developmental trajectory in male and female mice. This most likely contributes to sex-specific network formation. Morphological features such as microglial size, soma size, the number of primary branches and branches/processes ramification patterns could be potentially used as key features to classify microglia in the developing brain under normal conditions. In particular, different morphology of microglia between male and female mice might be one of the reasons why the classification of microglia is incredibly complicated especially in physiological conditions and during development.

In fact, the human and rodent brains have different microglia signatures and regional distribution. It remains unclear how morphological differences of microglia contribute to function and further studies correlating anatomy with function are necessary. Detailed microglial morphological and functional analysis would help to revolutionise neuropathological evaluation and avoid any bias since microglial phenotypes are still determined by visual investigation. Furthermore, it would help to understand microglial cells' precise dynamics and how they contribute to altering brain networks is likely to help design therapeutic strategies to enhance their activity, limit the damage that could be caused by their activation and/or use these cells as a diagnostic biomarker in disease.

In the following chapter I will be presenting results on microglial morphological and functional changes in the developing brain when synaptic activity is altered and the consequences that lead to miscommunication between microglia and neurons.

Chapter 4: Microglia are involved in activity-dependent neuronal network formation and maturation

4.1 Introduction

In the past decade, the study of microglia has rapidly expanded. One of the paradigms explaining synaptic pruning suggests that neuron-microglia interactions may be activity-dependent (Schafer et al., 2012; Wake et al., 2013). It has been shown that microglial cells are able to generate glutamate neurotransmitters as well as respond to any changes to in neurotransmission by changing their morphology (McMullan et al., 2012; Noda et al., 2000). Moreover, microglia stimulation with ionomycin, an ionophore that binds calcium ions (Ca^{2+}), indicates that microglia themselves release ATP and in a calcium and SNARE complex-dependent manner (Imura et al., 2013).

4.1.1 SNARE complex and microglia

The soluble N-ethylmaleimide fusion protein attachment protein receptor (SNARE) complex is universally involved in membrane fusion (Figure 29) (Han et al., 2017; Jena, 2011; Pobbati et al., 2006), synaptic vesicle trafficking and is essential for neuronal maintenance (Barrecheguren et al., 2017; Hay, 2001; Nicholson et al., 1998; Ulloa et al., 2018; Washbourne et al., 2002). The central components of the SNARE complex are synaptosomal-associated protein 25 (SNAP25), vesicle-associated membrane protein (VAMP) or synaptobrevin and syntaxin family proteins. Other essential proteins such as Munc13 and 18, synaptophysin and synaptotagmin interact and regulate the SNARE complex. SNARE protein expression changes throughout life suggesting a different role of these proteins during development (Greenlee et al., 2001, 2002; Prescott & Chamberlain, 2011). The formation of the SNARE complex

mediates exocytosis that occurs due to close interaction between the plasma and vesicle membrane proteins. SNARE complex machinery requires several steps, conformational changes of the molecules and involves different components as integral parts. Due to this reason each member of the SNARE complex has a precise role and even the slightest changes can disrupt synaptic vesicle fusion resulting in impaired neuronal formation, communication, and maintenance (Han et al., 2017; Hay, 2001; Jena, 2011; Ulloa et al., 2018).

Some studies indicate a microglial cells interaction with SNARE complex. In the absence of microglia, SNARE protein expression shows an upregulation of VAMP2 and seems to be involved in cross-talk within astrocytes by securing proper gliotransmission (Takata-Tsuji et al., 2021). Moreover, microglial cells themselves express Snap25 paralog Snap23 which is involved in phagocytic processes (Hepp et al., 1999; Rojewska et al., 2018). It has been shown that overexpression of Munc18 reduces the number of cortical microglia in mouse brains (Gil-Pisa et al., 2014). However, the relationship between microglia and SNARE complex machinery remains largely unexplored.

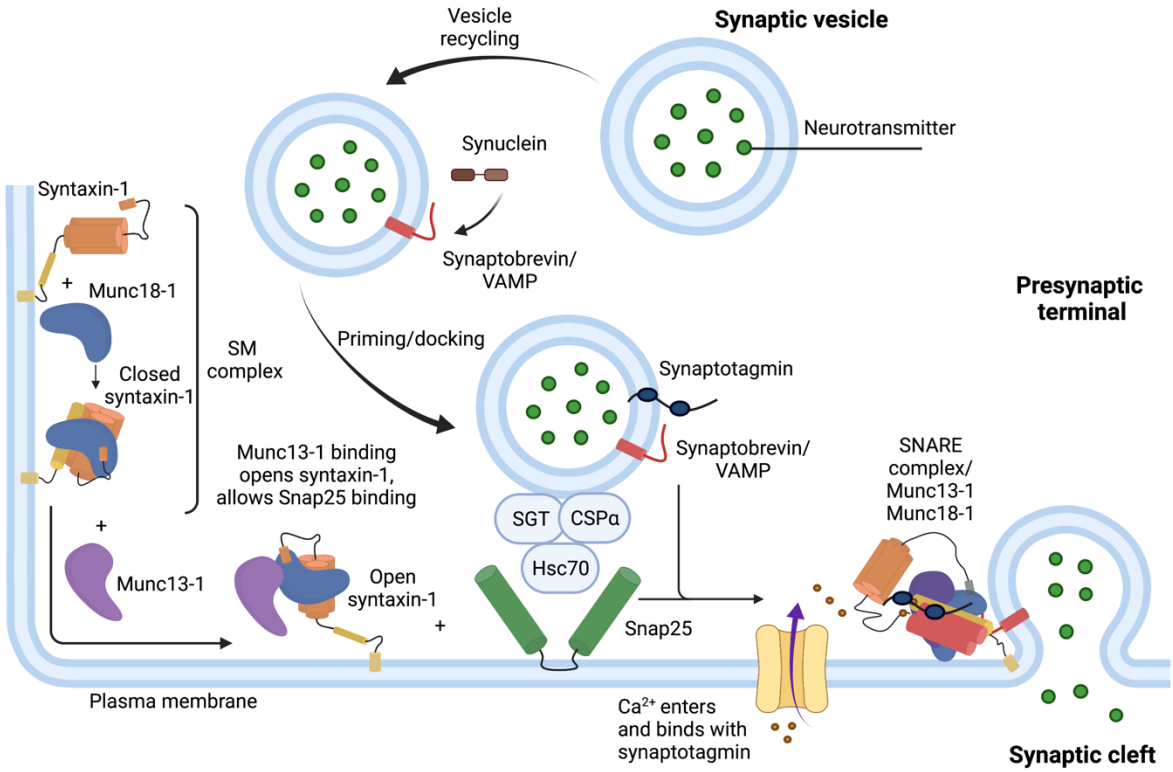


Figure 29: Overview of the functions of SNAREs, Snap25, and some of their accomplices at the synaptic terminal

Synaptobrevin (red) is shown on synaptic vesicles as a largely unstructured protein that binds to synuclein (brown). Syntaxin-1 [Habc domain and N-peptide (orange), SNARE motif (yellow)] is anchored on the plasma membrane and initially forms a closed conformation that binds to Munc18-1 (blue). SNAP-25 (green) is maintained in a state that is competent for SNARE-complex assembly by interactions with Hsc70 and its co-chaperones CSPα and SGT. Synaptic vesicle fusion requires assembly of the SNARE complex (bottom right), which is orchestrated in part by Munc18-1 and the Munc13-1 MUN domain (purple). Munc18-1 and perhaps also the MUN domain likely cooperate with the SNAREs in inducing membrane fusion. Synuclein assists in SNARE-complex assembly by as-yet unidentified interactions. After fusion, the SNARE complex is disassembled by NSF and SNAPs, and synaptobrevin is sorted to the synaptic vesicles. The same colour coding is used in all the figures, except that Munc18-1 is depicted with different shades of blue in Figure 4.1. Abbreviations: CSP, cysteine string protein; NSF, N-ethylmaleimide sensitive factor; SGT, small glutamine-rich protein; SNAPs, soluble NSF adaptor proteins; SNARE, SNAP receptor; SNAP-25 synaptosomal associated protein of 25 kDa (Adapted from (Rizo & Südhof, 2012)). Created with BioRender.com

4.1.2 Synaptosomal-associated protein 25 (Snap25)

Synaptosomal-associated protein of 25 kDa (Snap25) is an important component of the SNARE protein complex. Snap25 is highly expressed during early postnatal development in neurons and shifts its localization from axons and cell bodies to synaptic terminals in adults (Figure 29) (Oyler et al., 1991, 1992). Moreover, it is directly involved in neurotransmitter release, axonal growth and motor coordination (Heyser et al., 1995; Osen-Sand et al., 1993). Beyond neurotransmitter release SNAP25 protein plays a role in the modulation of voltage-gate calcium channels (Condliffe et al., 2010; Weiss et al., 2012), clathrin-dependent endocytosis (Xu et al., 2013; Z. Zhang et al., 2013), and postsynaptic receptor trafficking *in vitro* (Jurado et al., 2013; Lau et al., 2010).

Snap25 is found in two isoforms in neurons, Snap25a and Snap25b. It has been shown that Snap25a participates in axonal outgrowth and neurite sprouting, and Snap25b is necessary for rapid release of neurotransmitter (Bark et al., 1995; Boschert et al., 1996; Shirasu et al., 2000). Moreover, Snap25 is an important player for cognitive functioning (Gosso et al., 2006), long-term memory consolidation (Q. Hou et al., 2004; Q. L. Hou et al., 2006) and neuronal survival as it is responsible for the recycling of proteins on the plasma membrane (Peng et al., 2013).

However, it remains unclear how microglia are involved in synaptic vesicle release and trafficking under normal conditions, and whether there is direct or indirect interaction with SNARE complex proteins. To evaluate how neuronal activity changes the behaviour and

dynamic of microglia I removed the expression of Snap25, which is essential for regulated synaptic vesicles release and examined whether synaptic ‘silencing’ affects neuron-microglia interactions and neuronal network maturation in the developing brain.

4.2 Results

4.2.1 Conditional Snap25 knockout mouse model

A conditional Snap25 knockout mouse line was developed using the Cre-LoxP recombinase system (Figure 30). Snap25$^{fl/fl}$ is a transgene with LoxP sites flanking the alternatively spliced exons 5a and 5b of the SNARE gene *Snap25*. The *Snap25*$^{fl/fl}$ (B6-Snap25tm3mcw) strain was crossed to *Ai14* (B6;129S6-Gt(ROSA)26Sortm14(CAG-tdTomato)Hez/J). The LoxP sites themselves do not have any activity (behave as a normal wild type), and it was crossed to a mouse expressing Cre recombinase *Rbp4*^{Cre} (Tg(Rbp4-cre)KL100gsat). *Ai14* is a Cre-dependent reporter allele with a LoxP flanked STOP cassette. *Rbp4*^{Cre} is expressed in a subpopulation of layer 5 cortical neurons and expression starts. It has been previously shown by Molnár group that Cre recombinase expression starts during late embryonic development (Hoerder-Suabedissen et al., 2019). tdTomato (red fluorescent reporter) is expressed continuously once the STOP cassette has been removed by Cre-recombinase and labels all cells that expressed Cre at any stage of development (Figure 31). Importantly, in our breeding scheme, Cre recombinase was inherited through the female line, since inheritance through the male line was observed to result in body-wide Cre activation, rather than cell-type specific activation and would be predicted to result in full knock-out rather than conditional knock-out (Hoerder-Suabedissen et al., 2019).

The following abbreviations will be used: *Rbp4*^{Cre}*/+;Ai14;Snap25*$^{fl/fl}$ mouse as Snap25 cKO to indicate conditional knockout of SNAP25; Cre-negative littermates, *Rbp4+/+;Ai14;Snap25*$^{+/+}$ used as control.

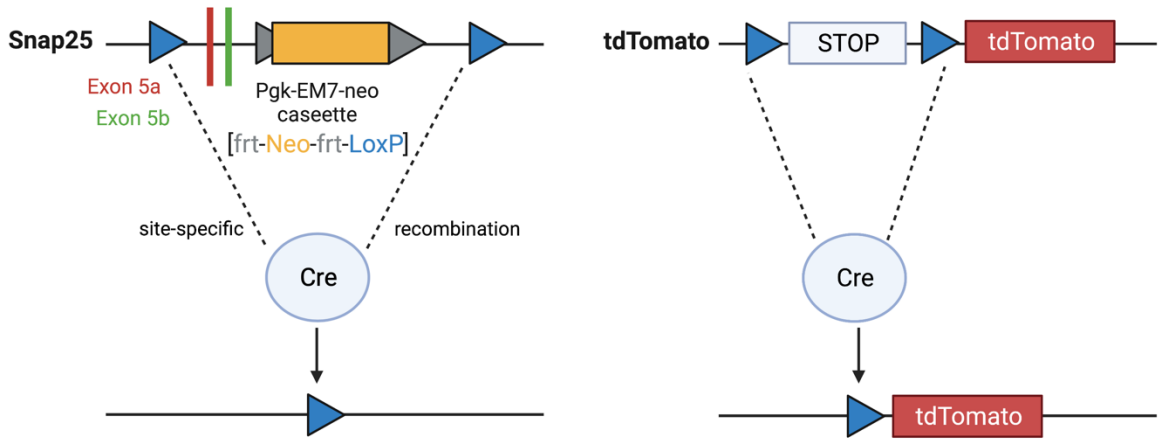


Figure 30: Cre-LoxP system to develop Snap25 cKO *(Rbp4^{Cre}/+;Ai14;Snap25$^{fl/fl}$)* mice strain

Snap25 schematic indicated the location of temporarily inserted recombination cassette and LoxP site location (blue triangle). Exons 5a and 5b were flanked by LoxP. In presence of Cre-recombinase, stop-codon (light blue rectangle) upstream of tdTomato-gene (red rectangle) is excised (adapted from (Hoerder-Suabedissen et al., 2019)). Created with BioRender.com

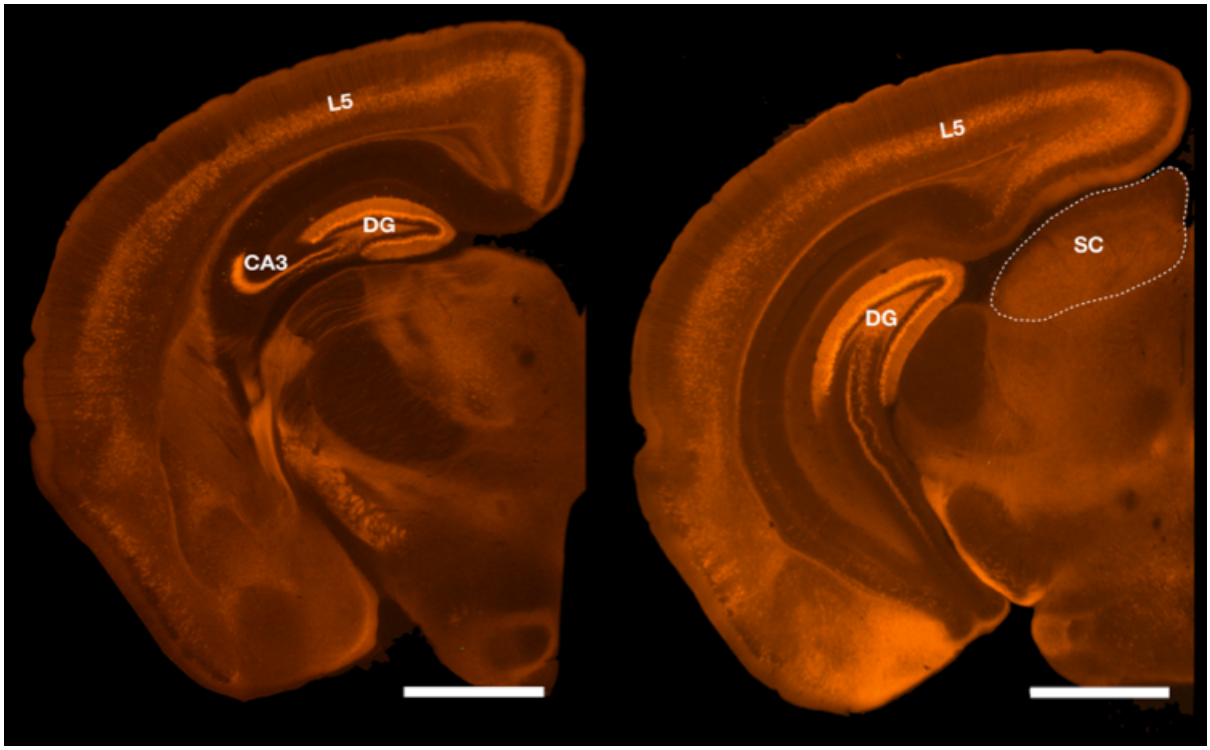


Figure 31: Cre expression in Snap25 cKO *(Rbp4^{Cre}/+;Ai14;Snap25$^{fl/fl}$)* mouse brains

Cre positive population of cortical layer 5 (L5) projection neurons and their projections to superior colliculus (SC), and higher order thalamic nuclei of PO and LP and Cre positive selected population of hippocampal dentate gyrus (DG) granule cells and their projections to cornus ammonis 3 (CA3) area. Scale bar = 1mm

To investigate whether abolished regulated release of neurotransmitter vesicles affects the dynamic of microglia in developing brains I studied a subgroup of layer 5 cortical projections neurons ($Rbp4^{Cre}$). I examined the microglial behaviour in proximity of the cell bodies in the visual cortex layer 5 and in their projection in the superior colliculus at P8, P14 and P21. I also examined the effects of changed neuronal activity within another projection neuron population that also had cre recombinase activity in the Rbp4-Cre line in the dentate gyrus of the hippocampus and at the terminal of their mossy fiber projections in the CA3 region at P8, P14 and P21. In my 'silenced' mouse model these particular neurons in cortical layer 5 and dentate gyrus were no longer able to release synaptic vesicles in an organized fashion from around birth which was validate in our previous studies (Hoerder-Suabedissen et al., 2019). In addition, I also studied the hippocampal CA1 region since CA3 pyramidal neurons project to the CA1 via the Schaffer collaterals and this region has been the most studied in terms of synaptic pruning, and neuronal network remodelling.

4.2.1 Synaptic 'silencing' affects microglial cell distribution and morphological features across brains during development

To understand whether abolished regulated release of neurotransmitter vesicles affects microglial behaviour across different brain regions in the developing Rbp4-Cre:$Snap25^{fl/fl}$ brain I first evaluated microglial density in control and Snap25 cKO mice visual cortex layer 5 (Figure 32A), superior colliculus (Figure 32B), hippocampal CA1 (Figure 32C) and CA3 (Figure 32D) at P8, P14 and P21. Microglial cells were identified through their immunoreactivity to Iba1 epitopes detected using anti-Iba1 antibody and visualized by confocal microscopy.

Microglial density was increased in Snap25 cKO compared to control mice only in visual cortex layer 5 at P21 (p = 0.0076, Figure 32A') and in the hippocampal CA3 at P8 (p = 0.0389) and P14 (p = 0.0004, Figure 32D'). The opposite effect of synaptic 'silencing' was observed in the hippocampal CA1 region where microglial density was decreased at P14 (p = 0.0091, Figure 32C'). However, no significant differences in microglial density were observed in superior colliculus (Figure 32B'). Interestingly, significant sex-specific differences in microglial density in Snap25 cKO mice were observed (Table 18). At P8, microglial density was increased in Snap25 cKO males compared to control males in visual cortex layer 5 (p = 0.0012), superior colliculus (p < 0.0001), and hippocampal CA1 (p < 0.0001) and CA3 (p = 0.0009), yet only in Snap25 cKO females compared to control females (p < 0.0001) in the CA3. Interestingly, microglial density was increased in Snap25 cKO males compared to Snap25 cKO females only in visual cortex layer 5 (p = 0.0074) yet decreased in the CA3 (p = 0.0065). Later in the development, microglial density was increased in Snap25 cKO males compared to control males in visual cortex layer 5 (P14: p = 0.0110 and P21: p < 0.0001) and in the hippocampal CA3 region (P14: p < 0.0001 and P21: p = 0.0081), and in the hippocampal CA1 but only at P21 (p = 0.0084). In females, microglia density was decreased only in the hippocampal CA1 Snap25 cKO mice (P14: p < 0.0001 and P21: p < 0.0001) yet increased in the hippocampal CA3 (P14: p < 0.0001 and P21: p < 0.0001). Sex-specific differences were also observed between Snap25 cKO males and females. Microglial density was increased in females at P14 (p = 0.0275) and P21 (p = 0.0006) in superior colliculus. In hippocampus, synaptic 'silencing' affected microglial density in the same fashion in both regions. Microglial density was decreased in Snap25 females compared to males at P14 (CA1: p = 0.0010 and CA3: p = 0.0119) yet increased at P21 (CA1: p = 0.0003 and CA3: p = 0.0003).

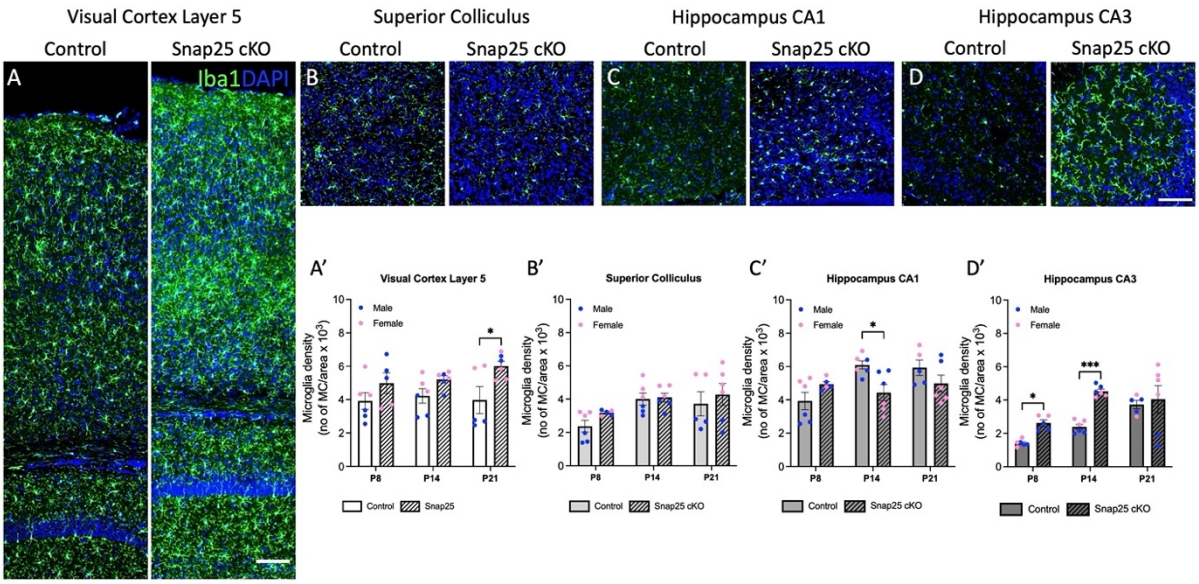


Figure 32: Sex-specific changes of microglial cells density across the brain in developing control and Snap25 cKO *(Rbp4^{Cre}/+;Ai14;Snap25$^{fl/fl}$)* mice

Representative images of Iba1+ microglia (green) counter stained with DAPI (blue) between control and Snap25 cKO (pattern) mice in visual cortex (A), superior colliculus (B), hippocampal CA1 (C) and CA3 (D) regions. Microglial density changes between control and Snap25 cKO animals and differences between male (blue) and female (pink) mice in developing visual cortex layer 5 (A'). I observed no significant changes in microglial density between control and Snap25 cKO mice at P8, P14 and P21 in superior colliculus (B') but my analysis revealed difference between male and female mice. In hippocampal CA1 (C'), microglial density changes between control and Snap25 cKO, and male and female mice. In hippocampal CA3 (D'), microglial density changes between control and Snap25 cKO, and male and female mice (two-way ANOVA, each dot represents an individual mouse, n = 5-6 per age group). All data presented as mean ± SEM, * $p < 0.05$, ** $p < 0.01$, *** $p < 0.001$, **** $p < 0.0001$. Scale bar, 100 µm.

Microglia Density (total number of microglial cells/μm^2 x10^3)									
Visual Cortex Layer 5									
P8	**Control Male, n = 3**	**Snap25 cKO Male, n = 3**	***p***	**Control Female, n = 3**	**Snap25 cKO Female, n = 2**	***p***	**Snap25 cKO Male, n = 3**	**Snap25 cKO Female, n = 2**	***p***
	2.9823 ± 0.2359	5.9186 ± 0.4230	0.0012	4.8592 ± 0.5595	3.5811 ± 0.1164	0.0813	5.9186 ± 0.4230	3.5811 ± 0.1164	0.0074
P14	**Control Male, n = 3**	**Snap25 cKO Male, n = 3**	***p***	**Control Female, n = 3**	**Snap25 cKO Female, n = 3**	***p***	**Snap25 cKO Male, n = 3**	**Snap25 cKO Female, n = 3**	***p***
	3.4107 ± 0.4229	4.9546 ± 0.3714	0.0110	5.0345 ± 0.3319	5.4732 ± 0.1139	0.3770	4.9546 ± 0.3714	5.4732 ± 0.1139	0.3010
P21	**Control Male, n = 3**	**Snap25 cKO Male, n 2**	***p***	**Control Female, n = 2**	**Snap25 cKO Female, n = 4**	***p***	**Snap25 cKO Male, n 2**	**Snap25 cKO Female, n = 4**	***p***
	2.6515 ± 0.0946	6.4688 ± 0.1398	0.0001	5.9625 ± 0.0731	5.7747 ± 0.4007	0.6992	6.4688 ± 0.1398	5.7747 ± 0.4007	0.1802
Superior Colliculus									
P8	**Control Male, n = 3**	**Snap25 cKO Male, n = 3**	***p***	**Control Female, n = 3**	**Snap25 cKO Female, n = 2**	***p***	**Snap25 cKO Male, n = 3**	**Snap25 cKO Female, n = 2**	***p***
	1.6027 ± 0.1833	3.1891 ± 0.0847	<0.0001	3.1522 ± 0.0728	3.1727 ± 0.1845	0.9222	3.1891 ± 0.0847	3.1727 ± 0.1845	0.9377
P14	**Control Male, n = 3**	**Snap25 cKO Male, n = 3**	***p***	**Control Female, n = 3**	**Snap25 cKO Female, n = 3**	***p***	**Snap25 cKO Male, n = 3**	**Snap25 cKO Female, n = 3**	***p***
	3.2936 ± 0.1616	3.5969 ± 0.2355	0.4409	4.7201 ± 0.3903	4.6032 ± 0.2144	0.7628	3.5969 ± 0.2355	4.6032 ± 0.2144	0.0275
P21	**Control Male, n = 3**	**Snap25 cKO Male, n 2**	***p***	**Control Female, n = 2**	**Snap25 cKO Female, n = 4**	***p***	**Snap25 cKO Male, n 2**	**Snap25 cKO Female, n = 4**	***p***
	2.5537 ± 0.1813	2.3703 ± 0.3658	0.7350	5.4876 ± 0.0092	5.2478 ± 0.3887	0.6423	2.3703 ± 0.3658	5.2478 ± 0.3887	0.0006
Hippocampus CA1									
P8	**Control Male, n = 3**	**Snap25 cKO Male, n = 3**	***p***	**Control Female, n = 3**	**Snap25 cKO Female, n = 2**	***p***	**Snap25 cKO Male, n = 3**	**Snap25 cKO Female, n = 2**	***p***
	2.7853 ± 0.1691	4.8021 ± 0.1496	<0.0001	5.0787 ± 0.1446	5.1371 ± 0.3413	0.8413	4.8021 ± 0.1496	5.1371 ± 0.3413	0.2722
P14	**Control Male, n = 3**	**Snap25 cKO Male, n = 3**	***p***	**Control Female, n = 3**	**Snap25 cKO Female, n = 3**	***p***	**Snap25 cKO Male, n = 3**	**Snap25 cKO Female, n = 3**	***p***
	5.7919 ± 0.3413	5.4722 ± 0.2469	0.4599	6.4007 ± 0.3259	3.4002 ± 0.2356	<0.0001	5.4722 ± 0.2469	3.4002 ± 0.2356	0.0010
P21	**Control Male, n = 3**	**Snap25 cKO Male, n 2**	***p***	**Control Female, n = 2**	**Snap25 cKO Female, n = 4**	***p***	**Snap25 cKO Male, n 2**	**Snap25 cKO Female, n = 4**	***p***
	5.2202 ± 0.2518	6.5114 ± 0.1845	0.0084	6.9909 ± 0.2951	4.2241 ± 0.1918	<0.0001	6.5114 ± 0.1845	4.2241 ± 0.1918	0.0003
Hippocampus CA3									
P8	**Control Male, n = 3**	**Snap25 cKO Male, n = 3**	***p***	**Control Female, n = 3**	**Snap25 cKO Female, n = 2**	***p***	**Snap25 cKO Male, n = 3**	**Snap25 cKO Female, n = 2**	***p***
	1.3834 ± 0.0464	2.3365 ± 0.1430	0.0009	1.4572 ± 0.1704	3.0712 ± 0.0092	<0.0001	2.3365 ± 0.1430	3.0712 ± 0.0092	0.0065
P14	**Control Male, n = 3**	**Snap25 cKO Male, n = 3**	***p***	**Control Female, n = 3**	**Snap25 cKO Female, n = 3**	***p***	**Snap25 cKO Male, n = 3**	**Snap25 cKO Female, n = 3**	***p***
	2.0623 ± 0.0527	4.7711 ± 0.1569	<0.0001	2.7238 ± 0.1034	4.2923 ± 0.0753	<0.0001	4.7711 ± 0.1569	4.2923 ± 0.0753	0.0119
P21	**Control Male, n = 3**	**Snap25 cKO Male, n 2**	***p***	**Control Female, n = 2**	**Snap25 cKO Female, n = 4**	***p***	**Snap25 cKO Male, n 2**	**Snap25 cKO Female, n = 4**	***p***
	3.7750 ± 0.2377	1.5634 ± 0.3257	0.0081	3.6613 ± 0.6557	5.2873 ± 0.3714	0.0252	1.5634 ± 0.3257	5.2873 ± 0.3714	0.0003

Table 18: Microglial density changes between control and Snap25 cKO mice in sex-specific manner

Sex-specific differences of microglial density in visual cortex layer 5, superior colliculus, and hippocampal CA1 and CA3 regions. All data presented as mean ± SEM, n = 2 – 3 mice per sex group.

To further understand the synaptic 'silencing' effect on microglial behaviour, I measured individual microglial cell volume, soma size, soma roundness, fractal dimension, primary branches and 3D Sholl in control and Snap25 cKO mice visual cortex layer 5 and hippocampal CA3 region of male and female mice at P8, P14 and P21. All measurements were performed on microglia that was revealed through their Iba1 immunoreactivity.

In visual cortex layer 5, microglial volume was significantly decreased in Snap25 cKO mice comparted to control at P14 and P21 (p = 0.0012 and p < 0.0001 respectively, Figurec33C). Sex-specific changes in microglial volume were observed. At P8, microglial volume was decreased in Snap25 cKO males compared to control males (p = 0.0068) and in control females compared to control males (p = 0.0036, Figure 33C'). At P14, microglial volume was increased in control females compared to control males (p < 0.0001) and Snap25 cKO females compared to Snap25 cKO males (p < 0.0001, Figure 33C"). Moreover, microglial volume was decreased in Snap25 cKO males compared to control males (p = 0.0009) and in Snap25 cKO females compared to control females (p = 0.0092, Figure 33C"). At P21, microglia volume was increased in control females compared to control males (p = 0.0004) and Snap25 cKO females compared to Snap25 cKO males (p = 0.0007, Figure 33C"'). In addition, microglial volume was decreased in Snap25 cKO males compared to control males (p = 0.0004) and in Snap25 cKO females compared to control females (p < 0.0001, Figure 33C"').

In the hippocampal CA3 region, microglial volume was significantly decreased in Snap25 cKO mice compared to control at P14 and P21 (p < 0.0001 and p = 0.0003 respectively, Figure 33D). No sex-specific changes in microglial volume were observed at P8 (Figure 33D') but microglial volume was different between male and female mice at P14 and P21. At P14, microglial volume was increased in control females compared to control males and Snap25 cKO females compared to Snap25 cKO males (p < 0.0001 and p = 0.0036 respectively, Figure 33D") but

decreased in Snap25 cKO females compared to control females ($p < 0.0001$, Figure 33D”). At P21, microglial volume was decreased in Snap25 cKO males compared to control males ($p = 0.0017$, Figure 33D”’).

No changes in primary branches were observed between control and Snap25 cKO mice visual cortex layer 5 (Figure 33E), and sex-specific changes were observed only at P14 ($p = 0.0006$, Figure 33E”), but no significant differences at P8 (Figure 33E’) and P21 (Figure 33E”’).

In the hippocampal CA3 area, primary branches were increased in Snap25 cKO at P14 ($p = 0.0014$), but decreased at P21 ($p = 0.0020$) compared to control mice (Figure 33F). No sex-specific differences were observed at P8 (Figure 33F’), but increased number of branches were observed in Snap25 cKO females compared to control females at P14 ($p = 0.0353$, Figure 33F”) and decreased in Snap25 cKO males compared to control males at P21 ($p = 0.0030$, Figure 33F”’).

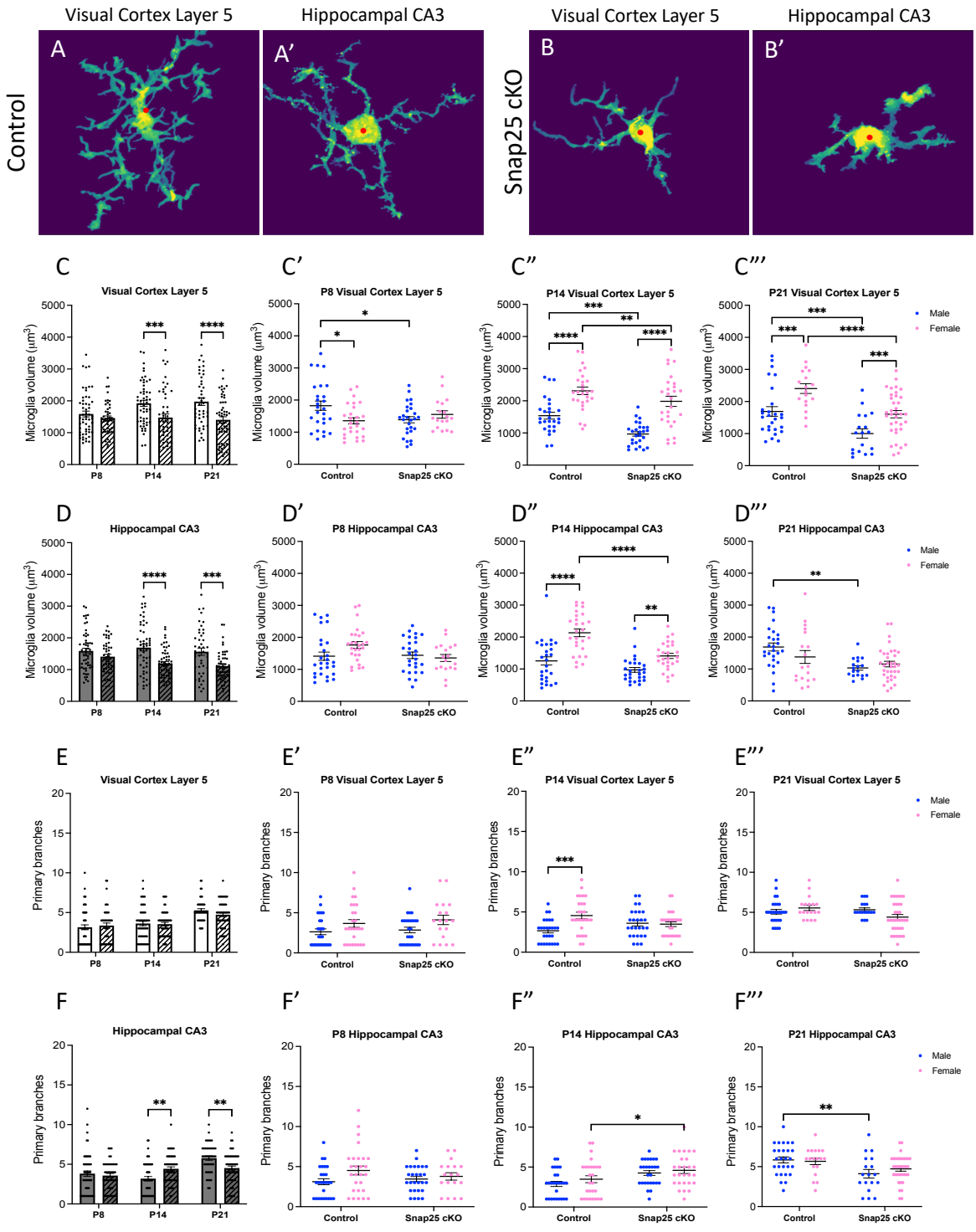


Figure 33:Lack of Snap25 affects microglial volume and primary branches in the developing brain

Visual cortex layer 5 control (white color) and Snap25 cKO (white color with pattern) mice. Hippocampal CA3 control (grey color) and Snap25 cKO (grey color with pattern) mice. Representative images of 3D reconstructed Iba1+ microglia in control mice visual cortex layer 5 (A) and hippocampus CA3 (A') and Snap25 cKO mice in visual cortex layer 5 (B) and hippocampal CA3 (B'). Microglial size as assessed as Iba1+ volume and microglial volume changes between control and Snap25 cKO mice in visual cortex layer 5 (C). Sex differences in microglial volume were observed in developing visual cortex

at P8 (C'), P14 (C") and P21 (C"'). In hippocampal CA3, microglial volume changes between control and Snap25 cKO mice (D). Sex differences in microglial volume were observed in developing hippocampal CA3 region at P8 (D'), P14 (D") and P21 (D"'). No changes in the number of primary branches were indicated between control and Snap25 cKO mice at P8, P14 and P21 in visual cortex layer 5 (E). Sex differences in primary branches were observed in developing visual cortex (E', E", E"'). The number of primary branches changes between control and Snap25 cKO in hippocampal CA3 (F). Sex differences in primary branches were observed in developing hippocampal CA3 region (F', F", F"'). (two-way ANOVA, each dot represents an individual cell, n = 18-27 per age group, males labelled in blue, females labelled in pink). All data presented as mean ± SEM, * $p < 0.05$, ** $p < 0.01$, *** $p < 0.001$, **** $p < 0.0001$.

I observed differences in microglial soma size in developing visual cortex layer 5 between control and Snap25 cKO mice (Figure 34A). Microglial soma size was increased in Snap25 cKO compared to control at P8 ($p = 0.0004$). No sex-specific differences were observed at P8 (Figure 34A') but microglial soma size was increased in control females compared to males at P14 ($p = 0.0014$, Figure 34A") and in Snap25 cKO males compared to control males at P21 ($p = 0.0306$). In hippocampal CA3 region, microglial soma size was increased in Snap25 cKO compared to control at P8 and P14 ($p = 0.0007$ and $p = 0.0066$ respectively, Figure 34B), however, I observed no significant sex-specific difference in microglial soma size at P8 (Figure 34B'), P14 (Figure 34B") and P21 (Figure 34B"'). Interestingly, no significant differences were observed in microglial soma roundness between control and Snap25 cKO mice visual cortex layer 5 and hippocampal CA3 region (Figure 34C-C"' and Figure 34D-D"').

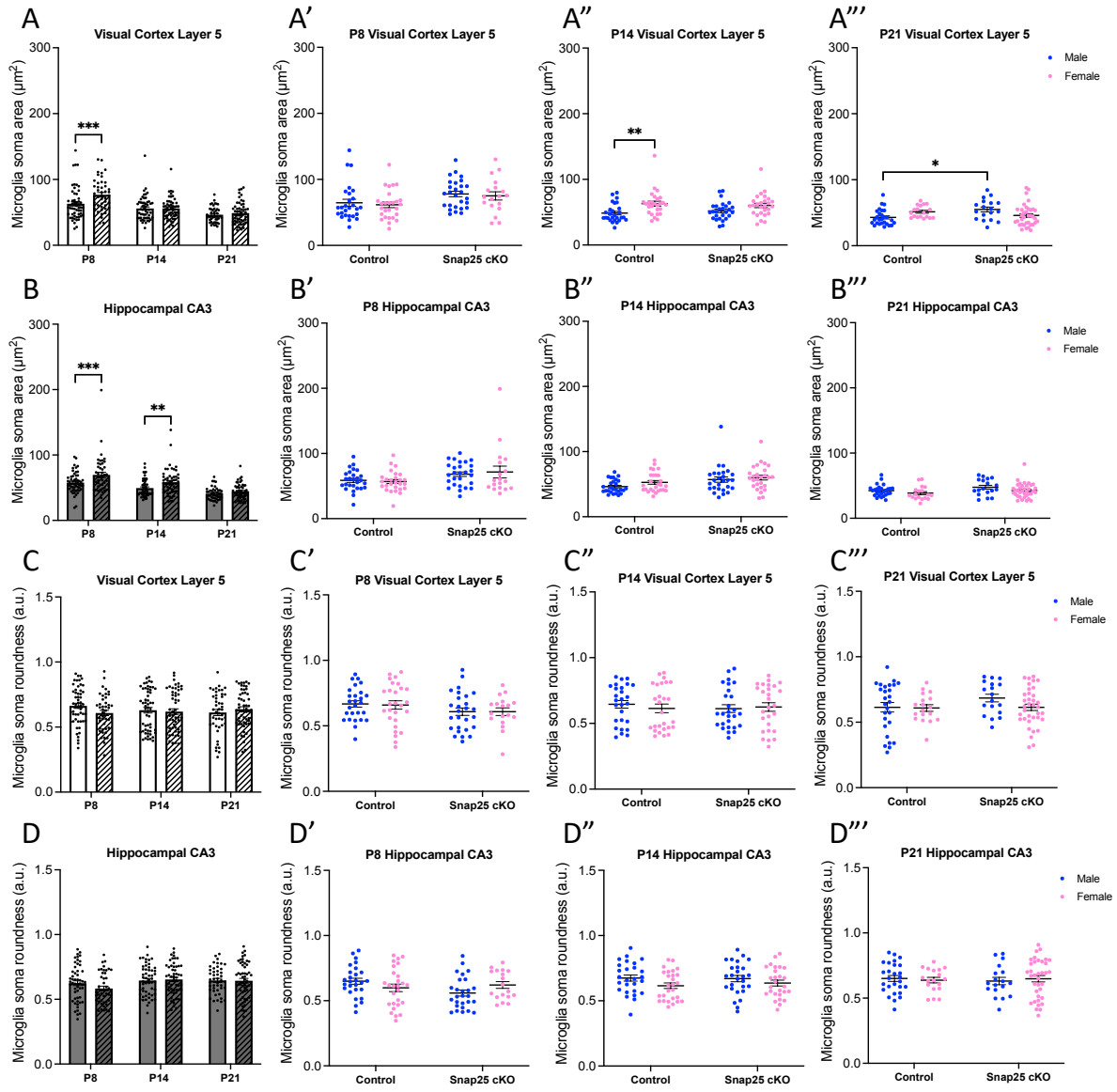


Figure 34: Increased microglial soma size in Snap25 cKO *(Rbp4^{Cre}/+;Ai14;Snap25$^{fl/fl}$)* mice

Visual cortex layer 5 control (white color) and Snap25 cKO (white color with pattern) mice. Hippocampal CA3 control (grey color) and Snap25 cKO (grey color with pattern) mice. Microglial soma size (manually measured using ImageJ software NIH polygon selection tool) differences between control and Snap25 cKO (A) in visual cortex layer 5. Sex-specific changes in microglial soma area between control and Snap25 cKO in visual cortex layer 5 at P8 (A'), P14 (A") and P21 (A"'). Soma area differences between control and Snap25 cKO (B) in hippocampal CA3 region. Sex-specific changes in microglial soma area between control and Snap25 cKO in hippocampal CA3 region at P8 (B'), P14 (B") and P21 (B"'). No differences in microglial soma roundness between control and Snap25 cKO (C) in visual cortex layer 5. No sex-specific differences in microglial soma roundness between control and Snap25 cKO in visual cortex layer 5 at P8 (C'), P14 (C") and P21 (C"'). No changes in microglial soma roundness between control and Snap25 cKO (D) in hippocampal CA3. No sex-specific changes in microglial soma roundness between control and Snap25 cKO in hippocampus CA3 at P8 (D'), P14 (D") and P21 (D"'). My results revealed differences between control and Snap25 cKO (two-way ANOVA,

each dot represents an individual cell, n = 45-54 per age group). Differences between male and female (two-way ANOVA, each dot represents an individual cell, n = 18-27 per age group, males labelled in blue, females labelled in pink). All data presented as mean ± SEM, * $p < 0.05$, ** $p < 0.01$, *** $p < 0.001$, **** $p < 0.0001$.

3D Sholl analysis was performed on Iba1-immunolabelled microglia in selected sectors of selected sections from *Rbp4^{Cre}/+;Ai14;Snap25$^{fl/fl}$* to quantify the number of microglial process intersections as a function of radial distance from individual cell soma. 3D Sholl analyses were completed on Iba1 labelled and individually imaged microglia in control and Snap25 cKO male and female mice visual cortex layer 5 and hippocampal CA3.

In visual cortex layer 5 (Figure 35A"), the 3D Sholl sum of intersections was significantly decreased in Snap25 cKO mice compared to control during development (P8: $p = 0.0015$, P14: $p = 0.0044$ and P21: $p = 0.0025$). Sex-specific differences in the number of intersections were observed on microglia in visual cortex layer 5 between control and Snap25 cKO mice. At P8, the number of intersections was higher in control females compared to control males ($p = 0.0068$) and in Snap25 cKO females compared to Snap25 cKO males ($p = 0.0024$) (Figure 35C). In males, significantly lower number of intersections was observed in Snap25 cKO compared to control ($p = 0.0229$). At P14, significantly lower numbers of intersections were observed in Snap25 cKO males compared to control males ($p < 0.0001$) and Snap25 cKO females ($p < 0.0001$, Figure 35C'). At P21, the number of intersections was higher in control females compared to control males ($p = 0.0039$) and Snap25 cKO females ($p = 0.0005$, Figure 35C"). In Snap25 cKO males, the number of intersections was decreased compared to control males ($p = 0.0004$) and Snap25 cKO females ($p = 0.0039$).

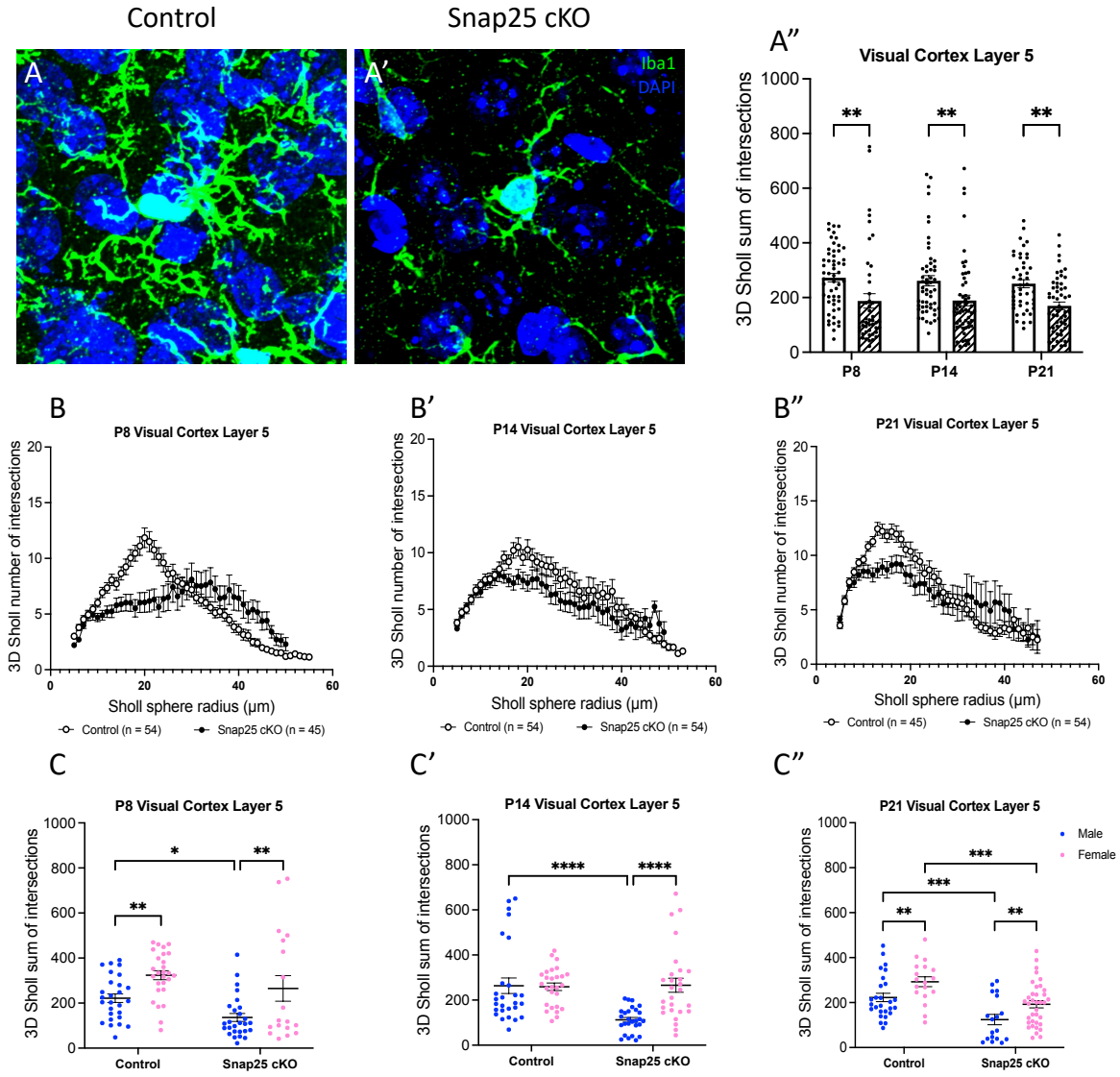


Figure 35: 3D Sholl analysis of microglia in the developing control and Snap25 cKO mice cortex

Visual cortex layer 5 control (white color) and Snap25 cKO (white color with pattern) mice. Representative cells with different ramification patterns immunolabeled with Iba1 (green) and counter stained with DAPI (blue) in control (white) (A) and Snap25 cKO (pattern) (A') mice in visual cortex. 3D Sholl analysis of control and Snap25 cKO in visual cortex layer 5 (A") at P8 (B), P14 (B') and P21 (B"). Sex-specific differences in 3D Sholl sum of intersections were observed between control and Snap25 cKO males and females at P8 (C), P14 (C') and P21 (C"). Differences between control and Snap25 cKO (two-way ANOVA, each dot represents an individual cell, n = 45-54 per age group). Differences between male and female (two-way ANOVA, each dot represents an individual cell, n = 18-27 per age group, males labelled in blue, females labelled in pink). All data presented as mean ± SEM, * $p < 0.05$, ** $p < 0.01$, *** $p < 0.001$, **** $p < 0.0001$. Scale bar, 20 µm.

The same differences in the sum of intersections were observed in the hippocampal CA3. The 3D Sholl sum of intersections was significantly decreased in Snap25 cKO mice comparted to control at P8 ($p < 0.0001$, Figure 36D" and 36E), but no significant differences were observed at P14 (Figure 36E') and P21 (Figure 36E"). Sex-specific differences were observed in the hippocampal CA3 region between control and Snap25 cKO mice. At P8, the number of intersections was higher in control females compared to Snap25 cKO females ($p = 0.0011$) and in control males compared to Snap25 cKO males ($p = 0.0016$, Figure 36F). At P14, a significantly higher number of intersections was observed in control females compared to control males ($p = 0.0026$) and in Snap25 cKO females compared to Snap25 cKO males ($p = 0.0161$, Figure 36F'). At P21, the number of intersections was higher in Snap25 cKO males compared to control males ($p = 0.0124$) and Snap25 cKO females ($p = 0.0001$, Figure 36F").

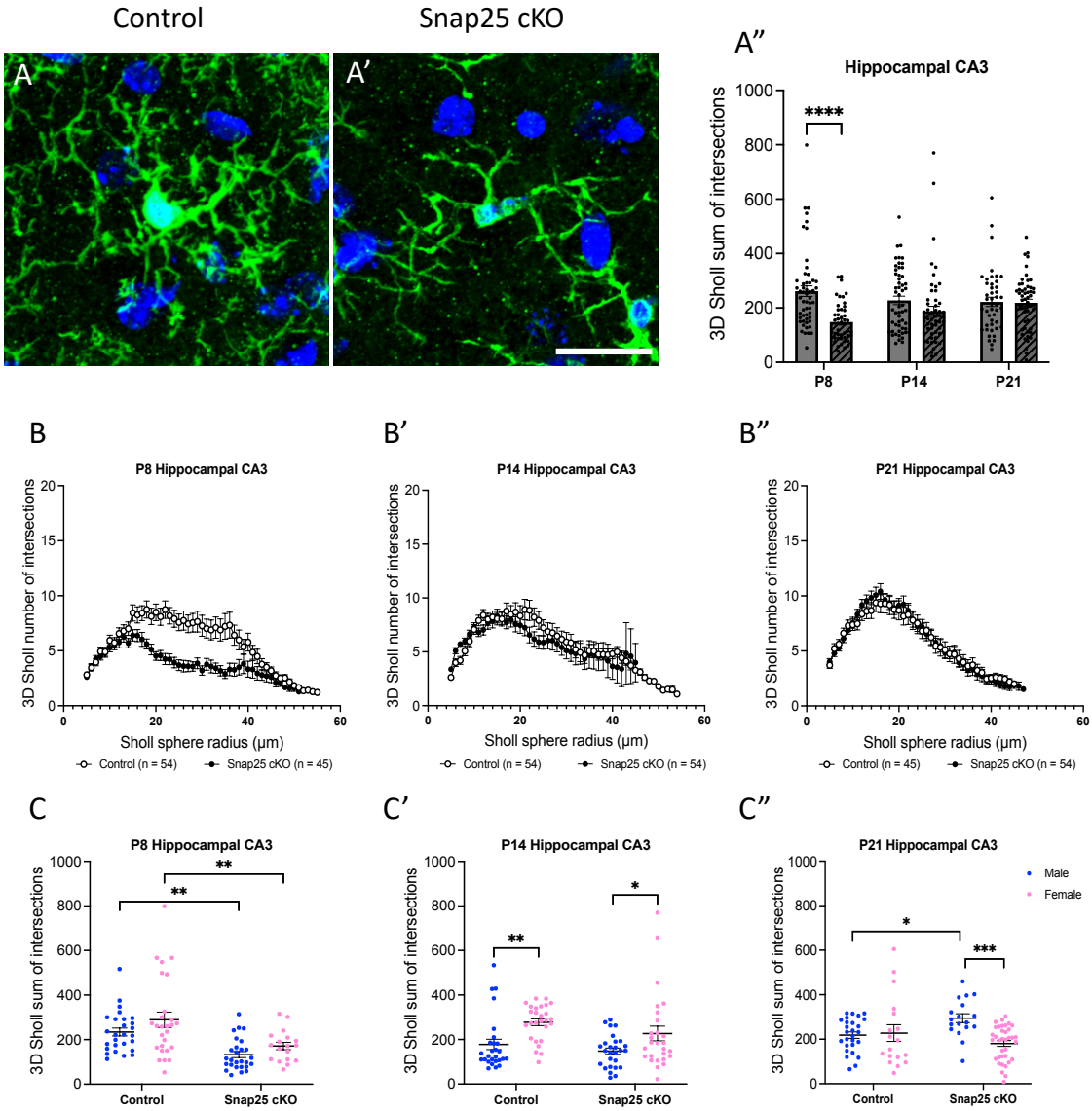


Figure 36: 3D Sholl analysis of microglia in the developing control and Snap25 cKO mice hippocampus

Hippocampal CA3 control (grey color) and Snap25 cKO (grey color with pattern) mice. Representative microglia cells with different ramification patterns revealed through their Iba1 immunoreactivity (green) and counter stained with DAPI (blue) in control (white) (A) and Snap25 cKO (pattern) (A') mice in visual cortex. 3D Sholl analysis of control and Snap25 cKO in the hippocampus CA3 (A") at P8 (B), P14 (B') and P21 (B"). Sex-specific differences in 3D Sholl sum of intersections were observed between control and Snap25 cKO males and females at P8 (C), P14 (C') and P21 (C"). Differences between control and Snap25 cKO (two-way ANOVA, each dot represents an individual cell, n = 45-54 per age group). Differences between male and female (two-way ANOVA, each dot represents an individual cell, n = 18-27 per age group, males labelled in blue, females labelled in pink). All data presented as mean ± SEM, * $p < 0.05$, ** $p < 0.01$, *** $p < 0.001$, **** $p < 0.0001$. Scale bar, 20 µm.

3D Sholl regression coefficient was used to describe changes in microglial processes. Regression coefficient is the slope of the linear regression and measure of the rate of decay of the number of branches with distance from the center of analysis. The higher regression coefficient value the less branches/processes microglia have moving from soma. Microglial complexity was expressed as fractal dimension using the Fractal box count method. Fractal dimension values range from 1 to 2, where 1 is considered to be a simple circle shape and 2 is considered to be the most complex shape. Both analyses were completed on Iba1 labelled and individually imaged microglia in control and Snap25 cKO male and female mice visual cortex layer 5 and hippocampal CA3.

In visual cortex layer 5, 3D Sholl regression coefficient was significantly increased in Snap25 cKO mice comparted to control at P8, P14 and P21 (p = 0.0242, p = 0.0004 and p = 0.0002 respectively, Figure 37G). No sex-specific differences in 3D Sholl regression coefficient were observed at P8 (Figure 37G'). At P14, the regression coefficient was higher in control males compared to females ($p < 0.0001$) and in Snap25 cKO males compared to Snap25 cKO females ($p < 0.0001$, Figure 37G"). Moreover, the regression coefficient was increased in Snap25 cKO males compared to control males (p = 0.0008) and in Snap25 cKO females compared to control (p = 0.0008). At P21, 3D Sholl regression coefficient was increased in Snap25 cKO males compared to control males (p = 0.0013), and in Snap25 cKO females compared to control females (p = 0.0106) and Snap25 cKO males (p = 0.0095, Figure 37G"').

In the hippocampal CA3 region, 3D Sholl regression coefficient was significantly increased in Snap25 cKO mice comparted to control at P8 and P14 (p = 0.0039 and p = 0.0002 respectively, Figure 37H). Sex-specific differences in the regression coefficient were observed in the hippocampal CA3 area between control and Snap25 cKO mice. At P8, the regression

coefficient was higher in control females compared to males (p = 0.0004) and in Snap25 cKO males compared to control males (p < 0.0001, Figure 37H'). At P14, the regression coefficient was higher in control males compared to control females (p < 0.0001) and in Snap25 cKO females compared to control females (p < 0.0001, Figure 37H"). At P21, 3D Sholl regression coefficient was increased in control females compared to control males (p = 0.0113) and in Snap25 cKO females compared to Snap25 cKO males (p = 0.0327, Figure 37H"').

Significant changes in fractal dimension were observed between Snap25 cKO and control mice. In visual cortex layer 5, microglial fractal dimension was significantly increased in Snap25 cKO mice comparted to control at P8 (p = 0.0137, Figure 37I). At P8, fractal dimension was higher in control males compared to control females (p = 0.0025) and in Snap25 cKO females compared to control females (p = 0.0048, Figure 37I'). At 14, fractal dimension was higher in control females compared to control males (p < 0.0001, Figure 37I"). At P21, fractal dimension was increased in Snap25 cKO males compared to control males (p = 0.0187) and significantly lower in Snap25 cKO females compared to Snap25 cKO males (p = 0.0115, Figure 37I"').

In hippocampal CA3, microglia fractal dimension was significantly increased in Snap25 cKO mice compared to control at P8 and P21 (p = 0.0006 and p = 0.0002 respectively, Figure 37J). No sex-specific differences in fractal dimension were observed between control and Snap25 cKO mice at P8 (Figure 37J') and P14 (Figure 37J"). At P21, fractal dimension was increased in Snap25 cKO males compared to control males (p = 0.0002, Figure 37J"'). In Snap25 cKO mice, fractal dimension was significantly lower in females compared to males (p = 0.0218). In females, fractal dimension was increased in Snap25 cKO compared to control (p = 0.0064).

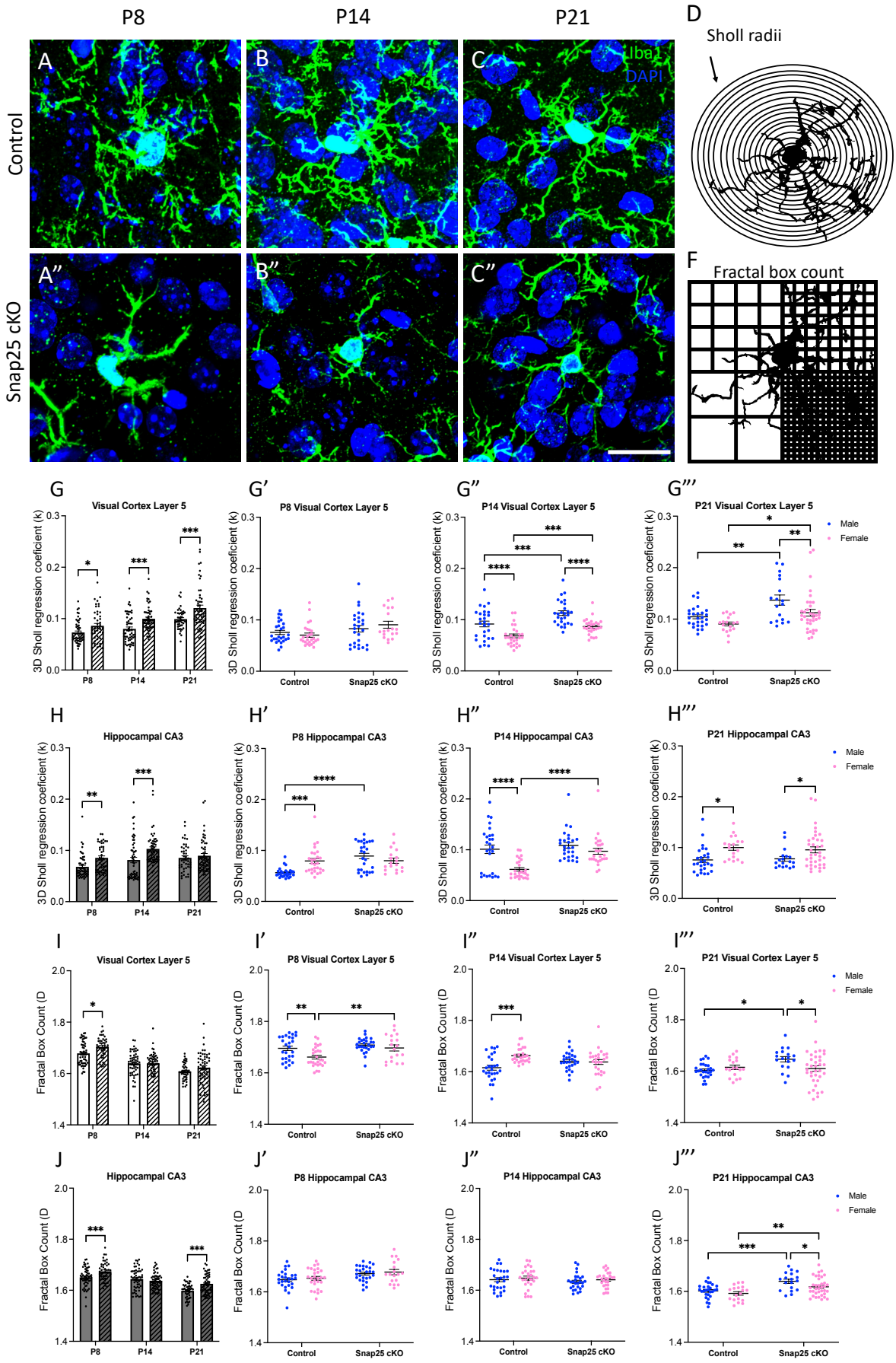

P8
P14
P21
Control
Snap25 cKO
A
B
C
A”
B”
C”
Iba1
DAPI
D
Sholl radii
F
Fractal box count
G
G’
G”
G”’
Visual Cortex Layer 5
P8 Visual Cortex Layer 5
P14 Visual Cortex Layer 5
P21 Visual Cortex Layer 5
3D Sholl regression coeficient (k)
Male
Female
H
H’
H”
H”’
Hippocampal CA3
P8 Hippocampal CA3
P14 Hippocampal CA3
P21 Hippocampal CA3
I
I’
I”
I”’
Fractal Box Count (D
J
J’
J”
J”’

Figure 37: Changes of microglial ramification and complexity during development in Snap25 cKO mice brain

Visual cortex layer 5 control (white color) and Snap25 cKO (white color with pattern) mice. Hippocampal CA3 control (grey color) and Snap25 cKO (grey color with pattern) mice. Representative cells with different ramification patterns immunolabelled with Iba1 (green) and counter stained with DAPI (blue) in control and Snap25 cKO (pattern) mice at P8 (A, A"), P14 (B, B") and P21 (C, C"). Sholl analysis (D). Fractal box analysis (F). 3D Sholl regression coefficient between control and Snap25 cKO mice in visual cortex layer 5 (G). Sex-specific differences in Sholl regression coefficient between male and female mice in visual cortex layer 5 at P8 (G'), P14 (G") and P21 (G"'). 3D Sholl regression coefficient between control and Snap25 cKO mice in hippocampal CA3 (H). Sex-specific differences in Sholl regression coefficient between male and female mice in hippocampal CA3 at P8 (H'), P14 (H") and P21 (H"'). Microglial complexity measured using fractal box count between control and Snap25 cKO mice in visual cortex layer 5 (I). Sex-specific differences in fractal dimension between male and female mice in visual cortex layer 5 at P8 (I'), P14 (I") and P21 (I"'). Fractal dimension of microglia between control and Snap25 cKO mice in hippocampal CA3 (J). Sex-specific differences in fractal dimension between male and female mice in hippocampal CA3 at P8 (J'), P14 (J") and P21 (J"'), but not at P8 (H') and P14 (H") (two-way ANOVA, each dot represents an individual cell, n = 18-27 per age group, males labelled in blue, females labelled in pink). All data presented as mean ± SEM, * $p < 0.05$, ** $p < 0.01$, *** $p < 0.001$, **** $p < 0.0001$. Scale bar, 20 µm.

Due to chronic synaptic 'silencing' microglial density increased but did not follow the same trajectory in males and females during development. Moreover, synaptic 'silencing' affected microglial morphological features in visual cortex layer 5 and hippocampal CA3 region. Microglial cells became smaller yet with bigger soma and with less processes. Interestingly, all these morphological changes were more evident in Snap25 cKO males compared to females. These results indicate that microglia were sensitive to abolished Snap25-mediated release of synaptic vesicles resulting in morphological changes in region and sex-specific manner. In the following chapter I shall discuss whether these morphological changes due to synaptic 'silencing' affected microglial activity.

4.2.2 Abolished regulated release of neurotransmitter vesicles affects microglial activity and microglia-neuron interactions in the developing brain

To evaluate changes in microglial activity and microglia-neuron interactions in 'silenced' brains, I measured the percentage of CD68 in microglia and synaptic density in control and Snap25 cKO visual cortex layer 5, superior colliculus, and hippocampal CA1 and CA3 regions of male and female mice at P8, P14 and P21. Moreover, I measured the number of phagocytic pouches of microglia and engulfment of presynaptic compartment in male and female control and Snap25 mice visual cortex layer 5 and hippocampus CA3 at P8, P14 and P21.

First, microglial active areas analysis was performed by immunocolocalization of Iba1-labelled microglia with the phagosomal marker CD68 in control and Snap25 cKO mice fixed brain sections.

The percentage of CD68 in microglia was reduced during development in visual cortex layer 5 (P8: $p < 0.0001$, P14: $p < 0.0001$ and P21: $p = 0.0021$, Figure 38A'), hippocampal CA1 (P8: $p < 0.0001$, P14: $p < 0.0001$ and P21: $p = 0.0082$, Figure 4.10C') and CA3 (P8: $p < 0.0001$, P14: $p < 0.0001$ and P21: $p = 0.0007$, Figure 38D')., but only at P8 and P14 in superior colliculus ($p < 0.0001$ for both, Figure 38B'). Sex-specific differences in the percentage of CD68 in microglia were observed (Table 19). First, microglial active areas were reduced in Snap25 cKO males compared to control males during development in visual cortex layer 5, hippocampal CA1 and CA3, but only at P8 and P14 in superior colliculus (visual cortex layer 5 P8: $p = 0.0063$, P14: $p = 0.0004$ and $p < 0.0001$ for the rest). The same trend was observed between Snap25 cKO and control females, the percentage of CD68 in microglia was reduced during development (CA1: P21 $p = 0.0003$ and $p < 0.0001$ for the rest). At P8, sex-specific differences between Snap25 cKO males and females were observed only in the hippocampal CA3 where less active areas of microglia were observed in males ($p = 0.0089$). At P14, the percentage of CD68 in microglia

was reduced in Snap25 cKO males compared to females only in superior colliculus (p = 0.0022). Interestingly, synaptic 'silencing' affected all brain regions in the same sex-specific way at P21 where the percentage of CD68 in microglia was reduced in Snap25 cKO females compared to males (visual cortex layer 5 and superior colliculus: $p < 0.0001$, CA1: $p = 0.0104$, CA3: $p = 0.0002$).

These results indicate that abolished Snap25-mediated release of synaptic vesicles not only affected microglial morphology but also reduced activity of microglia in the same fashion in the developing brain. Moreover, the percentage of CD68 in microglia between Snap25 cKO and control mice were affected in the same sex-specific fashion yet were more apparent in Snap25 cKO females than Snap25 cKO males at P21 in visual cortex layer 5, superior colliculus, and hippocampal CA1 and CA3.

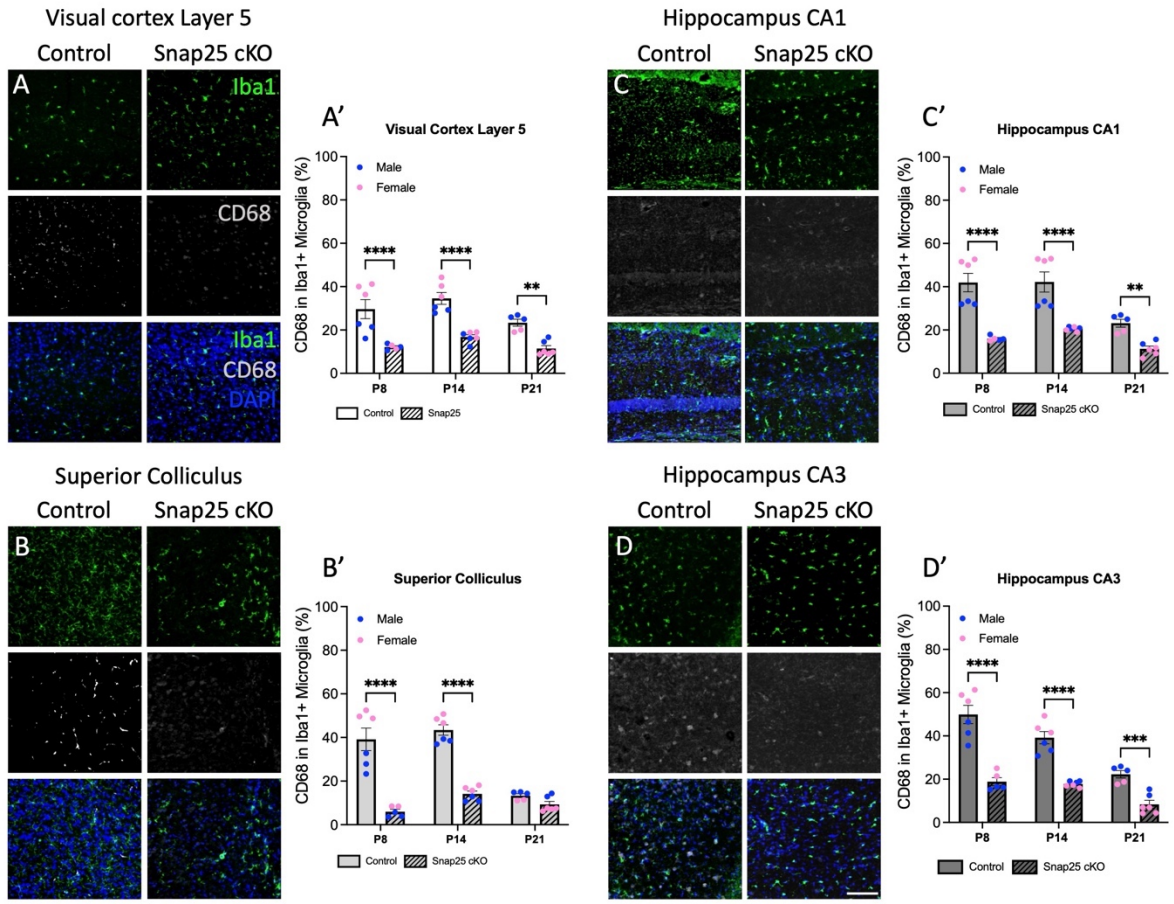


Figure 38: Reduction of the percentage of CD68 in Iba1 in Snap25 cKO mice

Representative images of Iba1 immunolabelled microglia (green) containing phagocytic compartments immunolabelled for CD68 in control and Snap25 cKO mice in visual cortex layer 5 (A), superior colliculus (B), hippocampus CA1 (C) and CA3 (D). Immunoreactivity for CD68 expressed as a percentage of CD68+ microglia cells with respect to total Iba1+ microglia cells decrease in Snap25 cKO mice compared to control in visual cortex layer 5 (A'), superior colliculus (B'), hippocampus CA1 (C') and CA3 (D') at P8, P14 and P21 (two-way ANOVA, each dot represents an individual mouse, n = 5-6 per age group, male mice labelled in blue, female mice labelled in pink). All data presented as mean ± SEM, * $p < 0.05$, ** $p < 0.01$, *** $p < 0.001$, **** $p < 0.0001$. Scale bar, 100 µm.

CD68 in Iba1+ microglia (%)									
Visual Cortex L5									
P8	**Control Male, n = 3**	**Snap25 cKO Male, n = 3**	***p***	**Control Female, n = 3**	**Snap25 cKO Female, n = 2**	***p***	**Snap25 cKO Male, n = 3**	**Snap25 cKO Female, n = 2**	***p***
	20.1092 ± 2.0477	12.1806 ± 0.9433	0.0063	39.1800 ± 1.4486	12.0956 ± 0.8456	<0.0001	12.1806 ± 0.9433	12.0956 ± 0.8456	0.9716
P14	**Control Male, n = 3**	**Snap25 cKO Male, n = 3**	***p***	**Control Female, n = 3**	**Snap25 cKO Female, n = 3**	***p***	**Snap25 cKO Male, n = 3**	**Snap25 cKO Female, n = 3**	***p***
	29.2005 ± 0.8026	15.5465 ± 1.7146	0.0004	39.9822 ± 2.6139	18.0558 ± 0.8904	<0.0001	15.5465 ± 1.7146	18.0558 ± 0.8904	0.3201
P21	**Control Male, n = 3**	**Snap25 cKO Male, n 2**	***p***	**Control Female, n = 2**	**Snap25 cKO Female, n = 4**	***p***	**Snap25 cKO Male, n 2**	**Snap25 cKO Female, n = 4**	***p***
	25.9497 ± 0.5553	15.6250 ± 1.0417	<0.0001	19.5238 ± 0.4762	9.3671 ± 0.2995	<0.0001	15.6250 ± 1.0417	9.3671 ± 0.2995	<0.0001
Superior Colliculus									
P8	**Control Male, n = 3**	**Snap25 cKO Male, n = 3**	***p***	**Control Female, n = 3**	**Snap25 cKO Female, n = 2**	***p***	**Snap25 cKO Male, n = 3**	**Snap25 cKO Female, n = 2**	***p***
	27.9792 ± 2.7257	4.3556 ± 0.6436	<0.0001	50.2831 ± 1.1315	8.4515 ± 0.0124	<0.0001	4.3556 ± 0.6436	8.4515 ± 0.0124	0.1527
P14	**Control Male, n = 3**	**Snap25 cKO Male, n = 3**	***p***	**Control Female, n = 3**	**Snap25 cKO Female, n = 3**	***p***	**Snap25 cKO Male, n = 3**	**Snap25 cKO Female, n = 3**	***p***
	38.2330 ± 0.7031	11.4426 ± 0.7412	<0.0001	48.6004 ± 1.2135	16.8563 ± 0.6945	<0.0001	11.4426 ± 0.7412	16.8563 ± 0.6945	0.0022
P21	**Control Male, n = 3**	**Snap25 cKO Male, n 2**	***p***	**Control Female, n = 2**	**Snap25 cKO Female, n = 4**	***p***	**Snap25 cKO Male, n 2**	**Snap25 cKO Female, n = 4**	***p***
	14.7400 ± 0.2126	13.6532 ± 0.7197	0.0914	11.2212 ± 0.2004	7.1483 ± 0.3171	0.0001	13.6532 ± 0.7197	7.1483 ± 0.3171	<0.0001
Hippocampus CA1									
P8	**Control Male, n = 3**	**Snap25 cKO Male, n = 3**	***p***	**Control Female, n = 3**	**Snap25 cKO Female, n = 2**	***p***	**Snap25 cKO Male, n = 3**	**Snap25 cKO Female, n = 2**	***p***
	32.4023 ± 0.4657	16.3615 ± 0.7832	<0.0001	51.4224 ± 0.7799	15.5000 ± 0.5000	<0.0001	16.3615 ± 0.7832	15.5000 ± 0.5000	0.4359
P14	**Control Male, n = 3**	**Snap25 cKO Male, n = 3**	***p***	**Control Female, n = 3**	**Snap25 cKO Female, n = 3**	***p***	**Snap25 cKO Male, n = 3**	**Snap25 cKO Female, n = 3**	***p***
	31.8260 ± 0.7538	21.0074 ± 0.2799	<0.0001	52.5648 ± 0.3225	20.1587 ± 0.6919	<0.0001	21.0074 ± 0.2799	20.1587 ± 0.6919	0.3106
P21	**Control Male, n = 3**	**Snap25 cKO Male, n 2**	***p***	**Control Female, n = 2**	**Snap25 cKO Female, n = 4**	***p***	**Snap25 cKO Male, n 2**	**Snap25 cKO Female, n = 4**	***p***
	26.0033 ± 0.5567	14.5693 ± 1.0557	0.0001	18.8131 ± 0.6313	9.6554 ± 1.0745	0.0003	14.5693 ± 1.0557	9.6554 ± 1.0745	0.0104
Hippocampus CA3									
P8	**Control Male, n = 3**	**Snap25 cKO Male, n = 3**	***p***	**Control Female, n = 3**	**Snap25 cKO Female, n = 2**	***p***	**Snap25 cKO Male, n = 3**	**Snap25 cKO Female, n = 2**	***p***
	41.1114 ± 3.1501	15.9133 ± 0.3562	<0.0001	58.7315 ± 1.5296	23.2143 ± 1.7857	<0.0001	15.9133 ± 0.3562	23.2143 ± 1.7857	0.0089
P14	**Control Male, n = 3**	**Snap25 cKO Male, n = 3**	***p***	**Control Female, n = 3**	**Snap25 cKO Female, n = 3**	***p***	**Snap25 cKO Male, n = 3**	**Snap25 cKO Female, n = 3**	***p***
	33.5897 ± 1.7073	18.8959 ± 0.2376	0.0001	44.8205 ± 2.3328	16.6792 ± 0.4134	<0.0001	18.8959 ± 0.2376	16.6792 ± 0.4134	0.3158
P21	**Control Male, n = 3**	**Snap25 cKO Male, n 2**	***p***	**Control Female, n = 2**	**Snap25 cKO Female, n = 4**	***p***	**Snap25 cKO Male, n 2**	**Snap25 cKO Female, n = 4**	***p***
	24.9753 ± 0.5561	13.9423 ± 1.4423	<0.0001	18.1985 ± 3.1787	5.5769 ± 0.7628	<0.0001	13.9423 ± 1.4423	5.5769 ± 0.7628	0.0002

Table 19: The percentage of CD68 in Iba1 positive microglia in male and female control and Snpa25 cKO mice

The percentage of Iba1 immunolabelled microglia containing phagocytic compartments immunostained for CD68 at P8, P14, and P21 in visual cortex layer 5, superior colliculus, and hippocampal CA1 and CA3 areas. All data presented as mean ± SEM, n = 2 – 3 mice per sex group.

To further investigate functional changes of microglia, I manually counted phagocytic pouches of individually 3D imaged microglial cells in control and Snap25 cKO visual cortex layer 5 and hippocampal CA3 region at P8, P14 and P21. Phagocytic pouches were defined as a formation of a 3D enclosed pouch of microglial branches around an apoptotic cell (apoptotic cells were identified based on their nuclear DAPI staining) (Sierra et al., 2010) (Figure 39A). In visual cortex layer 5, phagocytic pouches were decreased in Snap25 cKO compared to control mice at P8, P14 and P21 (p = 0.0014, p = 0.0068 and p = 0.0456 respectively, Figure 39B). Sex-specific differences in phagocytic pouches of microglia were observed. At P8, phagocytic pouches were lower in Snap25 cKO males compared to control males (p = 0.0025) and in Snap25 cKO females compared to control females (p = 0.0046, Figure 39B'). At P14 and P21, no sex-specific differences were observed. In the hippocampal CA3 area, phagocytic pouches were decreased in Snap25 cKO compared to control mice at P8 (p = 0.0037, Figure 39C). No sex-specific differences in phagocytic pouches were observed.

In recent years, it has been shown that microglia help remodel the developing neuronal network by 'nibbling' presynaptic compartments of excitatory synapses (process known as *trogocytosis*) (Weinhard, Di Bartolomei, et al., 2018). To evaluate microglial trogocytic activity *in vivo*, I measured Iba1 labelled microglia engulfment with excitatory presynaptic marker vGlut1 in control and Snap25 cKO visual cortex layer 5 and hippocampal CA3.

In visual cortex layer 5, vGlut1+ puncta engulfment by microglia was increased in Snap25 cKO compared to control mice at P8, P14 and P21 (p < 0.0001, p = 0.0166 and p = 0.0294 respectively, Figure 39D). Sex-specific differences in vGlut1 engulfment were observed only

at P8 and P14. At P8, vGlut1 engulfment was increased in Snap25 cKO males compared to control males ($p < 0.0001$) and Snap25 cKO females ($p = 0.0004$, Figure 39D'). At P14, vGlut1 engulfment was increased in Snap25 cKO males compared to control males ($p = 0.0271$, Figure 39D"). In hippocampal CA3, vGlut1 engulfment was decreased in Snap25 cKO compared to control mice at P14 and P21 ($p = 0.0053$ and $p = 0.0080$ respectively, Figure 39E). I observed no sex-specific differences in vGlut1+ puncta engulfment by microglia.

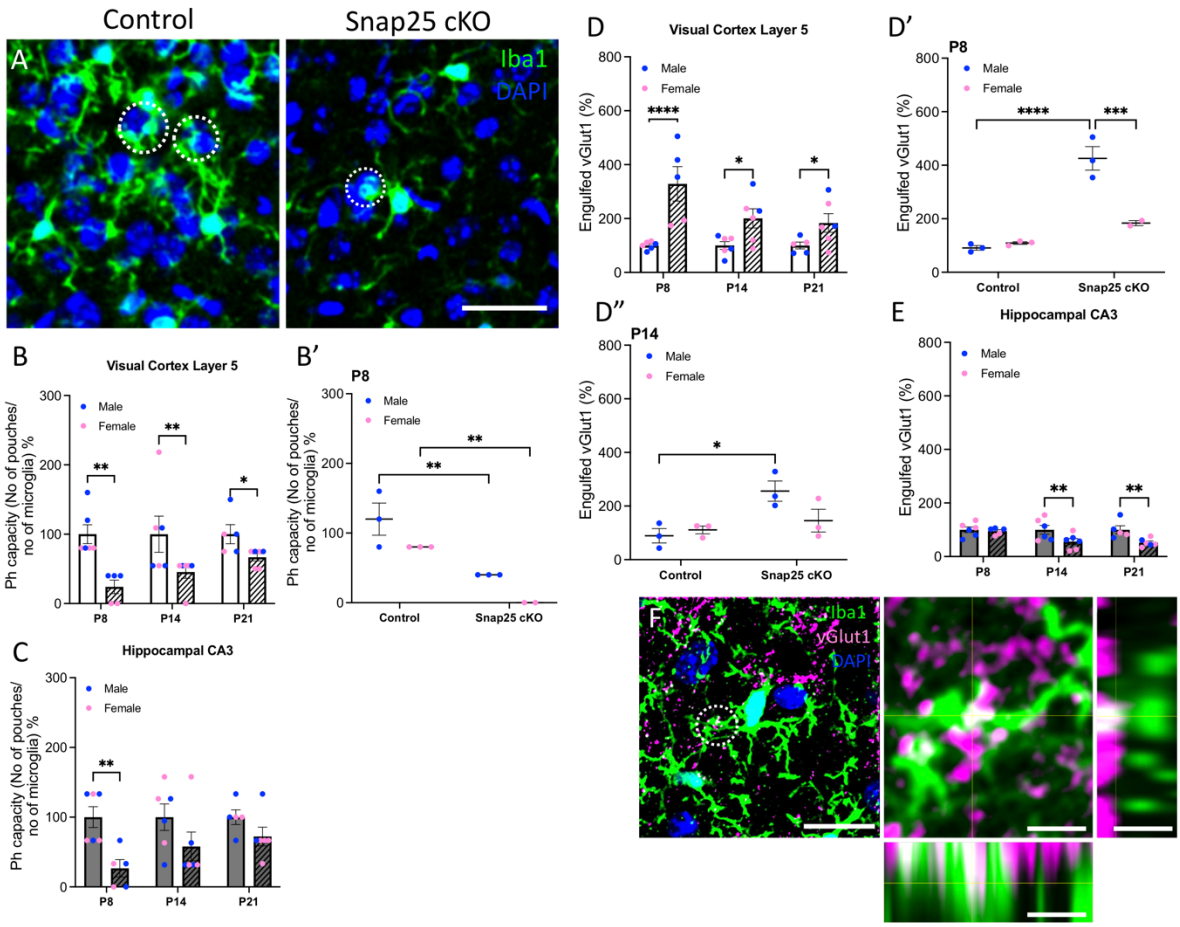


Figure 39: Microglial phagocytic pouches and presynaptic compartment engulfment differ between control and Snap25 cKO *(Rbp4^{Cre}/+;Ai14;Snap25$^{fl/fl}$)* brains

Visual cortex layer 5 control (white color) and Snap25 cKO (white color with pattern) mice. Hippocampal CA3 control (grey color) and Snap25 cKO (grey color with pattern) mice. Representative images of Iba1 immunolabelled microglia (green) with phagocytic pouches (circle) in control and Snap25 cKO mice (A). Phagocytic pouches decrease in Snap25 cKO (pattern) mice compared to control in developing visual cortex layer 5 (B) and hippocampus CA3 (C). vGlut1 (presynaptic marker) engulfment by microglia expressed as a percentage of vGlut1+ particles colocalized Iba1+. vGlut1

engulfment was increased in Snap25 cKO mice during development in visual cortex (D) but decreased in hippocampus CA3 (E). Representative images of Iba1+ microglia (green) with vGlut1+ particles (magenta) (F). Two-way ANOVA, each dot represents an individual mouse, n = 5-6 per age group, male mice labelled in blue, female mice labelled in pink). All data presented as mean ± SEM, * $p < 0.05$, ** $p < 0.01$, *** $p < 0.001$, **** $p < 0.0001$. Scale bar, 20 µm.

To further investigate whether synaptic 'silencing' affect microglia-neuron communications, I measured synaptic density. First, I quantified the number of synaptic puncta as the colocalization of the presynaptic (vGlut1) and postsynaptic (PSD95) markers that are specific for the excitatory synapses. Second, I measured the size of individual vGlut1+ and PSD95+ puncta.

Excitatory synaptic density was increased in Snap25 cKO compared to control only at P14 in visual cortex layer 5 ($p < 0.0001$, Figure 40A'). In the developing superior colliculus and hippocampal CA3 region, synaptic density was increased in the similar way (SC P8: $p = 0.0210$, P14: $p < 0.0001$ and P21: $p = 0.0137$, Figure 4.12B'; CA3: P8: $p = 0.0428$, P14: $p < 0.0001$ and P21: $p = 0.0137$ respectively, Figure 40D'). In the hippocampal CA1, excitatory synaptic density was increased at P14 and P21 ($p = 0.0003$ and $p = 0.0006$ respectively, Figure 40C'). Sex-specific differences in excitatory synaptic density were observed only at P14 in visual cortex layer 5, superior colliculus and hippocampal CA1. Synaptic density was increased in Snap25 cKO males compared to control males in visual cortex layer 5 (vGlut1/PSD95 synapse number expressed as %, 366.056 ± 28.994 and 46.359 ± 3.593 respectively, $p < 0.0001$), superior colliculus (vGlut1/PSD95 synapse number expressed as %, 275.232 ± 10.762 and 86.374 ± 8.734 respectively, $p = 0.0145$) and hippocampal CA1 (vGlut1/PSD95 synapse number expressed as %, 303.670 ± 59.375 and 70.744 ± 12.465 respectively, $p = 0.0016$). In addition, it was also increased in Snap25 cKO females compared to control females in visual cortex layer 5 (vGlut1/PSD95 synapse number expressed as %, 243.065 ± 49.902 and 153.641 ± 7.982

respectively, p = 0.0109) and superior colliculus (vGlut1/PSD95 synapse number expressed as %, 349.887 ± 82.131 and 113.626 ± 21.385 respectively, p = 0.0046). Excitatory synaptic density was increased in Snap25 cKO males compared to Snap25 cKO females but only in visual cortex layer 5 (vGlut1/PSD95 synapse number expressed as %, 366.056 ± 28.994 and 243.065 ± 49.902 respectively, p = 0.0176). In the hippocampal CA3, synaptic density was increased at P8 in Snap25 cKO females compared to control females (vGlut1/PSD95 synapse number expressed as %, 131.882 ± 22.762 and 78.466 ± 2.632 respectively, p = 0.0164) and at P14, there was an increase in Snap25 cKO males compared to control males (vGlut1/PSD95 synapse number expressed as %, 313.201 ± 71.852 and 101.594 ± 9.880 respectively, p = 0.0058). No significant differences between Snap25 cKO and control, and no sex-specific differences were observed in vGlut1+ and PSD95+ puncta size in visual cortex layer 5 (Figure 40A" - A"') and superior colliculus (Figure 40B" – B"'). Significant differences in vGlut1+ puncta size were observed in the hippocampal CA1 and CA3, but no differences in PSD95+ puncta size were observed. In the hippocampal CA1, vGlut1+ puncta were smaller in P21 control compared to P8 control mice (p = 0.0144, Figure 40C"). In addition, sex differences in vGlut1+ size was observed only at P14 where vGlut1 size was increased in Snap25 cKO males compared to control males (vGlut1 particle size: 0.194 ± 0.009 and 0.162 ± 0.004 respectively, p = 0.0094), but decreased in Snap25 cKO females compared to control females (vGlut1 particle size: 0.161 ± 0.002 and 0.223 ± 0.008 respectively, p = 0.0002) and Snap25 cKO males (vGlut1 particle size: 0.161 ± 0.002 and 0.194 ± 0.009, p = 0.0083). In the hippocampal CA3, vGlut1+ puncta size was lower in P14 compared to P8 control mice (p = 0.0002) and P21 compared to P8 control mice (p < 0.0001, Figure 40D"), but no significant sex-specific differences were observed.

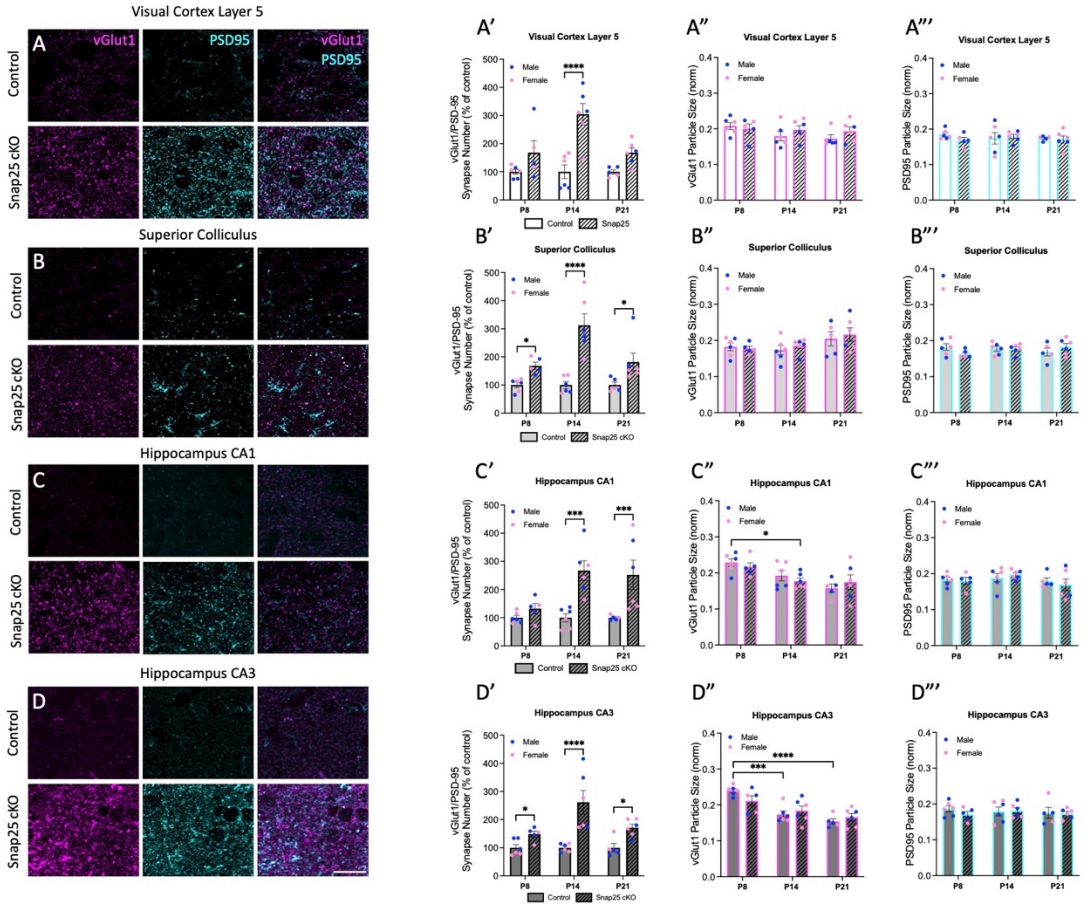


Figure 40: Synaptic density increases in sex-specific manner in 'silenced' brain during development

Representative images with excitatory markers vGlut1 (magenta) and PSD95 (cyan), show excitatory synapses, identified by colocalization between pre- (vGlut1+) and post-synaptic (PSD95) puncta in visual cortex layer 5 (A), superior colliculus (B), hippocampal CA1 (C) and CA3 (D) regions in control and Snap25 cKO (pattern) mice. The percentage of excitatory synapses between control and Snap25 cKO in visual cortex layer (A'). vGlut1+ and PSD95+ puncta size was normalized to control animals. vGlut1+ (A") and PSD95+ (A"') puncta size between control and Snap25 cKO males and females in developing visual cortex layer 5. The percentage of excitatory synapses between control and Snap25 cKO in superior colliculus (B'). vGlut1+ (B") and PSD95+ (B"') puncta size between control and Snap25 cKO males and females in developing superior colliculus. The percentage of excitatory synapses between control and Snap25 cKO in hippocampal CA1 (C'). vGlut1+ (C") and PSD95+ (C"') puncta size between control and Snap25 cKO males and females in developing hippocampal CA1. The percentage of excitatory synapse between control and Snap25 cKO in hippocampal CA3 (D'). vGlut1+ (D") and PSD95+ (D"') puncta size between control and Snap25 cKO males and females in developing hippocampal CA3 region. (two-way ANOVA, each dot represents an individual mouse, n = 5-6 per age group, male mice labelled in blue, female mice labelled in pink). All data presented as mean ± SEM, * $p < 0.05$, ** $p < 0.01$, *** $p < 0.001$, **** $p < 0.0001$. Scale bar, 20 µm.

Abolition of Snap25 affected microglial activation, microglia became less phagocytically active especially in males and it triggered increased engulfment of presynaptic compartments. Moreover, in silenced brains, synaptic density was increased, which was more pronounced in male brains during first two weeks of development in visual cortex layer 5, superior colliculus, and hippocampal CA1 and CA3.

4.2.3 Synaptic 'silencing' affects chemokine and phagocytic signalling pathways in the developing brain

4.2.3.1 Lack of Snap25 downregulates CX3CL1 but upregulates CX3CR1 expression

The chemokine signalling pathway via fractalkine was identified as one of the key players for normal synaptic pruning by microglia (Paolicelli et al., 2011). It is known that the fractalkine ligand (CX3CL1) is expressed on neurons and its receptor (CX3CR1) is only found on microglia. In a normal state, the CX3CL1/CX3CR1 axis plays a role in construction of the neuronal network, plasticity, maturation of synapses and control of immune processes (Owolabi & Saab, 2006; Paolicelli et al., 2011; Pawelec et al., 2020). Moreover, the CX3CL1/CX3CR1 signalling pathway modulates microglia dynamics and affects microglial morphology, migration, engulfment, and proliferation (Limatola & Ransohoff, 2014; Paolicelli et al., 2014). Importantly, normal levels of fractalkine inhibit microglial activation and keep microglia in the resting state (ramified microglia) (Biber et al., 2007b).

To investigate whether abolished regulated release of neurotransmitter vesicles in the developing brain affects the microglial chemokine signalling pathway, I examined CX3CL1 and CX3CR1 protein levels using Western Blot in control and Snap25 cKO mice cortex and hippocampus at P8, P14 and P21 (Figure 41A) and I used GAPDH as a control. However, this part of experiments had some limitations. GAPDH is the most commonly used control

antibody for Western Blot and by probing for GAPDH we usually are able to check that protein loading is the same across the gel. However, it has been reported that GAPDH protein level differs in different tissue and especially during development (Goasdoue et al., 2016; Kish et al., 1998; Vigels\o et al., 2015). Hence, it is necessary to evaluate whether GAPDH protein level differ in the loaded samples or remain similar level. To evaluate changes in fractalkine signalling in developing brain tissue as a control I used GAPDH for Western Blot since other controls that can be used were overlapping with the size of CX3CL1 and CX3CR1. Also, this part of experiments was performed in between Covid-19 pandemic (June 2020 – August 2020) and I had issues to order different control antibodies. Moreover, Abcam has recently knockout validated CX3CR1 (ab8021) antibody and found it to be non-specific/cross reactive. I was informed just recently and for my thesis I was not able to repeat Western Blot experiments using different anti-CX3CR1 antibody. For DPhil project paper I either have to repeat experiments or exclude CX3CR1 data. However, for my DPhil thesis I included CX3CR1 Western Blot data and discuss the results in the following paragraph. The results of anti-CX3CR1 antibody testing can be found on the datasheet here: https://www.abcam.com/cx3cr1-antibody-ab8021.html. More information on the knockout validation process can be found here: https://www.abcam.com/primary-antibodies/knockout-validation.

I also tested the expression of CX3CL1 and CX3CR1 mRNA using qPCR in control and Snap25 mice cortex and hippocampus at P8, P14 and P21. qPCR data were normalized to control P8 male and female mice expression levels and performed using the $2^{-\Delta\Delta Ct}$ method (Schmittgen & Livak, 2008) and expressed as fold change in arbitrary units. As an endogenous control I used TBP gene (TBP expression discussed in Appendix 1 and general methods chapter 2). Strict definition of endogenous genes is necessary since housekeeping genes have high variability

between different tissues and during brain development (Pérez et al., 2007; Sundaram et al., 2019). It has been shown that TBP expression increases at P23 in the cerebellum and spinal cord (Sundaram et al., 2019) and at P30 in choroid plexus (K. H. Ho & Patrizi, 2021) yet TBP is considered to be a sable endogenous genes in the developing brain. However, more detailed analysis of the housekeeping genes expression in the different developing brain regions would be necessary since the expression of endogenous genes might differ between cortical and subcortical regions.

In cortex, CX3CL1 protein (Figure 41B) and CX3CL1 mRNA (Figure 41C) expression levels fell significantly in Snap25 cKO mice compared to control during development (CX3CL1 protein P8: $p = 0.0001$, P14: $p = 0.0434$ and P21: $p < 0.0001$ and CX3CL1 mRNA P8: $p = 0.0034$, P14: $p < 0.0001$ and P21: $p < 0.0001$). I observed, sex-specific differences in CX3CL1 protein levels and CX3CL1 mRNA expression were observed in the developing cortex. CX3CL1 protein levels were lower in control females compared to control males and Snap25 cKO females at P8, P14 and P21 ($p < 0.0001$ for all, Figure 41B' – B"'). Moreover, in the developing cortex, CX3CL1 protein levels were lower in Snap25 cKO males compared to control males ($p < 0.0001$ for P8, P14 and P21) and Snap25 cKO females (P8: $p = 0.0092$, Figure 4.13B'; P14: $p < 0.0001$, Figure 41B"; P21: $p = 0.0011$, Figure 41B"'). The similar trend was observed in CX3CL1 mRNA expression in the developing cortex (Figure 41C'-C"'). CX3CL1 mRNA expression was significantly lower in Snap25 cKO males compared to control males ($p < 0.0001$ for P8, P14 and P21) and Snap25 cKO females ($p < 0.0001$ for P8 and P14). Lower CX3CL1 mRNA expression was observed in Snap25 cKO females compared to control females ($p < 0.0001$ for P8, P14 and P21). Interestingly, CX3CL1 mRNA was lower in control females compared to males at P14 ($p < 0.0001$) and slightly higher in control females compared to control males at P21 ($p = 0.0371$). CX3CR1 protein levels were significantly higher in Snap25 cKO mice

compared to control at P14 and P21 (p = 0.0001 and p = 0.0354 respectively), yet no significant differences between control and Snap25 cKO mice were observed in CX3CR1 mRNA expression during development (Figure 41D-E). Sex-specific changes in expression of both CX3CR1 protein and CX3CR1 mRNA were observed between control and Snap25 cKO mice. CX3CR1 protein levels were increased in control females compared to males in the developing cortex (P8: $p < 0.0001$, P14: $p < 0.0001$ and P21: p = 0.0093), yet decreased in Snap25 cKO females compared to males at P8 and P21 ($p < 0.0001$ and p = 0.0065, respectively). Moreover, CX3CR1 protein levels were increased in Snap25 cKO males compared to control ($p < 0.0001$ for P8, P14 and P21). In Snap25 females, CX3CR1 protein levels were lower compared to control at P8 ($p < 0.0001$) yet higher at P14 (p = 0.0007). CX3CR1 mRNA expression was significantly higher in Snap25 cKO males compared to control males ($p < 0.0001$) but lower in Snap25 cKO females compared to control females (p = 0.0005) at P8 (Figure 41E'). In addition, higher CX3CR1 mRNA expression was observed in Snap25 cKO males compared to Snap25 cKO females ($p < 0.0001$, Figure 41E'). At P14, CX3CR1 mRNA expression was lower in control females compared to males (p = 0.0052) and higher in Snap25 cKO females compared to control (p = 0.0128, Figure 41E"). At P21, CX3CR1 mRNA expression was lower in control females compared to males (p = 0.0009), but higher in Snap25 cKO females compared to males ($p < 0.0001$, Figure 41E"'). Moreover, CX3CR1 mRNA expression was lower in Snap25 cKO males compared to control males (p = 0.0456), but higher in Snap25 cKO females compared to control females ($p < 0.0001$).

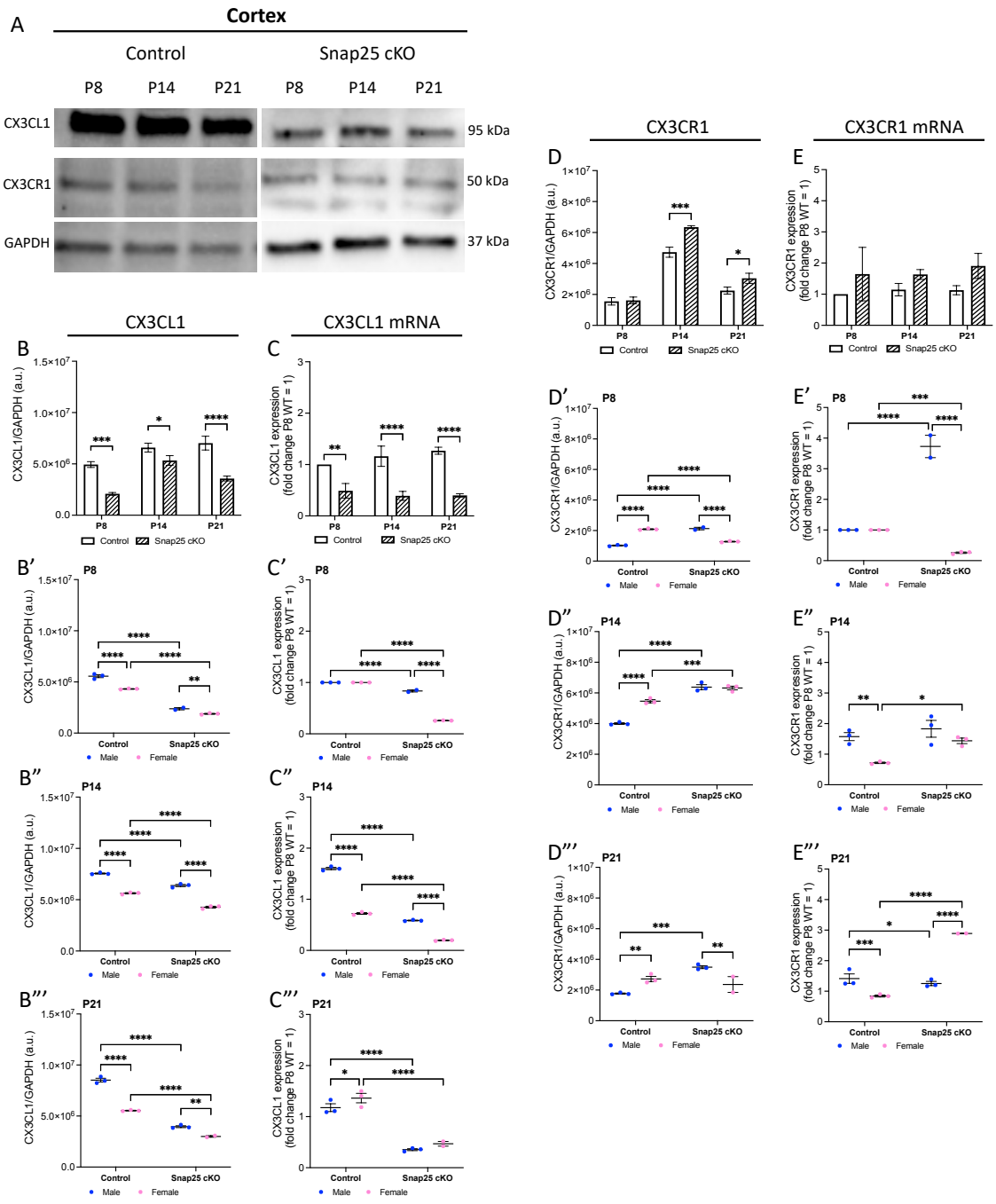


Figure 41: Abolition of Snap25 from a selected population of layer 5 projection neurons in *Rbp4^{Cre}/+;Ai14;Snap25$^{fl/fl}$* affects chemokine signalling in the developing cortex

CX3CL1 and CX3CR1 protein level demonstrated by western blotting in control and Snap25 cKO mice cortex (A). Densitometric analysis of western blotting of CX3CL1 between control and Snap25 cKO mice (B) at P8 (B'), P14 (B") and P21 (B"'); GAPDH was as a loading control. qPCR of the CX3CL1 mRNA expression level in control and Snap25 cKO mice cortex (C) at P8 (C'), P14 (C") and P21 (C"'). Densitometric analysis of western blotting of CX3CR1 between control and Snap25 cKO mice (D) at P8 (D'), P14 (D") and P21 (D"'); GAPDH was as a loading control. qPCR of the CX3CR1 mRNA expression level in control and Snap25 cKO mice cortex (E) at P8 (E'), P14 (E") and P21 (E"'). (two-way ANOVA,

each dot represents an individual mouse, n = 5-6 per age group, control – white, Snap25 cKO – pattern, male mice labelled in blue, female mice labelled in pink). All data presented as mean ± SEM, * $p < 0.05$, ** $p < 0.01$, *** $p < 0.001$, **** $p < 0.0001$.

In hippocampus, CX3CL1 (Figure 42B) protein levels were significantly lower in Snap25 cKO mice compared to control at P8, P14 and P21 (CX3CL1: $p < 0.0001$, $p < 0.0001$ and $p < 0.0001$ respectively) and CX3CL1 mRNA (Figure 42C) expression levels fell in Snap25 cKO at P8 and P14 ($p = 0.0340$ and $p = 0.0002$). Sex-specific changes in expression of both CX3CL1 protein and CX3CL1 mRNA were observed between control and Snap25 cKO mice in the developing hippocampus (Figure 42B'-B"' and 42C'-C"'). CX3CL1 protein levels were higher in control females compared to males at P8 and P14, yet lower at P21 ($p = 0.0461$, $p < 0.0001$ and $p < 0.0001$, respectively), and lower in Snap25 cKO females compared to males (P8: $p < 0.0001$, P14: $p < 0.0001$ and P21: $p = 0.0007$). Moreover, CX3CL1 protein levels were lower in Snap25 cKO males compared to control males ($p < 0.0001$ for P8, P14 and P21) and in Snap25 cKO females compared to control females ($p < 0.0001$ for P8, P14 and P21). CX3CL1 mRNA expression was significantly lower in Snap25 cKO males compared to control males at P8 and P14 ($p = 0.0041$ and $p = 0.0085$, respectively) and in Snap25 cKO females compared to control females ($p = 0.0003$) and Snap25 cKO males ($p = 0.0067$) at P8. Moreover, CX3CL1 mRNA expression was lower in control females compared to males ($p = 0.0181$) and lower in Snap25 cKO males compared to control males ($p = 0.0085$) at P14. No sex-specific differences in CX3CL1 mRNA expression were observed at P21. CX3CR1 protein levels were significantly higher in Snap25 cKO mice compared to control at P8, P14 and P21 ($p = 0.0024$, $p = 0.0002$ and $p = 0.0004$ respectively, Figure 42D) and CX3CR1 mRNA expression was lower only at P14 ($p = 0.0002$, Figure 42E). Sex-specific changes in expression of both CX3CR1 protein and CX3CR1 mRNA were observed between control and Snap25 cKO mice in the developing

hippocampus (Figure 42D'-D"' and 42E'-E"'). CX3CR1 protein levels were higher in control females compared to males at P8 and P14 ($p < 0.0001$ for both), yet lower at P21 ($p = 0.0323$). Lower levels were also observed in Snap25 cKO females compared to Snap25 cKO males but only at P8 ($p < 0.0001$). Moreover, there were higher levels of CX3CR1 in Snap25 cKO males compared to control males (P8: $p < 0.0001$, P14: $p < 0.0001$ and P21: $p = 0.0401$) and in Snap25 cKO females compared to control females at P14 and P21 ($p < 0.0001$ and $p = 0.0016$, respectively). CX3CR1 mRNA expression was significantly higher in Snap25 cKO females compared to control females (P8: $p = 0.0004$, P14: $p = 0.0064$ and P21: $p = 0.0002$) and compared to Snap25 cKO males at P8 and P21 ($p = 0.0002$ and $p = 0.0006$, respectively) yet lower at P14 ($p = 0.0004$). Moreover, CX3CR1 mRNA expression was higher in control males compared to females ($p = 0.0363$), yet lower Snap25 cKO males at P14 ($p = 0.0001$, Figure 4. 42E"').

Abolition of Snap25 from a selected group of layer 5 projection neurons and dentate gyrus neurons in *Rbp4^{Cre}/+;Ai14;Snap25$^{fl/fl}$* downregulates both CX3CL1 protein levels and mRNA expression in the developing brain. Interestingly, down regulation of CX3CL1 was more pronounced in females than in males. Moreover, abolished release of synaptic vesicles upregulates both CX3CR1 and protein levels and mRNA expression in the developing brain yet follows different expression patterns in males and females.

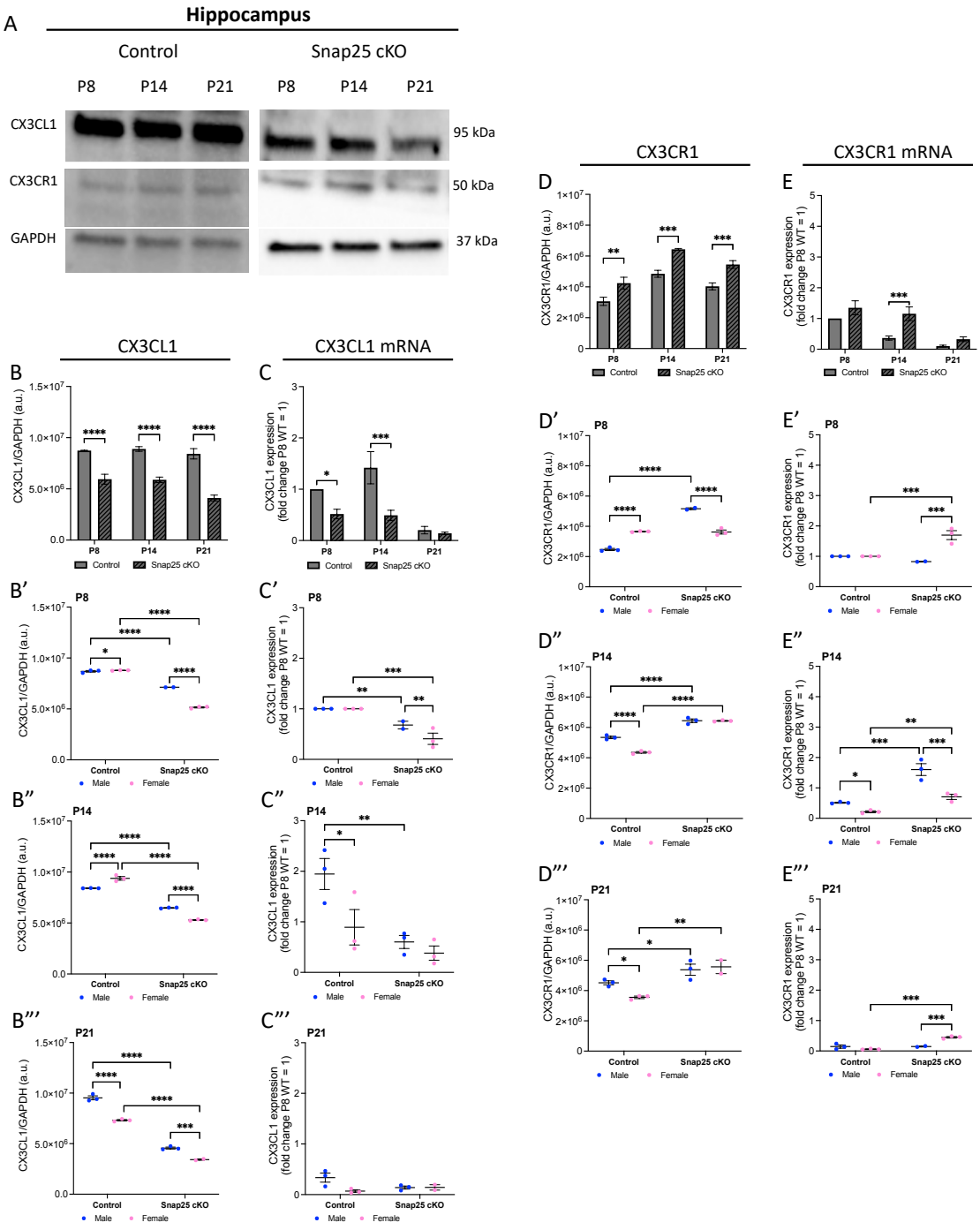


Figure 42: Abolition of Snap25 from dentate gyrus neurons in the *Rbp4^{Cre}/+;Ai14;Snap25$^{fl/fl}$* affects chemokine signalling in the developing hippocampus

CX3CL1 and CX3CR1 protein level demonstrated by western blotting in control and Snap25 cKO mice hippocampus (A). Densitometric analysis of western blotting of CX3CL1 between control and Snap25 cKO mice (B) at P8 (B'), P14 (B") and P21 (B"'); GAPDH was used as a loading control. qPCR of the CX3CL1 mRNA expression level in control and Snap25 cKO mouse hippocampus (C) at P8 (C'), P14 (C") and P21 (C"'). Densitometric analysis of western blotting of CX3CR1 between control and Snap25 cKO mice (D) at P8 (D'), P14 (D") and P21 (D"'); GAPDH was as a loading control. qPCR of the CX3CR1 mRNA expression level in control and Snap25 cKO mice hippocampus (E) at P8 (E'), P14 (E") and P21 (E"').

(two-way ANOVA, each dot represents an individual mouse, n = 5-6 per age group, control – white, Snap25 cKO – pattern, male mice labelled in blue, female mice labelled in pink). All data presented as mean ± SEM, * $p < 0.05$, ** $p < 0.01$, *** $p < 0.001$, **** $p < 0.0001$.

4.2.3.2 Lack of Snap25 affects C3 and CD11b expressions across the brain during development

The complement proteins C1q, C3 and C4 relocate to synapses and participate in synapse elimination by tagging synapses (Schafer et al., 2012; Stephan et al., 2012). Microglia express high affinity complement receptor 3 (CR3) and engulf tagged synapses (Presumey et al., 2017; Schafer et al., 2012). Complement component 3 (C3) is a soluble opsonin that binds to complement receptors on microglia and is commonly referred to as 'eat-me' signal. C3 helps promote phagocytosis by binding to unwanted or harmful material that needs to be eliminated (Elward & Gasque, 2003). In the brain, C3 localizes to developing synapses and promotes microglial engulfment (Schafer et al., 2012; Stevens et al., 2007). CD11b (also known as complement receptor 3A (CR3A)) is an alpha subunit that together with CD18 constructs CR3. CD11b is involved in adhesion, recognition and phagocytosis processes and uptake of complement-coated molecules (Jeong et al., 2013). Moreover, CD11b is expressed in both resting and active microglia (Lee et al., 2002).

To investigate whether synaptic 'silencing' affects the phagocytic signalling pathway through the complement system, I examined C3 and CD11b using western blot in control and Snap25 cKO cortex and hippocampus samples at P8, P14 and P21 (Figure 43A). I also tested the expression of C3 and CD11b mRNA using qPCR in cortex and hippocampus samples at P8, P14 and P21. qPCR data was normalized to control P8 expression levels and performed using the $2^{-\Delta\Delta Ct}$ method and expressed as fold change in arbitrary units (Schmittgen & Livak, 2008).

In cortex, C3 (Figure 43B) and C3 mRNA (Figure 43C) expression levels fell significantly in Snap25 cKO mice compared to control at P8, P14 and P21 (C3: $p < 0.0001$, $p <$, 0.0001 and $p = 0.0182$ respectively, and C3 mRNA: $p < 0.0001$, $p < 0.0001$ and $p < 0.0001$ respectively). Sex-specific differences in C3 protein levels followed the similar trend in the developing cortex (Figure 43B'-B"'). C3 protein levels were lower in Snap25 cKO males compared to control males (P8: $p = 0.0071$, P14: $p < 0.0001$ and P21: $p = 0.0002$), in Snap25 cKO females compared to control females at P8 and P14 ($p = 0.0072$ and $p < 0.0001$, respectively) and in control females compared to males but only at P21 ($p = 0.0023$). C3 mRNA expression was lower in Snap25 cKO males compared to control (P8: $p < 0.0001$, P14: $p = 0.0002$ and P21: $p < 0.0001$) and Snap25 cKO females compared to control (P8: $p < 0.0001$, P14: $p = 0.0105$ and P21: $p <$ 0.0001). Moreover, C3 mRNA expression was higher in Snap25 cKO females compared to males (P8: $p = 0.0041$, P14: $p = 0.0239$ and P21: $p = 0.0011$) and in control females compared to males ($p < 0.0001$). In the cortex, CD11b protein levels were significantly higher in Snap25 cKO mice compared to control at P8, P14 and P21 ($p < 0.0001$, $p < 0.0001$ and $p = 0.0044$ respectively), yet no significant changes in CD11b mRNA expression were found in the developing cortex (Figure 43D-E). Sex-specific differences in CD11b protein levels and mRNA expression were similar during development (Figure 43D'-D"', 43E'-E"'). Higher protein levels were observed in Snap25 cKO males compared to control males (P8: $p = 0.0011$, P14: $p <$ 0.0001 and P21: $p = 0.0009$), in Snap25 cKO females compared to control females (P8: $p =$ 0.0038, P14: $p < 0.0001$ and P21: $p = 0.0005$) and in Snap25 cKO females compared to Snap25 cKO males ($p = 0.0178$). CD11b mRNA expression was higher in Snap25 cKO males compared to control males only at P8 ($p < 0.0001$) and in Snap25 cKO females compared to control females during development (P8: $p = 0.0078$, P14: $p = 0.0002$ and P21: $p = 0.0002$). Moreover,

CD11b expression was higher in Snap25 cKO males compared to females at P8 ($p < 0.0001$) but lower at P14 and P21 ($p = 0.0009$ and $p = 0.0002$, respectively).

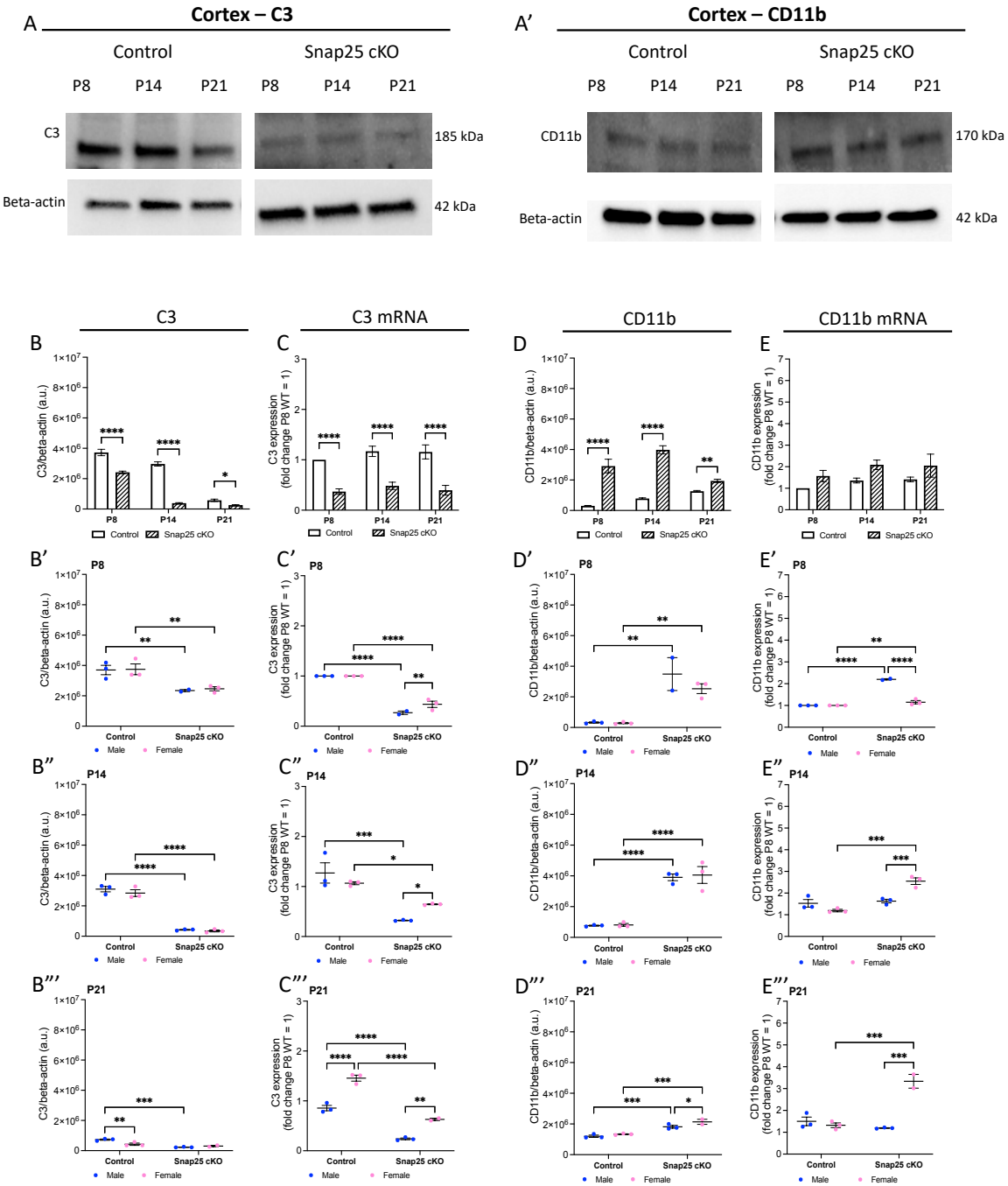


Figure 43: Synaptic 'silencing' of a subpopulation of layer 5 pyramidal neurons affects the expression of C3 and CD11b in the developing cortex

C3 and CD11b protein level demonstrated by western blotting in control and Snap25 cKO mice cortex (A). Densitometric analysis of western blotting of C3 between control and Snap25 cKO mice (B) at P8 (B'), P14 (B") and P21 (B"'); beta-actin was used as a loading control. qPCR of the C3 mRNA expression level in control and Snap25 cKO mice cortex (C) at P8 (C'), P14 (C") and P21 (C"'). Densitometric analysis of western blotting of CD11b between control and Snap25 cKO mice (D) at P8 (D'), P14 (D") and P21 (D"'); beta-actin was used as a loading control. qPCR of the CD11b mRNA expression level in control and Snap25 cKO mice cortex (E) at P8 (E'), P14 (E") and P21 (E"'). Two-way ANOVA, each dot represents an individual mouse, n = 5-6 per age group, control – white, Snap25 cKO – pattern, male mice labelled in blue, female mice labelled in pink. All data presented as mean ± SEM, * $p < 0.05$, ** $p < 0.01$, *** $p < 0.001$, **** $p < 0.0001$.

In hippocampus, C3 (Figure 44B) and C3 mRNA (Figure 44C) expression levels fell significantly in Snap25 cKO mice compared to control at P8, P14 and P21 (C3: $p < 0.0001$, $p <$, 0.0001 and $p < 0.0001$ respectively, and C3 mRNA: $p = 0.0002$, $p = 0.0006$ and $p = 0.0369$ respectively). Sex-specific changes in expression of both C3 protein and C3 mRNA were observed between control and Snap25 cKO mice during development. C3 protein levels were lower in Snap25 cKO males compared to control males during development (P8: $p = 0.0008$, P14: $p < 0.0001$ and P21: $p < 0.0001$) and in Snap25 females compared to control (P8: $p = 0.0009$, P14: $p < 0.0001$ and P21: $p < 0.0001$). C3 protein levels were lower in control females compared to males at P8 ($p = 0.0394$), yet higher at P21 ($p < 0.0001$). C3 mRNA expression was lower in Snap25 cKO males compared to control during the first two weeks of development ($p < 0.0001$ for P8 and P21) and Snap25 cKO males compared to females (P8: $p = 0.0189$ and P14: $p = 0.0002$). Lower C3 mRNA expression was in Snap25 cKO females compared to control at P8 ($p < 0.0001$), yet higher at P14 ($p = 0.0284$). In hippocampus, CD11b protein (Figure 44D) and CD11b mRNA (Figure 44E) expression levels increased significantly in Snap25 cKO mice compared to control at P8, P14 and P21 (CD11b: $p < 0.0001$, $p <$, 0.0001 and $p < 0.0001$ respectively, and CD11b mRNA: $p = 0.0015$, $p = 0.0002$ and $p = 0.0136$ respectively). Sex-specific differences in CD11b protein levels were similar in the developing hippocampus

(Figure 44D'-D"'). CD11b levels were higher in Snap25 cKO males compared to control males (P8: $p = 0.0007$, P14: $p < 0.0001$ and P21: $p < 0.0001$) and in Snap25 cKO females compared to control females (P8: $p = 0.0003$, P14: $p < 0.0001$ and P21: $p < 0.0001$). Moreover, sex-specific differences in CD11b mRNA expression followed different developmental trajectories (Figure 44E'-E"'). CD11b mRNA expression was higher in Snap25 cKO males compared to control males at P8 and P21 ($p < 0.0001$ and $p = 0.0002$, respectively) and in Snap25 cKO females compared to control females during development ($p < 0.0001$ for P8, P14 and P21). CD11b mRNA expression was higher in Snap25 cKO males compared to females only at P8 ($p < 0.0001$), and lower at P14 and P21 ($p < 0.0001$ for both). In control mice, lower CD11b mRNA expression was only observed in females at P14 ($p = 0.0194$).

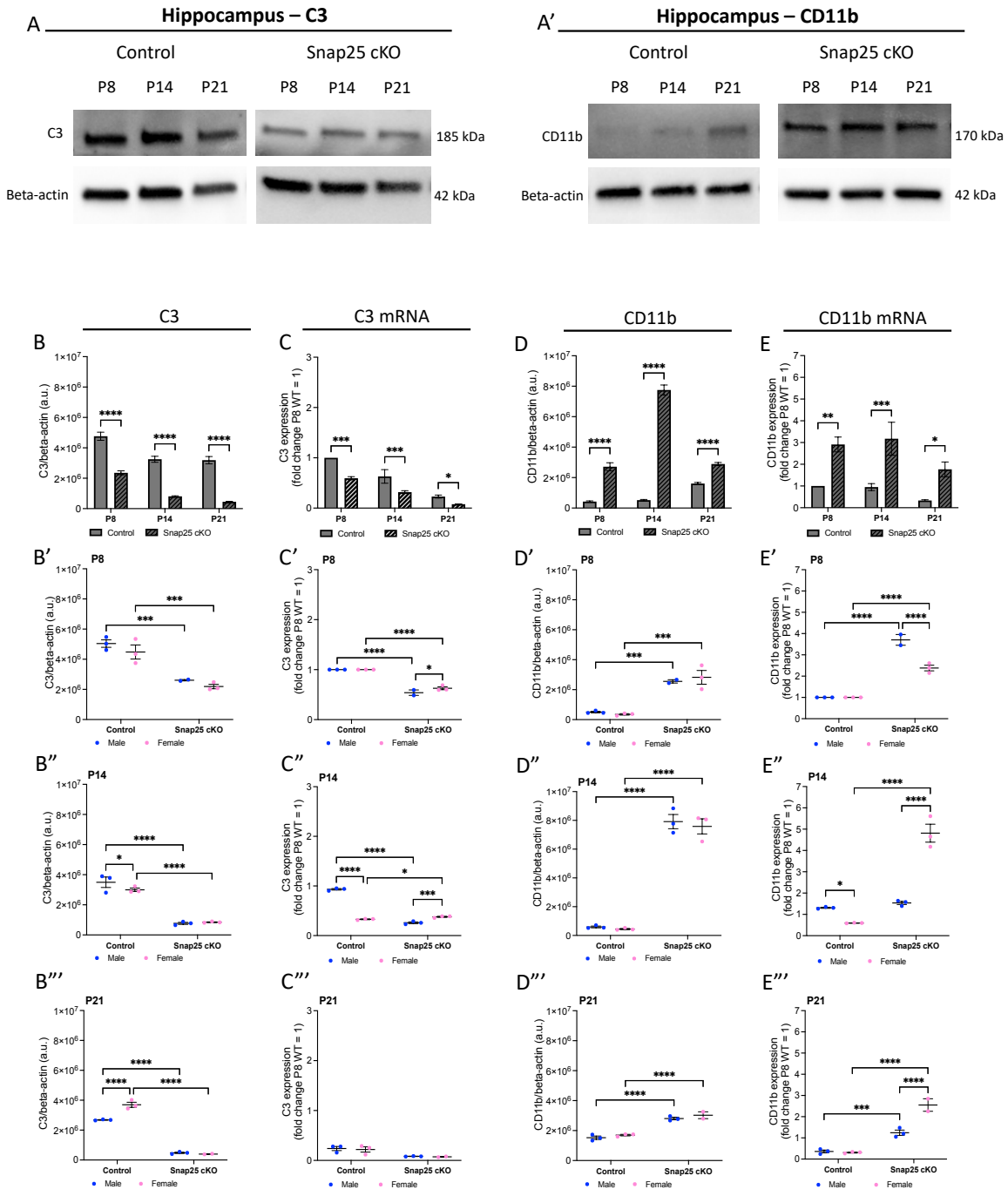


Figure 44: Synaptic 'silencing' of neurons in the dentate gyrus affects the expression of C3 and CD11b in the developing hippocampus

C3 and CD11b protein level demonstrated by western blotting in control and Snap25 cKO mice hippocampus (A). Densitometric analysis of western blotting of C3 between control and Snap25 cKO mice (B) at P8 (B'), P14 (B") and P21 (B"'); beta-actin was used as a loading control. qPCR of the C3 mRNA expression level in control and Snap25 cKO mice hippocampus (C) at P8 (C'), P14 (C") and P21 (C"'). Densitometric analysis of western blotting of CD11b between control and Snap25 cKO mice (D) at P8 (D'), P14 (D") and P21 (D"'); beta-actin was as a loading control. qPCR of the CD11b mRNA

expression level in control and Snap25 cKO mice hippocampus (E) at P8 (E'), P14 (E") and P21 (E"'). (two-way ANOVA, each dot represents an individual mouse, n = 5-6 per age group, control – white, Snap25 cKO – pattern, male mice labelled in blue, female mice labelled in pink). All data presented as mean ± SEM, * $p < 0.05$, ** $p < 0.01$, *** $p < 0.001$, **** $p < 0.0001$.

Abolition of Snap25 from a subset of layer 5 projection neurons and from dentate gyrus neurons downregulates both C3 protein levels and mRNA expression in the developing cortex and in hippocampus. Reduced C3 levels were more pronounced in males. Moreover, abolished release of synaptic vesicles increases CD11b protein levels and mRNA expression in the developing brain yet follows different expression patterns in males and females.

4.3 Discussion

In this part of the study, I demonstrated that abolished regulated release of synaptic vesicles affected microglia-neuron interactions and microglial behaviour in visual cortex layer 5, superior colliculus, and hippocampal CA1 and CA3 regions (Figure 45). First, abolition of Snap25 expression in selected subset of layer 5 neurons and dentate gyrus reduced microglial activity and affected morphological properties. Second, chronic synaptic 'silencing' altered synaptic maturation resulting in increased synaptic density and increased engulfment of presynaptic compartments. Third, abolition of Snap25 affected microglia-neuron communication by disrupting normal chemokine and phagocytic signalling. Lastly, sex-specific changes in microglia-neuron interactions were observed and indicated that male mice were more sensitive to abolished Snap25-mediated release of synaptic vesicles during brain development.

Synaptic pruning in the normal developing cerebral cortex has not been well studied due to the complex synaptic connectivity making it more challenging to trace pathway-specific synaptic inputs and the role of microglia during maturation and maintenance of the cerebral cortex. To better understand synaptic pruning and microglia-neuron interactions in an activity-dependent manner during early brain development, I used the Snap25 cKO (*Rbp4^{Cre};Ai14, Snap25$^{fl/fl}$*) mouse line where a selected population of cortical layer 5 projection neurons and a selected population of hippocampal dentate gyrus granule cells lack the ability to release synaptic vesicles in a regulated fashion starting shortly before birth. This model enabled me to investigate morphological and functional correlates of microglia activity that indicate communication between microglia and local and distant projections with aberrant neurotransmitter release. Little is known about the role of microglia in disrupted

neurotransmitter release through ablation of the SNARE complex proteins and more specifically in the transgenic *Rbp4^{Cre};Ai14;Snap25$^{fl/fl}$* (Snap25 cKO) mouse line. It has been reported that cortical development is unaffected in abolition of Snap25 from selected neuron populations, however 'silenced' brains shown early signs of axonal degeneration after P21 and degeneration of silenced neurons at 8 months (Hayashi et al., 2021; Hoerder-Suabedissen et al., 2019; Korrell et al., 2019). Similar silencing of different subpopulations of layers 6a (*Ntsr1^{Cre};Ai14;Snap25$^{fl/fl}$*) or layer 6b (*Drd1a^{Cre};Ai14;Snap25$^{fl/fl}$*) has less severe phenotype, the loss of synapses, demyelination and degeneration starts much later and we observed no cell death in these cKOs until the age of 8 months (Hoerder-Suabedissen et al., 2019)(Vadisiute et al., 2022 in press).

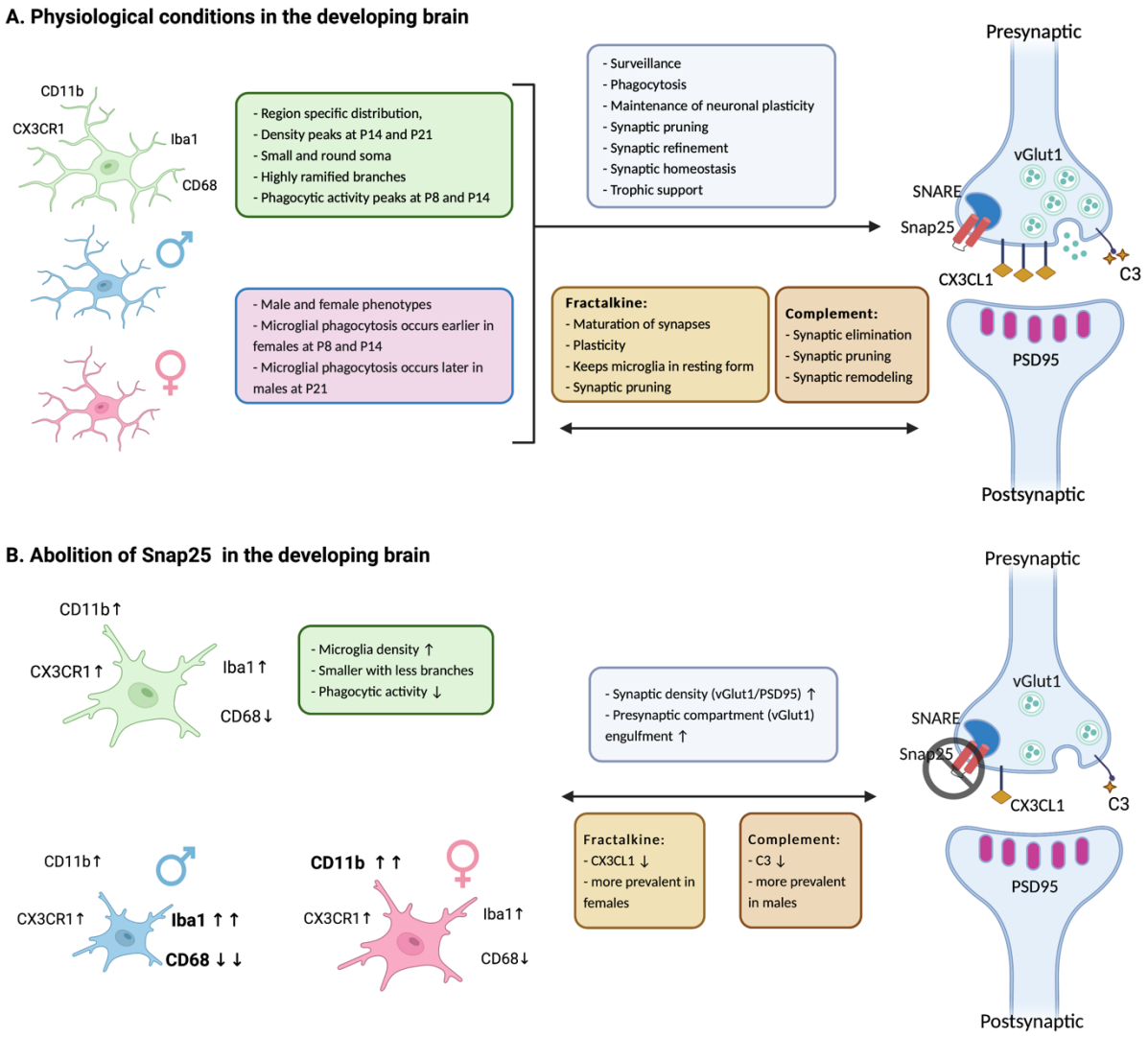


Figure 45: Abolition of Snap25 affected bidirectional communication between microglia and neurons in a sex-specific manner

(A) Indicates microglia-neuron interactions during normal development. (B) Indicates morphological, functional and molecular changes between microglia and neurons caused by abolished Snap25-mediated release of synaptic vesicles in the developing brain cortex and hippocampus. Created with BioRender.com

4.3.1 Synaptic 'silencing' affects microglia distribution and morphological features across developing brain in a sex-specific manner

It still remains largely unexplored how changes in brain activity affect heterogeneous distribution and morphology of microglia in the developing brain. Here I presented shifts in microglial morphology after chronic 'silencing'. Since sexual-dimorphism of microglia occurs

during normal brain development (discussed in Chapter 3) I further tested whether synaptic 'silencing' effects on microglia could be sex-specific. To evaluate microglial distribution, I labelled these cells using anti-Iba1 antibody and quantified the number of microglia in visual cortex layer 5, superior colliculus, hippocampal CA1 and CA3 regions. I demonstrated that at the location of the silenced layer 5 neurons in the visual cortex microglial density was increased only at P21 and was more pronounced in males. However, at the silenced mossy fiber projections in the CA3 region I observed an increase in microglial density at P8 and P14. Interestingly, in the hippocampal CA1 region, microglial density was reduced at P14, and lower density was more prevalent in silenced female mice. Even though the CA1 region did not receive direct projections from the subpopulation of layer 5 or dentate gyrus ($Rpb4^{Cre}$) neurons, abolition of Snap25 affected microglia density in this region. Moreover, I can speculate that these changes were either due to upstream altered circuitry/excitability or silenced $Rpb4^{Cre}$ neuron population have more extensive influence on general brain activity than we thought.

In the case of neurodevelopmental and neurodegenerative diseases, and other pathological conditions, microglia change their morphology. For example, in the presence of brain injury microglia shift morphology to amoeboid form (Arcuri et al., 2017; Hanisch & Kettenmann, 2007). To further investigate microglia, I analysed different morphological features of individual cells. In Snap25 cKO visual cortex layer 5 and hippocampal CA3, microglial volume was reduced yet microglial soma size was increased. Synaptic 'silencing' did not affect microglial soma roundness or the number of primary branches. Microglial process extension or retraction affects microglia-neuron interactions. In developing somatosensory cortex, increased microglial processes induce synapse formation (A. Miyamoto et al., 2016). Moreover, extracellular calcium reduction activates microglia and induces microglial

processes in the brain (Eyo et al., 2015). The authors concluded that even slight reductions in calcium can trigger microglial morphology changes, and microglia sense and contact dendrites via purinergic signalling (Eyo et al., 2015). Interestingly, abolition of Snap25 affected microglial ramification by inducing microglial process retraction in visual cortex layer 5 and hippocampal CA3 region. Increase in microglial soma size might be a compensatory mechanism due to processes retraction and/or intermediate stage towards complete transition to amoeboid form. However, to better understand if microglial process retraction affects synapse formation, it would be necessary to study microglial process interaction with silenced tdTomato+ neurons in the future.

These results provide evidence that abolition of Snap25 triggers microglial morphology changes, resulting in the reduction of microglial size and process retraction.

4.3.2 Abolished release of synaptic vesicles affects microglial function and excitatory synapse density in a sex-specific manner

To further investigate microglial activity, I determined changes in the percentage of CD68 in microglia and phagocytic pouches as well as changes in excitatory synapses size and density in the developing brain with abolished release of neurotransmitter vesicles. However, to investigate microglial activity and engulfment of synaptic compartments, the majority of the studies have been using double immunolabelling with CD68 and vGlut1 or PSD95 (He et al., 2019; Werneburg et al., 2019). Since my transgenic mouse model has a tdTomato red fluorescent reporter I could only use one of the markers together with Iba1. Two separate immunolabellings were performed: to determine active areas of microglia I used anti-Iba1 together with anti-CD68 (Paolicelli et al., 2017); to determine presynaptic compartment engulfment by microglia I used anti-Iba1 together with anti-vGlut1 (Ramaglia et al., 2021).

Changes in microglial phagocytic activity have been well studied in pathological conditions (Arcuri et al., 2017; Hanisch & Kettenmann, 2007; Sellgren et al., 2019). Moreover, it has been shown that defective microglial activity during brain development can lead to impaired phagocytosis and neuronal debris clearances and jeopardized neuronal connectivity (Casano & Peri, 2015; Kierdorf & Prinz, 2013; Prinz & Priller, 2014; Tay et al., 2017). I observed that due to abolished regulated release of neurotransmitter vesicles, phagocytic active areas of microglia decreased in all brain regions during brain development. In addition,I measured phagocytic pouches of microglia (Sierra et al., 2010). Changes in phagocytic pouches were similar to the changes of CD68 active areas of microglia. At the location of the silenced layer 5 neurons in the visual cortex, the percentage of phagocytic pouches was lower at P8, P14 and P21, but only at P8 in the silenced hippocampal CA3 region.

It has been reported that microglial activity is necessary for sex-dependent brain development. Microglial activity inhibition with minocycline (tetracycline antibiotic that also inhibits microglia) prevented the shift towards males during a critical stage for sexual differentiation (Lenz et al., 2013). Moreover, sex-specific differences of microglia have been shown in cognitive conditions such as autism, which is more prevalent in males (Tang et al., 2014; Velmeshev et al., 2019). I observed that during the first two weeks of development lower number of CD68 positive microglia was more pronounced in males but only in silenced superior colliculus and hippocampal CA3. Later in development, lower number of CD68 positive microglia was determined in females in all silenced brain regions.

To further investigate whether the abolition of Snap25 has an impact on developing synapses I measured excitatory synaptic density by labelling pre- and postsynaptic compartments (vGlut1 and PSD95 respectively). It has been shown that cortical layer 5 projections target higher order thalamic nuclei in the thalamus and form specialised synapses with thalamic

neurons (Hayashi et al., 2021; Hoerder-Suabedissen et al., 2019). Normally, the target thalamic neurons extend their dendritic protrusions into the layer 5 giant boutons (Groh et al., 2008; Hoogland et al., 1991). However, when *Snap25* expression is abolished specifically in a subtype of cortical layer 5 neurons from birth, the specialised synapses between the giant terminals and with the posterior thalamic neuronal dendritic protrusions fail to mature into the giant interdigitating shape, nevertheless synapses get established (Hayashi et al., 2021). This suggests that Snap25-mediated synaptic vesicle release by cortical layer 5 neurons is not crucial for initial formation of synapses in PO, but is fundamental for the growth and maturation of specialised synapses (Hayashi et al., 2021). More recent EM analysis by Hayashi and collaborators demonstrated the lack of specialised synapses in CA3 from dentate gyrus in the same model (*Rbp4*^{Cre}*;Ai14;Snap25*$^{fl/fl}$) (Hayashi et al., unpublished observations). In silenced brains, excitatory synaptic density was increased during development and more prevalent in males at P14. Moreover, I determined that abolished release of synaptic vesicles had no impact on vGlut1 and PSD95 puncta size in visual cortex layer 5, superior colliculus, and hippocampal CA1 and CA3 areas. However, I observed sex-specific differences in vGlut1 puncta size in the hippocampal CA1 area. The bigger vGlut1 puncta size was observed only in males at P14 in the hippocampal CA1. Interestingly, presynaptic compartment (vGlut1) engulfment by microglia was higher in silenced visual cortex layer 5 and more prevalent in males even though phagocytic activity of microglia was lower. At the silenced mossy fiber projections in the CA3 region, vGlut1 engulfment was lower at P14 and P21, and follows the same trajectory as phagocytic activity.

These results showed that abolished Snap25-mediated release of synaptic vesicles affected microglial function by reducing microglial activity. Thus, increased excitatory synaptic density triggered presynaptic compartments engulfment by microglia leading to impaired synaptic

maturation. My results suggest that Snap25-mediated regulated synaptic vesicle release is necessary for microglia-neuron interactions and normal synaptic maturation in a sex-specific manner during development.

4.3.3 Synaptic 'silencing' affects microglia-neuron interactions via chemokine and phagocytic signalling pathways

It has been shown that signalling between the neuronal chemokine fractalkine (CX3CL1) and its microglial receptor (CX3CR1) facilitates microglia-neuron interactions and is necessary for synaptic pruning (Jones et al., 2010; Maciejewski-Lenoir et al., 1999; Owolabi & Saab, 2006; Paolicelli et al., 2014). Interestingly, fractalkine is also associated with the SNARE complex components such as syntaxin 13 and VAMP3, and facilitates the protection of presynthesized CX3CL1 against premature degradation (G. Y. Liu et al., 2005). In the endothelial cells, SNARE complex protein SNAP23 together with syntaxin 3 and 4 help release endothelial-derived chemokines like CX3CL1, 8 and 10 (Schoppmeyer et al., 2022). However, developmental changes in CX3CL1-CX3CR1 signalling in relation to SNARE complex proteins are largely unexplored. To better understand the role of fractalkine signalling in microglia-neuron communications in mice with abolished Snap25-mediated release of synaptic vesicles, I measured CX3CL1 and CX3CR1[1] protein levels and mRNA expression. In cortex and hippocampus, CX3CL1 protein levels and mRNA expression were lower and more prevalent in Snap25 cKO females. Reduced CX3CL1 protein level was also found in schizophrenia patients

[1] Abcam has recently knockout validated ab8021 and found it to be non-specific/cross reactive. I was informed just recently and for my thesis I was not able to repeat western blot experiments using different anti-CX3CR1 antibody. The results of this testing can be found on the datasheet here: https://www.abcam.com/cx3cr1-antibody-ab8021.html.
More information on the knockout validation process can be found here: https://www.abcam.com/primary-antibodies/knockout-validation.

(Hill et al., 2021) suggesting that reduce fractalkine levels might be linked to neuronal loss (Fan et al., 2020) or impaired neuronal activity and/or network formation. Greater CX3CR1 protein levels were observed in Snap25 cKO mouse cortex and hippocampus and were more prevalent in males. Interestingly, greater CX3CR1 mRNA expression was more prevalent in females. Sex-specific differences in CX3CL1-CX3CR1 signalling have been shown in rats. Greater CX3CR1 expression was found in unstressed females (Bollinger et al., 2016). Furthermore, in an obese mouse model, high fat diet induced an increase of CX3CR1 in females (Dorfman et al., 2017) yet reduced CX3CL1-CX3CR1 signalling in the corticolimbic system (Kawamura et al., 2021). Microglia-neuron interactions may be activity-dependent through fractalkine signalling. Abolition of Snap25 caused reduced CX3CL1 expression and may result in impaired synaptic formation.

The phagocytic signalling pathway via the complement system plays an important role in microglia-neuron communication. The classical complement cascade components have been implicated in synapse elimination by microglia (Schafer et al., 2012; Stevens et al., 2007). To better understand the role of complement system in microglia-neuron interactions in mice with abolished Snap25-mediated release of synaptic vesicles, I measured C3 and CD11b protein levels and mRNA expression. C3 protein levels and mRNA expression were lower in both silenced cortex and hippocampus, and lower C3 mRNA expression was more prevalent in males. Interestingly, downregulation of C3 (tags synapses which need to be eliminated) correlates with loss of microglia phagocytic activity and was more prevalent in males. Moreover, mice lacking C1q or C3 show increased synaptic connectivity due to failed synaptic pruning (Chu et al., 2010; Stevens et al., 2007). In mice lacking complement receptor 3 (CR3) microglial phagocytosis was reduced between P5 and P20, and microglia engulfed inputs from the eye with less active neurons suggesting that microglia can act as a mediator of synaptic

remodelling in the developing retinothalamic system (Schafer et al., 2012). In silenced cortex, CD11b protein levels were increased but no changes in mRNA expression were observed. Moreover, CD11b protein levels and mRNA expression were increased in females at P14 and P21 silenced cortex. In silenced hippocampus, CD11b protein levels and mRNA expression were increased during development and mRNA expression was more prevalent in females at P14 and P21. This indicates that abolished Snap25-mediated release of synaptic vesicles caused downregulation of C3 and synapses that may need to be eliminated were not tagged. Since microglia are thus unable to recognize which synapses to eliminate, they may contact more synapses resulting in increased level of CD11b.

In conclusion, abolished Snap25-mediated release of synaptic vesicles affected microglial behaviour and dynamic, and microglia-neuron communications. The loss of microglial activity and impaired synaptic formation may be explained by altered chemokine and phagocytic signalling pathways. Given the differential effects of synaptic 'silencing' on microglial cell morphology and activity in males and females, it would be interesting to speculate that microglia may contribute to the sex-specific effects of synaptic 'silencing' on microglia-neuron interactions and synaptic maturation during development.

In the following chapter I will be presenting results and discuss whether the same changes in microglial behaviour and dynamics would apply for more acute silencing and activation without altering Snap25 expression. Manipulating activity using a different paradigm can distinguish whether the observed effects in this chapter were due to changes in neuronal synaptic activity or changes in receptor expressions that were influenced by Snap25 expression.

Chapter 5: Acute chemogenetic inhibition and activation of cortical layer 5 neurons and dentate gyrus affects microglial behaviour and dynamics

5.1 Introduction

Designer receptors exclusively activated by designer drugs (DREADDs) technology is a chemogenetic tool used to manipulate neuronal activity (Redfern et al., 2000; Sternson & Roth, 2014). Different protein classes have been chemogenetically engineered such as kinases (Bishop et al., 2000; Cohen et al., 2005; Y. Liu et al., 1998), enzymes (Klein et al., 2005; Strobel, 1998), G protein-coupled receptors (GPCRs) (Armbruster et al., 2007; Nakajima & Wess, 2012; Redfern et al., 2000; Vardy et al., 2015), and ligand-gated ion channels (Lerchner et al., 2007; Magnus et al., 2011). Here I presented the most commonly used GPCRs.

Gq-based DREADD is used to enhance neuronal firing and activate Gq signalling. Three Gq-based DREADDs were created based on different muscarinic receptors: hM1Dq, hM3Dq and hM5Dq (Armbruster et al., 2007) yet hM3Dq is the most used. hM3Dq can be activated by low concentrations of clozapine-N-oxide (CNO) actuator and mobilize intracellular calcium (Armbruster et al., 2007). Upon CNO binding, hM3Dq activates phospholipase C (PLC-β) and increases neuronal excitability by activating the protein kinase C (PKC) pathway via diacylglycerol (DAG) and Ca^{2+} through inositol-1,4,5-triphosphate (IP_3) (Guettier et al., 2009) (Figure 46).

Gi-based DREADD, an engineered human muscarinic receptor, is used to inhibit neuronal activity. The most common inhibitory DREADDs are hM2Di, hM4Di and KORD, yet hM4Di is the most used and can be activated by CNO (Armbruster et al., 2007). hM4Di inhibits neuronal activity by inducing hyperpolarization of Gβ/γ-mediated activation of G-protein inwardly rectifying potassium channels (GIRKs), which induces hyperpolarization (Armbruster et al.,

2007) and through inhibition of the synaptic vesicle release (Vardy et al., 2015) (Figure 46). Moreover, it has been indicated that hM4Di silences neurons via mild hyperpolarization and strong inhibition of release of neurotransmitter within minutes or hours (Vardy et al., 2015).

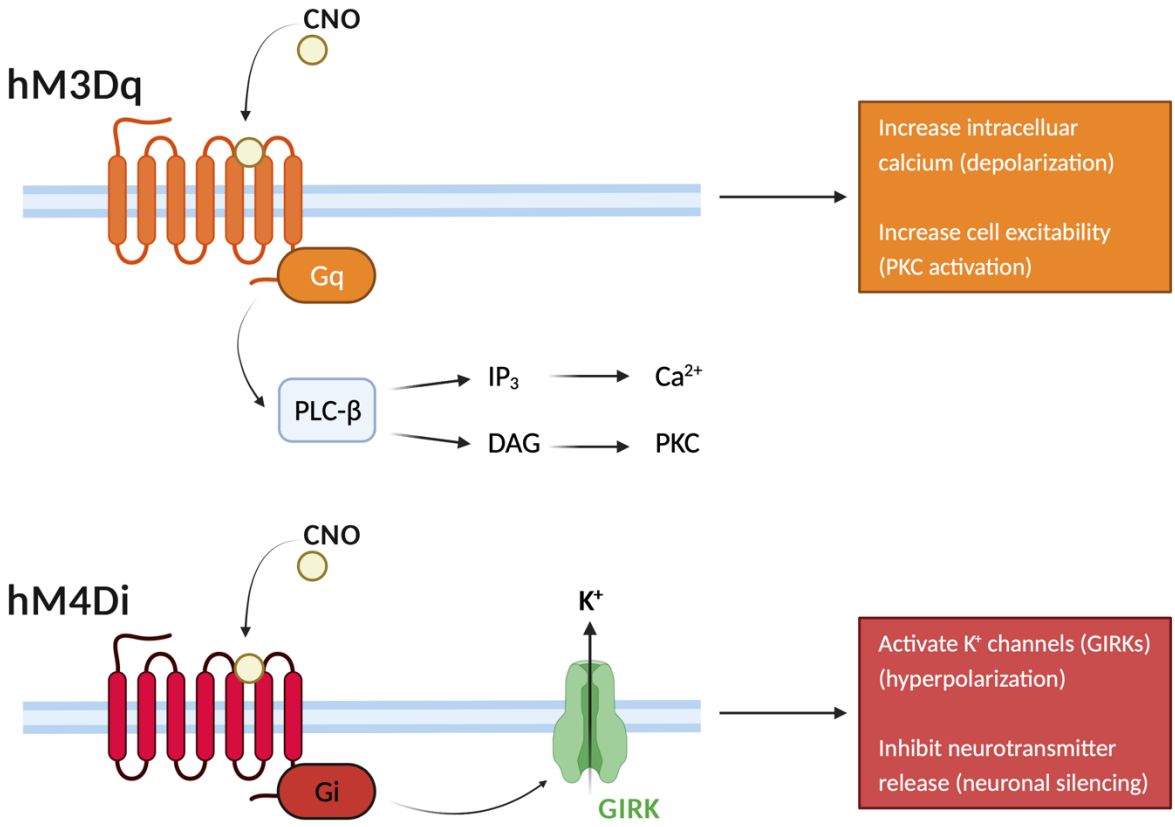


Figure 46: Excitatory and inhibitory DREADDs activation pathways

Excitatory DREADD (orange), inhibitory DREADD (red). PLC-β - phospholipase C, IP_3 - inositol-1,4,5-triphosphate, DAG – diacylglycerol, PKC – protein kinase C, GIRK - Gβ/γ-mediated activation of G-protein inwardly rectifying potassium channel. Created with BioRender.com

To better understand microglia-neuron interactions in an activity-dependent manner in the mature brain I used hM4Di and hM3Dq DREADDs and expressed them genetically within the same population of cortical and hippocampal neurons where I abolished Snap25 expression, thus abolishing regulated synaptic vesicular release in my previous experimental chapter. The Snap25 cKO model provides insight into chronic and continuous 'silencing' from the time of birth for the rest of the animal's life. To understand acute synaptic activation and inhibition I

used DREADDs to change the activity for hours rather than weeks in a selected population of cortical layer 5 and dentate gyrus neurons where Cre recombinase is expressed in the Rbp4^{Cre} mouse line (Hayashi et al., 2021; Hoerder-Suabedissen et al., 2019)

5.2 Results

5.2.1 Inhibitory and excitatory DREADDs mouse models

The R26-LSL-hM4Di-DREADD and CAG-LSL-hM3Dq-DREADD mouse lines were kindly provided by the Vyazovskiy laboratory who previously imported them from Jackson Laboratories. In the inhibitory DREADD line, Cre-recombinase causes the removal of a floxed-STOP cassette upstream of the *Gt(ROSA)26Sor* locus leading to the expression of a CAG promoter-driven HA-hM4Di-pta-mCitrine. In the excitatory DREADD line, Cre-recombinase mediated removal of an upstream floxed-STOP cassette leads to expression of CAG promoter-driven HA-hM3Dq-pta-mCitrine. Previously, the excitatory DREADD receptor was designed as a target insertion into the *Gt(ROSA)26Sor* locus as well as inhibitory DREADD receptor. However, in 2017 The Jackson Laboratory reported and confirmed a randomly integrated construct CAG-LSL-hM3Dq-pta-mCitrine instead of *Gt(ROSA)26Sor* locus and that the random insertion has not affected the functionality of the allele. hM4Di activation via CNO is predicted to cause acute neuronal silencing by inducing the canonical Gi-pathway in the expressing cells and hM3Dq activation via CNO is predicted to cause acute activation by inducing the canonical Gq-pathway in the expressing cells of subpopulation of cortical layer 5 and dentate gyrus neurons.

The following abbreviations were used: inhibitory DREADD (Rbp4^{Cre};hM4Di) and excitatory DREADD (Rbp4^{Cre};hM3Dq).

5.2.2 Experimental design and procedures

DREADD actuators are designer drugs that allow activation of the receptors in order to increase or suppress neuronal activity of the DREADD construct expressing cells. To activate DREADD constructs in transgenic mice I used CNO (clozapine-N-oxide), the most commonly used chemical ligand that activates hM4Di and hM3Dq DREADDs. However, CNO can be metabolized via back-transformation to clozapine in guinea pigs, humans (Jann et al., 1994) and mice (Gomez et al., 2017). Clozapine is an antipsychotic drug used to treat schizophrenia (Khan & Zaidi, 2017) and has a broad spectrum of side effects such as hypotension, sedation, and anticholinergic syndrome (Jann et al., 1994; Khan & Zaidi, 2017). Since CNO is back-metabolized to clozapine and other metabolites, it has off-target effects and binds to other neurotransmitter receptors (Gomez et al., 2017; van der Veen et al., 2021). Due to back-metabolism of CNO to clozapine another actuator has been used to activate DREADDs. Compound 21 has minimal off-site activity and cannot be metabolized to clozapine, and can be used as alternative to CNO (Chen et al., 2015; Thompson et al., 2018). However both clozapine and compound 21 have effects on sleep that has to be considered when chemogenetic paradigms are used in sleep models (Traut et al., 2022).

After systematic application of CNO the behaviour effects induced via DREADDs can be expected at least from 15 min (Jendryka et al., 2019) post injection and relative time course of CNO concentration in plasma peaks within 90 min (Allen et al., 2019). Based on the literature review about CNO pharmacokinetic and pharmacodynamic, for my experiments I chose to inject animals with CNO and perfuse them after 90 min (Table 20). All animals used for this part of experiments were adults and littermates.

Inhibitory DREADD (Rbp4^{Cre};hM4Di)			Excitatory DREADD (Rbp4^{Cre};hM3Dq)		
No of mice	**Compound**	**Concentration**	**No of mice**	**Compound**	**Concentration**
n = 2	Saline (control)	0.25 mg/ml	n = 6	Saline (control)	0.25 mg/ml
n = 2	CNO	1 mg/kg	n = 2	CNO	0.05 mg/kg
n = 2	CNO	5 mg/kg	n = 2	CNO	0.1 mg/kg
			n = 1	CNO	0.5 mg/kg
			n = 1*	CNO	1 mg/kg
			n = 3 (4*)	CNO	10 mg/kg
All animals were perfused 90 min after CNO administration					

Table 20: IP injections of saline and CNO

Red asterisks indicate dead mice. The brains of these mice were collected but were not included in further data analysis.

5.2.2.1 Inhibitory DREADD: *Rbp4^{Cre};hM4Di*

Inhibitory DREADD experiments were performed together with Dr. Elise Meijer. Rbp4^{Cre};hM4Di mice were used before by Dr. Lukas Krone (Molnár and Vyazovskiy groups) and we used the same CNO doses since Lukas did not observe any adverse effect on the Rbp4^{Cre};hM4Di transgenic mouse line after CNO administration. Inhibitory DREADD mice were injected with saline, 1 mg/kg CNO and 5 mg/kg CNO (Table 20) with 2 animals per dose for statistical analysis of the results. All animals were closely monitored, and their behaviour was recorded with video in ANYmaze software. During this experiment, animal behaviour was normal, they were not in pain or distress, and adverse effect of CNO was not observed.

5.2.2.2 Excitatory DREADD: *Rbp4^{Cre};hM3Dq*

The first pilot experiment was performed on Rbp4^{Cre};hM3Dq adult mice using 10 mg/kg CNO based on our literature review (Jendryka et al., 2019; Koike et al., 2016; Manvich et al., 2018; Martinez et al., 2019) In collaboration with Elise Meijer (Molnár and Vyazovskiy groups) we injected 4 animals with saline and 4 animals with 10 mg/kg CNO. CNO solution was prepared under sterile conditions and passed through a Millipore filter by Dr. Lukas Krone and Dr. Elise

Meijer (Molnár and Vyazovskiy groups). CNO was kept at -20 °C and defrosted on the day of use and diluted using sterile saline. 15 min after CNO intraperitoneal injection we observed an adverse effect of a sedation-like state (one mouse died after 55 min*), likely caused by a CNO dosage that was too high for this particular transgenic mouse line. An SC18 report was filed, and the PPL was amended to include drastically reduced activity as expected adverse event in addition to drastically increased activity as expected adverse event. After approval of the amendment, we repeated the experiments with the following adjustments: 1) we started with a 100x lower dose of CNO (0.1 mg/kg, compared to 10 mg/kg injected in the first pilot experiment) and gradually increasing the dose to 10x lower dose of CNO (1 mg/kg) with 2 animals per dose for statistical analysis of the results; 2) animals were injected, one animal at a time to closely monitor the animal before increasing the dose in the next animal. To have a proper documentation of animal behaviour following CNO administration we recorded the behaviour of the animals with video in ANYmaze software. We proposed to inject the saline (control) animals concomitantly with the experimental animals since we had no evidence from the previous experiment that these animals could have any adverse effect. As expected, we did not observe any behavioural changes in animals injected with saline. When starting with the lowest CNO dose (0.1 mg/kg), the animal seemed less active but was easily arousable. We increased CNO to 0.5 mg/kg and observed the same behaviour. Then, we increased CNO to 1 mg/kg*, however after 20 minutes following the IP administration the animal had seizures and died. After this observation and consultations with NACWO and VET, it was decided to reduce CNO 200x to 0.05 mg/kg. We observed a milder behavioural effect of reduced activity and slower locomotor activity with no signs of distress. In all $Rbp4^{Cre}$;hM3Dq animals, the CNO effect seemed to peak about 1 h after IP administration, and then gradually wear off again. We suspect that the death was due to strong reaction to

CNO acting on this particular neuronal population in the cerebral cortex that was generated to react to CNO in the Rbp4^{Cre};hM3Dq transgenic mouse. The activity of each neuronal population can have different effects on the overall brain activity and the behaviour of an animal. These effects are uncharted territories and in fact this is what we wanted to find out with our experiments to understand the functions of the different cortical projection neuron populations (Rbp4-Cre; Ntsr1-Cre and Drd1a-Cre) in behaviour of the animals. The effect of CNO in the neuron populations of cortical layer 5 and dentate gyrus in the Rbp4^{Cre};hM3Dq mice seems to have a very narrow functional range and it is difficult to control.

5.2.2.3 *Rbp4^{Cre}*, *hM4Di* and *hM3Dq* control experiments

To better understand if the DREADD itself has an impact on cortical neurons without CNO administration, I performed additional control experiments. I injected with saline and perfused after 90 min 2 animals of cortical layer 5 driver line (Rbp4^{Cre}), inhibitory DREADD receptor line (*hM4Di*) and excitatory DREADD receptor (*hM3Dq*) (Table 21). No changes of animal behaviour were observed after the saline injection. All animals used for this part of the experiments were adults and littermates.

Number of animals	Mouse line	Compounds	Concentration	Injection
n = 2	*Rbp4^{Cre}*	Saline	0.25 mg/ml	IP
n = 2	*hM4Di*	Saline	0.25 mg/ml	IP
n = 2	*hM3Dq*	Saline	0.25 mg/ml	IP
All animals were perfused 90 min after CNO administration				

Table 21: Animals used for control experiments

5.2.3 DREADDs validation

5.2.3.1 Methods

All animals were perfused as described in the General Methods Chapter in the section 'Perfusion' and brain tissue was sectioned as describes in section 'Fixed-tissue sectioning'. To evaluate changes of activation and silencing after CNO administration in Rbp4^{Cre};hM4Di and Rbp4^{Cre};hM3Dq I used cFos staining. All brain sections were blocked in 20 % normal goat serum (Sigma Aldrich) and 0.3 % Triton X-100 in PBS for 2 hours at room temperature. cFos was immunodetected by overnight incubation at 4 °C with primary antibodies (rabbit anti-cFos 1:500, Synaptic Systems, 226-003) followed by secondary antibodies (goat anti-rabbit A488) in PBS with 5% normal goat serum and 0.3% Triton X-100 for 2 hours at room temperature. Immunolabelled sections were counterstained with DAPI, mounted with FluorSave^{TM} reagent (MerckMillipore). To evaluate cFos+ cells in visual cortex layer 5, superior colliculus, hippocampus CA1 and hippocampus CA3 regions, immunolabelled sections were imaged with a laser-scanning confocal microscope (Zeiss LSM710) using 20x/0.6 air objective and 1x optical zoom at 0.42 µm pixel size, and frame size 1024 x 1024. Image size: 424.7 µm x 424.7 µm. cFos+ cell density was analysed using 'Cell counter' as described in the general method section before.

The same Rbp4^{Cre};hM4Di and Rbp4^{Cre};hM3Dq brain sections were used to detect changes in microglia density, morphology and activity as well as synaptic density in visual cortex layer 5, superior colliculus, hippocampus CA1 and CA3 regions. Iba1, CD68, vGlut1 and PSD95 staining were used as described before. Microglia density and morphology, microglia phagocytic

activity, and synaptic density imaging and analysis were performed as described in Chapters 3 and 4 previously.

5.2.3.2 Inhibitory DREADD validation

To validate inhibitory DREADD (Figure 47A) anti-cFos antibody was used. Saline injected mice were used as control. cFos+ cells density was measured in saline (Figure 47C) and CNO (Figure 47C') injected adult mice visual cortex layer 5, superior colliculus, hippocampal CA1 and CA3 regions.

In visual cortex layer 5 and superior colliculus, cFos+ cells density was decreased in mice injected with 1 mg/kg CNO (L5: saline = 3.818± 0.111, CNO = 1.812±0.042; SC: saline = 2.379±0.166, CNO = 0.249±0.028) and 5 mg/kg CNO (L5: saline = 3.818± 0.014, CNO = 0.816±0.042; SC: saline = 2.379±0.166, CNO = 0.097±0.028) compared to saline (main effect of CNO: $F(2,12) = 530.4$, $p < 0.0001$ for both, Figure 47G). No significant differences in cFos+ cells density after CNO application were observed in the hippocampal CA1 and CA3 regions. This data shows that application of CNO to $Rbp4^{Cre}$;hM4Di mouse leads to decreased density of cFos+ cells in visual cortex layer 5 and superior colliculus suggesting that neuronal activity was inhibited in the $Rbp4^{Cre}$ population of cortical layer 5 neurons and their target regions in the superior colliculus.

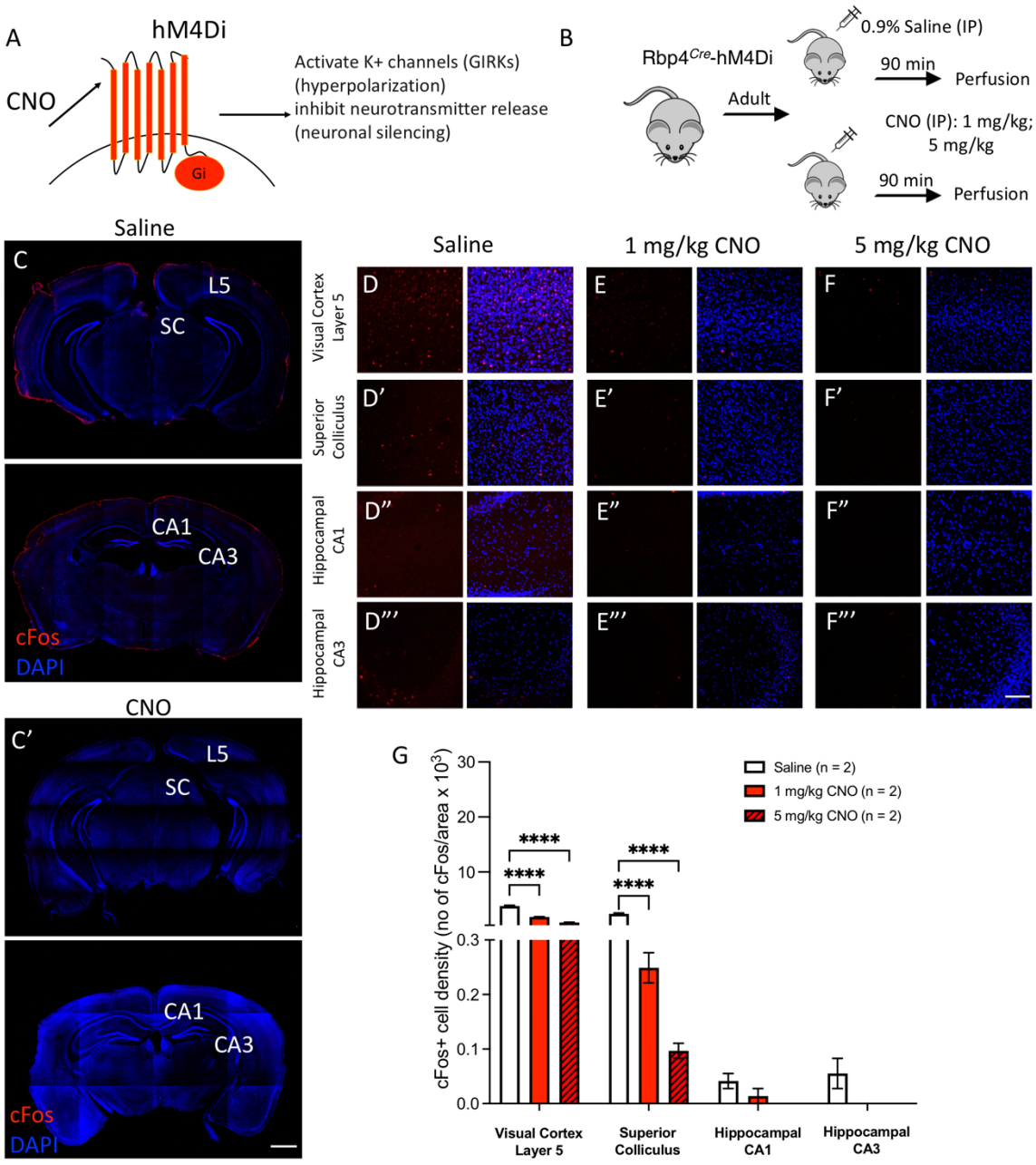


Figure 47: cFos+ cells density decreases in *Rbp4^{Cre};hM4Di* mice 90 minutes after CNO application

Schematic of inhibitory DREADD (A). Experimental procedures of inhibitory DREADD (B). Representative images of cFos+ cells (red) in saline (C) and CNO (C') injected mice brain. Representative images of cFos+ cells in saline injected mice visual cortex layer 5 (D), superior colliculus (D'), hippocampal CA1 (D") and CA3 (D"') regions. Representative images of cFos+ cells in 1 mg/kg CNO injected mice visual cortex layer 5 (E), superior colliculus (E'), hippocampal CA1 (E") and CA3 (E"') regions. Representative images of cFos+ cells (red) in saline (C) and CNO (C') injected mice brain. Representative images of cFos+ cells in 5 mg/kg CNO injected mice visual cortex layer 5 (F), superior colliculus (F'), hippocampal CA1 (F") and CA3 (F"') regions. Changes in cFos+ cells density after CNO application in visual cortex layer 5, superior colliculus, hippocampus CA1 and CA3 regions (G). Two-

way ANOVA, n = 2 per group, all data presented as mean ± SEM, * $p < 0.05$, ** $p < 0.01$, *** $p < 0.001$, **** $p < 0.0001$. Scale bar of C-C' - 1000 µm, D-F"' 100 µm

5.2.3.3 Excitatory DREADD validation

I next validated excitatory DREADD (Figure 48A) using cFos immunolabelling. Saline injected mice were used as control. Animals were perfused after 90 mins of CNO application, and their brains were processed for cFos immunohistochemistry, counterstained with DAPI. cFos+ cells density was measured in saline (Figure 48C-D) and CNO (Figure 48E-F) injected adult mice visual cortex layer 5, superior colliculus, hippocampal CA1 and CA3 regions.

Immunolabelling with cFos showed that $Rbp4^{Cre}$;hM3Dq mice treatment with CNO leads to increased density of cFos+ cells in the visual cortex layer 5, superior colliculus and hippocampal CA3 region (main CNO effect: $F(3,36) = 108.5$, $p < 0.0001$, Figure 48G). In visual cortex layer 5, cFos+ cells density was increased in mice injected with 0.05 mg/kg CNO (saline = 4.178±0.169 vs CNO = 5.963±0.014, $p = 0.0015$), 0.1 mg/kg CNO (saline = 4.178±0.169 vs CNO = 6.737±0.041, $p < 0.0001$) and 10 mg/kg CNO (saline = 4.178±0.169 vs CNO = 14.194±1.156, $p < 0.0001$) compared to saline. In superior colliculus, increased cFos+ cells density was observed only in mice injected with 10 mg/kg CNO compared to saline (saline = 1.328± 0.108 vs CNO = 3.228±1 0.621, $p = 0.0005$). In the hippocampal CA3 area, increased cFos+ cells density was observed only in mice injected with the higher dose of 10 mg/kg CNO compared to saline (saline = 0.028± 0.005 vs CNO = 1.549±1 0.085 $p = 0.0087$). These results suggest that neuronal activity was increased in the $Rbp4^{Cre}$ population of cortical layer 5 neurons, their target regions in the superior colliculus and at the terminal of their mossy fiber projections in the CA3 region.

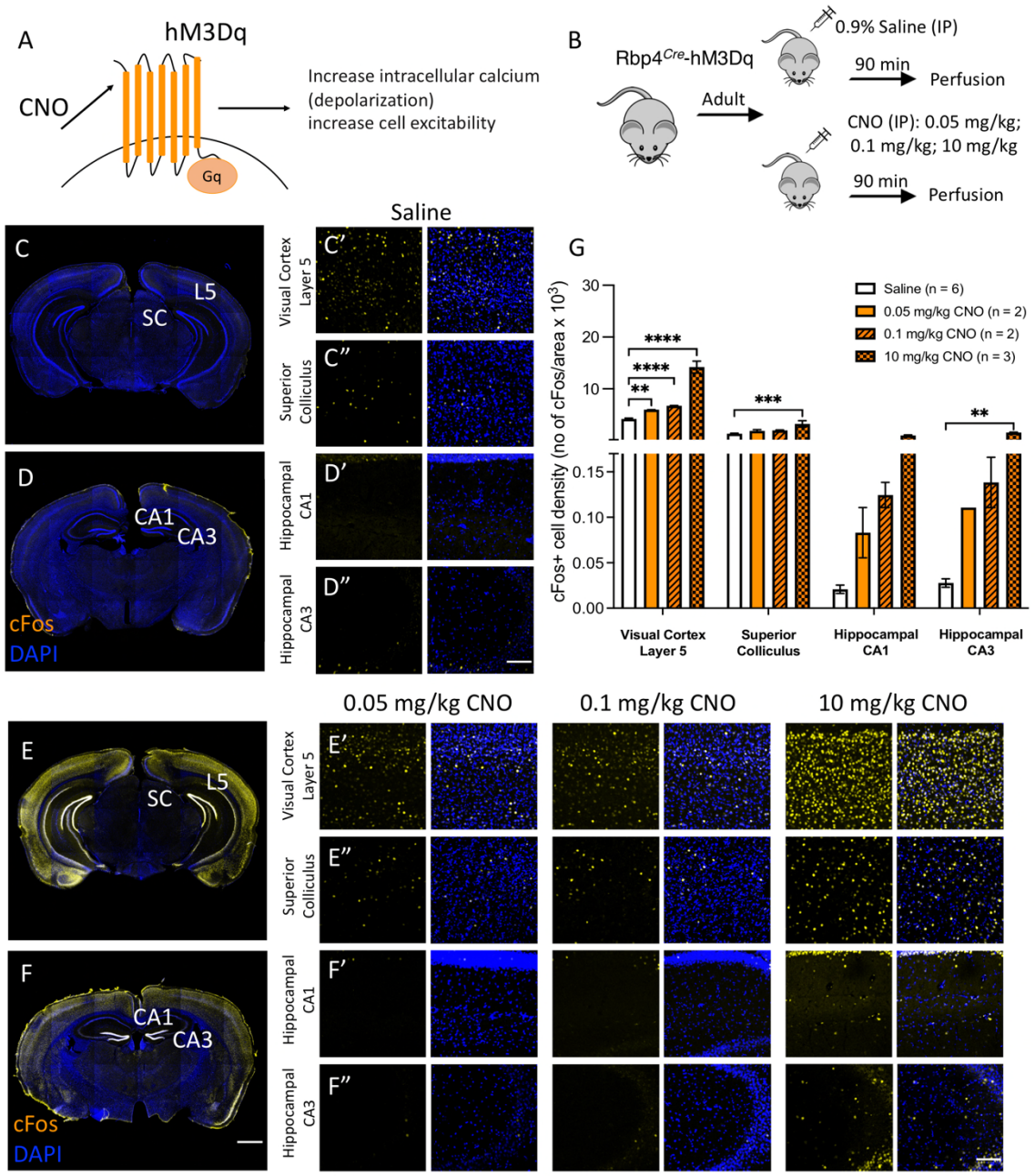


Figure 48: cFos+ cells increases in *Rbp4^{Cre};hM3Dq* mice 90 minutes after CNO application

Schematic of excitatory DREADD (A). Experimental procedures of excitatory DREADD (B). Representative images of cFos+ cells (orange) in saline (C-D) injected mice visual cortex layer 5 (C'), superior colliculus (C''), hippocampal CA1 (D') and CA3 (D"') regions. Representative images of cFos+ cells in CNO injected mice visual cortex layer 5 (E-E), superior colliculus (E-E'), hippocampal CA1 (F-F') and CA3 (F-F") regions. Representative images of cFos+ cells (red) in saline (C) and CNO (C') injected mice brain. Changes in cFos+ cells density after CNO administration in visual cortex layer 5, superior colliculus, hippocampal CA1 and CA3 regions (G). Two-way ANOVA, saline n = 6, 0.05 mg/kg CNO n = 2, 0.1 mg/kg CNO n = 2 and 10 mg/kg CNO n = 2, all data presented as mean ± SEM, * $p < 0.05$, ** $p < 0.01$, *** $p < 0.001$, **** $p < 0.0001$. Scale bar of C-F - 1000 µm, the rest of the images - 100 µm.

5.2.3.4 Rbp4^{Cre}, hM4Di and hM3Dq control validation

Cortical layer 5 driver line (Rbp4^{Cre}), inhibitory DREADD receptor line (hM4Di) and excitatory DREADD receptor (hM3Dq) mice were injected only with saline and for validation I used cFos labelling. In visual cortex layer 5 and superior colliculus, higher cFos+ cells density was observed in hM4Di and hM3Dq mice ($F(2,12) = 159.8$, $p<0.0001$). In visual cortex layer 5, cFos+ cells density was increased in hM4Di and hM3Dq compared to Rbp4^{Cre} (Rbp4^{Cre} = 5.727±0.277 vs hM4Di = 6.641±0.166, $p = 0.0214$ and Rbp4^{Cre} = 5.727±0.277 vs hM3Dq = 14.692±0.747, $p < 0.0001$), and in hM3Dq compared to hM4Di (hM4Di = 6.641±0.166 vs hM3Dq = 14.692±0.747, $p < 0.0001$). In superior colliculus, cFos+ cells density was increased in hM3Dq compared to Rbp4^{Cre} and hM4Di (Rbp4^{Cre} = 1.466±0.001 vs hM3Dq = 3.445±0.124, $p < 0.0001$ and hM4Di = 1.480±0.179 vs hM3Dq = 3.445±0.124, $p < 0.0001$).

For further validation I compared cFos+ cells density between saline injected Rbp4^{Cre}, hM4Di and hM3Dq to saline injected Rbp4^{Cre};hM4Di and Rbp4^{Cre};hM3Dq. Differences in cFos+ cells density were observed only in visual cortex layer 5 and superior colliculus. cFos+ cell density was decreased in transgenic inhibitory and/or excitatory DREADDs mice crossed with Rbp4^{Cre} driver line compared to only Rbp4^{Cre} driver line and DREADD receptor hM4Di and hM3Dq lines (L5: Rbp4^{Cre} = 5.727±0.277, hM4Di = 6.641±0.166, Rbp4^{Cre};hM4Di = 3.818±0.111, hM3Dq = 14.692±0.747, Rbp4^{Cre};hM3Dq = 4.177±0.169; SC: Rbp4^{Cre} = 1.466±0.001, hM3Dq = 3.445±0.124, Rbp4^{Cre};hM4Di = 2.379±0.166, Rbp4^{Cre};hM3Dq = 1.328±0.108, $F(4,36) = 213.6$, $p < 0.0001$).

These results showed that without CNO treatment inhibitory DREADD and excitatory DREADDs had lower cFos+ cells density than Rbp4^{Cre}, hM4Di and hM3Dq.

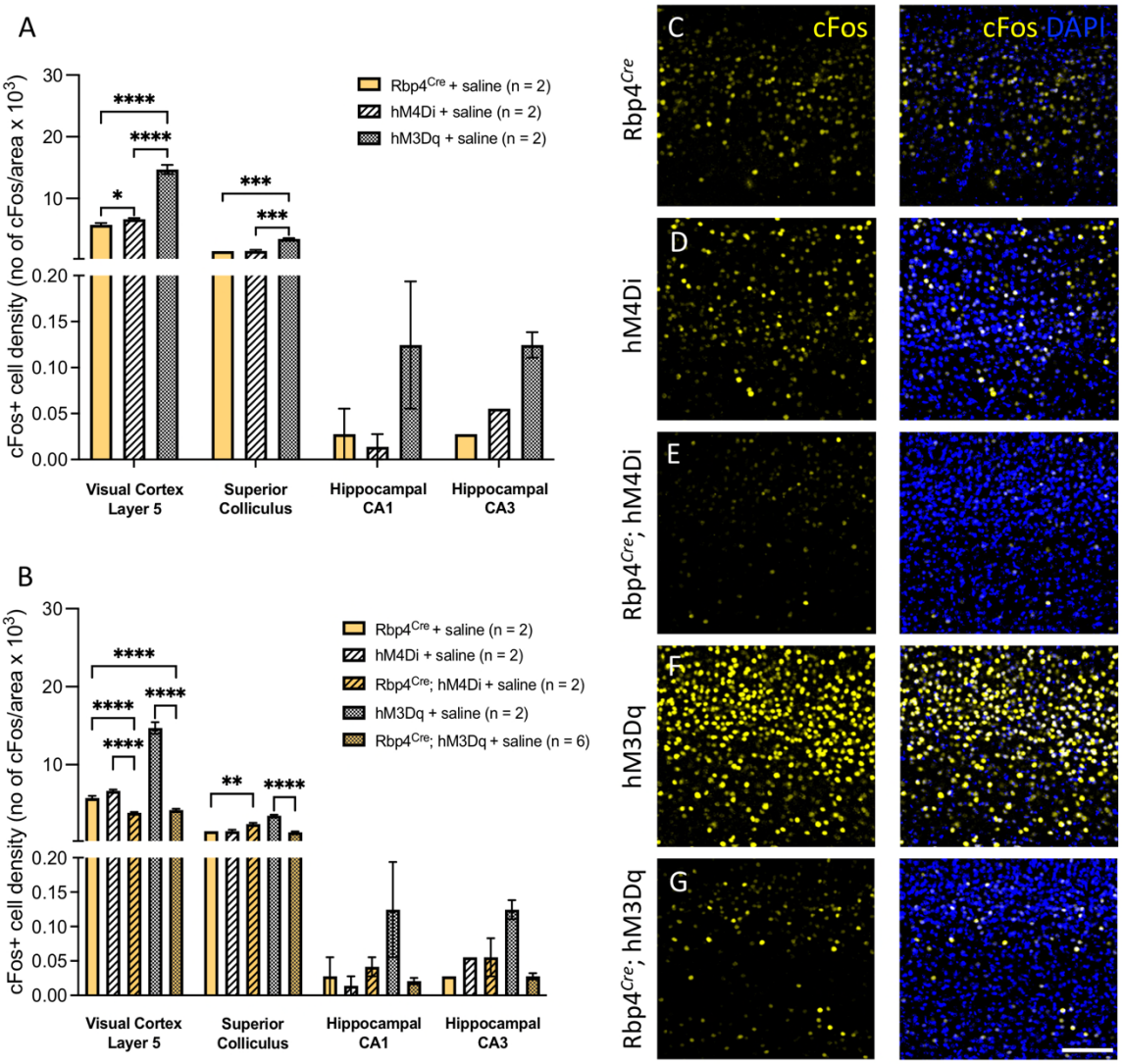


Figure 49: Changes in cFos+ density in mice injected with saline

Changes in cFos+ cells density in saline injected Rbp4^{Cre};hM4Di and Rbp4^{Cre};hM3Dq (A) and comparison with saline injected Rbp4^{Cre};hM4Di and Rbp4^{Cre};hM3Dq (B). Representative images of cFos+ cells (yellow) density in saline injected Rbp4^{Cre} (C), hM4Di (D), Rbp4^{Cre};hM4Di (E), hM3Dq (F) and Rbp4^{Cre};hM3Dq (G) mice brain. Two-way ANOVA, n = 2 per group, all data presented as mean ± SEM, * $p < 0.05$, ** $p < 0.01$, *** $p < 0.001$, **** $p < 0.0001$. Scale bar, 100 µm.

5.2.3 Chronic and acute 'silencing' and acute activation of cortical layer 5 subtypes and dentate gyrus neurons affects microglial behaviour and synaptic density in the visual cortex layer 5, superior colliculus, hippocampal CA1 and CA3 regions of the mature brain

To investigate whether short-term 'silencing' and activation have any impact on microglia, I evaluated microglial density, phagocytic activity, morphological features and synaptic density in adult mice visual cortex layer 5, superior colliculus, hippocampal CA1 and CA3 regions. To further understand microglia's role in activity-dependent neuronal network maintenance I also used chronically silenced Snap25 cKO adult mice. Due to synaptic 'silencing' microglial density was increased in adult mice brain (main Snap25 effect, $F(1,16) = 158.3$, $p < 0.0001$). In Snap25 cKO adult mice, microglial density was increased in visual cortex layer 5 (control = 2.742±0.125 vs Snap25 cKO = 4.209±0.157, $p < 0.0001$) hippocampal CA1 (control = 1.397±0.064 vs Snap25 cKO = 3.209±0.055, $p < 0.0001$) and CA3 (control = 1.453±0.102 vs Snap25 cKO = 1.928±0.028, $p = 0.0055$) regions compared to control mice but no significant differences were observed in superior colliculus (Figure 50A'). Moreover, the percentage of CD68 in microglia was decreased only in Snap25 cKO mice visual cortex layer 5 (control = 9.647±1.143 vs Snap25 cKO = 4.416±0.129, main Snap25 cKO effect: $F(1,16) = 9.256$, $p = 0.0078$, Figure 50A") out of all the regions investigated. In $Rbp4^{Cre}$;hM4Di mice, differences in microglial density were observed only in the hippocampal CA1 region (Figure 50B'). Microglial density was increased in mice injected with 5 mg/kg CNO compared to saline injected mice (saline = 1.328±0.055 vs CNO = 2.670±0.374, $p = 0.0007$, main CNO effect: $F(2,12) = 10.70$, $p = 0.0022$ Figure 50B'). Moreover, the percentage of CD68 in microglia was decreased in mice injected with 1 mg/kg and/or 5 mg/kg CNO compared to saline injected mice (main CNO effect: $F(2,12) = 25.75$, $p < 0.0001$ Figure 50B").

In visual cortex layer 5, the percentage of CD68 in microglia was decreased in mice injected with 1 mg/kg and 5 mg/kg CNO compared to saline injected mice (saline = 6.978±0.751 vs 1 mg/kg CNO = 3.689±1.644, *p* = 0.0196 and vs 5 mg/kg CNO = 2.586±0.436, *p* = 0.0037). In superior colliculus, the percentage of CD68 in microglia was decreased in mice injected with 1 mg/kg and 5 mg/kg CNO compared to saline injected mice (saline = 7.791±0.064 vs 1 mg/kg CNO = 4.991±0.041, *p* = 0.0408 and vs 5 mg/kg CNO = 4.216±0.621, *p* = 0.0127). In the hippocampal CA1 and CA3 regions, the percentage of CD68 in microglia was decreased in mice injected with 5 mg/kg CNO compared to saline injected mice (CA1: saline = 7.425±1.226 vs CNO = 2.562±0.135, *p* = 0.0018 and CA3: saline = 7.321±0.797 vs CNO = 2.621±1.601, *p* = 0.0023 Figure 50B').

In $Rbp4^{Cre}$;hM3Dq, microglial density was decreased in mice injected with 0.05 mg/kg, 0.1 mg/kg and 10 mg/kg CNO compared to saline injected mice (main CNO effect: $F(3,36) = 52.98$, $p < 0.0001$, Figure 50C', Table 22).

CD68 in microglia increases in excitatory DREADD mice injected with CNO (main CNO effect: $F(3,36) = 121,2$, $p < 0.0001$ Figure 50C"). In visual cortex layer 5 and superior colliculus, the percentage of CD68 in microglia was increased in mice injected with 10 mg/kg CNO compared to saline injected mice (*p* = 0.0017 and *p* = 0.0050 respectively, Figure 50C"). In the hippocampal CA1 area, the percentage of CD68 in microglia was increased in mice injected with 0.05 mg/kg, 0.1 mg/kg and 10 mg/kg CNO compared to saline injected mice (*p* = 0.0055, *p* < 0.0001 and *p* < 0.0001 respectively, Figure 50C"). In the hippocampal CA3 region, the percentage of CD68 in microglia was increased in mice injected with 0.05 mg/kg, 0.1 mg/kg and 10 mg/kg CNO compared to saline injected mice (*p* < 0.0001 for all, Figure 50C").

These findings show that chronic and acute 'silencing' affected microglial cells behaviour in a similar fashion. Microglial density was increased, yet the percentage of CD68 in microglia was

decreased in Snap25 cKO and Rbp4^{Cre};hM3Dq mouse brains. Acute chemogenetic activation of selected neuronal populations of the Rbp4-cre neurons had a very strong effect on microglia in visual cortex layer 5, superior colliculus, hippocampal CA1 and CA3 regions of the brains that I selected to study in detail. CNO injected Rbp4^{Cre};hM3Dq mice showed reduced microglial density and increased CD68 in Iba1. The strongest changes of microglia were observed in excitatory DREADD mice injected with the highest dose of CNO. Interestingly, even 100x and 200x lower concentrations of CNO had an effect on microglial density and the percentage of CD68 in microglia suggesting that microglia are particularly sensitive to synaptic activation.

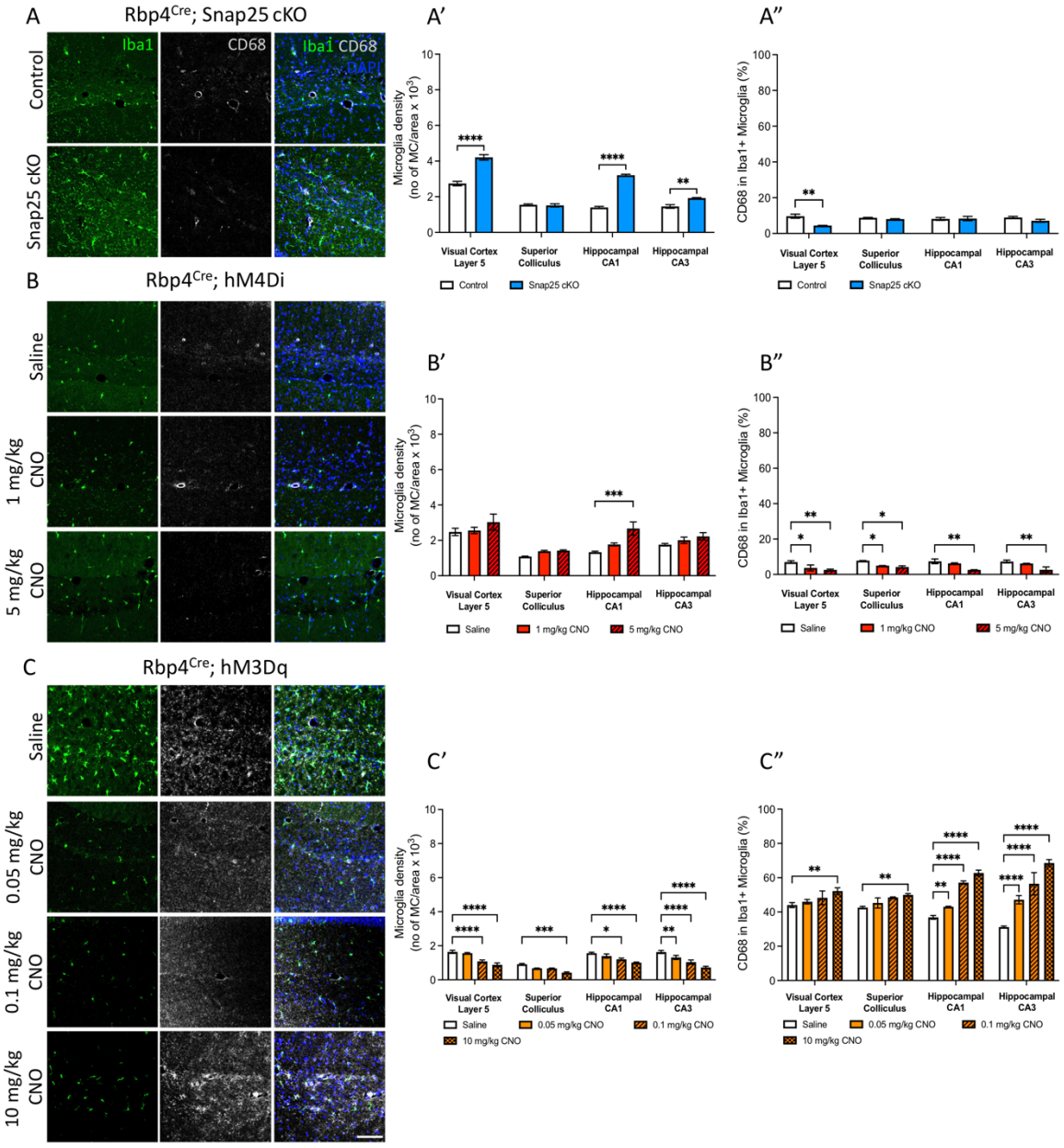


Figure 50: Changes in microglial distribution and phagocytic activity in the chronic 'silencing' model of Snap25 cKO (*Rbp4^{Cre};Snap25$^{fl/fl}$*), and after 90 minutes of chemogenetic manipulation in the inhibitory (*Rbp4^{Cre};hM4Di*) and excitatory (*Rbp4Cre;hM3Dq*) DREADDs mice

Representative images of microglial (Iba1 – green) density and phagocytic activity (CD68 – grey) in Snap25 cKO (A), Rbp4^{Cre};hM4Di (B) and Rbp4^{Cre};hM3Dq (C) mice. Changes in microglial density (A') and the percentage of CD68 in microglia (A") between control and Snap25 cKO mice (two-way ANOVA, control n = 4, Snap25 cKO = 2). Changes in microglial density (B') and the percentage of CD68 in microglia (B") in Rbp4^{Cre};hM4Di (two-way ANOVA, n = 2 per group). Changes in microglial density (C') and the percentage of CD68 in microglia (C") in Rbp4^{Cre};hM3Dq (two-way ANOVA, saline n = 6, 0.05 mg/kg CNO n = 2, 0.1 mg/kg CNO n = 2 and 10 mg/kg CNO n = 2). All data presented as mean ± SEM, * $p < 0.05$, ** $p < 0.01$, *** $p < 0.001$, **** $p < 0.0001$. Scale bar, 100 µm.

Microglial Density				
	Treatment conditions	Mean values ± standard error	*t*	*p*
Visual Cortex Layer 5	Saline vs 0.05 mg/kg CNO	1.641±0.091 vs 1.563±0.041	t=0.6037 df=36.00	0.5499
	Saline vs 0.1 mg/kg CNO	1.641±0.091 vs 1.079±0.083	t=4.332 df=36.00	0.0001
	Saline vs 10 mg/kg CNO	1.641±0.091 vs 0.878±0.113	t=6.786 df=36.00	0.0001
Superior colliculus	Saline vs 0.05 mg/kg CNO	0.916±0.044 vs 0.673±0.018	t=1.870 df=36.00	0.0696
	Saline vs 0.1 mg/kg CNO	0.916±0.044 vs 0.668±0.023	t=1.906 df=36.00	0.0647
	Saline vs 10 mg/kg CNO	0.916±0.044 vs 0.421±0.044	t=4.394 df=36.00	0.0001
Hippocampal CA1	Saline vs 0.05 mg/kg CNO	1.563±0.056 vs 1.397±0.124	t=1.278 df=36.00	0.2093
	Saline vs 0.1 mg/kg CNO	1.563±0.056 vs 1.203±0.069	t=2.770 df=36.00	0.0088
	Saline vs 10 mg/kg CNO	1.563±0.056 vs 1.009±0.032	t=4.920 df=36.00	0.0001
Hippocampal CA3	Saline vs 0.05 mg/kg CNO	1.632±0.092 vs 1.314±0.124	t=2.450 df=36.00	0.0193
	Saline vs 0.1 mg/kg CNO	1.632±0.092 vs 1.037±0.124	t=4.581 df=36.00	0.0001
	Saline vs 10 mg/kg CNO	1.632±0.092 vs 0.726±0.069	t=8.057 df=36.00	0.0001

Table 22: Changes in microglial density after CNO application in excitatory DREADD mice

To further investigate microglial morphology in chronic and acute 'silencing' and acute activation, I measured microglial volume, soma size and primary branches, and microglial ramification using 3D Sholl analysis.

In Snap25 cKO mice, no significant differences in microglial volume (Figure 51D) and the number of primary branches (Figure 51D") were observed. Microglial soma size was increased in Snap25 cKO mice compared to control (main Snap25 cKO effect: F(1,104) =12.16, p = 0.0007, Figure 51 D') but only in visual cortex layer 5 (p = 0.0012).

In Rbp4^{Cre};hM4Di mice, no significant differences in microglial volume were observed in visual cortex layer 5, superior colliculus, hippocampal CA1 and CA3 regions (Figure 51E). Due to CNO application, microglial soma size was increased (L5 saline = 47.025±0.381, L5 CNO = 49.378±0.767, CA3 saline = 46.674±0.517, CA3 CNO = 48.592±0.021, main CNO effect: F(2,66) = 15.83, p < 0.0001). In visual cortex layer 5 and the hippocampal CA3 region, microglial soma size was increased in mice injected with 5 mg/kg CNO compared to saline injected mice (p =

0.0002 and $p = 0.0023$ respectively, Figure 51E'). In visual cortex layer 5 and hippocampal CA3 area, microglial primary branches were decreased in mice injected with 1 mg/kg and 5 mg/kg CNO compared to saline injected mice (main CNO effect: $F(2,66) = 25.45$, $p < 0.0001$, Figure 51E").

In Rbp4^{Cre};hM3Dq mice injected with CNO, I observed changes in microglial cells morphology: microglial volume was decreased (main CNO effect: $F(3,160) = 80.15$, $p < 0.0001$ (Figure 51F), as well as soma size (main CNO effect: $F(3,160) = 37.77$, $p < 0.0001$, Figure 51F') and the number of primary branches (main CNO effect: $F(3,160) = 113.0$, $p < 0.0001$, Figure 51F").

Microglial volume was decreased in mice injected with 0.05 mg/kg and 0.1 mg/kg CNO compared to saline injected mice ($p < 0.0001$ for both, Figure 51F) in visual cortex layer 5. In the hippocampal CA3 region, microglial volume was decreased in mice injected with 0.05 mg/kg, 0.1 mg/kg and 10 mg/kg CNO compared to saline injected mice ($p < 0.0001$, $p < 0.0001$ and $p = 0.0081$ respectively, Figure 51F). In Rbp4^{Cre};hM3Dq, 90 minutes after CNO application I observed that microglial soma size was decreased in mice injected with 0.05 mg/kg and 0.1 mg/kg CNO but increased in mice injected with 10 mg/kg CNO compared to saline injected mice in visual cortex layer 5 ($p = 0.0024$, $p < 0.0001$ and $p = 0.0380$ respectively) and hippocampal CA3 ($p = 0.0047$, $p < 0.0001$ and $p = 0.0054$ respectively, Figure 51F'). In visual cortex layer 5, the number of primary branches was decreased in mice injected with 0.05 mg/kg and 10 mg/kg CNO compared to saline injected mice ($p < 0.0001$ for both, Figure 51F"). In the hippocampal CA3 region, the number of primary branches was decreased in mice injected with 0.05 mg/kg, 0.1 mg/kg and 10 mg/kg CNO compared to saline injected mice ($p = 0.0028$, $p < 0.0001$ and $p < 0.0001$ respectively, Figure 51F").

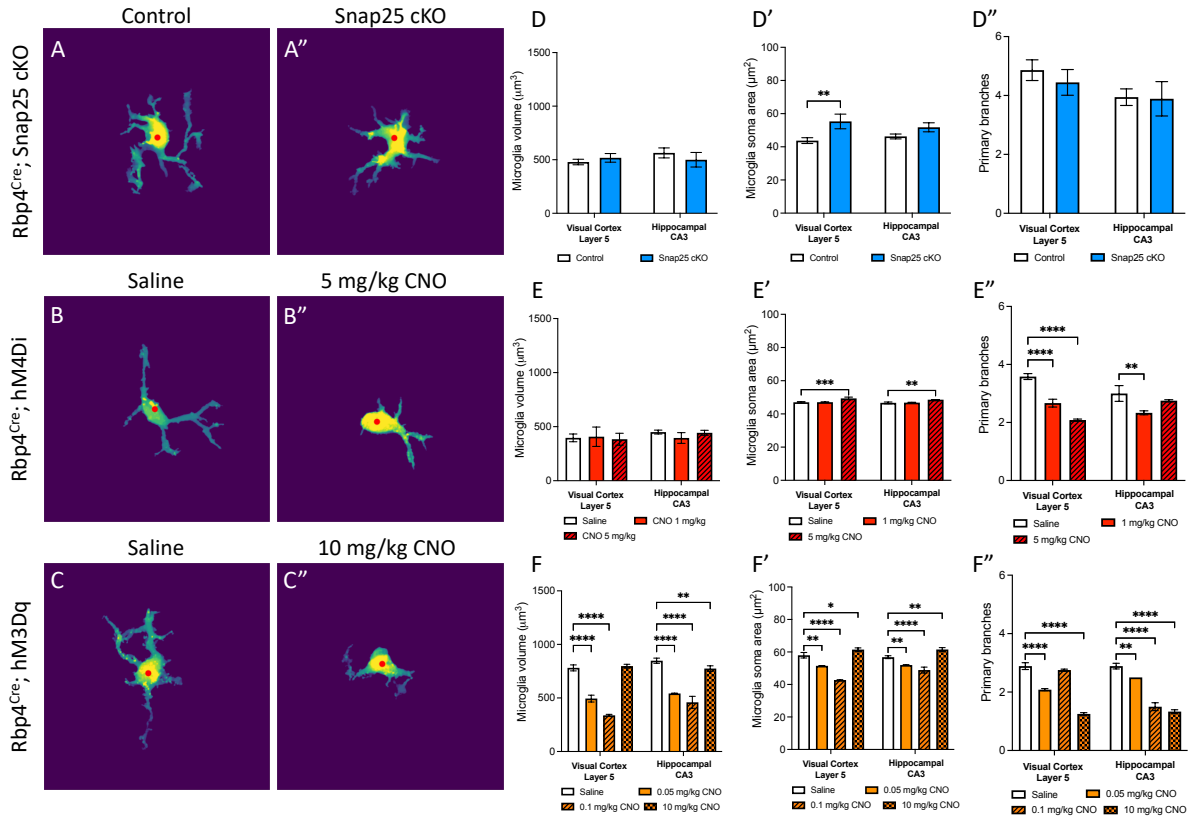


Figure 51: Changes in microglial morphology in in the chronic 'silencing' model of Snap25 cKO, and after 90 minutes of chemogenetic manipulation in the inhibitory (*Rbp4^{Cre};hM4Di*) and excitatory (*Rbp4^{Cre};hM3Dq*) DREADDs mice

Representative images of microglia in control (A) and Snap25 cKO (A”), in saline (B) and 5mg/kg CNO (B”) injected Rbp4^{Cre};hM4Di mice, and in saline (C) and in 10 mg/kg CNO (C”) injected Rbp4^{Cre};hM3Dq mice. Changes in microglial volume (D), soma area (D’) and primary branches (D”) between control and Snap25 cKO (two-way ANOVA, control n = 4, Snap25 cKO = 2). Changes in microglial volume (E), soma area (E’) and primary branches (E”) in Rbp4^{Cre};hM4Di (two-way ANOVA, n = 2 per group). Changes in microglial volume (F), soma area (F’) and primary branches (F”) in Rbp4^{Cre};hM3Dq (two-way ANOVA, saline n = 6, 0.05 mg/kg CNO n = 2, 0.1 mg/kg CNO n = 2 and 10 mg/kg CNO n = 2). All data presented as mean ± SEM, * $p < 0.05$, ** $p < 0.01$, *** $p < 0.001$, **** $p < 0.0001$.

3D Sholl analysis was performed on Iba1-immunolabelled sections to quantify the number of microglial process intersections as a function of radial distance from individual cell soma and describe changes in branch patterns by measuring Sholl regression coefficient. 3D Sholl analysis revealed changes only in Snap25 cKO mice hippocampal CA3 region (main Snap25

cKO effect: F(1,104) = 1.575, p = 0.2123, Figure 52D). 3D Sholl intersections were lower in Snap25 cKO compared to control mice (p = 0.0205, Figure 52D).

In Rbp4^{Cre};hM3Dq mice brain, the number of intersections was decreased in mice injected with CNO (main CNO effect: $F(2,66) = 1194$, $p < 0.0001$, Figure 52E). Sholl number of intersections where lower in mice injected with 0.05 mg/kg and 0.1 mg/kg CNO compared to saline injected mice in both visual cortex layer 5 ($p < 0.0001$ for both) and hippocampal CA3 ($p < 0.0001$ for both, Figure 52E). No significant differences in Sholl regression coefficient were observed (Figure 52E').

In Rbp4^{Cre};hM3Dq mice injected with CNO, decreased number of intersections (main CNO effect: $F(3,160) = 6.706$, $p = 0.0003$, Figure 52F) and increased regression coefficient (main CNO effect: $F(3,160) = 50.0$, $p < 0.0001$, Figure 52F') were observed. The 3D Sholl number of intersections was decreased in mice injected with 0.05 mg/kg, 0.1 mg/kg and 10 mg/kg CNO compared to saline injected mice but only in the hippocampal CA3 region (p = 0.0208, p = 0.0034 and p = 0.0001 respectively, Figure 52F). In visual cortex layer 5, the Sholl regression coefficient was increased in mice injected with 0.05 mg/kg and 0.1 mg/kg CNO compared to saline injected mice ($p < 0.0001$ for both Figure 52F'). In the hippocampal CA3 region, Sholl regression coefficient was increased in mice injected with 0.05 mg/kg, 0.1 mg/kg and 10 mg/kg CNO compared to saline injected mice ($p < 0.0001$, $p < 0.0001$ and $p = 0.0002$ respectively, Figure 52F').

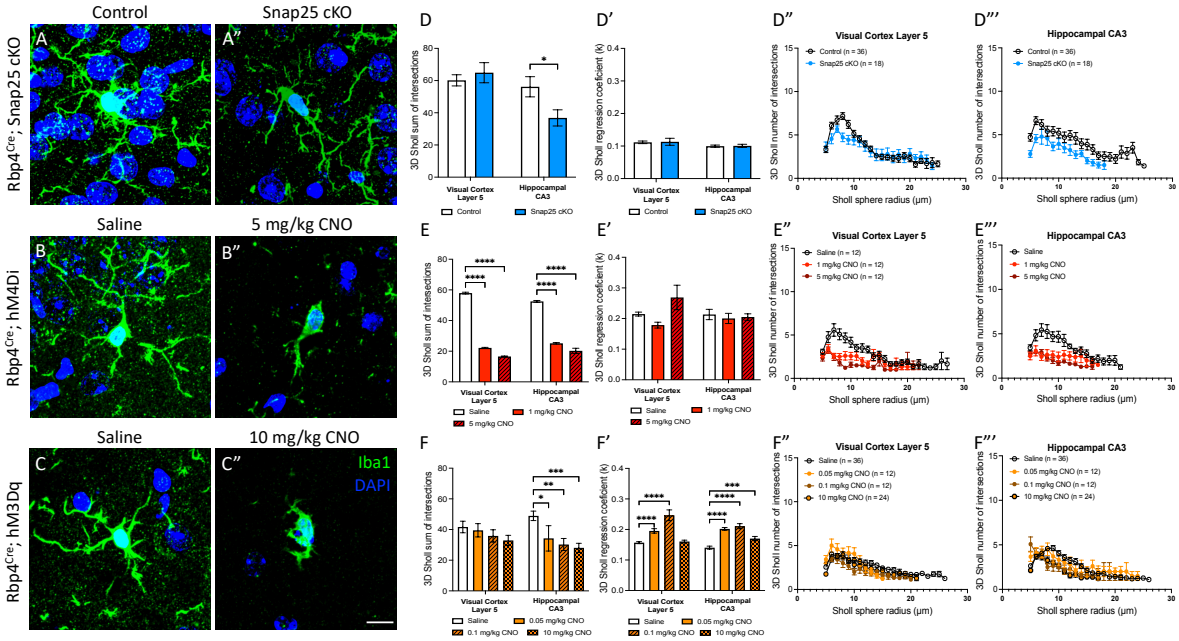


Figure 52: Changes in microglia ramification patterns in the chronic 'silencing' model of Snap25 cKO, and after 90 minutes of chemogenetic manipulation in the inhibitory (*Rbp4^{Cre};hM4Di*) and excitatory (*Rbp4^{Cre};hM3Dq*) DREADDs mice

Representative images of microglia in control (A) and Snap25 cKO (A''), in saline (B) and 5mg/kg CNO (B'') injected Rbp4^{Cre};hM4Di mice, and in saline (C) and in 10 mg/kg CNO (C'') injected Rbp4^{Cre};hM3Dq mice after 90 minutes of CNO application. Changes in 3D Sholl sum of intersections (D), regression coefficient (D') in visual cortex layer 5 (D'') and hippocampal CA3 region (D''') between control and Snap25 cKO (two-way ANOVA, control n = 4, Snap25 cKO = 2). Changes in 3D Sholl sum of intersections (E), regression coefficient (E') in visual cortex layer 5 (E'') and hippocampal CA3 region (E''') in Rbp4^{Cre};hM4Di (two-way ANOVA, n = 2 per group). Changes in 3D Sholl sum of intersections (F), regression coefficient (F') in visual cortex layer 5 (F'') and hippocampal CA3 region (F''') in Rbp4^{Cre};hM3Dq (two-way ANOVA, saline n = 6, 0.05 mg/kg CNO n = 2, 0.1 mg/kg CNO n = 2 and 10 mg/kg CNO n = 2). All data presented as mean ± SEM, * $p < 0.05$, ** $p < 0.01$, *** $p < 0.001$, **** $p < 0.0001$. Scale bar, 100 µm

These results show changes in microglial morphology in mice with chronic and acute synaptic 'silencing' and acute activation. In mouse brains with abolished Snap25-mediated release of synaptic vesicles, microglial cells had bigger soma and fewer branches. In Rbp4^{Cre};hM3Dq mice, microglial cells were smaller with bigger soma area and less branches. These

morphological changes of microglia suggest that excitatory DREADD mice brain had two different types of microglia: ramified and amoeboid.

To further examine chronic and acute 'silencing' and acute activation effect on synaptic density, I quantified the number of synaptic puncta as the colocalization of the presynaptic (vGlut1) and postsynaptic (PSD95) markers that are specific for the excitatory synapses in visual cortex layer 5, superior colliculus, hippocampal CA1 and CA3 region. In Snap25 cKO brain, synaptic density was increased (main Snap25 cKO effect: $F(1,16) = 536.0$, $p < 0.0001$, Figure 53A"). Moreover, synaptic density was increased in visual cortex layer ($p < 0.0001$), superior colliculus ($p = 0.0251$), hippocampal CA1 ($p < 0.0001$) and CA3 ($p < 0.0001$) regions compared to control mice. In $Rbp4^{Cre}$;hM4Di mice, synaptic density was increased in mice injected with CNO (main CNO effect: $F(2,12) = 164,7$, $p < 0.0001$, Figure 53B"). In addition, synaptic density was increased in mice injected with 1 mg/kg and 5 mg/kg CNO compared to saline injected mice in visual cortex layer 5 ($p < 0.0001$), hippocampal CA1 ($p < 0.0001$) and CA3 ($p < 0.0001$). In $Rbp4^{Cre}$;hM3Dq, synaptic density was only measured in saline and 10 mg/kg CNO injected mice and I observed lower synaptic density in mice after 90 min CNO application (main CNO effect: $F(1, 24) = 23.95$, $p < 0.0001$ (Figure 53C").

Moreover, synaptic density was decreased in mice injected with CNO compared to saline injected mice visual cortex layer 5 ($p = 0.0012$) and superior colliculus ($p = 0.0124$). These results suggest that even acute changes in synaptic activity can affect mature neuronal network synaptic density. Excitatory synaptic density was increased in both Snap25 cKO and $Rbp4^{Cre}$;hM4Di mice brain yet decreased in $Rbp4^{Cre}$;hM3Dq. To better explore these changes in synaptic density further experiments are needed.

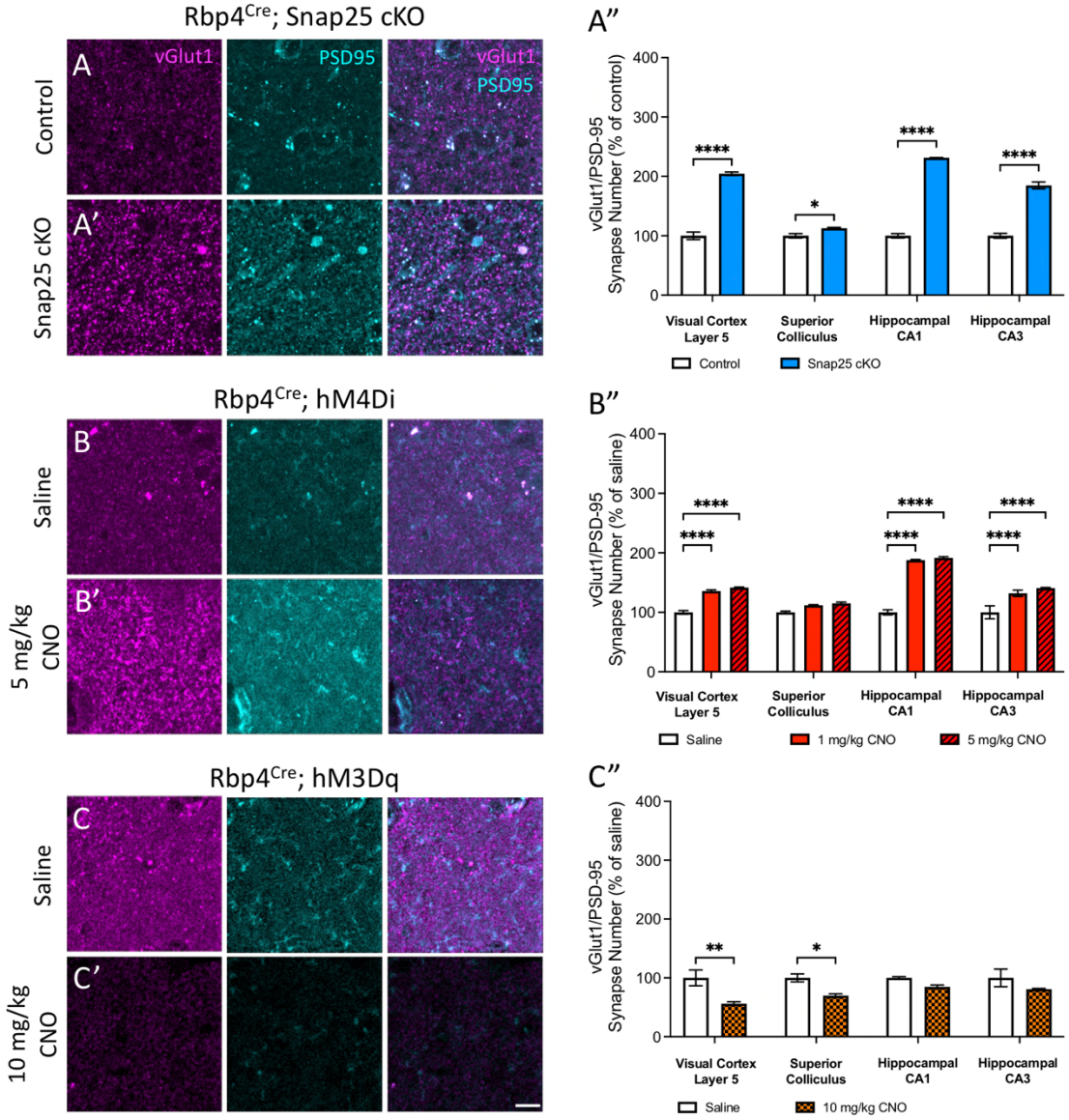


Figure 53: Changes in synaptic density in in the chronic 'silencing' model of Snap25 cKO, and after 90 minutes of chemogenetic manipulation in the inhibitory (*Rbp4^{Cre};hM4Di*) and excitatory (*Rbp4^{Cre};hM3Dq*) DREADDs mice

Representative images with excitatory markers vGlut1 (magenta) and PSD95 (cyan), show excitatory synapses, identified by colocalization between pre- (vGlut1+) and post-synaptic (PSD95) puncta in control (A) and Snap25 cKO mice (A'), and changes in excitatory synapses between control and Snap25 cKO (A") (two-way ANOVA, control n = 4, Snap25 cKO = 2). Representative images with excitatory markers vGlut1 and PSD95 show excitatory synapses, identified by colocalization between vGlut1+ and PSD95+ puncta in saline (B) and 5 mg/kg CNO (B') injected Rbp4^{Cre};hM4Di mice and changes in excitatory synapses between saline and CNO injected mice (B") (two-way ANOVA, n = 2 per group). Representative images with excitatory markers vGlut1 and PSD95 show excitatory synapses, identified by colocalization between vGlut1+ and PSD95+ puncta in saline (C) and 10 mg/kg CNO (C') injected Rbp4^{Cre};hM3Dq mice and changes in excitatory synapses between saline and CNO injected mice (C") (two-way ANOVA, saline n = 6, 10 mg/kg CNO n = 2). All data presented as mean ± SEM, * $p < 0.05$, ** $p < 0.01$, *** $p < 0.001$, **** $p < 0.0001$. Scale bar, 20 µm

5.3 Discussion

In this part of my study, I provided several experimental observations regarding the effects of short-term activation of selected neuronal populations on microglia function. I demonstrated that acute inhibition and activation of cell type-specific neuronal activity using Rbp4^{Cre};hM4Di and Rbp4^{Cre};hM3Dq in mature brains changes microglial morphology and phagocytic activity extremely rapidly, in less than two hours. In addition, chronic synaptic (Snap25 cKO) and acute chemogenetic (Rbp4^{Cre};hM4Di) 'silencing' affects microglial cells in the similar manner. Acute chemogenetic activation (Rbp4^{Cre}:hM3Dq) hyperactivates microglia and increases the number of amoeboid type of microglia. Lastly, acute inhibition and activation of neuronal activity affects excitatory synaptic density in the short period of time.

5.3.1 Inhibitory and excitatory DREADDs model to study microglial behaviour and dynamics

To better understand how changes in neuronal network activity affect microglia behaviour, I developed, validated and utilised inhibitory and excitatory DREADDs mice. The majority of previous chemogenetic studies have been using viral injections to deliver the receptors to a particular neuronal population (Scofield et al., 2015; Sternson & Roth, 2014; Zhu et al., 2014) yet I selected to use DREADD transgenic mice. I had several reasons to make this decision. Microglia scan their environment all the time and are able to check the brain in under a few hours (Kierdorf & Prinz, 2013; Priller & Prinz, 2019). The main disadvantage of DREADD viral injections is that microglia, as first responders, would first migrate to the injection site and react to the virus as a pathogen. Due to this function of microglia, it is difficult to study further changes of microglia caused by DREADD neuromodulation and not by injection itself. Moreover, injections can only influence a relatively small population of neurons, injection

sizes can vary and therefore the quantitative assessment of the responses across different animals is more difficult.

It has recently been reported that both hM4Di and hM3Dq DREADDs can be used to silence or activate microglia (Grace et al., 2018; Yi et al., 2021). Direct silencing and activation using DREADDS have been driven by CX3CR1 or CD68 (Grace et al., 2018; Saika et al., 2020; Yi et al., 2021). Manipulation of microglia activity through DREADDs allows us to study microglia in an activity-dependent manner by manipulating both neuronal and microglial activity and could be used to study intracellular pathways to better understand microglia-neuron interactions in the future.

Here I studied the effect of synaptic activation and inhibition in a selected population of cortical layer 5 and dentate gyrus neurons $Rbp4^{Cre}$ on microglia. First, I validated inhibitory and excitatory DREADDs through immunohistochemistry for the immediate early gene cFos (Dulka et al., 2020). Inhibitory DREADD mice treatment with CNO decreased cFos in the visual cortex layer 5 and superior colliculus yet no changes in cFos expressing cells were indicated in hippocampal CA1 and CA3 regions. In addition, no behaviour changes in $Rbp4^{Cre}$;hM4Di mice after 1 mg/kg and 5 mg/kg IP injection with CNO were observed. Van der Veen et al., used 10 mg/kg of CNO on the same $Rbp4^{Cre}$;hM4Di mice and did not observed any behaviour changes as well either (van der Veen et al., 2021). However, hM4Di viral injection into the cortex of layer 5 $Rbp4^{Cre}$ mice showed that inhibition of $Rbp4^{Cre}$ mice induced deficits in advancements, pronation, grasping and food release (Ueno et al., 2018). Decreased cFos expression suggests that neuronal activity was inhibited in the $Rbp4^{Cre}$ population of cortical layer 5 neurons and their target regions in the superior colliculus. However, for inhibitory DREADD validation cFos immunolabelling is not the best approach, and to further validate $Rbp4^{Cre}$;hM4Di electrophysiological experiments are needed. In excitatory DREADD mice 10

mg/kg application increased cFos after 90 minutes. Moreover, we observed behavioural changes such as reduced motor activity and sedation-like state in Rbp4^{Cre};hM3Dq mice. In similar studies in mice, 10 mg/kg was used as the default dose of CNO (Koike et al., 2016) and we performed our initial experiments using 10 mg/kg, but one mouse had an adverse effect of a sedation-like state and died shortly after. For animal welfare reasons we reduced CNO dosage to 10x, 100x and 200x lower. However, using reduced dose of CNO 10x to 1 mg/kg, one animal still had seizures and died. By reducing CNO 100x to 0.1 mg/kg, the animal seemed less active yet easily arousable and with reduced CNO 200x to 0.05 mg/kg we observed a milder behaviour effect of reduced activity and slower locomotor activity and no signs of distress. Changes in Rbp4^{Cre};hM3Dq mice behaviour after CNO treatment were observed by Van der Veen and colleagues (van der Veen et al., 2021). Similar to our experiment, they started with 10 mg/kg and reduced to 1 mg/kg CNO since they observed seizures in two mice (van der Veen et al., 2021). Authors discussed that seizures were caused due to unilateral off-site expression in the motor cortex (van der Veen et al., 2021). Moreover, these behaviour changes and adverse effects and deaths most likely were caused due to strong reaction to CNO acting on Rbp4^{Cre} neuronal population in the cerebral cortex of Rbp4^{Cre};hM3Dq mice. Overall, it seems that the effect of CNO in this particular DREADD line is difficult to control and for the future experiments much lowers doses or another actuator such as compound 21 should be used in combination with EEG recording.

5.3.2 Chronic synaptic and acute chemogenetic 'silencing', and acute chemogenetic activation affects microglial distribution and morphology

Next, I studied microglial distribution and morphology in chronic and acute synaptic 'silencing' and acute activation. To label microglial cells I used the most commonly used anti-Iba1 (Wako)

antibody (https://labchem-wako.fujifilm.com/us/product/detail/W01W0101-1974.html. To evaluate microglial distribution, I quantified the number of microglia in visual cortex layer 5, superior colliculus, and hippocampal CA1 and CA3 regions. My results indicate that chronic and acute synaptic 'silencing' affected microglial cell behaviour in a similar fashion. In chronically silenced brains, more microglial cells were observed in visual cortex layer 5 and hippocampal CA1 and CA3 regions. Acute silencing affected only the hippocampal CA1 region from these regions and more microglia were observed only in mice that were treated with a higher dose of CNO. Interestingly, acute chemogenetic neuronal activation reduced microglial density. The strongest changes of microglia density were observed in $Rbp4^{Cre}$;hM3Dq mice injected with the highest dose of CNO. Although, even with 1/100 and 1/200 lower doses of CNO microglial density was reduced suggesting that microglia are particularly sensitive to synaptic activation. Interestingly, direct activation of microglia in CX3CR1-hM3Dq mice showed that CNO administration upregulated Iba1 expression and the number of Iba1+ microglia were increased (Saika et al., 2020). This data suggests that due to synaptic activation the number of Iba1+ microglia were reduced yet increased by directly activating microglia.

A number of studies indicated that the main changes of microglial morphology, under physiological and pathological conditions are size, soma area and branching (S. Choi et al., 2021; A. Karperien et al., 2013; Morrison & Filosa, 2013; Soltys et al., 2005; Torres-Platas et al., 2014). To better understand whether manipulations of neuronal activity have an impact on microglia, I individually imaged Iba1 labelled microglia, to analyse their volume, soma area, primary branches, and the ramification of processes in three paradigms (chronic silencing model of $Rbp4^{Cre}$:$Snap25^{fl/fl}$ and after 90 minutes of chemogenetic manipulation in the inhibitory (Rbp4Cre;hM4Di) and excitatory (Rbp4Cre;hM3Dq) DREADDs mice). Microglial morphological changes were similar in Snap25 cKO and inhibitory DREADD mouse brains.

Chronic and acute ‘silencing’ had no effect on microglial volume. Although, microglial soma size was increased in visual cortex layer 5 in Snap25 cKO mice and in both regions in inhibitory DREADD mice but only treated with 5 mg/kg CNO. Moreover, chronic synaptic ‘silencing’ had no effect on the number of primary branches of microglia yet acute synaptic ‘silencing’ reduced microglial primary branches in both visual cortex layer 5 and hippocampal CA3 region. Microglial process ramification was decreased in Snap25 cKO mice brain but only in hippocampal CA3 region yet in both visual cortex layer 5 and hippocampal CA3 region in inhibitory DREADD mice brain. Acute synaptic activation had a strong effect on microglial morphology. First, microglial volume and soma size were reduced in excitatory DREADD mice administered with 0.05 mg/kg and 0.1 mg/kg CNO yet increased in mice treated with 10 mg/kg CNO. Secondly, microglial primary branches and process ramification was reduced in excitatory DREADD mice. However, the lowest numbers of processes were observed in mice treated with 10 mg/kg CNO. These findings indicate that microglial cells were sensitive to different concentrations of CNO. It seems that in $Rbp4^{Cre}$;hM3Dq mice treated with 10 mg/kg CNO, microglial morphology shifts to amoeboid type yet remained still ramified type treated with 0.05 mg/kg and 0.1 mg/kg CNO. Badimon et al., showed that manipulation of neuronal activity using inhibitory and excitatory DREADDs affects microglial gene expression (Badimon et al., 2020). Moreover, neuronal activation altered microglia-neuron interactions by affecting microglial process extension and motility (Badimon et al., 2020). These results show that microglia respond to neuronal ‘silencing’ or activation by adapting their morphology.

5.3.3 Chronic synaptic and acute chemogenetic 'silencing', and acute chemogenetic activation affects CD68 in microglia and excitatory synaptic density

To further explore whether manipulations of neuronal activity affect microglial function, I evaluated microglial phagocytic activity in three paradigms (chronic silencing model of $Rbp4^{Cre}$:$Snap25^{fl/fl}$ and after 90 minutes of chemogenetic manipulation in the inhibitory (Rbp4Cre;hM4Di) and excitatory (Rbp4Cre;hM3Dq) DREADDs mice). I used Iba1 immunolabelling together with the phagosomal marker CD68. CD68 is a commonly used marker to evaluate microglial phagocytic activity. CD68 is expressed at high levels in amoeboid microglia and at low levels in ramified microglia (Tay et al., 2017). I observed that the percentage of CD68 in microglia was lower in Snap25 cKO and $Rbp4^{Cre}$;hM4Di mice. Interestingly, chronic synaptic 'silencing' reduced the percentage of CD68 in microglia only in visual cortex layer 5, yet acute synaptic 'silencing' reduced CD68 in all tested brain regions. Yi and colleagues showed that induction of inhibitory DREADD in microglia suppressed microglial activation (Yi et al., 2021). Increased CD68 in microglia were observed in excitatory DREADD mice 90 minutes after the injection with the highest dose of CNO in visual cortex layer 5, superior colliculus, and hippocampal CA1 and CA3 regions. Interestingly, increased CD68 in microglia correlates with amoeboid or active microglial morphology observed in $Rbp4^{Cre}$;hM3Dq mice treated with 10 mg/kg CNO. Moreover, I observed that even at 1/100 and 1/200 lower concentrations of CNO the percentage of CD68 in microglia was increased, but only in hippocampal CA1 and CA3 regions. Only CA3 region receives direct input from dentate gyrus, CA1 has been influenced indirectly. It seems that microglia are particularly sensitive to synaptic activation in the hippocampus. Microglial density was reduced in $Rbp4^{Cre}$;hM3Dq mice yet microglia shifted their morphology to amoeboid type and were more active. Amoeboid microglial phagocytic activity is very high. This type of microglia are usually

associated with neuroinflammation (Casano & Peri, 2015; Hanisch & Kettenmann, 2007; Tay et al., 2017). Microglia association with neuroinflammation was indicated using chemogenetic tools. It has been shown that using DREADDs under a CD68 promoter, the activation of microglia results in inflammation (Grace et al., 2018). Moreover, it has been recently observed that manipulation of neuronal activity using DREADDs affected microglia-neuron interactions. The authors showed that microglia tends to suppress excessive neuronal activity in adult mice (Badimon et al., 2020). Together these results suggest that microglia-neuron communication is tightly controlled, and microglia respond to any changes of neuronal activity by changing their activity and morphology.

Lastly, to further investigate whether manipulations of neuronal activity affect microglia-neuron interactions, I measured excitatory synaptic density. Pre- and postsynaptic compartments were immunolabelled using anti-vGlut1 and anti-PSD95 antibodies and synaptic density was measured by colocalization between vGlut1+ and PSD95+ puncta. In Snap25 cKO mice, synaptic density was increased in all tested brain regions. Similar increase in synaptic density was observed in $Rbp4^{Cre}$;hM4Di mice brain jut 90 minutes after the start of chemogenetic stimulation. I observed that different concentrations of CNO affected synaptic density in the same fashion and synaptic density was increased in visual cortex layer 5 and hippocampal CA1 and CA3 regions, yet no changes were observed in superior colliculus. Furthermore, acute activation reduced synaptic density in visual cortex layer 5 and superior colliculus but no changes were observed in hippocampal CA1 and CA3 regions. Jayachandran and colleagues showed that in nucleus reuniens of the thalamus hM4Di silenced fiber density was increased (Jayachandran et al., 2019). Moreover, in Snap25 het mice dendritic spine density was reduced but PSD95 puncta size was not affected (Fossati et al., 2015) and by

reducing Snap25 levels synaptic density was reduced at P50 (Sharma et al., 2012). These data suggest that impaired neuronal activity affects synaptic density.

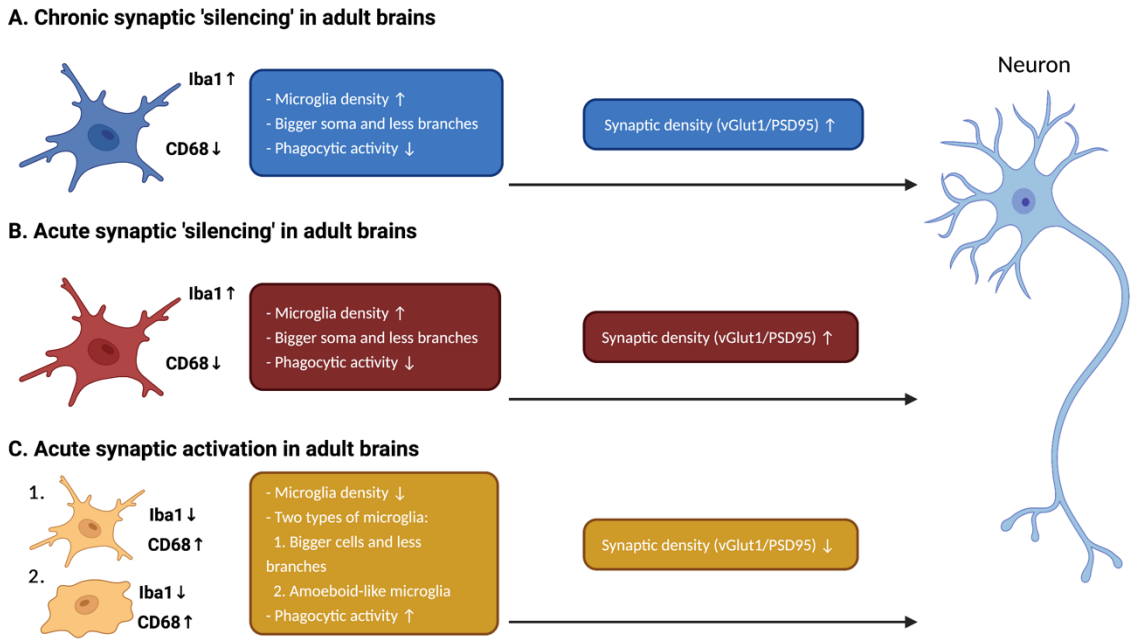


Figure 54: Microglial cells morphological and functional adaptation to the changes of synaptic activity

(A) Indicates abolition of Snap25 and this chronic synaptic 'silencing' started from birth and continued throughout postnatal development until adulthood. (B) Inhibitory and (C) excitatory DREADDs effect on microglia and synapses in the mature brain. Created with BioRender.com

In conclusion, these findings indicate that chronic or acute manipulations of neuronal activity both change microglia-neuron communication. Microglial cells adapt to neuronal inhibition or activation by changing their morphology and function (Figure 54). Chronic and acute synaptic 'silencing' affects microglia in the same manner by increasing the number of microglia yet reducing microglial activity which can be related with the increase in synaptic density. Acute neuronal activation with chemogenetic methods alters microglial morphology and microglia response by retracting their processes and shifting to amoeboid form after 90

minutes starting the stimulation. Moreover, acute chemogenetic activation of selected neurons reduces the number of microglia yet increases their phagocytic activity. This morphological and functional activation of microglia might be related to the reduction of synaptic density in the brains with activated synaptic activity.

Chapter 6: Discussion

In my DPhil project I investigated whether chronic or acute manipulations of neuronal activity of a selected population of cortical projection neurons affect microglia-neuron interactions and microglial behaviour during early postnatal brain development and in the adult mouse. I have shown that microglia are uniformly distributed in the visual cortex layer 5, superior colliculus, and hippocampal CA1 and CA3 regions and do not follow the same developmental trajectory in male and female mice. Moreover, I demonstrated that chronic synaptic 'silencing' by abolishing regulated synaptic vesicle release from a subpopulation of cortical projection neurons altered microglia-neuron interactions and impaired neuronal network maturation in the developing mouse brain. Abolished Snap25-mediated release of synaptic vesicles triggered morphological changes of microglia resulting in the reduction of microglial size and induced microglial process retraction in visual cortex layer 5, superior colliculus, and hippocampal CA1 and CA3 areas. Thus, increased excitatory synaptic density and presynaptic compartments elimination by microglia lead to impaired synaptic maturation. Notably, I found that abolition of Snap25 from a subpopulation of cortical layer 5 projection neurons disrupted microglia-neuron interactions by altering chemokine and phagocytic signalling pathways. Given the differential effects of synaptic 'silencing' on microglial cell morphology and activity in males and females, I speculate that microglia may contribute to the sex-specific effects of synaptic 'silencing' on microglia-neuron interactions and synaptic maturation during development. Lastly, I demonstrated that microglial cells adapt to acute chemogenetic neuronal inhibition or activation by changing their morphology and functional status in less than two hours. Chronic synaptic and acute chemogenetic 'silencing' increased the number of microglia, yet reduced microglial activity in visual cortex layer 5, superior colliculus, and hippocampal CA1 and CA3, which can be related to the increase in synaptic density. On the

other hand, acute neuronal activation altered microglial morphology and response by retracting their processes and shifting to amoeboid form, which led to an increase in CD68 in microglia. All this might have contributed to reduced synaptic density. My work suggests that inhibition or excitation of neuronal activity changes microglia-neuron interactions and excitatory synapses maintenance in the mature brain.

6.1: Inhibition or excitation of neuronal activity affects microglial distribution in the developing brain in a sex-specific manner

My study raises the questions of whether inhibition or activation of specific elements of the cerebral cortical neuronal network affects microglial behaviour and microglia-neuron communications during neuronal network maturation and maintenance. It has been shown that synaptic pruning by microglia is activity-dependent in the somatosensory cortex layer 4 callosal axons (De León Reyes et al., 2019) and in the retinogeniculate system (Schafer et al., 2012) raising the possibility that Snap25-mediated release of synaptic vesicles might play a crucial role in microglia-neuron interactions to secure normal neuronal network development and maintenance. In the developing CNS, microglia are not evenly distributed and have different density and morphological heterogeneity across the brain. It has been demonstrated that microglial distribution changes rapidly during the first month of mouse postnatal development (DiBona et al., 2019; Li et al., 2019; Mondo et al., 2020; Paolicelli et al., 2011). Moreover, the sexual dimorphism of microglial distribution has been shown in mouse parietal cortex, amygdala and hippocampus (Guneykaya et al., 2018; Schwarz et al., 2012; Weinhard, Neniskyte, et al., 2018). I observed that in the developing visual cortex and across different cortical layers microglial density remains stable yet increases in the subcortical regions in mice (Figure 24). Different regions have different developmental

profiles. In the hippocampal CA1 region and superior colliculus microglial density peaks at P14, yet peaks a week later in the hippocampal CA3. During the first week of postnatal development, the sexual dimorphism of microglial density appears to emerge slower in the visual cortex than in the subcortical regions. Afterwards, sexual dimorphism of microglial density becomes evident and higher in female brains with the exception of hippocampal CA3. The Snap25 cKO model gave me the opportunity to compare cerebral cortical and hippocampal circuits with chronic synaptic 'silencing' by abolition of Snap25 expression and thus removing the ability of the nerve terminals to release synaptic vesicles in a regulated fashion. At the silenced mossy fibre projections in the hippocampal CA3 regions, microglial cells seem to be affected earlier in the developing brain yet later at the location of silenced layer 5 projection neurons (Figure 32). The opposite effect of synaptic 'silencing' was observed in the hippocampal CA1 region. It seems that the lack of regulated vesicular release of neurotransmitters in the Rbp4^{Cre} projection neurons in the layer 5 and CA3 leads to an increase of microglial density yet decreases in the CA1. The CA1 region does not receive direct inputs from layer 5 projection neurons but communicates with the CA3 region through Schaffer collaterals (Daumas et al., 2009). Even though Schaffer collaterals were not directly silenced, a subpopulation of mossy fibre projections was silenced in the CA3. Here I can speculate that indirect reduction of the regulated vesicular release of neurotransmitters through abolition of Snap25 affects microglial distribution in a different manner than direct 'silencing' during early postnatal brain development. Notably, in the mature Snap25 cKO mice brain, microglial density remains increased in silenced Rbp4^{Cre} projection neurons population in the visual cortex layer 5, and hippocampal CA1 and CA3 (Figure 50). Because in Snap25 cKO mice Rbp4^{Cre} projection neurons in cortical layer 5 and dentate gyrus were no longer able to release synaptic vesicles in a regulated fashion coupled to action potentials from around birth,

it was essential to evaluate if acute chemogenetic 'silencing' ('silencing' for minutes or hours rather than weeks or months) of mice Rbp4^{Cre} projection neurons affects microglia in the same fashion. In the mature brain, acute chemogenetic 'silencing' affected microglia in a histochemically detectable fashion only in the CA1 region. Microglial density was increased in animals injected with the highest dose of CNO, yet other regions remained unaffected. Acute chemogenetic 'silencing' affects microglial density in the similar way as chronic 'silencing' with conditional Snap25 KO yet it can be related with the off-site effect of CNO and its binding to other neurotransmitter receptors (Gomez et al., 2017; van der Veen et al., 2021). The opposite trend was observed in mice with acute chemogenetic activation of Rpb4^{Cre} projection neurons. Significantly decreased microglial density was observed in the visual cortex layer 5 and subcortical regions just after 90 minutes of chemogenetic activation. It seems that microglia are particularly sensitive to acute activation since the highest dose of 10 mg/kg of CNO and 200x lower dose of CNO affects microglial density in the similar fashion.

6.2: Microglia adapt their morphology in activity-dependent manner

During brain development, not only microglial distribution but also morphology experiences dramatic changes. These morphological changes reflect different functional states. Microglia can change or adapt their morphology as a response to different environmental, physiological and pathological stimulus (Antonson et al., 2017; Bolton et al., 2013, 2017; Gunner et al., 2019; Hartz et al., 2008; Lin et al., 2017; Pang et al., 2005; Shankardass et al., 2009). During embryonic and early postnatal development microglial morphology shifts from amoeboid to ramified, and it has been shown that ramified form of microglia is the most common in the developing and mature brain (A. Karperien et al., 2013; Lawson et al., 1990; Torres-Platas et

al., 2014)). I observed that in the developing visual cortex layer 5 and hippocampal CA3 region, microglial cells become bigger with more primary branches, and microglia soma size reduces as well as microglial branching complexity. All these morphological changes were more evident in females (Figure 26). Although microglial processes remain consistent during development, sex-specific differences were apparent in female visual cortex layer 5 at P8 and P21 and in hippocampal CA3 at P14. In contrast, abolished Snap25-mediated release of synaptic vesicles in the developing visual cortex layer 5 and hippocampal CA3 leads to significant changes in microglial morphology. Microglia reduce in size (Figure 33), soma becomes bigger (Figure 34), microglia processes are retracted (Figure 35-36) and these changes are more apparent in males. My results gave evidence that microglia are sensitive to chronic 'silencing' of selected population of neurons and their projections which shifts their morphology into the transition state from ramified to amoeboid. However, in the mature brain, the effect of chronic 'silencing' on microglial morphology does not seem that evident. Microglial soma size was slightly increased only in the visual cortex layer 5 and reduced processes were observed only in the hippocampal CA3 region. One of the explanations of the morphological changes is that microglia are more sensitive to abolition of Snap25 during critical periods of development than the synaptic pruning and synaptogenesis occurs (Morimoto & Nakajima, 2019; Seeman et al., 1987). On the other hand, different mechanisms can take a place and other glial cells might be involved to support the maintenance of mature neuronal network (Biswas et al., 2020; Domingues et al., 2016; Flynn et al., 2003; Irfan et al., 2021; N. Miyamoto et al., 2015; Neniskyte & Gross, 2017; Palpagama et al., 2019). Acute chemogenetic 'silencing' had a stronger and more evident effect on microglial morphology (Figure 51-52). In both visual cortex layer 5 and hippocampal CA3, microglial soma increased in size, yet the number of primary branches and processes was reduced suggesting that acute

'silencing' caused microglial transition to a less ramified state. In contrast, acute activation caused a dramatic shift of microglia from ramified to amoeboid, yet it seems that two types of microglia were evident. The shift to amoeboid type was caused by the highest dose of CNO: microglial volume and soma size increased, microglia lost their primary branches and only had 1 or 2, and retracted their processes. Acute chemogenetic activation using lower doses of CNO (0.05 mg/kg and 0.1 mg/kg) seems to affect microglia slightly yet microglia remain ramified only smaller and with fewer branches compared to the control group. These results indicate that microglia react to inhibition in one manner and to activation in opposite manner suggesting that microglia are able to respond to both acute and chronic neuronal activity changes of the brain. If so, microglial activity must be affected as well. It has been shown that defective microglial activity can lead to impaired phagocytosis and jeopardised neuronal connectivity in the developing brain (Casano & Peri, 2015; Priller & Prinz, 2019; Prinz & Priller, 2014; Tay et al., 2017).

6.3: Changes in microglial activity during postnatal development in activity-dependent manner

During normal development, the percentage of CD68 in microglia significantly increased during the first two weeks of development and decreased thereafter (Figure 25). In the superior colliculus, and hippocampal CA1 and CA3 regions, phagocytically active areas of microglia (CD68 signal in Iba1+ microglia) occurs earlier in females at P8 and P14, and later in males. The same trend was observed in the hippocampal CA1 where the percentage of CD68 in microglia was higher in females at P8 and P15 yet in males at P28 (Weinhard, Neniskyte, et al., 2018). Due to abolished Snap25-mediated regulated release of synaptic vesicles, CD68

signal in Iba1+ microglia and phagocytic pouches in Iba1+ microglia (Sierra et al., 2010)) decreased in all brain regions in the developing brain yet phagocytic pouches were lower only in hippocampal CA3 at P8 (Figure 38-39). In Snap25 cKO, lower CD68 in microglia was determined in males at P8 and P14 in superior colliculus and hippocampal CA3. Moreover, later in development, lower CD68 in Iba1 was observed in Snap25 cKO females. Similar reduction in CD68 was observed in the mature brain (Figure 50). In Snap25 cKO mice, lower CD68 in microglia was indicated only in the visual cortex layer 5 yet acute 'silencing' reduced CD68 in visual cortex layer 5, superior colliculus, and hippocampal CA1 and CA3. Furthermore, in the chemogenetic activation model of Rbp4Cre;hM3Dq, changes in the percentage of CD68 in microglia correlate with differences in microglial morphology. Excitatory DREADD mice injected with the highest 10 mg/kg CNO showed microglia shift to amoeboid form and significantly increased CD68 in microglia across the brain. Lower CNO doses increased CD68 in microglia as well but the changes that I could detect only reached significance in the hippocampus. Higher percentage of CD68 in microglia might be more present in microglia that are in transition state from ramified to amoeboid. Since amoeboid microglia in the mature brain are usually found in pathological conditions and/or inflammation, this data suggests that higher doses of CNO hyper-activate microglia and might be toxic for the brain. Moreover, I observed and documented severe adverse effects on mice injected with 10 mg/kg CNO and had to reduce the CNO dose. It seems that "too high" $Rbp4^{Cre}$ neuron activation in cerebral cortex or dentate gyrus elicits seizure activities and has a negative impact on mice well-being and behaviour, and even on microglial cells' behaviour and dynamics. Further chronic EEG recordings would help to reveal the nature of the possible abnormal activity patterns in these models during chemogenetic manipulations.

6.4: Changes in neuronal activity alters microglia-neuron interactions during development

6.4.1: Changes in excitatory synaptic density and microglial trogocytic activity

The role of the Snap25 protein in neuron-neuron communications through regulated synaptic vesicle release is not essential for synapse formation (Washbourne et al., 2002), but it is fundamental for the maturation of specialised synapses from cortical layer 5 to Po thalamus (Hayashi et al., 2021) or dentate gyrus to CA3 synapse (Hayashi et al., unpublished). Here I identified that abolition of Snap25 altered synapses maturation and maintenance, and microglia-neuron interactions. In Snap25 cKO mice, excitatory synaptic density was affected in all brain regions that I investigated in the same manner (Figure 40). Thus, excitatory synaptic density dramatically increased at P14 in the visual cortex layer 5. It is important to note that several studies have shown that microglial cell activity and synaptic pruning peaks during the second week of postnatal development in mice (Paolicelli et al., 2011; Weinhard, Neniskyte, et al., 2018). This increase in excitatory synaptic density correlates with reduced microglial functional activity and morphological changes resulting in impaired synaptic maturation. Although abolition of Snap25 had no impact on pre- and postsynaptic compartments size, I observed changes in the efficiency of synaptic trogocytosis (partial phagocytosis or when one cell contacts and nibbles another cell) (Figure 39), a process of microglia-dependent synaptic remodelling demonstrated in the developing brain (Weinhard, Di Bartolomei, et al., 2018). In proximity with the silenced cell bodies in the visual cortex layer 5 neurons, higher trogocytosis efficiency might be related with altered synaptic maturation and weaker formation of synapses. It has been shown that during brain development “weaker” synapses are eliminated and the “stronger” ones - maintained (Katz & Shatz, 1996; Presumey et al., 2017). The opposite effect was observed in the mossy fibre projections in the

hippocampal CA3 region where trogocytosis efficiency was reduced. Although it is difficult to explain why synaptic trogocytosis differs between visual cortex layer 5 and hippocampal CA3 synapses. One of the possible explanations might be related to local and distant projection silencing. At the distant projections in the CA3, microglia are either unable to recognize which synaptic connections to eliminate or in this region there are less weaker synapses than in layer 5. Notably, abolition of Snap25 from these neuronal populations has a long-term consequence and contributes to the discrimination of synapses to be eliminated or maintained in the mature brain (Figure 53). The same tendency in increased excitatory synaptic density was observed in mature Snap25 cKO and $Rbp4^{Cre}$;hM4Di visual cortex layer 5, superior colliculus, and hippocampal CA1 and CA3. On the other hand, acute chemogenetic activation leads to decreased excitatory synaptic density due to increased microglial phagocytic activity in visual cortex layer 5 silenced neurons and their projections to superior colliculus.

6.4.2: Molecular mechanisms of microglia-neuron interactions

Manipulation of neuronal activity of a selected neuronal population in the developing mouse brain leads to severe changes in microglial behaviour and impaired synaptic maturation and maintenance, raising the possibility that Snap25 is necessary for microglia-neuron interactions in an activity-dependent manner during development. It has been demonstrated in a number of studies that the fractalkine axis plays a key role in synaptic pruning and microglia-neuron communications via CX3CR1 signalling, yet all those studies concentrated on manipulations of CX3CR1 expression on microglia (Dorfman et al., 2017; Liang et al., 2009; Maciejewski-Lenoir et al., 1999; Maggi et al., 2011; Paolicelli et al., 2014; Wynne et al., 2010). However, little is known about CX3CL1 signalling in an activity-dependent manner, and under

normal and pathological conditions. Abolition of regulated synaptic vesicular release and thus abolition of synaptic activity through the abolition of Snap25 leads to downregulation of CX3CL1 that is necessary for normal synaptic pruning and microglia-neuron interactions (Figure 41-42) (Jones et al., 2010; Maciejewski-Lenoir et al., 1999; Paolicelli et al., 2014). Moreover, the downregulation of CX3CL1 protein levels and mRNA expression were evident in females in both the cortex and hippocampus. It has been shown that reduced CX3CL1 levels can be linked to neuronal loss and/or impaired neuronal network formation (Fan et al., 2020; Hill et al., 2021). The downregulation of CX3CL1 in Snap25 cKO correlates with impaired neuronal maturation as well as impaired microglial activity. The opposite tendency was observed in CX3CR1 expression. The upregulation of CX3CR1 protein levels was more apparent in males yet it is difficult to interpret my data since my recent validation of CX3CR1 demonstrated it to be non-specific/cross reactive. On the other hand, I determined that CX3CR1 mRNA expression follows the same trend as CX3CR1 protein levels and upregulation were more evident in males during the first two weeks of postnatal development in cortex yet only at P14 in hippocampus. To confirm if chronic abolition of Snap25 expression in selected neuronal populations in the mouse brain leads to upregulation of the fractalkine receptor, more experiments need to be performed using CX3CR1 KO mouse or microglia-depletion models. While the overall profile of microglia-neuron interactions may be Snap25-dependent through CX3CL1-CX3CR1 signalling, there may be links between Snap25 and the complement system. The classical complement system has been identified as a key player in synapse elimination by microglia in an activity-dependent manner (Schafer et al., 2012; Stevens et al., 2007). Apparently, abolition of Snap25 leads to the downregulation of C3 and correlates with a loss of microglial phagocytic activity since C3 tags synapses that need to be eliminated. Similar to CX3CL1 downregulation effect on the neuronal network, lack of C3 also

leads to increased synaptic connectivity caused by failed synaptic pruning by (Schafer et al., 2012; Stevens et al., 2007). Abolition of Snap25 affects CX3CL1 and C3 expression in the same manner, resulting in failed synaptic pruning that leads to increased synaptic density. Upregulation of CD11b was found in the silenced cortex and hippocampus and more evident in females during the second and third week of postnatal development. Reduced CD11b expression may be related with the loss of C3 signalling and impaired synaptic pruning. Whether C3 down regulation is related with CD11b upregulation in a mouse model with abolished Snap25-mediated release of neurotransmitter, it is necessary to test C3 – CR3 signalling not only on the CR3 subunit CD11b. Moreover, C1q expression evaluation is necessary to better understand Snap25 impact on phagocytic signalling via the complement system.

In conclusion, Snap25 is necessary for microglia-neuron interactions and for region-specific developmental synaptic pruning to secure normal maturation and maintenance of the neuronal network through fractalkine and complement signalling. Microglia are sensitive to acute manipulations of neuronal activity and rapidly respond to different stimuli. Inhibition and activation of the neuronal network has different effects on microglial function and morphology resulting in impaired neuronal network maintenance. Given the differential profiles of microglia response to chemogenetic inhibition and excitation, it seems that microglia contribute to the region- and sex-specific synaptic maturation and microglia-neuron interactions in an activity-dependent manner. Understanding the cellular and molecular mechanisms of these interactions is key to reveal the pathomechanisms of several cognitive conditions.

6.5: Limitations and future directions

The role of microglia in activity-dependent neuronal network maturation presented in this thesis highlighted mechanisms of bidirectional communication between microglia and neurons. These findings indicate a novel and potential role of Snap25-mediated microglia-neuron interactions. However, Snap25 is one of the proteins of the SNARE complex and other components such as Munc13 and Munc18 may play a crucial role in the bidirectional interaction between microglia and neurons. Snap25 plays a role in regulated activity where Munc is a key component in vesicular release during spontaneous activity. It would be important to investigate whether abolishing vesicular release completely through Munc13 and Munc18 ablation have an impact on microglia-neuron interactions in the developing brain. Chemokine and phagocytic signalling pathways are necessary to secure normal neuronal network formation and remodelling, and microglia-neuron communication yet some neuronal projections can also be maintained through the release of trophic factors. One of those factors are brain derived neurotrophic factor (BDNF) that plays a role in microglial maintenance and may play a role in the control of neuronal network excitability (Ferrini & De Koninck, 2013; Huang et al., 2021). It has been shown that not only neurons but also microglia secrete BDNF. It would be important to test whether activation or 'silencing' of the neuronal network can be rescued/restored by microglial BDNF and whether BDNF can help to re-establish the activity of genetically silenced neurons. If the release of microglial BDNF can control neuronal excitability, this neurotrophic factor may lead to novel therapeutic approaches for various neurodevelopmental disorders.

Moreover, to develop new automated ML or PC methods of microglial classification is pivotal as well as understanding microglia's role during normal brain development. Most studies

focus on the treatment of neurological disorders, while only a minority of the research in this area seeks to understand their causes. Understanding microglia function is key to recognise and treat neuronal dysfunction during development and in the adult. Once we understand what is hiding behind strictly regulated neuronal network formation and refinement, we might be able to monitor microglia pathologies and manipulate microglia-neuron interactions as novel therapeutic approaches.

Bibliography

Allen, D. C., Carlson, T. L., Xiong, Y., Jin, J., Grant, K. A., & Cuzon Carlson, V. C. (2019). A Comparative Study of the Pharmacokinetics of Clozapine N-Oxide and Clozapine N-Oxide Hydrochloride Salt in Rhesus Macaques. *The Journal of Pharmacology and Experimental Therapeutics*, *368*(2), 199–207. https://doi.org/10.1124/jpet.118.252031

Andoh, M., Ikegaya, Y., & Koyama, R. (2019). Synaptic Pruning by Microglia in Epilepsy. *Journal of Clinical Medicine*, *8*(12), 2170. https://doi.org/10.3390/jcm8122170

Antonson, A. M., Radlowski, E. C., Lawson, M. A., Rytych, J. L., & Johnson, R. W. (2017). Maternal viral infection during pregnancy elicits anti-social behavior in neonatal piglet offspring independent of postnatal microglial cell activation. *Brain, Behavior, and Immunity*, *59*, 300–312.

Arcuri, C., Mecca, C., Bianchi, R., Giambanco, I., & Donato, R. (2017). The Pathophysiological Role of Microglia in Dynamic Surveillance, Phagocytosis and Structural Remodeling of the Developing CNS. *Frontiers in Molecular Neuroscience*, *10*, 191. https://doi.org/10.3389/fnmol.2017.00191

Armbruster, B. N., Li, X., Pausch, M. H., Herlitze, S., & Roth, B. L. (2007). Evolving the lock to fit the key to create a family of G protein-coupled receptors potently activated by an inert ligand. *Proceedings of the National Academy of Sciences of the United States of America*, *104*(12), 5163–5168. https://doi.org/10.1073/pnas.0700293104

Askew, K., & Gomez-Nicola, D. (2018). A story of birth and death: Insights into the formation and dynamics of the microglial population. *Brain, Behavior, and Immunity*, *69*, 9–17. https://doi.org/https://doi.org/10.1016/j.bbi.2017.03.009

Baalman, K., Marin, M. A., Ho, T. S.-Y., Godoy, M., Cherian, L., Robertson, C., & Rasband, M. N. (2015). Axon Initial Segment–Associated Microglia. *The Journal of Neuroscience*, *35*(5), 2283 LP – 2292. https://doi.org/10.1523/JNEUROSCI.3751-14.2015

Bachstetter, A. D., Ighodaro, E. T., Hassoun, Y., Aldeiri, D., Neltner, J. H., Patel, E., Abner, E. L., & Nelson, P. T. (2017). Rod-shaped microglia morphology is associated with aging in 2 human autopsy series. *Neurobiology of Aging*, *52*, 98–105. https://doi.org/10.1016/j.neurobiolaging.2016.12.028

Badimon, A., Strasburger, H. J., Ayata, P., Chen, X., Nair, A., Ikegami, A., Hwang, P., Chan, A. T., Graves, S. M., Uweru, J. O., Ledderose, C., Kutlu, M. G., Wheeler, M. A., Kahan, A.,

Ishikawa, M., Wang, Y.-C., Loh, Y.-H. E., Jiang, J. X., Surmeier, D. J., … Schaefer, A. (2020). Negative feedback control of neuronal activity by microglia. *Nature*, *586*(7829), 417–423. https://doi.org/10.1038/s41586-020-2777-8

Bark, C. I., Hahn, K. M., Ryabinin, A. E., & Wilson, M. C. (1995). Differential expression of SNAP-25 protein isoforms during divergent vesicle fusion events of neural development. *Proceedings of the National Academy of Sciences of the United States of America*. https://doi.org/10.1073/pnas.92.5.1510

Barkal, A. A., Brewer, R. E., Markovic, M., Kowarsky, M., Barkal, S. A., Zaro, B. W., Krishnan, V., Hatakeyama, J., Dorigo, O., & Barkal, L. J. (2019). CD24 signalling through macrophage Siglec-10 is a target for cancer immunotherapy. *Nature*, *572*(7769), 392–396.

Barrecheguren, P. J., Ros, O., Cotrufo, T., Kunz, B., Soriano, E., Ulloa, F., Stoeckli, E. T., & Araújo, S. J. (2017). SNARE proteins play a role in motor axon guidance in vertebrates and invertebrates. *Developmental Neurobiology*. https://doi.org/10.1002/dneu.22481

Bazan, J. F., Bacon, K. B., Hardiman, G., Wang, W., Soo, K., Rossi, D., Greaves, D. R., Zlotnik, A., & Schall, T. J. (1997). A new class of membrane-bound chemokine with a CX3C motif. *Nature*, *385*(6617), 640–644. https://doi.org/10.1038/385640a0

Biber, K., Neumann, H., Inoue, K., & Boddeke, H. W. G. M. (2007a). Neuronal “On” and “Off” signals control microglia. *Trends in Neurosciences*, *30*(11), 596–602. https://doi.org/10.1016/j.tins.2007.08.007

Biber, K., Neumann, H., Inoue, K., & Boddeke, H. W. G. M. (2007b). Neuronal ‘On’ and ‘Off’ signals control microglia. *Trends in Neurosciences*, *30*(11), 596–602. https://doi.org/10.1016/j.tins.2007.08.007

Bilimoria, P. M., & Stevens, B. (2015). Microglia function during brain development: New insights from animal models. *Brain Research*, *1617*, 7–17. https://doi.org/10.1016/j.brainres.2014.11.032

Bishop, A. C., Ubersax, J. A., Petsch, D. T., Matheos, D. P., Gray, N. S., Blethrow, J., Shimizu, E., Tsien, J. Z., Schultz, P. G., Rose, M. D., Wood, J. L., Morgan, D. O., & Shokat, K. M. (2000). A chemical switch for inhibitor-sensitive alleles of any protein kinase. *Nature*, *407*(6802), 395–401. https://doi.org/10.1038/35030148

Bisht, K., Sharma, K. P., Lecours, C., Sánchez, M. G., El Hajj, H., Milior, G., Olmos-Alonso, A., Gómez-Nicola, D., Luheshi, G., Vallières, L., Branchi, I., Maggi, L., Limatola, C., Butovsky,

O., & Tremblay, M.-È. (2016). Dark microglia: A new phenotype predominantly associated with pathological states. *Glia*, *64*(5), 826–839. https://doi.org/10.1002/glia.22966

Biswas, S., Cottarelli, A., & Agalliu, D. (2020). Neuronal and glial regulation of CNS angiogenesis and barriergenesis. *Development (Cambridge, England)*, *147*(9). https://doi.org/10.1242/dev.182279

Bollinger, J. L., Bergeon Burns, C. M., & Wellman, C. L. (2016). Differential effects of stress on microglial cell activation in male and female medial prefrontal cortex. *Brain, Behavior, and Immunity*, *52*, 88–97. https://doi.org/https://doi.org/10.1016/j.bbi.2015.10.003

Bolte, S., & Cordelières, F. P. (2006). A guided tour into subcellular colocalization analysis in light microscopy. *Journal of Microscopy*, *224*(Pt 3), 213–232. https://doi.org/10.1111/j.1365-2818.2006.01706.x

Bolton, J. L., Huff, N. C., Smith, S. H., Mason, S. N., Foster, W. M., Auten, R. L., & Bilbo, S. D. (2013). Maternal stress and effects of prenatal air pollution on offspring mental health outcomes in mice. *Environmental Health Perspectives*, *121*(9), 1075–1082.

Bolton, J. L., Marinero, S., Hassanzadeh, T., Natesan, D., Le, D., Belliveau, C., Mason, S. N., Auten, R. L., & Bilbo, S. D. (2017). Gestational exposure to air pollution alters cortical volume, microglial morphology, and microglia-neuron interactions in a sex-specific manner. *Frontiers in Synaptic Neuroscience*, *9*, 10.

Boschert, U., O'Shaughnessy, C., Dickinson, R., Tessari, M., Bendotti, C., Catsicas, S., & Pich, E. M. (1996). Developmental and plasticity-related differential expression of two SNAP-25 isoforms in the rat brain. *Journal of Comparative Neurology*. https://doi.org/10.1002/(SICI)1096-9861(19960401)367:2<177::AID-CNE2>3.0.CO;2-2

Brioschi, S., Zhou, Y., & Colonna, M. (2020). Brain Parenchymal and Extraparenchymal Macrophages in Development, Homeostasis, and Disease. *The Journal of Immunology*, *204*(2), 294 LP – 305. https://doi.org/10.4049/jimmunol.1900821

Brockhaus, J., Möller, T., & Kettenmann, H. (1996). Phagocytozing ameboid microglial cells studied in a mouse corpus callosum slice preparation. *Glia*, *16*(1), 81–90.

Brown, G. C., & Neher, J. J. (2014). Microglial phagocytosis of live neurons. *Nature Reviews Neuroscience*, *15*(4), 209–216. https://doi.org/10.1038/nrn3710

Cardona, A. E., Pioro, E. P., Sasse, M. E., Kostenko, V., Cardona, S. M., Dijkstra, I. M., Huang,

D., Kidd, G., Dombrowski, S., Dutta, R., Lee, J.-C., Cook, D. N., Jung, S., Lira, S. A., Littman, D. R., & Ransohoff, R. M. (2006). Control of microglial neurotoxicity by the fractalkine receptor. *Nature Neuroscience*, *9*(7), 917–924. https://doi.org/10.1038/nn1715

Casano, A. M., & Peri, F. (2015). Microglia: Multitasking specialists of the brain. In *Developmental Cell*. https://doi.org/10.1016/j.devcel.2015.01.018

Chapman, G. A., Moores, K. E., Gohil, J., Berkhout, T. A., Patel, L., Green, P., Macphee, C. H., & Stewart, B. R. (2000). The role of fractalkine in the recruitment of monocytes to the endothelium. *European Journal of Pharmacology*, *392*(3), 189–195. https://doi.org/10.1016/s0014-2999(00)00117-5

Chen, X., Choo, H., Huang, X.-P., Yang, X., Stone, O., Roth, B. L., & Jin, J. (2015). The first structure-activity relationship studies for designer receptors exclusively activated by designer drugs. *ACS Chemical Neuroscience*, *6*(3), 476–484. https://doi.org/10.1021/cn500325v

Cheng, J., Dong, Y., Ma, J., Pan, R., Liao, Y., Kong, X., Li, X., Li, S., Chen, P., Wang, L., Yu, Y., & Yuan, Z. (2021). Microglial Calhm2 regulates neuroinflammation and contributes to Alzheimer's disease pathology. *Science Advances*, *7*(35). https://doi.org/10.1126/sciadv.abe3600

Chianella, S., Semprevivo, M., Peng, Z. C., Zaccheo, D., Bentivoglio, M., & Grassi-Zucconi, G. (1999). Microglia activation in a model of sleep disorder: an immunohistochemical study in the rat brain during Trypanosoma brucei infection. *Brain Research*, *832*(1–2), 54–62. https://doi.org/10.1016/s0006-8993(99)01449-3

Choi, B. H. (1981). Hematogenous cells in the central nervous system of developing human embryos and fetuses. *The Journal of Comparative Neurology*, *196*(4), 683–694. https://doi.org/10.1002/cne.901960412

Choi, S., Guo, L., & Cordeiro, M. F. (2021). Retinal and Brain Microglia in Multiple Sclerosis and Neurodegeneration. *Cells*, *10*(6). https://doi.org/10.3390/cells10061507

Chu, Y., Jin, X., Parada, I., Pesic, A., Stevens, B., Barres, B., & Prince, D. A. (2010). Enhanced synaptic connectivity and epilepsy in C1q knockout mice. *Proceedings of the National Academy of Sciences of the United States of America*, *107*(17), 7975–7980. https://doi.org/10.1073/pnas.0913449107

Chugh, D., & Ekdahl, C. T. (2016). Interactions Between Microglia and Newly Formed

Hippocampal Neurons in Physiological and Seizure-Induced Inflammatory Environment. *Brain Plasticity (Amsterdam, Netherlands)*, *1*(2), 215–221. https://doi.org/10.3233/BPL-150014

Cockram, T. O. J., Dundee, J. M., Popescu, A. S., & Brown, G. C. (2021). The Phagocytic Code Regulating Phagocytosis of Mammalian Cells . In *Frontiers in Immunology* (Vol. 12). https://www.frontiersin.org/article/10.3389/fimmu.2021.629979

Cohen, M. S., Zhang, C., Shokat, K. M., & Taunton, J. (2005). Structural bioinformatics-based design of selective, irreversible kinase inhibitors. *Science (New York, N.Y.)*, *308*(5726), 1318–1321. https://doi.org/10.1126/science1108367

Combadiere, C., Gao, J., Tiffany, H. L., & Murphy, P. M. (1998). Gene cloning, RNA distribution, and functional expression of mCX3CR1, a mouse chemotactic receptor for the CX3C chemokine fractalkine. *Biochemical and Biophysical Research Communications*, *253*(3), 728–732. https://doi.org/10.1006/bbrc.1998.9849

Condliffe, S. B., Corradini, I., Pozzi, D., Verderio, C., & Matteoli, M. (2010). Endogenous SNAP-25 regulates native voltage-gated calcium channels in glutamatergic neurons. *Journal of Biological Chemistry*, *285*(32), 24968–24976.

Constanzo, J., Midavaine, É., Fouquet, J., Lepage, M., Descoteaux, M., Kirby, K., Tremblay, L., Masson-Côté, L., Geha, S., Longpré, J.-M., Paquette, B., & Sarret, P. (2020). Brain irradiation leads to persistent neuroinflammation and long-term neurocognitive dysfunction in a region-specific manner. *Progress in Neuro-Psychopharmacology and Biological Psychiatry*, *102*, 109954. https://doi.org/https://doi.org/10.1016/j.pnpbp.2020.109954

Crain, J. M., & Watters, J. J. (2010). Estrogen and P2 Purinergic Receptor Systems in Microglia: Therapeutic Targets for Neuroprotection. *The Open Drug Discovery Journal*, *2*, 148–167. https://doi.org/10.2174/1877381801002010148

Crehan, H., Hardy, J., & Pocock, J. (2012). Microglia, Alzheimer's Disease, and Complement. *International Journal of Alzheimer’s Disease*, *2012*, 983640. https://doi.org/10.1155/2012/983640

Dailey, M. E., & Waite, M. (1999). Confocal imaging of microglial cell dynamics in hippocampal slice cultures. *Methods*, *18*(2), 222–230.

Dalman, C., Allebeck, P., Gunnell, D., Harrison, G., Kristensson, K., Lewis, G., Lofving, S., Rasmussen, F., Wicks, S., & Karlsson, H. (2008). Infections in the CNS during childhood

and the risk of subsequent psychotic illness: a cohort study of more than one million Swedish subjects. *American Journal of Psychiatry*, *165*(1), 59–65.

Darabid, H., Perez-Gonzalez, A. P., & Robitaille, R. (2014). Neuromuscular synaptogenesis: coordinating partners with multiple functions. *Nature Reviews Neuroscience*, *15*(11), 703–718.

Das, G. D. (1976). Gitter cells and their relationship to macrophages in the developing cerebellum: an electron microscopic study. *Virchows Archiv. B, Cell Pathology*, *20*(4), 299–305. https://doi.org/10.1007/BF02890348

Daumas, S., Ceccom, J., Halley, H., Francés, B., & Lassalle, J.-M. (2009). Activation of metabotropic glutamate receptor type 2/3 supports the involvement of the hippocampal mossy fiber pathway on contextual fear memory consolidation. *Learning & Memory (Cold Spring Harbor, N.Y.)*, *16*(8), 504–507. https://doi.org/10.1101/lm.1418309

Davalos, D., Grutzendler, J., Yang, G., Kim, J. V, Zuo, Y., Jung, S., Littman, D. R., Dustin, M. L., & Gan, W.-B. (2005). ATP mediates rapid microglial response to local brain injury in vivo. *Nature Neuroscience*, *8*(6), 752–758. https://doi.org/10.1038/nn1472

Davis, E. J., Foster, T. D., & Thomas, W. E. (1994). Cellular forms and functions of brain microglia. *Brain Research Bulletin*, *34*(1), 73–78. https://doi.org/10.1016/0361-9230(94)90189-9

de Cossío, L. F., Guzmán, A., van der Veldt, S., & Luheshi, G. N. (2017). Prenatal infection leads to ASD-like behavior and altered synaptic pruning in the mouse offspring. *Brain, Behavior, and Immunity*, *63*, 88–98.

De Haas, A. H., Boddeke, H. W. G. M., & Biber, K. (2008). Region-specific expression of immunoregulatory proteins on microglia in the healthy CNS. *Glia*, *56*(8), 888–894.

De León Reyes, N. S., Mederos, S., Varela, I., Weiss, L. A., Perea, G., Galazo, M. J., & Nieto, M. (2019). Transient callosal projections of L4 neurons are eliminated for the acquisition of local connectivity. *Nature Communications*, *10*(1), 4549. https://doi.org/10.1038/s41467-019-12495-w

De, S., Van Deren, D., Peden, E., Hockin, M., Boulet, A., Titen, S., & Capecchi, M. R. (2018). Two distinct ontogenies confer heterogeneity to mouse brain microglia. *Development*, *145*(13), dev152306. https://doi.org/10.1242/dev.152306

del Rio-Hortega, P. (1932). *Cytology & [and] cellular pathology of the nervous system*.

Hoeber.

Denizet, M., Cotter, L., Lledo, P.-M., & Lazarini, F. (2017). Sensory deprivation increases phagocytosis of adult-born neurons by activated microglia in the olfactory bulb. *Brain, Behavior, and Immunity*, *60*, 38–43. https://doi.org/10.1016/j.bbi.2016.09.015

DeVries, M. E., Cao, H., Wang, J., Xu, L., Kelvin, A. A., Ran, L., Chau, L. A., Madrenas, J., Hegele, R. A., & Kelvin, D. J. (2003). Genomic Organization and Evolution of the CX3CR1/CCR8 Chemokine Receptor Locus*. *Journal of Biological Chemistry*, *278*(14), 11985–11994. https://doi.org/https://doi.org/10.1074/jbc.M211422200

DiBona, V. L., Zhu, W., Shah, M. K., Rafalia, A., Ben Cheikh, H., Crockett, D. P., & Zhang, H. (2019). Loss of Par1b/MARK2 primes microglia during brain development and enhances their sensitivity to injury. *Journal of Neuroinflammation*, *16*(1), 11. https://doi.org/10.1186/s12974-018-1390-3

Domingues, H. S., Portugal, C. C., Socodato, R., & Relvas, J. B. (2016). Oligodendrocyte, Astrocyte, and Microglia Crosstalk in Myelin Development, Damage, and Repair . In *Frontiers in Cell and Developmental Biology* (Vol. 4). https://www.frontiersin.org/article/10.3389/fcell.2016.00071

Dorfman, M. D., Krull, J. E., Douglass, J. D., Fasnacht, R., Lara-Lince, F., Meek, T. H., Shi, X., Damian, V., Nguyen, H. T., Matsen, M. E., Morton, G. J., & Thaler, J. P. (2017). Sex differences in microglial CX3CR1 signalling determine obesity susceptibility in mice. *Nature Communications*, *8*, 14556. https://doi.org/10.1038/ncomms14556

Dulka, B. N., Bagatelas, E. D., Bress, K. S., Grizzell, J. A., Cannon, M. K., Whitten, C. J., & Cooper, M. A. (2020). Chemogenetic activation of an infralimbic cortex to basolateral amygdala projection promotes resistance to acute social defeat stress. *Scientific Reports*, *10*(1), 6884. https://doi.org/10.1038/s41598-020-63879-8

Eggen, B. J. L., Boddeke, E. W. G. M., & Kooistra, S. M. (2019). Regulation of Microglia Identity from an Epigenetic and Transcriptomic Point of View. *Neuroscience*, *405*, 3—13. https://doi.org/10.1016/j.neuroscience.2017.12.010

Ehlers, M. R. W. (2000). CR3: a general purpose adhesion-recognition receptor essential for innate immunity. *Microbes and Infection*, *2*(3), 289–294.

Ehninger, D., & Kempermann, G. (2003). Regional effects of wheel running and environmental enrichment on cell genesis and microglia proliferation in the adult murine neocortex. *Cerebral Cortex (New York, N.Y. : 1991)*, *13*(8), 845–851.

https://doi.org/10.1093/cercor/13.8.845

Elward, K., & Gasque, P. (2003). “Eat me” and “don’t eat me” signals govern the innate immune response and tissue repair in the CNS: emphasis on the critical role of the complement system. *Molecular Immunology*, *40*(2–4), 85–94. https://doi.org/10.1016/s0161-5890(03)00109-3

Enayati, M., Solati, J., Hosseini, M.-H., Shahi, H.-R., Saki, G., & Salari, A.-A. (2012). Maternal infection during late pregnancy increases anxiety-and depression-like behaviors with increasing age in male offspring. *Brain Research Bulletin*, *87*(2–3), 295–302.

Eyo, U. B., Gu, N., De, S., Dong, H., Richardson, J. R., & Wu, L.-J. (2015). Modulation of microglial process convergence toward neuronal dendrites by extracellular calcium. *The Journal of Neuroscience : The Official Journal of the Society for Neuroscience*, *35*(6), 2417–2422. https://doi.org/10.1523/JNEUROSCI.3279-14.2015

Fan, Q., He, W., Gayen, M., Benoit, M. R., Luo, X., Hu, X., & Yan, R. (2020). Activated CX3CL1/Smad2 Signals Prevent Neuronal Loss and Alzheimer{\textquoteright}s Tau Pathology-Mediated Cognitive Dysfunction. *Journal of Neuroscience*, *40*(5), 1133–1144. https://doi.org/10.1523/JNEUROSCI.1333-19.2019

Ferrini, F., & De Koninck, Y. (2013). Microglia control neuronal network excitability via BDNF signalling. *Neural Plasticity*, *2013*, 429815. https://doi.org/10.1155/2013/429815

Finneran, D. J., Morgan, D., Gordon, M. N., & Nash, K. R. (2019). CNS-Wide over Expression of Fractalkine Improves Cognitive Functioning in a Tauopathy Model. *Journal of Neuroimmune Pharmacology : The Official Journal of the Society on NeuroImmune Pharmacology*, *14*(2), 312–325. https://doi.org/10.1007/s11481-018-9822-5

Fiore, N. T., Yin, Z., Guneykaya, D., Gauthier, C. D., Hayes, J., D’Hary, A., Butovsky, O., & Moalem-Taylor, G. (2021). Sex-specific transcriptome of spinal microglia in neuropathic pain due to peripheral nerve injury. *BioRxiv*, 2021.05.27.446082. https://doi.org/10.1101/2021.05.27.446082

Flynn, S. W., Lang, D. J., Mackay, A. L., Goghari, V., Vavasour, I. M., Whittall, K. P., Smith, G. N., Arango, V., Mann, J. J., Dwork, A. J., Falkai, P., & Honer, W. G. (2003). Abnormalities of myelination in schizophrenia detected in vivo with MRI, and post-mortem with analysis of oligodendrocyte proteins. *Molecular Psychiatry*. https://doi.org/10.1038/sj.mp.4001337

Fossati, G., Morini, R., Corradini, I., Antonucci, F., Trepte, P., Edry, E., Sharma, V., Papale, A.,

Pozzi, D., Defilippi, P., Meier, J. C., Brambilla, R., Turco, E., Rosenblum, K., Wanker, E. E., Ziv, N. E., Menna, E., & Matteoli, M. (2015). Reduced SNAP-25 increases PSD-95 mobility and impairs spine morphogenesis. *Cell Death & Differentiation*, *22*(9), 1425–1436. https://doi.org/10.1038/cdd.2014.227

Fujimoto, E., Miki, A., & Mizoguti, H. (1989). Histochemical study of the differentiation of microglial cells in the developing human cerebral hemispheres. *Journal of Anatomy*, *166*, 253.

Fujita, S., & Kitamura, T. (1975). Origin of brain macrophages and the nature of the so-called microglia. *Acta Neuropathologica. Supplementum*. https://doi.org/10.1007/978-3-662-08456-4_51

Gardai, S. J., McPhillips, K. A., Frasch, S. C., Janssen, W. J., Starefeldt, A., Murphy-Ullrich, J. E., Bratton, D. L., Oldenborg, P.-A., Michalak, M., & Henson, P. M. (2005). Cell-surface calreticulin initiates clearance of viable or apoptotic cells through trans-activation of LRP on the phagocyte. *Cell*, *123*(2), 321–334. https://doi.org/10.1016/j.cell.2005.08.032

Gasque, P., Singhrao, S. K., Neal, J. W., Wang, P., Sayah, S., Fontaine, M., & Morgan, B. P. (1998). The receptor for complement anaphylatoxin C3a is expressed by myeloid cells and nonmyeloid cells in inflamed human central nervous system: analysis in multiple sclerosis and bacterial meningitis. *The Journal of Immunology*, *160*(7), 3543–3554.

Gil-Pisa, I., Cebrián, C., Ortega, J. E., Meana, J. J., & Sulzer, D. (2014). Cytokine pathway disruption in a mouse model of schizophrenia induced by Munc18-1a overexpression in the brain. *Journal of Neuroinflammation*. https://doi.org/10.1186/1742-2094-11-128

Ginhoux, F., Greter, M., Leboeuf, M., Nandi, S., See, P., Gokhan, S., Mehler, M. F., Conway, S. J., Ng, L. G., Stanley, E. R., Samokhvalov, I. M., & Merad, M. (2010). Fate mapping analysis reveals that adult microglia derive from primitive macrophages. *Science*. https://doi.org/10.1126/science.1194637

Ginhoux, F., Lim, S., Hoeffel, G., Low, D., & Huber, T. (2013). Origin and differentiation of microglia. In *Frontiers in Cellular Neuroscience*. https://doi.org/10.3389/fncel.2013.00045

Glantz, L. A., & Lewis, D. A. (2000). Decreased dendritic spine density on prefrontal cortical pyramidal neurons in schizophrenia. *Archives of General Psychiatry*. https://doi.org/10.1001/archpsyc.57.1.65

Glenn, J. A., Booth, P. L., & Thomas, W. E. (1991). Pinocytotic activity in ramified microglia. *Neuroscience Letters*, *123*(1), 27–31. https://doi.org/https://doi.org/10.1016/0304-3940(91)90150-R

Goasdoue, K., Awabdy, D., Bjorkman, S. T., & Miller, S. (2016). Standard loading controls are not reliable for Western blot quantification across brain development or in pathological conditions. *Electrophoresis*, *37*(4), 630–634. https://doi.org/10.1002/elps.201500385

Goldmann, T., Wieghofer, P., Jordão, M. J. C., Prutek, F., Hagemeyer, N., Frenzel, K., Amann, L., Staszewski, O., Kierdorf, K., Krueger, M., Locatelli, G., Hochgerner, H., Zeiser, R., Epelman, S., Geissmann, F., Priller, J., Rossi, F. M. V, Bechmann, I., Kerschensteiner, M., … Prinz, M. (2016). Origin, fate and dynamics of macrophages at central nervous system interfaces. *Nature Immunology*, *17*(7), 797–805. https://doi.org/10.1038/ni.3423

Gomez, J. L., Bonaventura, J., Lesniak, W., Mathews, W. B., Sysa-Shah, P., Rodriguez, L. A., Ellis, R. J., Richie, C. T., Harvey, B. K., Dannals, R. F., Pomper, M. G., Bonci, A., & Michaelides, M. (2017). Chemogenetics revealed: DREADD occupancy and activation via converted clozapine. *Science (New York, N.Y.)*, *357*(6350), 503–507. https://doi.org/10.1126/science.aan2475

Gordon, S. R., Maute, R. L., Dulken, B. W., Hutter, G., George, B. M., McCracken, M. N., Gupta, R., Tsai, J. M., Sinha, R., & Corey, D. (2017). PD-1 expression by tumour-associated macrophages inhibits phagocytosis and tumour immunity. *Nature*, *545*(7655), 495–499.

Gosso, M. F., De Geus, E. J. C., Van Belzen, M. J., Polderman, T. J. C., Heutink, P., Boomsma, D. I., & Posthuma, D. (2006). The SNAP-25 gene is associated with cognitive ability: Evidence from a family-based study in two independent Dutch cohorts. *Molecular Psychiatry*. https://doi.org/10.1038/sj.mp.4001868

Grace, P. M., Wang, X., Strand, K. A., Baratta, M. V, Zhang, Y., Galer, E. L., Yin, H., Maier, S. F., & Watkins, L. R. (2018). DREADDed microglia in pain: Implications for spinal inflammatory signaling in male rats. *Experimental Neurology*, *304*, 125–131. https://doi.org/10.1016/j.expneurol.2018.03.005

Green, T. R. F., Ortiz, J. B., Wonnacott, S., Williams, R. J., & Rowe, R. K. (2020). The Bidirectional Relationship Between Sleep and Inflammation Links Traumatic Brain

Injury and Alzheimer's Disease . In *Frontiers in Neuroscience* (Vol. 14). https://www.frontiersin.org/article/10.3389/fnins.2020.00894

Greenlee, M. H. W., Roosevelt, C. B., & Sakaguchi, D. S. (2001). Differential localization of SNARE complex proteins SNAP-25, Syntaxin, and VAMP during development of the mammalian retina. *Journal of Comparative Neurology*. https://doi.org/10.1002/1096-9861(20010212)430:3<306::AID-CNE1032>3.0.CO;2-B

Greenlee, M. H. W., Wilson, M. C., & Sakaguchi, D. S. (2002). Expression of SNAP-25 during mammalian retinal development: Thinking outside the synapse. *Seminars in Cell and Developmental Biology*. https://doi.org/10.1016/S1084-9521(02)00015-0

Groh, A., de Kock, C. P. J., Wimmer, V. C., Sakmann, B., & Kuner, T. (2008). Driver or Coincidence Detector: Modal Switch of a Corticothalamic Giant Synapse Controlled by Spontaneous Activity and Short-Term Depression. *Journal of Neuroscience*, *28*(39), 9652–9663. https://doi.org/10.1523/JNEUROSCI.1554-08.2008

Guerrero, B. L., & Sicotte, N. L. (2020). Microglia in Multiple Sclerosis: Friend or Foe? . In *Frontiers in Immunology* (Vol. 11). https://www.frontiersin.org/article/10.3389/fimmu.2020.00374

Guettier, J.-M., Gautam, D., Scarselli, M., Ruiz de Azua, I., Li, J. H., Rosemond, E., Ma, X., Gonzalez, F. J., Armbruster, B. N., Lu, H., Roth, B. L., & Wess, J. (2009). A chemical-genetic approach to study G protein regulation of beta cell function in vivo. *Proceedings of the National Academy of Sciences of the United States of America*, *106*(45), 19197–19202. https://doi.org/10.1073/pnas.0906593106

Guillot-Sestier, M.-V., Araiz, A. R., Mela, V., Gaban, A. S., O'Neill, E., Joshi, L., Chouchani, E. T., Mills, E. L., & Lynch, M. A. (2021). Microglial metabolism is a pivotal factor in sexual dimorphism in Alzheimer's disease. *Communications Biology*, *4*(1), 711. https://doi.org/10.1038/s42003-021-02259-y

Guneykaya, D., Ivanov, A., Hernandez, D. P., Haage, V., Wojtas, B., Meyer, N., Maricos, M., Jordan, P., Buonfiglioli, A., Gielniewski, B., Ochocka, N., Cömert, C., Friedrich, C., Artiles, L. S., Kaminska, B., Mertins, P., Beule, D., Kettenmann, H., & Wolf, S. A. (2018). Transcriptional and Translational Differences of Microglia from Male and Female Brains. *Cell Reports*, *24*(10), 2773-2783.e6. https://doi.org/10.1016/j.celrep.2018.08.001

Gunner, G., Cheadle, L., Johnson, K. M., Ayata, P., Badimon, A., Mondo, E., Nagy, M. A., Liu,

L., Bemiller, S. M., Kim, K. W., Lira, S. A., Lamb, B. T., Tapper, A. R., Ransohoff, R. M., Greenberg, M. E., Schaefer, A., & Schafer, D. P. (2019). Sensory lesioning induces microglial synapse elimination via ADAM10 and fractalkine signaling. *Nature Neuroscience*. https://doi.org/10.1038/s41593-019-0419-y

Gutmann, D. H., & Kettenmann, H. (2019). Microglia/Brain Macrophages as Central Drivers of Brain Tumor Pathobiology. *Neuron*, *104*(3), 442–449. https://doi.org/10.1016/j.neuron.2019.08.028

Hagemeyer, N., Hanft, K.-M., Akriditou, M.-A., Unger, N., Park, E. S., Stanley, E. R., Staszewski, O., Dimou, L., & Prinz, M. (2017). Microglia contribute to normal myelinogenesis and to oligodendrocyte progenitor maintenance during adulthood. *Acta Neuropathologica*, *134*(3), 441–458. https://doi.org/10.1007/s00401-017-1747-1

Han, J., Pluhackova, K., & Böckmann, R. A. (2017). The multifaceted role of SNARE proteins in membrane fusion. In *Frontiers in Physiology*. https://doi.org/10.3389/fphys.2017.00005

Hanisch, U.-K., & Kettenmann, H. (2007). Microglia: active sensor and versatile effector cells in the normal and pathologic brain. *Nature Neuroscience*, *10*(11), 1387–1394. https://doi.org/10.1038/nn1997

Hansen, D. V, Hanson, J. E., & Sheng, M. (2018). Microglia in Alzheimer's disease. *The Journal of Cell Biology*, *217*(2), 459–472. https://doi.org/10.1083/jcb.201709069

Harrison, J. K., Jiang, Y., Chen, S., Xia, Y., Maciejewski, D., McNamara, R. K., Streit, W. J., Salafranca, M. N., Adhikari, S., Thompson, D. A., Botti, P., Bacon, K. B., & Feng, L. (1998). Role for neuronally derived fractalkine in mediating interactions between neurons and CX3CR1-expressing microglia. *Proceedings of the National Academy of Sciences of the United States of America*, *95*(18), 10896–10901. https://doi.org/10.1073/pnas.95.18.10896

Hartz, A. M. S., Bauer, B., Block, M. L., Hong, J.-S., & Miller, D. S. (2008). Diesel exhaust particles induce oxidative stress, proinflammatory signaling, and P-glycoprotein up-regulation at the blood-brain barrier. *The FASEB Journal*, *22*(8), 2723–2733.

Hashimoto, K., & Kano, M. (2013). Synapse elimination in the developing cerebellum. *Cellular and Molecular Life Sciences*, *70*(24), 4667–4680.

Hay, J. C. (2001). SNARE complex structure and function. *Experimental Cell Research*. https://doi.org/10.1006/excr.2001.5368

Hayakawa, K., Pham, L.-D. D., Seo, J. H., Miyamoto, N., Maki, T., Terasaki, Y., Sakadžić, S., Boas, D., van Leyen, K., Waeber, C., Kim, K.-W., Arai, K., & Lo, E. H. (2016). CD200 restrains macrophage attack on oligodendrocyte precursors via toll-like receptor 4 downregulation. *Journal of Cerebral Blood Flow and Metabolism : Official Journal of the International Society of Cerebral Blood Flow and Metabolism*, *36*(4), 781–793. https://doi.org/10.1177/0271678X15606148

Hayashi, S., Hoerder-Suabedissen, A., Kiyokage, E., Maclachlan, C., Toida, K., Knott, G., & Molnár, Z. (2021). Maturation of Complex Synaptic Connections of Layer 5 Cortical Axons in the Posterior Thalamic Nucleus Requires SNAP25. *Cerebral Cortex*, *31*(5), 2625–2638. https://doi.org/10.1093/cercor/bhaa379

He, J., Zhao, C., Dai, J., Weng, C. H., Bian, B. S. J., Gong, Y., Ge, L., Fang, Y., Liu, H., Xu, H., & Yin, Z. Q. (2019). Microglia Mediate Synaptic Material Clearance at the Early Stage of Rats With Retinitis Pigmentosa . In *Frontiers in Immunology* (Vol. 10). https://www.frontiersin.org/article/10.3389/fimmu.2019.00912

Heindl, S., Gesierich, B., Benakis, C., Llovera, G., Duering, M., & Liesz, A. (2018). Automated Morphological Analysis of Microglia After Stroke. *Frontiers in Cellular Neuroscience*, *12*. https://doi.org/10.3389/fncel.2018.00106

Hepp, R., Perraut, M., Chasserot-Golaz, S., Galli, T., Aunis, D., Langley, K., & Grant, N. J. (1999). Cultured glial cells express the SNAP-25 analogue SNAP-23. *GLIA*. https://doi.org/10.1002/(SICI)1098-1136(199908)27:2<181::AID-GLIA8>3.0.CO;2-9

Heppner, F. L., Skutella, T., Hailer, N. P., Haas, D., & Nitsch, R. (1998). Activated microglial cells migrate towards sites of excitotoxic neuronal injury inside organotypic hippocampal slice cultures. *European Journal of Neuroscience*, *10*(10), 3284–3290.

Hernadez-Ontiveros, D., Tajiri, N., Acosta, S., Giunta, B., Tan, J., & Borlongan, C. (2013). Microglia Activation as a Biomarker for Traumatic Brain Injury . In *Frontiers in Neurology* (Vol. 4). https://www.frontiersin.org/article/10.3389/fneur.2013.00030

Hertz, L., & Fedoroff, S. (1980). *Advances in cellular neurobiology*.--.

Heyser, C. J., Wilson, M. C., & Gold, L. H. (1995). Coloboma hyperactive mutant exhibits delayed neurobehavioral developmental milestones. *Developmental Brain Research*. https://doi.org/10.1016/0165-3806(95)00130-6

Hill, S. L., Shao, L., & Beasley, C. L. (2021). Diminished levels of the chemokine fractalkine in post-mortem prefrontal cortex in schizophrenia but not bipolar disorder. *The World*

Journal of Biological Psychiatry : The Official Journal of the World Federation of Societies of Biological Psychiatry, *22*(2), 94–103. https://doi.org/10.1080/15622975.2020.1755451

Hiragi, T., Ikegaya, Y., & Koyama, R. (2018). Microglia after Seizures and in Epilepsy. *Cells*, *7*(4). https://doi.org/10.3390/cells7040026

Ho, K. H., & Patrizi, A. (2021). Assessment of common housekeeping genes as reference for gene expression studies using RT-qPCR in mouse choroid plexus. *Scientific Reports*, *11*(1), 3278. https://doi.org/10.1038/s41598-021-82800-5

Ho, M. S. (2019). Microglia in Parkinson's Disease. *Advances in Experimental Medicine and Biology*, *1175*, 335–353. https://doi.org/10.1007/978-981-13-9913-8_13

Ho, Y.-M., Au, N.-P. B., Wong, K.-L., Chan, C. T.-L., Kwok, W.-M., Law, G.-L., Tang, K.-K., Wong, W.-Y., Ma, C.-H. E., & Lam, M. H.-W. (2014). A lysosome-specific two-photon phosphorescent binuclear cyclometalated platinum(II) probe for in vivo imaging of live neurons. *Chemical Communications (Cambridge, England)*, *50*(32), 4161–4163. https://doi.org/10.1039/c3cc48934e

Hoerder-Suabedissen, A., Korrell, K. V., Hayashi, S., Jeans, A., Ramirez, D. M. O., Grant, E., Christian, H. C., Kavalali, E. T., Wilson, M. C., & Molnár, Z. (2019). Cell-Specific Loss of SNAP25 from Cortical Projection Neurons Allows Normal Development but Causes Subsequent Neurodegeneration. *Cerebral Cortex (New York, N.Y. : 1991)*. https://doi.org/10.1093/cercor/bhy127

Hoogland, P. V, Wouterlood, F. G., Welker, E., & Van der Loos, H. (1991). Ultrastructure of giant and small thalamic terminals of cortical origin: a study of the projections from the barrel cortex in mice using Phaseolus vulgaris leuco-agglutinin (PHA-L). *Experimental Brain Research*, *87*(1), 159–172. https://doi.org/10.1007/BF00228517

Hooks, B. M., & Chen, C. (2006). Distinct roles for spontaneous and visual activity in remodeling of the retinogeniculate synapse. *Neuron*, *52*(2), 281–291.

Hoshiko, M., Arnoux, I., Avignone, E., Yamamoto, N., & Audinat, E. (2012). Deficiency of the microglial receptor CX3CR1 impairs postnatal functional development of thalamocortical synapses in the barrel cortex. *Journal of Neuroscience*. https://doi.org/10.1523/JNEUROSCI.1167-12.2012

Hou, Q., Gao, X., Zhang, X., Kong, L., Wang, X., Bian, W., Tu, Y., Jin, M., Zhao, G., Li, B., Jing, N., & Yu, L. (2004). SNAP-25 in hippocampal CA1 region is involved in memory

consolidation. *European Journal of Neuroscience*. https://doi.org/10.1111/j.1460-9568.2004.03600.x

Hou, Q. L., Gao, X., Lu, Q., Zhang, X. H., Tu, Y. Y., Jin, M. L., Zhao, G. P., Yu, L., Jing, N. H., & Li, B. M. (2006). SNAP-25 in hippocampal CA3 region is required for long-term memory formation. *Biochemical and Biophysical Research Communications*. https://doi.org/10.1016/j.bbrc.2006.06.184

Huang, L., Jin, J., Chen, K., You, S., Zhang, H., Sideris, A., Norcini, M., Recio-Pinto, E., Wang, J., Gan, W.-B., & Yang, G. (2021). BDNF produced by cerebral microglia promotes cortical plasticity and pain hypersensitivity after peripheral nerve injury. *PLoS Biology*, *19*(7), e3001337–e3001337. https://doi.org/10.1371/journal.pbio.3001337

Hui, C. W., Vecchiarelli, H. A., Gervais, É., Luo, X., Michaud, F., Scheefhals, L., Bisht, K., Sharma, K., Topolnik, L., & Tremblay, M.-È. (2020). Sex Differences of Microglia and Synapses in the Hippocampal Dentate Gyrus of Adult Mouse Offspring Exposed to Maternal Immune Activation. *Frontiers in Cellular Neuroscience*, *14*. https://doi.org/10.3389/fncel.2020.558181

Hutchins, K. D., Dickson, D. W., Rashbaum, W. K., & Lyman, W. D. (1990). Localization of morphologically distinct microglial populations in the developing human fetal brain: implications for ontogeny. *Developmental Brain Research*, *55*(1), 95–102.

Huttenlocher, P. R. (1979). Synaptic density in human frontal cortex-developmental changes and effects of aging. *Brain Res*, *163*(2), 195–205.

Imai, T., Hieshima, K., Haskell, C., Baba, M., Nagira, M., Nishimura, M., Kakizaki, M., Takagi, S., Nomiyama, H., Schall, T. J., & Yoshie, O. (1997). Identification and molecular characterization of fractalkine receptor CX3CR1, which mediates both leukocyte migration and adhesion. *Cell*, *91*(4), 521–530. https://doi.org/10.1016/s0092-8674(00)80438-9

Imura, Y., Morizawa, Y., Komatsu, R., Shibata, K., Shinozaki, Y., Kasai, H., Moriishi, K., Moriyama, Y., & Koizumi, S. (2013). Microglia release ATP by exocytosis. *GLIA*. https://doi.org/10.1002/glia.22517

Irfan, M., Evonuk, K. S., & DeSilva, T. M. (2021). Microglia phagocytose oligodendrocyte progenitor cells and synapses during early postnatal development: implications for white versus gray matter maturation. *The FEBS Journal*. https://doi.org/10.1111/febs.16190

Ishihara, Y., Itoh, K., Ishida, A., & Yamazaki, T. (2015). Selective estrogen-receptor modulators suppress microglial activation and neuronal cell death via an estrogen receptor-dependent pathway. *The Journal of Steroid Biochemistry and Molecular Biology*, *145*, 85–93. https://doi.org/10.1016/j.jsbmb.2014.10.002

Jann, M. W., Lam, Y. W., & Chang, W. H. (1994). Rapid formation of clozapine in guinea-pigs and man following clozapine-N-oxide administration. *Archives Internationales de Pharmacodynamie et de Therapie*, *328*(2), 243–250.

Jayachandran, M., Linley, S. B., Schlecht, M., Mahler, S. V, Vertes, R. P., & Allen, T. A. (2019). Prefrontal Pathways Provide Top-Down Control of Memory for Sequences of Events. *Cell Reports*, *28*(3), 640-654.e6. https://doi.org/10.1016/j.celrep.2019.06.053

Jena, B. P. (2011). Role of SNAREs in membrane fusion. *Advances in Experimental Medicine and Biology*. https://doi.org/10.1007/978-94-007-0763-4_3

Jendryka, M., Palchaudhuri, M., Ursu, D., van der Veen, B., Liss, B., Kätzel, D., Nissen, W., & Pekcec, A. (2019). Pharmacokinetic and pharmacodynamic actions of clozapine-N-oxide, clozapine, and compound 21 in DREADD-based chemogenetics in mice. *Scientific Reports*, *9*(1), 4522. https://doi.org/10.1038/s41598-019-41088-2

Jeong, H.-K., Ji, K., Min, K., & Joe, E.-H. (2013). Brain inflammation and microglia: facts and misconceptions. *Experimental Neurobiology*, *22*(2), 59–67. https://doi.org/10.5607/en.2013.22.2.59

Jia, J., Yang, L., Chen, Y., Zheng, L., Chen, Y., Xu, Y., & Zhang, M. (2022). The Role of Microglial Phagocytosis in Ischemic Stroke. *Frontiers in Immunology*, *12*, 790201. https://doi.org/10.3389/fimmu.2021.790201

Jinno, S., Fleischer, F., Eckel, S., Schmidt, V., & Kosaka, T. (2007). Spatial arrangement of microglia in the mouse hippocampus: a stereological study in comparison with astrocytes. *Glia*, *55*(13), 1334–1347. https://doi.org/10.1002/glia.20552

Jones, B. A., Beamer, M., & Ahmed, S. (2010). Fractalkine/CX3CL1: A potential new target for inflammatory diseases. In *Molecular Interventions*. https://doi.org/10.1124/mi.10.5.3

Jurado, S., Goswami, D., Zhang, Y., Molina, A. J. M., Südhof, T. C., & Malenka, R. C. (2013). LTP requires a unique postsynaptic SNARE fusion machinery. *Neuron*, *77*(3), 542–558.

Jurga, A. M., Paleczna, M., & Kuter, K. Z. (2020). Overview of General and Discriminating Markers of Differential Microglia Phenotypes . In *Frontiers in Cellular Neuroscience* (Vol. 14). https://www.frontiersin.org/article/10.3389/fncel.2020.00198

Karperien, A., Ahammer, H., & Jelinek, H. (2013). Quantitating the subtleties of microglial morphology with fractal analysis. *Frontiers in Cellular Neuroscience*, *7*. https://doi.org/10.3389/fncel.2013.00003

Karperien, A. L., & Jelinek, H. F. (2015). Fractal, multifractal, and lacunarity analysis of microglia in tissue engineering. *Frontiers in Bioengineering and Biotechnology*, *3*, 51. https://doi.org/10.3389/fbioe.2015.00051

Karperien, A. L., & Jelinek, H. F. (2016). *Box-Counting Fractal Analysis: A Primer for the Clinician BT - The Fractal Geometry of the Brain* (A. Di Ieva (ed.); pp. 13–43). Springer New York. https://doi.org/10.1007/978-1-4939-3995-4_2

KARPERIEN, A. L., JELINEK, H. F., & BUCHAN, A. M. (2008). BOX-COUNTING ANALYSIS OF MICROGLIA FORM IN SCHIZOPHRENIA, ALZHEIMER'S DISEASE AND AFFECTIVE DISORDER. *Fractals*, *16*(02), 103–107. https://doi.org/10.1142/S0218348X08003880

Karve, I. P., Taylor, J. M., & Crack, P. J. (2016). The contribution of astrocytes and microglia to traumatic brain injury. *British Journal of Pharmacology*, *173*(4), 692–702. https://doi.org/10.1111/bph.13125

Katz, L. C., & Shatz, C. J. (1996). Synaptic activity and the construction of cortical circuits. *Science (New York, N.Y.)*, *274*(5290), 1133–1138. https://doi.org/10.1126/science.274.5290.1133

Kawamura, N., Katsuura, G., Yamada-Goto, N., Novianti, E., Inui, A., & Asakawa, A. (2021). Impaired brain fractalkine-CX3CR1 signaling is implicated in cognitive dysfunction in diet-induced obese mice. *BMJ Open Diabetes Research & Care*, *9*(1). https://doi.org/10.1136/bmjdrc-2020-001492

Kerr, N., Dietrich, D. W., Bramlett, H. M., & Raval, A. P. (2019). Sexually dimorphic microglia and ischemic stroke. *CNS Neuroscience & Therapeutics*, *25*(12), 1308–1317. https://doi.org/10.1111/cns.13267

Kershman, J. (1939). Genesis of microglia in the human brain. *Archives of Neurology And Psychiatry*. https://doi.org/10.1001/archneurpsyc.1939.02270130034002

Khan, A. H., & Zaidi, S. (2017). Clozapine: Improvement of Negative Symptoms of Schizophrenia. In *Cureus* (Vol. 9, Issue 12, p. e1973). https://doi.org/10.7759/cureus.1973

Kierdorf, K., Katzmarski, N., Haas, C. A., & Prinz, M. (2013). Bone Marrow Cell Recruitment to the Brain in the Absence of Irradiation or Parabiosis Bias. *PLoS ONE*.

https://doi.org/10.1371/journal.pone.0058544

Kierdorf, K., & Prinz, M. (2013). Factors regulating microglia activation. *Frontiers in Cellular Neuroscience*, *7*. https://doi.org/10.3389/fncel.2013.00044

Kim, K.-W., Vallon-Eberhard, A., Zigmond, E., Farache, J., Shezen, E., Shakhar, G., Ludwig, A., Lira, S. A., & Jung, S. (2011). In vivo structure/function and expression analysis of the CX3C chemokine fractalkine. *Blood*, *118*(22), e156–e167. https://doi.org/https://doi.org/10.1182/blood-2011-04-348946

Kish, S. J., Lopes-Cendes, I., Guttman, M., Furukawa, Y., Pandolfo, M., Rouleau, G. A., Ross, B. M., Nance, M., Schut, L., Ang, L., & DiStefano, L. (1998). Brain Glyceraldehyde-3-Phosphate Dehydrogenase Activity in Human Trinucleotide Repeat Disorders. *Archives of Neurology*, *55*(10), 1299–1304. https://doi.org/10.1001/archneur.55.10.1299

Klein, G., Humbert, N., Gradinaru, J., Ivanova, A., Gilardoni, F., Rusbandi, U. E., & Ward, T. R. (2005). Tailoring the active site of chemzymes by using a chemogenetic-optimization procedure: towards substrate-specific artificial hydrogenases based on the biotin-avidin technology. *Angewandte Chemie (International Ed. in English)*, *44*(47), 7764–7767. https://doi.org/10.1002/anie.200502000

Klocke, C., Allen, J. L., Sobolewski, M., Mayer-Pröschel, M., Blum, J. L., Lauterstein, D., Zelikoff, J. T., & Cory-Slechta, D. A. (2017). Neuropathological consequences of gestational exposure to concentrated ambient fine and ultrafine particles in the mouse. *Toxicological Sciences*, *156*(2), 492–508.

Koike, H., Demars, M. P., Short, J. A., Nabel, E. M., Akbarian, S., Baxter, M. G., & Morishita, H. (2016). Chemogenetic Inactivation of Dorsal Anterior Cingulate Cortex Neurons Disrupts Attentional Behavior in Mouse. *Neuropsychopharmacology : Official Publication of the American College of Neuropsychopharmacology*, *41*(4), 1014–1023. https://doi.org/10.1038/npp.2015.229

Kongsui, R., Beynon, S. B., Johnson, S. J., & Walker, F. R. (2014). Quantitative assessment of microglial morphology and density reveals remarkable consistency in the distribution and morphology of cells within the healthy prefrontal cortex of the rat. *Journal of Neuroinflammation*, *11*(1), 182. https://doi.org/10.1186/s12974-014-0182-7

Konigsmark, B. W., & Sidman, R. L. (1963). Origin of brain macrophages in the mouse. *Journal of Neuropathology & Experimental Neurology*, *22*(4), 643–676.

Korrell, K. V., Disser, J., Parley, K., Vadisiute, A., Requena-Komuro, M. C., Fodder, H., Pollart,

C., Knott, G., Molnár, Z., & Hoerder-Suabedissen, A. (2019). Differential effect on myelination through abolition of activity-dependent synaptic vesicle release or reduction of overall electrical activity of selected cortical projections in the mouse. *Journal of Anatomy*, *235*(3), 452–467. https://doi.org/10.1111/joa.12974

Korzhevskii, D. E., & Kirik, O. V. (2016). Brain Microglia and Microglial Markers. *Neuroscience and Behavioral Physiology*, *46*(3), 284–290. https://doi.org/10.1007/s11055-016-0231-z

Kosonowska, E., Janeczko, K., & Setkowicz, Z. (2015). Inflammation induced at different developmental stages affects differently the range of microglial reactivity and the course of seizures evoked in the adult rat. *Epilepsy and Behavior*. https://doi.org/10.1016/j.yebeh.2015.04.063

LaMantia, A. S., & Rakic, P. (1990). Axon overproduction and elimination in the corpus callosum of the developing rhesus monkey. *The Journal of Neuroscience : The Official Journal of the Society for Neuroscience*, *10*(7), 2156–2175. https://doi.org/10.1523/JNEUROSCI.10-07-02156.1990

Lau, C. G., Takayasu, Y., Rodenas-Ruano, A., Paternain, A. V, Lerma, J., Bennett, M. V. L., & Zukin, R. S. (2010). SNAP-25 is a target of protein kinase C phosphorylation critical to NMDA receptor trafficking. *Journal of Neuroscience*, *30*(1), 242–254.

Lauro, C., Catalano, M., Trettel, F., & Limatola, C. (2015). Fractalkine in the nervous system: neuroprotective or neurotoxic molecule? *Annals of the New York Academy of Sciences*, *1351*, 141–148. https://doi.org/10.1111/nyas.12805

Lawson, L. J., Perry, V. H., Dri, P., & Gordon, S. (1990). Heterogeneity in the distribution and morphology of microglia in the normal adult mouse brain. *Neuroscience*, *39*(1), 151–170. https://doi.org/10.1016/0306-4522(90)90229-w

Lawson, L. J., Perry, V. H., & Gordon, S. (1992). Turnover of resident microglia in the normal adult mouse brain. *Neuroscience*, *48*(2), 405–415. https://doi.org/10.1016/0306-4522(92)90500-2

Lee, Y. B., Nagai, A., & Kim, S. U. (2002). Cytokines, chemokines, and cytokine receptors in human microglia. *Journal of Neuroscience Research*, *69*(1), 94–103. https://doi.org/10.1002/jnr.10253

Lehrman, E. K., Wilton, D. K., Litvina, E. Y., Welsh, C. A., Chang, S. T., Frouin, A., Walker, A. J., Heller, M. D., Umemori, H., Chen, C., & Stevens, B. (2018). CD47 Protects Synapses

from Excess Microglia-Mediated Pruning during Development. *Neuron*, *100*(1), 120-134.e6. https://doi.org/10.1016/j.neuron.2018.09.017

Lenz, K. M., Nugent, B. M., Haliyur, R., & McCarthy, M. M. (2013). Microglia are essential to masculinization of brain and behavior. *The Journal of Neuroscience : The Official Journal of the Society for Neuroscience*, *33*(7), 2761–2772. https://doi.org/10.1523/JNEUROSCI.1268-12.2013

Lerchner, W., Xiao, C., Nashmi, R., Slimko, E. M., van Trigt, L., Lester, H. A., & Anderson, D. J. (2007). Reversible silencing of neuronal excitability in behaving mice by a genetically targeted, ivermectin-gated Cl- channel. *Neuron*, *54*(1), 35–49. https://doi.org/10.1016/j.neuron.2007.02.030

Levesque, S., Taetzsch, T., Lull, M. E., Kodavanti, U., Stadler, K., Wagner, A., Johnson, J. A., Duke, L., Kodavanti, P., & Surace, M. J. (2011). Diesel exhaust activates and primes microglia: air pollution, neuroinflammation, and regulation of dopaminergic neurotoxicity. *Environmental Health Perspectives*, *119*(8), 1149–1155.

Leyh, J., Paeschke, S., Mages, B., Michalski, D., Nowicki, M., Bechmann, I., & Winter, K. (2021). Classification of Microglial Morphological Phenotypes Using Machine Learning. *Frontiers in Cellular Neuroscience*, *15*, 701673. https://doi.org/10.3389/fncel.2021.701673

Li, F., Jiang, D., & Samuel, M. A. (2019). Microglia in the developing retina. *Neural Development*, *14*(1), 12. https://doi.org/10.1186/s13064-019-0137-x

Liang, K. J., Lee, J. E., Wang, Y. D., Ma, W., Fontainhas, A. M., Fariss, R. N., & Wong, W. T. (2009). Regulation of dynamic behavior of retinal microglia by CX3CR1 signaling. *Investigative Ophthalmology and Visual Science*. https://doi.org/10.1167/iovs.08-3357

Limatola, C., & Ransohoff, R. M. (2014). Modulating neurotoxicity through CX3CL1/CX3CR1 signaling. *Frontiers in Cellular Neuroscience*, *8*, 229. https://doi.org/10.3389/fncel.2014.00229

Lin, X., Cheng, C., Terry, P., Chen, J., Cui, H., & Wu, J. (2017). Rapid and sensitive detection of bisphenol a from serum matrix. *Biosensors and Bioelectronics*, *91*, 104–109.

Linnartz, B., & Neumann, H. (2013). Microglial activatory (immunoreceptor tyrosine-based activation motif)-and inhibitory (immunoreceptor tyrosine-based inhibition motif)-signaling receptors for recognition of the neuronal glycocalyx. *Glia*, *61*(1), 37–46.

Liu, G. Y., Kulasingam, V., Alexander, R. T., Touret, N., Fong, A. M., Patel, D. D., & Robinson,

L. A. (2005). Recycling of the membrane-anchored chemokine, CX2CL1. *Journal of Biological Chemistry*. https://doi.org/10.1074/jbc.M413073200

Liu, H., Wang, X., Chen, L., Chen, L., Tsirka, S. E., Ge, S., & Xiong, Q. (2021). Microglia modulate stable wakefulness via the thalamic reticular nucleus in mice. *Nature Communications*, *12*(1), 4646. https://doi.org/10.1038/s41467-021-24915-x

Liu, P., Liang, Y., Jiang, L., Wang, H., Wang, S., & Dong, J. (2018). CX3CL1/fractalkine enhances prostate cancer spinal metastasis by activating the Src/FAK pathway. *International Journal of Oncology*, *53*(4), 1544–1556.

Liu, Y., Shah, K., Yang, F., Witucki, L., & Shokat, K. M. (1998). Engineering Src family protein kinases with unnatural nucleotide specificity. *Chemistry & Biology*, *5*(2), 91–101. https://doi.org/10.1016/s1074-5521(98)90143-0

London, A., Cohen, M., & Schwartz, M. (2013). Microglia and monocyte-derived macrophages: functionally distinct populations that act in concert in CNS plasticity and repair. *Frontiers in Cellular Neuroscience*, *7*, 34.

Lowery, R. L., Tremblay, M.-E., Hopkins, B. E., & Majewska, A. K. (2017). The microglial fractalkine receptor is not required for activity-dependent plasticity in the mouse visual system. *Glia*, *65*(11), 1744–1761. https://doi.org/10.1002/glia.23192

Lyons, A., Lynch, A. M., Downer, E. J., Hanley, R., O'Sullivan, J. B., Smith, A., & Lynch, M. A. (2009). Fractalkine-induced activation of the phosphatidylinositol-3 kinase pathway attentuates microglial activation in vivo and in vitro. *Journal of Neurochemistry*, *110*(5), 1547–1556. https://doi.org/10.1111/j.1471-4159.2009.06253.x

Lyu, J., Jiang, X., Leak, R. K., Shi, Y., Hu, X., & Chen, J. (2021). Microglial Responses to Brain Injury and Disease: Functional Diversity and New Opportunities. *Translational Stroke Research*, *12*(3), 474–495. https://doi.org/10.1007/s12975-020-00857-2

Mabrouk, R. (2022). Principal Component Analysis versus Subject’s Residual Profile Analysis for Neuroinflammation Investigation in Parkinson Patients: A PET Brain Imaging Study. *Journal of Imaging*, *8*(3). https://doi.org/10.3390/jimaging8030056

Maciejewski-Lenoir, D., Chen, S., Feng, L., Maki, R., & Bacon, K. B. (1999). Characterization of fractalkine in rat brain cells: migratory and activation signals for CX3CR-1-expressing microglia. *Journal of Immunology (Baltimore, Md. : 1950)*.

Maezawa, I., & Jin, L.-W. (2010). Rett syndrome microglia damage dendrites and synapses by the elevated release of glutamate. *The Journal of Neuroscience : The Official Journal*

of the Society for Neuroscience, *30*(15), 5346–5356. https://doi.org/10.1523/JNEUROSCI.5966-09.2010

Maggi, L., Scianni, M., Branchi, I., D'Andrea, I., Lauro, C., & Limatola, C. (2011). CX(3)CR1 deficiency alters hippocampal-dependent plasticity phenomena blunting the effects of enriched environment. *Frontiers in Cellular Neuroscience*, *5*, 22. https://doi.org/10.3389/fncel.2011.00022

Magnus, C. J., Lee, P. H., Atasoy, D., Su, H. H., Looger, L. L., & Sternson, S. M. (2011). Chemical and genetic engineering of selective ion channel-ligand interactions. *Science (New York, N.Y.)*, *333*(6047), 1292–1296. https://doi.org/10.1126/science.1206606

Maho, A., Bensimon, A., Vassart, G., & Parmentier, M. (1999). Mapping of the CCXCR1, CX3CR1, CCBP2 and CCR9 genes to the CCR cluster within the 3p21.3 region of the human genome. *Cytogenetics and Cell Genetics*, *87*(3–4), 265–268. https://doi.org/10.1159/000015443

Manvich, D. F., Webster, K. A., Foster, S. L., Farrell, M. S., Ritchie, J. C., Porter, J. H., & Weinshenker, D. (2018). The DREADD agonist clozapine N-oxide (CNO) is reverse-metabolized to clozapine and produces clozapine-like interoceptive stimulus effects in rats and mice. *Scientific Reports*, *8*(1), 3840. https://doi.org/10.1038/s41598-018-22116-z

Martinez, V. K., Saldana-Morales, F., Sun, J. J., Zhu, P. J., Costa-Mattioli, M., & Ray, R. S. (2019). Off-Target Effects of Clozapine-N-Oxide on the Chemosensory Reflex Are Masked by High Stress Levels . In *Frontiers in Physiology* (Vol. 10). https://www.frontiersin.org/article/10.3389/fphys.2019.00521

McCarthy, M. M., Wright, C. L., & Schwarz, J. M. (2009). New tricks by an old dogma: mechanisms of the organizational/activational hypothesis of steroid-mediated sexual differentiation of brain and behavior. *Hormones and Behavior*, *55*(5), 655–665.

McMullan, S. M., Phanavanh, B., Li, G. G., & Barger, S. W. (2012). Metabotropic glutamate receptors inhibit microglial glutamate release. *ASN Neuro*, *4*(5). https://doi.org/10.1042/AN20120044

Menassa, D. A., & Gomez-Nicola, D. (2018). Microglial dynamics during human brain development. In *Frontiers in Immunology*. https://doi.org/10.3389/fimmu.2018.01014

Mildenberger, W., Stifter, S. A., & Greter, M. (2022). Diversity and function of brain-associated macrophages. *Current Opinion in Immunology*, *76*, 102181.

https://doi.org/https://doi.org/10.1016/j.coi.2022.102181

Mittelbronn, M., Dietz, K., Schluesener, H. J., & Meyermann, R. (2001). Local distribution of microglia in the normal adult human central nervous system differs by up to one order of magnitude. *Acta Neuropathologica*. https://doi.org/10.1007/s004010000284

Miyamoto, A., Wake, H., Ishikawa, A. W., Eto, K., Shibata, K., Murakoshi, H., Koizumi, S., Moorhouse, A. J., Yoshimura, Y., & Nabekura, J. (2016). Microglia contact induces synapse formation in developing somatosensory cortex. *Nature Communications*. https://doi.org/10.1038/ncomms12540

Miyamoto, N., Maki, T., Shindo, A., Liang, A. C., Maeda, M., Egawa, N., Itoh, K., Lo, E. K., Lok, J., Ihara, M., & Arai, K. (2015). Astrocytes promote oligodendrogenesis after white matter damage via brain-derived neurotrophic factor. *Journal of Neuroscience*. https://doi.org/10.1523/JNEUROSCI.1592-15.2015

Mondo, E., Becker, S. C., Kautzman, A. G., Schifferer, M., Baer, C. E., Chen, J., Huang, E. J., Simons, M., & Schafer, D. P. (2020). A developmental analysis of juxtavascular microglia dynamics and interactions with the vasculature. *BioRxiv*. https://doi.org/10.1101/2020.05.25.110908

Monier, A., Adle-Biassette, H., Delezoide, A.-L., Evrard, P., Gressens, P., & Verney, C. (2007). Entry and Distribution of Microglial Cells in Human Embryonic and Fetal Cerebral Cortex. *Journal of Neuropathology & Experimental Neurology*, *66*(5), 372–382. https://doi.org/10.1097/nen.0b013e3180517b46

Monier, A., Evrard, P., Gressens, P., & Verney, C. (2006). Distribution and differentiation of microglia in the human encephalon during the first two trimesters of gestation. *The Journal of Comparative Neurology*, *499*(4), 565–582. https://doi.org/10.1002/cne.21123

Monroe, K. M., & Di Paolo, G. (2021). Microglia clean up toxic lipids in multiple sclerosis. *Nature Neuroscience*, *24*(4), 451–452. https://doi.org/10.1038/s41593-021-00829-1

Morimoto, K., & Nakajima, K. (2019). Role of the Immune System in the Development of the Central Nervous System . In *Frontiers in Neuroscience* (Vol. 13). https://www.frontiersin.org/article/10.3389/fnins.2019.00916

Morrison, H. W., & Filosa, J. A. (2013). A quantitative spatiotemporal analysis of microglia morphology during ischemic stroke and reperfusion. *Journal of Neuroinflammation*, *10*(1), 782. https://doi.org/10.1186/1742-2094-10-4

Mosser, C.-A., Baptista, S., Arnoux, I., & Audinat, E. (2017). Microglia in CNS development: Shaping the brain for the future. *Progress in Neurobiology*, *149–150*, 1–20. https://doi.org/https://doi.org/10.1016/j.pneurobio.2017.01.002

Nagata, S., Suzuki, J., Segawa, K., & Fujii, T. (2016). Exposure of phosphatidylserine on the cell surface. *Cell Death & Differentiation*, *23*(6), 952–961. https://doi.org/10.1038/cdd.2016.7

Nakajima, K., & Wess, J. (2012). Design and functional characterization of a novel, arrestin-biased designer G protein-coupled receptor. *Molecular Pharmacology*, *82*(4), 575–582. https://doi.org/10.1124/mol.112.080358

Nakamura, K., Casey, M., Oey, H., Vari, F., Stagg, J., Gandhi, M. K., & Smyth, M. J. (2020). Targeting an adenosine-mediated "don't eat me signal" augments anti-lymphoma immunity by anti-CD20 monoclonal antibody. *Leukemia*, *34*(10), 2708–2721.

Nelson, L. H., Warden, S., & Lenz, K. M. (2017). Sex differences in microglial phagocytosis in the neonatal hippocampus. *Brain, Behavior, and Immunity*, *64*, 11–22. https://doi.org/10.1016/j.bbi.2017.03.010

Neniskyte, U., & Gross, C. T. (2017). Errant gardeners: Glial-cell-dependent synaptic pruning and neurodevelopmental disorders. In *Nature Reviews Neuroscience*. https://doi.org/10.1038/nrn.2017.110

Nicholson, K. L., Munson, M., Miller, R. B., Filip, T. J., Fairman, R., & Hughson, F. M. (1998). Regulation of SNARE complex assembly by an N-terminal domain of the t- SNARE Sso1p. *Nature Structural Biology*. https://doi.org/10.1038/1834

Nimmerjahn, A., Kirchhoff, F., & Helmchen, F. (2005). Resting microglial cells are highly dynamic surveillants of brain parenchyma in vivo. *Science (New York, N.Y.)*, *308*(5726), 1314–1318. https://doi.org/10.1126/science.1110647

Nishiyori, A., Minami, M., Ohtani, Y., Takami, S., Yamamoto, J., Kawaguchi, N., Kume, T., Akaike, A., & Satoh, M. (1998). Localization of fractalkine and CX3CR1 mRNAs in rat brain: Does fractalkine play a role in signaling from neuron to microglia? *FEBS Letters*. https://doi.org/10.1016/S0014-5793(98)00583-3

Noda, M., Nakanishi, H., Nabekura, J., & Akaike, N. (2000). AMPA-kainate subtypes of glutamate receptor in rat cerebral microglia. *The Journal of Neuroscience : The Official Journal of the Society for Neuroscience*, *20*(1), 251–258. https://doi.org/10.1523/JNEUROSCI.20-01-00251.2000

Nomiyama, H., Imai, T., Kusuda, J., Miura, R., Callen, D. F., & Yoshie, O. (1998). Human chemokines fractalkine (SCYD1), MDC (SCYA22) and TARC (SCYA17) are clustered on chromosome 16q13. *Cytogenetics and Cell Genetics*, *81*(1), 10–11. https://doi.org/10.1159/000015000

Nomura, K., Vilalta, A., Allendorf, D. H., Hornik, T. C., & Brown, G. C. (2017). Activated Microglia Desialylate and Phagocytose Cells via Neuraminidase, Galectin-3, and Mer Tyrosine Kinase. *The Journal of Immunology*, *198*(12), 4792 LP – 4801. https://doi.org/10.4049/jimmunol.1502532

Noris, M., & Remuzzi, G. (2013). Overview of Complement Activation and Regulation. *Seminars in Nephrology*, *33*(6), 479–492. https://doi.org/https://doi.org/10.1016/j.semnephrol.2013.08.001

O'Leary, D. D. M., Bicknese, A. R., De Carlos, J. A., Heffner, C. D., Koester, S. E., Kutka, L. J., & Terashima, T. (1990). Target selection by cortical axons: alternative mechanisms to establish axonal connections in the developing brain. *Cold Spring Harbor Symposia on Quantitative Biology*, *55*, 453–468.

O'Leary, D. D. M., & Koester, S. E. (1993). Development of projection neuron types, axon pathways, and patterned connections of the mammalian cortex. *Neuron*, *10*(6), 991–1006.

Ogden, C. A., deCathelineau, A., Hoffmann, P. R., Bratton, D., Ghebrehiwet, B., Fadok, V. A., & Henson, P. M. (2001). C1q and mannose binding lectin engagement of cell surface calreticulin and CD91 initiates macropinocytosis and uptake of apoptotic cells. *The Journal of Experimental Medicine*, *194*(6), 781–795. https://doi.org/10.1084/jem.194.6.781

Osen-Sand, A., Catsicas, M., Staple, J. K., Jones, K. A., Ayala, G., Knowles, J., Grenningloh, G., & Catsicas, S. (1993). Inhibition of axonal growth by SNAP-25 antisense oligonucleotides in vitro and in vivo. *Nature*, *364*(6436), 445–448. https://doi.org/10.1038/364445a0

Owolabi, S. A., & Saab, C. Y. (2006). Fractalkine and minocycline alter neuronal activity in the spinal cord dorsal horn. *FEBS Letters*, *580*(18), 4306–4310. https://doi.org/10.1016/j.febslet.2006.06.087

Oyler, G. A., Polli, J. W., Higgins, G. A., Wilson, M. C., & Billingsley, M. L. (1992). Distribution and expression of SNAP-25 immunoreactivity in rat brain, rat PC-12 cells and human

SMS-KCNR neuroblastoma cells. *Developmental Brain Research*. https://doi.org/10.1016/0165-3806(92)90172-S

Oyler, G. A., Polli, J. W., Wilson, M. C., & Billingsley, M. L. (1991). Developmental expression of the 25-kDa synaptosomal-associated protein (SNAP-25) in rat brain. *Proceedings of the National Academy of Sciences of the United States of America*. https://doi.org/10.1073/pnas.88.12.5247

Pabon, M. M., Bachstetter, A. D., Hudson, C. E., Gemma, C., & Bickford, P. C. (2011). CX3CL1 reduces neurotoxicity and microglial activation in a rat model of Parkinson's disease. *Journal of Neuroinflammation*, *8*, 9. https://doi.org/10.1186/1742-2094-8-9

Palpagama, T. H., Waldvogel, H. J., Faull, R. L. M., & Kwakowsky, A. (2019). The Role of Microglia and Astrocytes in Huntington's Disease. *Frontiers in Molecular Neuroscience*, *12*, 258. https://doi.org/10.3389/fnmol.2019.00258

Pang, Y., Rodts-Palenik, S., Cai, Z., Bennett, W. A., & Rhodes, P. G. (2005). Suppression of glial activation is involved in the protection of IL-10 on maternal E. coli induced neonatal white matter injury. *Developmental Brain Research*, *157*(2), 141–149.

Paolicelli, R. C., Bisht, K., & Tremblay, M. È. (2014). Fractalkine regulation of microglial physiology and consequences on the brain and behavior. In *Frontiers in Cellular Neuroscience*. https://doi.org/10.3389/fncel.2014.00129

Paolicelli, R. C., Bolasco, G., Pagani, F., Maggi, L., Scianni, M., Panzanelli, P., Giustetto, M., Ferreira, T. A., Guiducci, E., Dumas, L., Ragozzino, D., & Gross, C. T. (2011). Synaptic pruning by microglia is necessary for normal brain development. *Science*. https://doi.org/10.1126/science.1202529

Paolicelli, R. C., Jawaid, A., Henstridge, C. M., Valeri, A., Merlini, M., Robinson, J. L., Lee, E. B., Rose, J., Appel, S., Lee, V. M.-Y., Trojanowski, J. Q., Spires-Jones, T., Schulz, P. E., & Rajendran, L. (2017). TDP-43 Depletion in Microglia Promotes Amyloid Clearance but Also Induces Synapse Loss. *Neuron*, *95*(2), 297-308.e6. https://doi.org/https://doi.org/10.1016/j.neuron.2017.05.037

Pawelec, P., Ziemka-Nalecz, M., Sypecka, J., & Zalewska, T. (2020). The Impact of the CX3CL1/CX3CR1 Axis in Neurological Disorders. *Cells*, *9*(10). https://doi.org/10.3390/cells9102277

Pelvig, D. P., Pakkenberg, H., Stark, A. K., & Pakkenberg, B. (2008). Neocortical glial cell numbers in human brains. *Neurobiology of Aging*, *29*(11), 1754–1762.

https://doi.org/https://doi.org/10.1016/j.neurobiolaging.2007.04.013

Penfield, W. (1928). *Neuroglia and microglia: the interstitial tissue of the central nervous system*. Paul B. Hoeber.

Peng, L., Liu, H., Ruan, H., Tepp, W. H., Stoothoff, W. H., Brown, R. H., Johnson, E. A., Yao, W. D., Zhang, S. C., & Dong, M. (2013). Cytotoxicity of botulinum neurotoxins reveals a direct role of syntaxin 1 and SNAP-25 in neuron survival. *Nature Communications*. https://doi.org/10.1038/ncomms2462

Pérez, S., Royo, L. J., Astudillo, A., Escudero, D., Álvarez, F., Rodríguez, A., Gómez, E., & Otero, J. (2007). Identifying the most suitable endogenous control for determining gene expression in hearts from organ donors. *BMC Molecular Biology*, *8*(1), 1–7.

Pobbati, A. V., Stein, A., & Fasshauer, D. (2006). N- to C-terminal SNARE complex assembly promotes rapid membrane fusion. *Science*. https://doi.org/10.1126/science.1129486

Poniatowski, Ł. A., Wojdasiewicz, P., Krawczyk, M., Szukiewicz, D., Gasik, R., Kubaszewski, Ł., & Kurkowska-Jastrzębska, I. (2017). Analysis of the Role of CX3CL1 (Fractalkine) and Its Receptor CX3CR1 in Traumatic Brain and Spinal Cord Injury: Insight into Recent Advances in Actions of Neurochemokine Agents. *Molecular Neurobiology*, *54*(3), 2167–2188. https://doi.org/10.1007/s12035-016-9787-4

Prescott, G. R., & Chamberlain, L. H. (2011). Regional and developmental brain expression patterns of SNAP25 splice variants. *BMC Neuroscience*. https://doi.org/10.1186/1471-2202-12-35

Presumey, J., Bialas, A. R., & Carroll, M. C. (2017). Complement System in Neural Synapse Elimination in Development and Disease. In *Advances in Immunology*. https://doi.org/10.1016/bs.ai.2017.06.004

Priller, J., & Prinz, M. (2019). Targeting microglia in brain disorders. In *Science*. https://doi.org/10.1126/science.aau9100

Prinz, M., Erny, D., & Hagemeyer, N. (2017). Ontogeny and homeostasis of CNS myeloid cells. *Nature Immunology*, *18*(4), 385–392.

Prinz, M., & Priller, J. (2014). Microglia and brain macrophages in the molecular age: From origin to neuropsychiatric disease. In *Nature Reviews Neuroscience*. https://doi.org/10.1038/nrn3722

Qin, C., Zhou, L.-Q., Ma, X.-T., Hu, Z.-W., Yang, S., Chen, M., Bosco, D. B., Wu, L.-J., & Tian, D.-S. (2019). Dual Functions of Microglia in Ischemic Stroke. *Neuroscience Bulletin*,

35(5), 921–933. https://doi.org/10.1007/s12264-019-00388-3

Ramaglia, V., Dubey, M., Malpede, M. A., Petersen, N., de Vries, S. I., Ahmed, S. M., Lee, D. S. W., Schenk, G. J., Gold, S. M., Huitinga, I., Gommerman, J. L., Geurts, J. J. G., & Kole, M. H. P. (2021). Complement-associated loss of CA2 inhibitory synapses in the demyelinated hippocampus impairs memory. *Acta Neuropathologica*, *142*(4), 643–667. https://doi.org/10.1007/s00401-021-02338-8

Ransohoff, R. M., & Perry, V. H. (2009). Microglial physiology: unique stimuli, specialized responses. *Annual Review of Immunology*, *27*, 119–145.

Raport, C. J., Schweickart, V. L., Eddy, R. L., Shows, T. B., & Gray, P. W. (1995). The orphan G-protein-coupled receptor-encoding gene V28 is closely related to genes for chemokine receptors and is expressed in lymphoid and neural tissues. *Gene*, *163*(2), 295–299. https://doi.org/https://doi.org/10.1016/0378-1119(95)00336-5

Redfern, C. H., Degtyarev, M. Y., Kwa, A. T., Salomonis, N., Cotte, N., Nanevicz, T., Fidelman, N., Desai, K., Vranizan, K., Lee, E. K., Coward, P., Shah, N., Warrington, J. A., Fishman, G. I., Bernstein, D., Baker, A. J., & Conklin, B. R. (2000). Conditional expression of a Gi-coupled receptor causes ventricular conduction delay and a lethal cardiomyopathy. *Proceedings of the National Academy of Sciences of the United States of America*, *97*(9), 4826–4831. https://doi.org/10.1073/pnas.97.9.4826

Reemst, K., Noctor, S. C., Lucassen, P. J., & Hol, E. M. (2016). The Indispensable Roles of Microglia and Astrocytes during Brain Development . In *Frontiers in Human Neuroscience* (Vol. 10). https://www.frontiersin.org/article/10.3389/fnhum.2016.00566

Rezaie, P., & Male, D. (2002). Mesoglia and microglia - A historical review of the concept of mononuclear phagocytes within the central nervous system. In *Journal of the History of the Neurosciences*. https://doi.org/10.1076/jhin.11.4.325.8531

Rio-Hortega, P. (1939). The microglia. *The Lancet*, *233*(6036), 1023–1026.

Rivas-Fuentes, S., Salgado-Aguayo, A., Arratia-Quijada, J., & Gorocica-Rosete, P. (2021). Regulation and biological functions of the CX3CL1-CX3CR1 axis and its relevance in solid cancer: A mini-review. *Journal of Cancer*, *12*(2), 571–583. https://doi.org/10.7150/jca.47022

Rizo, J., & Südhof, T. C. (2012). The membrane fusion enigma: SNAREs, Sec1/Munc18 proteins, and their accomplices guilty as charged? In *Annual Review of Cell and*

Developmental Biology (Vol. 28). https://doi.org/10.1146/annurev-cellbio-101011-155818

Rojewska, E., Piotrowska, A., Popiolek-Barczyk, K., & Mika, J. (2018). Botulinum toxin type A—a modulator of spinal neuron–glia interactions under neuropathic pain conditions. In *Toxins*. https://doi.org/10.3390/toxins10040145

Rossi, D. L., Hardiman, G., Copeland, N. G., Gilbert, D. J., Jenkins, N., Zlotnik, A., & Bazan, J. F. (1998). Cloning and characterization of a new type of mouse chemokine. *Genomics*, *47*(2), 163–170. https://doi.org/10.1006/geno.1997.5058

Roumier, A., Pascual, O., Béchade, C., Wakselman, S., Poncer, J.-C., Réal, E., Triller, A., & Bessis, A. (2008). Prenatal activation of microglia induces delayed impairment of glutamatergic synaptic function. *PloS One*, *3*(7), e2595.

Sagar, M. A. K., Cheng, K. P., Ouellette, J. N., Williams, J. C., Watters, J. J., & Eliceiri, K. W. (2020). Machine Learning Methods for Fluorescence Lifetime Imaging (FLIM) Based Label-Free Detection of Microglia. *Frontiers in Neuroscience*, *14*. https://doi.org/10.3389/fnins.2020.00931

Saika, F., Matsuzaki, S., Kobayashi, D., Ideguchi, Y., Nakamura, T. Y., Kishioka, S., & Kiguchi, N. (2020). Chemogenetic Regulation of CX3CR1-Expressing Microglia Using Gi-DREADD Exerts Sex-Dependent Anti-Allodynic Effects in Mouse Models of Neuropathic Pain. *Frontiers in Pharmacology*, *11*. https://doi.org/10.3389/fphar.2020.00925

Sarma, J. V., & Ward, P. A. (2011). The complement system. *Cell and Tissue Research*, *343*(1), 227–235. https://doi.org/10.1007/s00441-010-1034-0

Savage, J. C., St-Pierre, M.-K., Carrier, M., El Hajj, H., Novak, S. W., Sanchez, M. G., Cicchetti, F., & Tremblay, M.-È. (2020). Microglial physiological properties and interactions with synapses are altered at presymptomatic stages in a mouse model of Huntington's disease pathology. *Journal of Neuroinflammation*, *17*(1), 98. https://doi.org/10.1186/s12974-020-01782-9

Savchenko, V. L., McKanna, J. A., Nikonenko, I. R., & Skibo, G. G. (2000). Microglia and astrocytes in the adult rat brain: comparative immunocytochemical analysis demonstrates the efficacy of lipocortin 1 immunoreactivity. *Neuroscience*, *96*(1), 195–203. https://doi.org/10.1016/s0306-4522(99)00538-2

Schaafsma, W., Basterra, L. B., Jacobs, S., Brouwer, N., Meerlo, P., Schaafsma, A., Boddeke, E. W. G. M., & Eggen, B. J. L. (2017). Maternal inflammation induces immune activation

of fetal microglia and leads to disrupted microglia immune responses, behavior, and learning performance in adulthood. *Neurobiology of Disease*, *106*, 291–300.

Schafer, D. P., Lehrman, E. K., Kautzman, A. G., Koyama, R., Mardinly, A. R., Yamasaki, R., Ransohoff, R. M., Greenberg, M. E., Barres, B. A., & Stevens, B. (2012). Microglia Sculpt Postnatal Neural Circuits in an Activity and Complement-Dependent Manner. *Neuron*. https://doi.org/10.1016/j.neuron.2012.03.026

Schecter, R. W., Maher, E. E., Welsh, C. A., Stevens, B., Erisir, A., & Bear, M. F. (2017). Experience-Dependent Synaptic Plasticity in V1 Occurs without Microglial CX3CR1. *The Journal of Neuroscience : The Official Journal of the Society for Neuroscience*, *37*(44), 10541–10553. https://doi.org/10.1523/JNEUROSCI.2679-16.2017

Schmittgen, T. D., & Livak, K. J. (2008). Analyzing real-time PCR data by the comparative C(T) method. *Nature Protocols*, *3*(6), 1101–1108. https://doi.org/10.1038/nprot.2008.73

Schoppmeyer, R., van Steen, A. C. I., Kempers, L., Timmerman, A. L., Nolte, M. A., Hombrink, P., & van Buul, J. D. (2022). The endothelial diapedesis synapse regulates transcellular migration of human T lymphocytes in a CX3CL1- and SNAP23-dependent manner. *Cell Reports*, *38*(3), 110243. https://doi.org/10.1016/j.celrep.2021.110243

Schwarz, J. M., Sholar, P. W., & Bilbo, S. D. (2012). Sex differences in microglial colonization of the developing rat brain. *Journal of Neurochemistry*, *120*(6), 948–963. https://doi.org/10.1111/j.1471-4159.2011.07630.x

Scofield, M. D., Boger, H. A., Smith, R. J., Li, H., Haydon, P. G., & Kalivas, P. W. (2015). Gq-DREADD Selectively Initiates Glial Glutamate Release and Inhibits Cue-induced Cocaine Seeking. *Biological Psychiatry*, *78*(7), 441–451. https://doi.org/10.1016/j.biopsych.2015.02.016

Seeman, P., Bzowej, N. H., Guan, H. C., Bergeron, C., Becker, L. E., Reynolds, G. P., Bird, E. D., Riederer, P., Jellinger, K., & Watanabe, S. (1987). Human brain dopamine receptors in children and aging adults. *Synapse (New York, N.Y.)*, *1*(5), 399–404. https://doi.org/10.1002/syn.890010503

Sellgren, C. M., Gracias, J., Watmuff, B., Biag, J. D., Thanos, J. M., Whittredge, P. B., Fu, T., Worringer, K., Brown, H. E., Wang, J., Kaykas, A., Karmacharya, R., Goold, C. P., Sheridan, S. D., & Perlis, R. H. (2019). Increased synapse elimination by microglia in schizophrenia patient-derived models of synaptic pruning. *Nature Neuroscience*. https://doi.org/10.1038/s41593-018-0334-7

Shankardass, K., McConnell, R., Jerrett, M., Milam, J., Richardson, J., & Berhane, K. (2009). Parental stress increases the effect of traffic-related air pollution on childhood asthma incidence. *Proceedings of the National Academy of Sciences*, *106*(30), 12406–12411.

Sharma, M., Burré, J., Bronk, P., Zhang, Y., Xu, W., & Südhof, T. C. (2012). CSPα knockout causes neurodegeneration by impairing SNAP-25 function. *The EMBO Journal*, *31*(4), 829–841. https://doi.org/10.1038/emboj.2011.467

Shen, Y., Li, R., McGeer, E. G., & McGeer, P. L. (1997). Neuronal expression of mRNAs for complement proteins of the classical pathway in Alzheimer brain. *Brain Research*, *769*(2), 391–395.

Shimaoka, T., Nakayama, T., Fukumoto, N., Kume, N., Takahashi, S., Yamaguchi, J., Minami, M., Hayashida, K., Kita, T., & Ohsumi, J. (2004). Cell surface-anchored SR-PSOX/CXC chemokine ligand 16 mediates firm adhesion of CXC chemokine receptor 6-expressing cells. *Journal of Leukocyte Biology*, *75*(2), 267–274.

Shirasu, M., Kimura, K., Kataoka, M., Takahashi, M., Okajima, S., Kawaguchi, S., Hirasawa, Y., Ide, C., & Mizoguchi, A. (2000). VAMP-2 promotes neurite elongation and SNAP-25A increases neurite sprouting in PC12 cells. *Neuroscience Research*. https://doi.org/10.1016/S0168-0102(00)00125-5

Sierra, A., Encinas, J. M., Deudero, J. J. P., Chancey, J. H., Enikolopov, G., Overstreet-Wadiche, L. S., Tsirka, S. E., & Maletic-Savatic, M. (2010). Microglia shape adult hippocampal neurogenesis through apoptosis-coupled phagocytosis. *Cell Stem Cell*. https://doi.org/10.1016/j.stem.2010.08.014

Silva, C. G., Peyre, E., & Nguyen, L. (2019). Cell migration promotes dynamic cellular interactions to control cerebral cortex morphogenesis. *Nature Reviews. Neuroscience*, *20*(6), 318–329. https://doi.org/10.1038/s41583-019-0148-y

Silvin, A., & Ginhoux, F. (2018). Microglia heterogeneity along a spatio-temporal axis: More questions than answers. *Glia*, *66*(10), 2045–2057. https://doi.org/10.1002/glia.23458

Soltys, Z., Orzylowska-Sliwinska, O., Zaremba, M., Orlowski, D., Piechota, M., Fiedorowicz, A., Janeczko, K., & Oderfeld-Nowak, B. (2005). Quantitative morphological study of microglial cells in the ischemic rat brain using principal component analysis. *Journal of Neuroscience Methods*, *146*(1), 50–60. https://doi.org/10.1016/j.jneumeth.2005.01.009

Stanfield, B. B. (1992). The development of the corticospinal projection. *Progress in*

Neurobiology, *38*(2), 169–202.

Stanfield, B. B., O'Leary, D. D. M., & Fricks, C. (1982). Selective collateral elimination in early postnatal development restricts cortical distribution of rat pyramidal tract neurones. *Nature*, *298*(5872), 371–373.

Stence, N., Waite, M., & Dailey, M. E. (2001). Dynamics of microglial activation: A confocal time-lapse analysis in hippocampal slices. *Glia*, *33*(3), 256–266.

Stephan, A. H., Barres, B. A., & Stevens, B. (2012). The Complement System: An Unexpected Role in Synaptic Pruning During Development and Disease. *Annual Review of Neuroscience*. https://doi.org/10.1146/annurev-neuro-061010-113810

Sternson, S. M., & Roth, B. L. (2014). Chemogenetic tools to interrogate brain functions. *Annual Review of Neuroscience*, *37*, 387–407. https://doi.org/10.1146/annurev-neuro-071013-014048

Stevens, B., Allen, N. J., Vazquez, L. E., Howell, G. R., Christopherson, K. S., Nouri, N., Micheva, K. D., Mehalow, A. K., Huberman, A. D., Stafford, B., Sher, A., Litke, A. M., Lambris, J. D., Smith, S. J., John, S. W. M., & Barres, B. A. (2007). The Classical Complement Cascade Mediates CNS Synapse Elimination. *Cell*, *131*(6), 1164–1178. https://doi.org/https://doi.org/10.1016/j.cell.2007.10.036

Stowell, R. D., Wong, E. L., Batchelor, H. N., Mendes, M. S., Lamantia, C. E., Whitelaw, B. S., & Majewska, A. K. (2018). Cerebellar microglia are dynamically unique and survey Purkinje neurons in vivo. *Developmental Neurobiology*, *78*(6), 627–644. https://doi.org/10.1002/dneu.22572

Stratoulias, V., Venero, J. L., Tremblay, M.-È., & Joseph, B. (2019). Microglial subtypes: diversity within the microglial community. *The EMBO Journal*, *38*(17), e101997–e101997. https://doi.org/10.15252/embj.2019101997

Streit, W. J., Xue, Q.-S., Tischer, J., & Bechmann, I. (2014). Microglial pathology. *Acta Neuropathologica Communications*, *2*(1), 142. https://doi.org/10.1186/s40478-014-0142-6

Strobel, S. A. (1998). Ribozyme chemogenetics. *Biopolymers*, *48*(1), 65–81. https://doi.org/10.1002/(SICI)1097-0282(1998)48:1<65::AID-BIP7>3.0.CO;2-D

Sundaram, V. K., Sampathkumar, N. K., Massaad, C., & Grenier, J. (2019). Optimal use of statistical methods to validate reference gene stability in longitudinal studies. *PloS One*, *14*(7), e0219440. https://doi.org/10.1371/journal.pone.0219440

Takata-Tsuji, F., Chounlamountri, N., Do, L. D., Philippot, C., Novion Ducassou, J., Couté, Y., Ben Achour, S., Honnorat, J., Place, C., & Pascual, O. (2021). Microglia modulate gliotransmission through the regulation of VAMP2 proteins in astrocytes. *GLIA*. https://doi.org/10.1002/glia.23884

Tan, Y.-L., Yuan, Y., & Tian, L. (2020). Microglial regional heterogeneity and its role in the brain. *Molecular Psychiatry*, *25*(2), 351–367. https://doi.org/10.1038/s41380-019-0609-8

Tang, G., Gudsnuk, K., Kuo, S. H., Cotrina, M. L., Rosoklija, G., Sosunov, A., Sonders, M. S., Kanter, E., Castagna, C., Yamamoto, A., Yue, Z., Arancio, O., Peterson, B. S., Champagne, F., Dwork, A. J., Goldman, J., & Sulzer, D. (2014). Loss of mTOR-Dependent Macroautophagy Causes Autistic-like Synaptic Pruning Deficits. *Neuron*. https://doi.org/10.1016/j.neuron.2014.07.040

Tarozzo, G., Bortolazzi, S., Crochemore, C., Chen, S.-C., Lira, A. S., Abrams, J. S., & Beltramo, M. (2003). Fractalkine protein localization and gene expression in mouse brain. *Journal of Neuroscience Research*, *73*(1), 81–88. https://doi.org/10.1002/jnr.10645

Tay, T. L., Savage, J. C., Hui, C. W., Bisht, K., & Tremblay, M.-È. (2017). Microglia across the lifespan: from origin to function in brain development, plasticity and cognition. *The Journal of Physiology*, *595*(6), 1929–1945. https://doi.org/10.1113/JP272134

Tetreault, N. A., Hakeem, A. Y., Jiang, S., Williams, B. A., Allman, E., Wold, B. J., & Allman, J. M. (2012). Microglia in the Cerebral Cortex in Autism. *Journal of Autism and Developmental Disorders*, *42*(12), 2569–2584. https://doi.org/10.1007/s10803-012-1513-0

Thion, M. S., Low, D., Silvin, A., Chen, J., Grisel, P., Schulte-Schrepping, J., Blecher, R., Ulas, T., Squarzoni, P., Hoeffel, G., Coulpier, F., Siopi, E., David, F. S., Scholz, C., Shihui, F., Lum, J., Amoyo, A. A., Larbi, A., Poidinger, M., … Garel, S. (2018). Microbiome Influences Prenatal and Adult Microglia in a Sex-Specific Manner. *Cell*, *172*(3), 500-516.e16. https://doi.org/10.1016/j.cell.2017.11.042

Thompson, K. J., Khajehali, E., Bradley, S. J., Navarrete, J. S., Huang, X. P., Slocum, S., Jin, J., Liu, J., Xiong, Y., Olsen, R. H. J., Diberto, J. F., Boyt, K. M., Pina, M. M., Pati, D., Molloy, C., Bundgaard, C., Sexton, P. M., Kash, T. L., Krashes, M. J., … Tobin, A. B. (2018). DREADD Agonist 21 Is an Effective Agonist for Muscarinic-Based DREADDs in Vitro and in Vivo. *ACS Pharmacology & Translational Science*, *1*(1), 61–72.

https://doi.org/10.1021/acsptsci.8b00012

Torres-Platas, S. G., Comeau, S., Rachalski, A., Bo, G. D., Cruceanu, C., Turecki, G., Giros, B., & Mechawar, N. (2014). Morphometric characterization of microglial phenotypes in human cerebral cortex. *Journal of Neuroinflammation*. https://doi.org/10.1186/1742-2094-11-12

Traut, J., Mengual, J. P., Meijer, E. J., McKillop, L. E., Alfonsa, H., Hoerder-Suabedissen, A., Song, S. M., Molnár, Z., Akerman, C. J., Vyazovskiy, V. V, & Krone, L. B. (2022). Effects of clozapine-N-oxide and compound 21 on sleep in laboratory mice. *BioRxiv*, 2022.02.01.478652. https://doi.org/10.1101/2022.02.01.478652

Tremblay, M.-È., Lowery, R. L., & Majewska, A. K. (2010). Microglial interactions with synapses are modulated by visual experience. *PLoS Biology*, *8*(11), e1000527. https://doi.org/10.1371/journal.pbio.1000527

Tremblay, M.-È., Zettel, M. L., Ison, J. R., Allen, P. D., & Majewska, A. K. (2012). Effects of aging and sensory loss on glial cells in mouse visual and auditory cortices. *Glia*, *60*(4), 541–558. https://doi.org/10.1002/glia.22287

Tuan, L.-H., & Lee, L.-J. (2019). Microglia-mediated synaptic pruning is impaired in sleep-deprived adolescent mice. *Neurobiology of Disease*, *130*, 104517. https://doi.org/10.1016/j.nbd.2019.104517

Ueno, M., Fujita, Y., Tanaka, T., Nakamura, Y., Kikuta, J., Ishii, M., & Yamashita, T. (2013). Layer V cortical neurons require microglial support for survival during postnatal development. *Nature Neuroscience*, *16*(5), 543–551. https://doi.org/10.1038/nn.3358

Ueno, M., Nakamura, Y., Li, J., Gu, Z., Niehaus, J., Maezawa, M., Crone, S. A., Goulding, M., Baccei, M. L., & Yoshida, Y. (2018). Corticospinal Circuits from the Sensory and Motor Cortices Differentially Regulate Skilled Movements through Distinct Spinal Interneurons. *Cell Reports*, *23*(5), 1286-1300.e7. https://doi.org/10.1016/j.celrep.2018.03.137

Ulloa, F., Cotrufo, T., Ricolo, D., Soriano, E., & Araújo, S. J. (2018). SNARE complex in axonal guidance and neuroregeneration. In *Neural Regeneration Research*. https://doi.org/10.4103/1673-5374.228710

van den Elsen, J. M. H., & Isenman, D. E. (2011). A crystal structure of the complex between human complement receptor 2 and its ligand C3d. *Science*, *332*(6029), 608–611.

van der Veen, B., Kapanaiah, S. K. T., Kilonzo, K., Steele-Perkins, P., Jendryka, M. M., Schulz,

S., Tasic, B., Yao, Z., Zeng, H., Akam, T., Nicholson, J. R., Liss, B., Nissen, W., Pekcec, A., & Kätzel, D. (2021). Control of impulsivity by Gi-protein signalling in layer-5 pyramidal neurons of the anterior cingulate cortex. *Communications Biology*, *4*(1), 662. https://doi.org/10.1038/s42003-021-02188-w

Van Der Walt, S., Schönberger, J. L., Nunez-Iglesias, J., Boulogne, F., Warner, J. D., Yager, N., Gouillart, E., & Yu, T. (2014). Scikit-image: Image processing in python. *PeerJ*. https://doi.org/10.7717/peerj.453

Vanderhaeghen, P., & Cheng, H.-J. (2010). Guidance molecules in axon pruning and cell death. *Cold Spring Harbor Perspectives in Biology*, *2*(6), a001859. https://doi.org/10.1101/cshperspect.a001859

VanRyzin, J. W., Pickett, L. A., & McCarthy, M. M. (2018). Microglia: Driving critical periods and sexual differentiation of the brain. *Developmental Neurobiology*, *78*(6), 580–592. https://doi.org/10.1002/dneu.22569

Vardy, E., Robinson, J. E., Li, C., Olsen, R. H. J., DiBerto, J. F., Giguere, P. M., Sassano, F. M., Huang, X.-P., Zhu, H., Urban, D. J., White, K. L., Rittiner, J. E., Crowley, N. A., Pleil, K. E., Mazzone, C. M., Mosier, P. D., Song, J., Kash, T. L., Malanga, C. J., … Roth, B. L. (2015). A New DREADD Facilitates the Multiplexed Chemogenetic Interrogation of Behavior. *Neuron*, *86*(4), 936–946. https://doi.org/10.1016/j.neuron.2015.03.065

Velmeshev, D., Schirmer, L., Jung, D., Haeussler, M., Perez, Y., Mayer, S., Bhaduri, A., Goyal, N., Rowitch, D. H., & Kriegstein, A. R. (2019). Single-cell genomics identifies cell type–specific molecular changes in autism. *Science*. https://doi.org/10.1126/science.aav8130

Vigels\o, A., Dybboe, R., Hansen, C. N., Dela, F., Helge, J. W., & Guadalupe Grau, A. (2015). GAPDH and β-actin protein decreases with aging, making Stain-Free technology a superior loading control in Western blotting of human skeletal muscle. *Journal of Applied Physiology*, *118*(3), 386–394. https://doi.org/10.1152/japplphysiol.00840.2014

Vilalta, A., & Brown, G. C. (2018). Neurophagy, the phagocytosis of live neurons and synapses by glia, contributes to brain development and disease. *The FEBS Journal*, *285*(19), 3566–3575. https://doi.org/10.1111/febs.14323

Villa, A., Della Torre, S., & Maggi, A. (2019). Sexual differentiation of microglia. *Frontiers in Neuroendocrinology*, *52*, 156–164. https://doi.org/10.1016/j.yfrne.2018.11.003

Villa, A., Gelosa, P., Castiglioni, L., Cimino, M., Rizzi, N., Pepe, G., Lolli, F., Marcello, E., Sironi, L., Vegeto, E., & Maggi, A. (2018). Sex-Specific Features of Microglia from Adult Mice.

Cell Reports, *23*(12), 3501–3511. https://doi.org/10.1016/j.celrep.2018.05.048

Vinet, J., van Weering, H. R. J., Heinrich, A., Kälin, R. E., Wegner, A., Brouwer, N., Heppner, F. L., van Rooijen, N., Boddeke, H. W. G. M., & Biber, K. (2012). Neuroprotective function for ramified microglia in hippocampal excitotoxicity. *Journal of Neuroinflammation*, *9*(1), 27. https://doi.org/10.1186/1742-2094-9-27

Wake, H., Moorhouse, A. J., Jinno, S., Kohsaka, S., & Nabekura, J. (2009). Resting Microglia Directly Monitor the Functional State of Synapses In Vivo and Determine the Fate of Ischemic Terminals. *The Journal of Neuroscience*, *29*(13), 3974 LP – 3980. https://doi.org/10.1523/JNEUROSCI.4363-08.2009

Wake, H., Moorhouse, A. J., Miyamoto, A., & Nabekura, J. (2013). Microglia: Actively surveying and shaping neuronal circuit structure and function. In *Trends in Neurosciences*. https://doi.org/10.1016/j.tins.2012.11.007

Wakselman, S., Béchade, C., Roumier, A., Bernard, D., Triller, A., & Bessis, A. (2008). Developmental Neuronal Death in Hippocampus Requires the Microglial CD11b Integrin and DAP12 Immunoreceptor. *The Journal of Neuroscience*, *28*(32), 8138 LP – 8143. https://doi.org/10.1523/JNEUROSCI.1006-08.2008

Walker, D. G., Kim, S. U., & McGeer, P. L. (1995). Complement and cytokine gene expression in cultured microglia derived from postmortem human brains. *Journal of Neuroscience Research*, *40*(4), 478–493.

Walker, F. R., Beynon, S. B., Jones, K. A., Zhao, Z., Kongsui, R., Cairns, M., & Nilsson, M. (2014). Dynamic structural remodelling of microglia in health and disease: a review of the models, the signals and the mechanisms. *Brain, Behavior, and Immunity*, *37*, 1–14. https://doi.org/10.1016/j.bbi.2013.12.010

WALTON, W. H. (1948). Feret‘s Statistical Diameter as a Measure of Particle Size. *Nature*, *162*(4113), 329–330. https://doi.org/10.1038/162329b0

Washbourne, P., Thompson, P. M., Carta, M., Costa, E. T., Mathews, J. R., Lopez-Benditó, G., Molnár, Z., Becher, M. W., Valenzuela, C. F., Partridge, L. D., & Wilson, M. C. (2002). Genetic ablation of the t-SNARE SNAP-25 distinguishes mechanisms of neuroexocytosis. *Nature Neuroscience*. https://doi.org/10.1038/nn783

Weinhard, L., Di Bartolomei, G., Bolasco, G., Machado, P., Schieber, N. L., Neniskyte, U., Exiga, M., Vadisiute, A., Raggioli, A., Schertel, A., Schwab, Y., & Gross, C. T. (2018). Microglia remodel synapses by presynaptic trogocytosis and spine head filopodia

induction. *Nature Communications*. https://doi.org/10.1038/s41467-018-03566-5

Weinhard, L., Neniskyte, U., Vadisiute, A., di Bartolomei, G., Aygün, N., Riviere, L., Zonfrillo, F., Dymecki, S., & Gross, C. (2018). Sexual dimorphism of microglia and synapses during mouse postnatal development. *Developmental Neurobiology*. https://doi.org/10.1002/dneu.22568

Weiss, N., Hameed, S., Fernández-Fernández, J. M., Fablet, K., Karmazinova, M., Poillot, C., Proft, J., Chen, L., Bidaud, I., & Monteil, A. (2012). A Cav3. 2/syntaxin-1A signaling complex controls T-type channel activity and low-threshold exocytosis. *Journal of Biological Chemistry*, *287*(4), 2810–2818.

Werneburg, S., Jung, J., Kunjamma, R. B., Ha, S.-K., Luciano, N. J., Willis, C. M., Gao, G., Crocker, S. J., Popko, B., Reich, D. S., & Schafer, D. P. (2019). Targeted complement inhibition at synapses prevents microglial synaptic engulfment and synapse loss in demyelinating disease. *BioRxiv*, 841601. https://doi.org/10.1101/841601

White, G. E., McNeill, E., Channon, K. M., & Greaves, D. R. (2014). Fractalkine promotes human monocyte survival via a reduction in oxidative stress. *Arteriosclerosis, Thrombosis, and Vascular Biology*, *34*(12), 2554–2562.

Wierzba-Bobrowicz, T., Gwiazda, E., Kosno-Kruszewska, E., Lewandowska, E., Lechowicz, W., Bertrand, E., Szpak, G. M., & Schmidt-Sidor, B. (2002). Morphological analysis of active microglia--rod and ramified microglia in human brains affected by some neurological diseases (SSPE, Alzheimer's disease and Wilson's disease). *Folia Neuropathologica*, *40*(3), 125–131.

Wirenfeldt, M., Clare, R., Tung, S., Bottini, A., Mathern, G. W., & Vinters, H. V. (2009). Increased activation of Iba1+ microglia in pediatric epilepsy patients with Rasmussen's encephalitis compared with cortical dysplasia and tuberous sclerosis complex. *Neurobiology of Disease*, *34*(3), 432–440. https://doi.org/https://doi.org/10.1016/j.nbd.2009.02.015

Wlodarczyk, A., Holtman, I. R., Krueger, M., Yogev, N., Bruttger, J., Khorooshi, R., Benmamar-Badel, A., de Boer-Bergsma, J. J., Martin, N. A., Karram, K., Kramer, I., Boddeke, E. W., Waisman, A., Eggen, B. J., & Owens, T. (2017). A novel microglial subset plays a key role in myelinogenesis in developing brain. *The EMBO Journal*, *36*(22), 3292–3308. https://doi.org/10.15252/embj.201696056

Wojdasiewicz, P., Poniatowski, Ł. A., Kotela, A., Deszczyński, J., Kotela, I., & Szukiewicz, D.

(2014). The Chemokine CX3CL1 (Fractalkine) and its Receptor CX3CR1: Occurrence and Potential Role in Osteoarthritis. *Archivum Immunologiae et Therapiae Experimentalis*, *62*(5), 395–403. https://doi.org/10.1007/s00005-014-0275-0

Wouters, D., Wiessenberg, H. D., Hart, M., Bruins, P., Voskuyl, A., Daha, M. R., & Hack, C. E. (2005). Complexes between C1q and C3 or C4: novel and specific markers for classical complement pathway activation. *Journal of Immunological Methods*, *298*(1–2), 35–45. https://doi.org/10.1016/j.jim.2004.12.018

Wynne, A. M., Henry, C. J., Huang, Y., Cleland, A., & Godbout, J. P. (2010). Protracted downregulation of CX3CR1 on microglia of aged mice after lipopolysaccharide challenge. *Brain, Behavior, and Immunity*, *24*(7), 1190–1201. https://doi.org/10.1016/j.bbi.2010.05.011

Xiao, J., Dong, H., Wu, Y., Tian, W., & Liu, L. (2009). Gene expression profiling of Cx3cl1 in bone marrow mesenchymal stem cells by osteogenic induction. *Omics : A Journal of Integrative Biology*, *13*(4), 337–343. https://doi.org/10.1089/omi.2009.0018

Xu, J., Luo, F., Zhang, Z., Xue, L., Wu, X.-S., Chiang, H.-C., Shin, W., & Wu, L.-G. (2013). SNARE proteins synaptobrevin, SNAP-25, and syntaxin are involved in rapid and slow endocytosis at synapses. *Cell Reports*, *3*(5), 1414–1421.

Yamagata, M., Sanes, J. R., & Weiner, J. A. (2003). Synaptic adhesion molecules. *Current Opinion in Cell Biology*, *15*(5), 621–632. https://doi.org/https://doi.org/10.1016/S0955-0674(03)00107-8

Yang, H.-M., Yang, S., Huang, S.-S., Tang, B.-S., & Guo, J.-F. (2017). Microglial Activation in the Pathogenesis of Huntington's Disease . In *Frontiers in Aging Neuroscience* (Vol. 9). https://www.frontiersin.org/article/10.3389/fnagi.2017.00193

Yanguas-Casás, N., Crespo-Castrillo, A., de Ceballos, M. L., Chowen, J. A., Azcoitia, I., Arevalo, M. A., & Garcia-Segura, L. M. (2018). Sex differences in the phagocytic and migratory activity of microglia and their impairment by palmitic acid. *Glia*, *66*(3), 522–537. https://doi.org/10.1002/glia.23263

Yi, M.-H., Liu, Y. U., Liu, K., Chen, T., Bosco, D. B., Zheng, J., Xie, M., Zhou, L., Qu, W., & Wu, L.-J. (2021). Chemogenetic manipulation of microglia inhibits neuroinflammation and neuropathic pain in mice. *Brain, Behavior, and Immunity*, *92*, 78–89. https://doi.org/https://doi.org/10.1016/j.bbi.2020.11.030

Zerrate, M. C., Pletnikov, M., Connors, S. L., Vargas, D. L., Seidler, F. J., Zimmerman, A. W.,

Slotkin, T. A., & Pardo, C. A. (2007). Neuroinflammation and Behavioral Abnormalities after Neonatal Terbutaline Treatment in Rats: Implications for Autism. *Journal of Pharmacology and Experimental Therapeutics*, *322*(1), 16 LP – 22. https://doi.org/10.1124/jpet.107.121483

Zhan, Y., Paolicelli, R. C., Sforazzini, F., Weinhard, L., Bolasco, G., Pagani, F., Vyssotski, A. L., Bifone, A., Gozzi, A., & Ragozzino, D. (2014). Deficient neuron-microglia signaling results in impaired functional brain connectivity and social behavior. *Nature Neuroscience*, *17*(3), 400–406.

Zhang, S. (2019). Microglial activation after ischaemic stroke. *Stroke and Vascular Neurology*, *4*(2), 71 LP – 74. https://doi.org/10.1136/svn-2018-000196

Zhang, Z., Wang, D., Sun, T., Xu, J., Chiang, H.-C., Shin, W., & Wu, L.-G. (2013). The SNARE proteins SNAP25 and synaptobrevin are involved in endocytosis at hippocampal synapses. *Journal of Neuroscience*, *33*(21), 9169–9175.

Zhao, D., Mokhtari, R., Pedrosa, E., Birnbaum, R., Zheng, D., & Lachman, H. M. (2017). Transcriptome analysis of microglia in a mouse model of Rett syndrome: differential expression of genes associated with microglia/macrophage activation and cellular stress. *Molecular Autism*, *8*(1), 17. https://doi.org/10.1186/s13229-017-0134-z

Zhao, H., Alam, A., Chen, Q., Eusman, M. A., Pal, A., Eguchi, S., Wu, L., & Ma, D. (2017). The role of microglia in the pathobiology of neuropathic pain development: what do we know? *British Journal of Anaesthesia*, *118*(4), 504–516. https://doi.org/https://doi.org/10.1093/bja/aex006

Zhu, H., Pleil, K. E., Urban, D. J., Moy, S. S., Kash, T. L., & Roth, B. L. (2014). Chemogenetic inactivation of ventral hippocampal glutamatergic neurons disrupts consolidation of contextual fear memory. *Neuropsychopharmacology : Official Publication of the American College of Neuropsychopharmacology*, *39*(8), 1880–1892. https://doi.org/10.1038/npp.2014.35

Zhuo, M., Wu, G., & Wu, L.-J. (2011). Neuronal and microglial mechanisms of neuropathic pain. *Molecular Brain*, *4*(1), 31. https://doi.org/10.1186/1756-6606-4-31

Zusso, M., Methot, L., Lo, R., Greenhalgh, A. D., David, S., & Stifani, S. (2012). Regulation of postnatal forebrain amoeboid microglial cell proliferation and development by the transcription factor Runx1. *The Journal of Neuroscience : The Official Journal of the Society for Neuroscience*, *32*(33), 11285–11298.

https://doi.org/10.1523/JNEUROSCI.6182-11.2012

Appendix 1

The broad variability in the expression of housekeeping genes in the developing brain requires strict definition of endogenous controls. For synaptic 'silencing' using abolition of Snap25 gene expression as an endogenous control I used TBP. Here I showed that housekeeping gene TBP are adequate reference for CX3CL1, CX3CR1, C3 and CD11b gene expression analysis in the developing cortex and hippocampus.

In the developing cortex, no statistically significant differences in TBP expression were observed (control mice: P8 = 29.111±0.279, n = 6; P14 = 29.803±0.233, n = 6; P21 = 30.126±0.215, n = 6; $F(2, 28) = 0.735$, $p = 0.4886$, Figure A1A). Moreover, no statistically significant differences between control and Snap25 cKO control mice were observed in the developing cortex (Snap25 cKO: P8 = 29.874±0.290, n = 5; P14 = 29.479±0.116, n = 6; P21 = 29.399±0.089, n = 5; $F(1, 28) = 0.286$, $p = 0.5968$, Figure A1A).

In the developing hippocampus, no statistically significant differences in TBP expression were observed (control mice: P8 = 28.969±0.391, n = 6; P14 = 29.656±0.443, n = 6; P21 = 29.571±0.220, n = 6; $F(2, 28) = 2.49$, $p = 0.1014$, Figure A1B). No statistically significant differences between control and Snap25 cKO mice in the developing hippocampus were observed (Snap25 cKO: P8 = 28.401±0.501, n = 5; P14 = 29.033±0.457, n = 6; P21 = 29.512±0.287, n = 5; $F(1, 28) = 1.66$, $p = 0.2086$ Figure A1B).

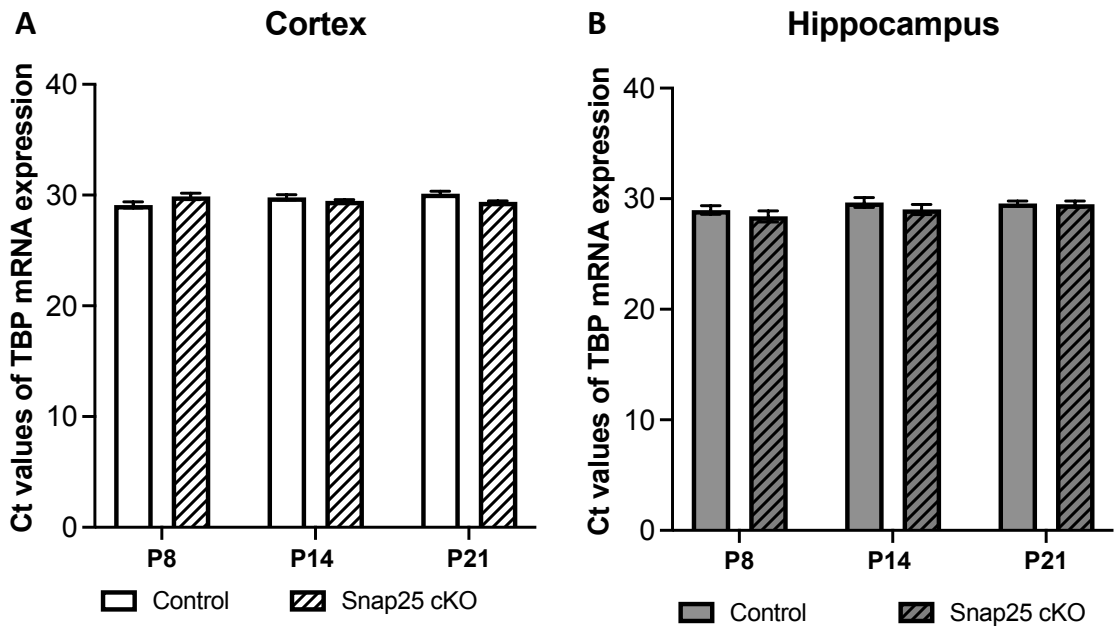


Figure A1: TBP expression in the developing brain

A) TBP expression in the developing cortex at P8, P14 and P21 between control and Snap25 cKO mice. B) TBP expression in the developing hippocampus at P8, P14 and P21 between control and Snap25 cKO mice. Two-way ANOVA, all data presented as mean ± SEM, * $p < 0.05$, ** $p < 0.01$, *** $p < 0.001$, **** $p < 0.0001$.